RADIOCHEMICAL AND SPECTROSCOPIC STUDIES OF CESIUM, BARIUM, AND COBALT SORPTION ON SOME NATURAL CLAYS

A THESIS
SUBMITTED TO THE DEPARTMENT OF CHEMISTRY
AND THE INSTITUTE OF ENGINEERING AND SCIENCES
OF BİLKENT UNIVERSITY
IN PARTIAL FULFILLMENT OF THE REQUIREMENTS
FOR THE DEGREE OF
DOCTOR OF PHILOSOPHY

By
TALAL SHAHWAN

AUGUST 2000

I certify that I have read this thesis and that in my opinion it is fully adequate, in scope and in quality, as a thesis of the degree of Doctor of Philosophy

Prof. Dr. Hasan N. Erten (Principal Advisor)

I certify that I have read this thesis and that in my opinion it is fully adequate, in scope and in quality, as a thesis of the degree of Doctor of Philosophy

Prof. Dr. Hale Göktürk

I certify that I have read this thesis and that in my opinion it is fully adequate, in scope and in quality, as a thesis of the degree of Doctor of Philosophy

Prof. Dr. Atilla Aydınlı

I certify that I have read this thesis and that in my opinion it is fully adequate, in scope and in quality, as a thesis of the degree of Doctor of Philosophy

Assoc. Prof Margarita Kantcheva

I certify that I have read this thesis and that in my opinion it is fully adequate, in scope and in quality, as a thesis of the degree of Doctor of Philosophy

Assist. Prof Serdar Özçelik

Approved for the Institute of Engineering and Sciences

Prof. Dr. Mehmet Baray
Director of Institute of Engineering and Science

ABSTRACT

RADIOCHEMICAL AND SPECTROSCOPIC SORPTION STUDIES OF CESIUM, BARIUM, AND COBALT ON SOME NATURAL CLAYS

TALAL SHAHWAN

Ph.D. in Chemistry

Supervisor: Prof. Dr. Hasan N. Erten

August 2000

The wide growth in the nuclear activities results in an increasing subsequent influx of radioactive wastes into the environment. This problem has manifested a great deal of interest aiming at finding out ways through which those wastes can be harmlessly isolated from the human environment. Geological disposal is considered as one of the most promising solutions that ensures a safe storage of radioactive wastes as long as their activities are above the accepted levels. Clay minerals are proposed as backfill buffering materials in the geological repositories that can delay the migration of the radionuclides through sorption and thus decrease the contamination of underground waters. The extent of retardation of the radionuclide

migration is dependent on factors like time of contact, pH and Eh of groundwater, concentration, temperature and grain size of the mineral particles.

In this study radiochemical, spectroscopic (ToF-SIMS, XPS), and X-ray diffraction techniques were applied to examine different aspects of the sorption behavior of Cs^{+}, Ba^{2+}, and Co^{2+} on three natural clay minerals containing primarily kaolinite, illite-chlorite, and bentonite.

The elements cesium (Z=55), barium (Z=56), and cobalt (Z=27) have the radioactive isotopes ^{137}Cs ($t_{1/2}$= 30.17 years), ^{140}Ba ($t_{1/2}$= 12.79 day), and ^{60}Co ($t_{1/2}$=5.3 y) which are important in radioactive waste management. The first two radionuclides are produced in high yields in nuclear fission, whereas the third is an activation product. The natural clay samples that were used in this study originated from natural mineralogical beds at Sındırgı, Afyon, and Giresun regions in Turkey. The characterization of these clay samples showed that the primary clay minerals were kaolinite in Sındırgı clay, chlorite and illite in Afyon clay, and montmorillonite in Giresun clay. Each of these clays possess different structural properties that result in different sorption capabilities.

Radiochemical batch experiments were carried out to examine the effects of time, concentration, and temperature on the sorption of Cs^{+}, Ba^{2+}, and Co^{2+} on clays. Solutions of these cations spiked with several microliters of the radionuclides ^{137}Cs ($t_{1/2}$=30.1 y), ^{133}Ba($t_{1/2}$=10.7 y), and ^{60}Co($t_{1/2}$=5.3 y) were monitored using γ-ray

Spectroscopy prior to and after each sorption experiment. These results showed that equilibrium is achieved within two days in all cases. The sorption data was adequately described by Freundlich and Dubinin-Radushkevich isotherm models. Based on the parameters of those isotherm models, it was found that sorption was nonlinear, and that bentonite showed the highest sorption affinity and sorption capacity towards the sorbed ions. The thermodynamic parameters indicated that while sorption of Cs^+ and Ba^{2+} on the three clays is exothermic that of Co^{2+} is endothermic. The obtained values of Gibbs free energy change, ΔG^o, were generally in the 8-16 (kJ/mol) energy range that corresponds to ion exchange type sorption mechanism.

Since sorption is mainly a surface phenomenon, part of our sorption studies were carried out using the surface sensitive techniques; Time of Flight- Secondary Ion Mass Spectroscopy (ToF-SIMS) and X-ray Photoelectron Spectroscopy (XPS). In addition, depth profiling up to 70 Å was performed using ToF-SIMS to investigate Cs^+, Ba^{2+}, and Co^{2+} concentrations through the clay surface. ToF-SIMS and XPS studies were helpful in figuring out the surface composition of different clays prior to and after sorption. Quantification of the depletion of different alkali and alkaline-earth metals initially contained within the analyzed clay surface showed that ion exchange plays a primary role in the sorption process. In addition, X-Ray Diffraction (XRD) technique was applied to figure out the mineralogical composition of the clay minerals used and examine any structural change a accompanying the sorption process. XRD spectra of the clay samples after sorption

showed that -apart from some intensity reductions in some clay features-, no primary changes were detected in the sorption cases of Cs^{+} and Co^{2+}. In Ba^{2+} sorption , however, features belonging $BaCO_3$ were present in the spectra corresponding to sorption on chlorite-illite and bentonite.

Keywords: Sorption, Cesium, Barium, Cobalt, Kaolinite, Chlorite-Illite, Bentonite, Batch Operation, Radiotracer Method, Time of Flight-Secondary Ion Mass Spectroscopy, X-ray Photoelectron Spectroscopy, X-ray Diffraction, Distribution Ratio, Depletion Factor, Percentage Contribution to Depletion, Isotherm Models, Enthalpy Change, Entropy Change, Gibbs Free Energy Change.

ÖZET

SEZYUM, BARYUM, VE COBALT İYONLARININ BAZI KİL MİNERALLERCE TUTULMASININ RADYOKİMYASAL VE SPEKTROSKOPİK YÖNTEMLERİ İLE İNCELENMESİ

TALAL SHAHWAN

Doktora Tezi, Kimya Bölümü

Tez Yöneticisi : Prof. Dr. Hasan N. Erten

Ağustus 2000

Radyoaktif maddelerin kullanışından meydana gelen artış sonucunda oluşan radyoaktif atıklar biolojik çevre açısından gün geçtikçe büyüyen bir sorun olarak ortaya çıkmaktadır. Bu atıkların yaratabilecekleri zararlardan korunmak için, jeolojik oluşumlara depolanması konusunda çeşitli projeler geliştirilmektedir. Bu oluşumlarda kullanılması planlanan kil mineralleri, radyoaktif izotopların dağılımını sorpsiyon yoluyla azaltmaktadır. Bunun sonucunda, bu izotopların yeraltı sularına

ulaşmaları ve meydana getirebilecekleri radyoaktif kirlenme önemli ölçüde önlenebilmektedir. Radyoaktif maddelerin killer üzerine tutulma davranışları çeşitli faktörlerce etkilenmektedir. Bunların arasında temas süresi, yeraltısularının pH'ı ve Eh'ı, iyon konsantrasyonu, ısı, ve mineral taneciklerinin büyüklüğü sayılabilir. Radyoaktif atıkların depolanması ile ilgili güvenlik çalışmaları, radyoaktif izotopların jeolojik ortamdaki davranışlarının ayrıntılı bir şekilde anlaşılmasını gerektirmektedir.

Bu çalışmada sezyum, baryum, ve kobalt iyonlarının Türkiye'de bulanan üç tane kil çeşiti üzerindeki farklı sorpsiyon yönleri incelenmiştir. ^{137}Cs ($t_{1/2}$= 30.1 y), ^{140}Ba ($t_{1/2}$= 12.8 d), ve ^{60}Co ($t_{1/2}$= 5.3 y) izotopları radyoaktif atıklar bakımından önemli olan radyoizotoplardır. . ^{137}Cs ve ^{140}Ba nükleer fizyon neticesinde yüksek verimle meydana gelen izotoplardır. ^{60}Co ise, nükleer aktivasyon yoluyla ortaya çıkmaktadır. İncelenen kil örnekleri Sındırgı, Afyon, ve Giresun bölgelerinden alınmıştır. X-ışını Kırınımı (XRD) ve Fourier Dönüşümlü Kızıl Ötesi Spektroskopisi (FTIR) verilerine göre, Sındırgı kili büyük ölçüde kaolinit, Afyon kili klorit ve illit, ve Giresun kili bentonit (montmorrilonit) tipi kil çeşitlerinden oluşmaktadır.

Yapılan bütün deneylerde baç metodu kullanılmıştır. Sorpsiyon çalışmalarında radyokimyasal yöntemle beraber güçlü birer yüzeysel teknik olan

Time of Flight-Kütle Spektoskopisi (ToF-SIMS) ve X-ışını Fotoelektron Spektroskopisi (XPS) de kullanılmıştır.

Radyokimyasal yöntemle yürütülen çalışmada temas süresi, çözeltinin derişimi, ve ısı etkenlerinin, sezyum, baryum, ve kobalt iyonlarının killer üzerine sorpsiyonunu nasıl etkilediği araştırılmıştır. Sorpsiyon kinetiği çalışmaları dengeye iki gün içinde ulaşıldığını göstermiştir. Elde edilen sorpsiyon verilerine değişik izoterm modelleri uygulanmıştır. Sorpsiyon verileri Freundlich ve Dubinin-Radushkevich izoterm modellerine iyi uyduğu görülmüştür. Değişik sıcaklıklarda elde edilen deneysel verileri kullanarak sorpsiyonda entalpi değişimi, $\Delta H°$, entropi değişimi, $\Delta S°$ ve Gibbs serbest enerjisi değişimi, $\Delta G°$, hesaplanmıştır. Killerin üçünde de sezyum ve baryum iyonlarının sorpsiyonu ekzotermik olduğunu gözlenirken, kobalt iyonun sorpsiyonu endotermik olduğu tesbit edilmiştir. Değişik sıcaklıklarda yapılan $\Delta G°$ hesaplamalarında negatif değerler elde edilmiştir. Bunlar ise, sorpsiyonun kendiliğinden oluştuğunu göstermektedir. Hesaplanan $\Delta G°$ değerlerinin tümü, 8-16 kJ/moL değerleri arasında bulunmaktadır. Bu düzeyedeki enerjiler, sorpsiyonun daha çok iyon değişimi yoluyla meydana geldiğini göstermektedir.

Sorpsiyon olayı daha çok yüzeyde yer aldığı için, ToF-SIMS ve XPS gibi etkili yüzeysel teknikler kullanılmıştır. Ayrıca, ToF-SIMS kullanılarak 70Å' a varan derinlik analizi de yapılmıştır. Bu çalışmaların sonucunda, sorpsiyon deneylerinin

öncesi ve sonrasında kilin yapısında bulunan değişik elementlerin oranları belirlenmiştir Sorpsiyon esnasında killerden salıverilen iyonların miktarlarının, killerce tutulan sezyum, baryum, ve kobalt iyonların miktarları ile karşılaştırılması sonucunda iyon değişiminin sorpsiyon mekanizmasında etkin bir rol oynadığı gözlenmiştir.

XRD tekniği kullanılarak killerin yapılarında sorpsiyonla birlikte meydana gelen değişimler incelenmiştir. XRD verilerine göre, sezyum ve kobalt iyonlarının sorpsiyonu sonucunda önemli bir değişiklik olmazken, baryumun klorıt-illit ve bentonit killerince sorpsiyonu sonucunda $BaCO_3$ çökelti şeklinde oluştuğu tesbit edilmiştir.

Anahtar Kelimeler: Sorpsiyon, Sezyum, Baryum, Kobalt, Kaolinit, Klorit-İllit, Bentonit, Baç Metodu, İyon Değişimi, Radyokimya, ToF-SIMS, XPS, XRD Dağılım Oranı, Izoterm Modelleri, Sorpsiyon Entalpisi, Sorpsiyon Entropisi, Gibbs Serbest Enerjisi.

ACKNOWLEDGEMENT

I wish to express my gratitude towards my supervisor Prof. Dr. Hasan N. Erten for his guidance and support throughout the course of this study.

I would like to thank Prof. Dr. Şefik Süzer, Assoc. Prof. Margarita Kantcheva, and Prof. Dr. Attila Aydınlı for their help in developing this thesis. I wish to thank Prof. Dr. G. Allen, Dr. L. Black, and Dr. K. Hallam at the Interface Centre/Bristol University for their help in ToF-SIMS, XPS, and XRD Measurements.

I debt thanks also to my friend Şafak Sayan and all other friends for their help and encouragement.

I would like to express my endless thanks to my beloved family and my dear wife, Faten, for their unseized sacrifices and support throughout the course of my studies.

TABLE OF CONTENTS

1. INTRODUCTION 1

1.1- Radioactive Waste Management 1

1.1.1- Catagories of Radioactive Waste 2

1.1.2- Disposal Options of Radioactive Waste 5

1.1.3- Nuclear Waste Repository 6

1.2- Clay Minerals 8

1.2.1- General Description 8

1.2.2- Structural Features of Some Clay Minerals 8

1.2.3- Cation Exchange Capacity 14

1.2.4- Clay-Solution Interaction and Sorption Affinity 17

1.3- Groundwater and Radionuclide Migration 19

1.4- Retardation Mechanisms of Radionuclide Migration 21

1.5- The Batch Method 24

1.6- Literature Review 25

1.7- The Present Study 28

1.7.1- General Objectives 28

1.7.2- Techniques Used 31

1.7.2.1- The Radiotracer Method 31

1.7.2.2- Time of Flight-Secondary Ion Mass Spectroscopy 32

1.7.2.3- X-ray Photoelectron Spectroscopy 34

1.7.2.4- X-ray Diffraction 35

2. MATHEMATICAL RELATIONS 37

2.1- The Distribution Ratio 37

2.2- Sorption Isotherm Models 39

2.2.1- Langmuir Isotherm Model 39

2.2.2- Freundlich Isotherm Model 40

2.2.3- Dubinin-Radushkevich Isotherm Model 41

2.3- Thermodynamic Relations 43

2.4- ToF-SIMS Calculations 44

3. EXPERIMENTAL 47

3.1- Experiments Using the Radiotracer Method 47

3.1.1- Analysis of Bilkent Tapwater 47

3.1.2- Pretreatment of the Clay Samples 48

3.1.3- Isotopic Tracers 49

3.1.4- Effect of Time 53

3.1.5- Effects of Loading and Temperature 53

3.2- Experiments Using Time of Flight-Secondary Ion Mass Spectroscopy (ToF-SIMS), X-ray Photoelectron Spectroscopy (XPS), and X-ray Diffraction (XRD) 54

3.2.1- Sorption Experiments 54

3.2.2- ToF-SIMS Analysis of Clay Samples Before and After Sorption 55

3.2.3- XPS Analysis of Clay Samples Before and After Sorption 56

3.2.4- XRD Analysis of Clay Samples Before and After Sorption 56

3.2.5- FTIR Analysis of Natural Clay Samples..... 57

4. RESULTS AND DISCUSSIONS 58

4.1- Characterization of the Clay Minerals 58

4.2- Radiochemical Sorption Studies 69

4.2.1- Effect of Time on Sorption 69

4.2.2- Loading and Temperature Studies 74

4.2.2.1- Loading Curves 75

4.2.2.2- The Sorption Isotherms 80

4.2.2.3- The Thermodynamic Parameters 96

4.3- Sorption Studies Using ToF-SIMS 105

4.3.1- Analysis of the Exchanged Ions 110

4.3.2- Analysis of the Sorbed Cations 119

4.4- Sorption Studies Using XPS 130

4.5- XRD Sorption Studies 137

4.6- Empirical Equations 142

4.6.1- Equations Based on Data Obtained Using Radiochemical Studies 142

4.6.2- Equations Based on Data Obtained Using ToF-SIMS Studies 147

5. CONCLUSIONS 150

REFERENCES 153

APPENDICES..... 162

LIST OF FIGURES

1.1: Diagram of a Radioactive Waste Repository (E B S) 7

1.2: The Kaolinite Structure 10

1.3: The Structure of Hydrous Mica (Illite) 12

1.4: The Chlorite Structure 12

1.5: The Montmorillonite Structure 13

1.6: Schematic Picture of the Fixed (Stern) and Diffuse (Gouy) Layers 18

1.7: Retardation Mechanisms in Migration Behavior Considerations Through Geomedia 23

3.1: Schematic Draw of the Ge Detector 52

4.1: X-ray Diffraction Spectra of; (a) Kaolinite (b) Chlorite-Illite, and (c) Bentonite 60

4.2: IR Spectrum of Kaolinite. The Inset in the Figure Gives the IR Spectrum of Pure Kaolinite..... 61

4.3: IR Spectrum of Chlorite-Illite. The Insets in the Figure Gives the IR Spectra of; (a) Pure Chlorite, and (b) Pure Illite 62

4.4: IR Spectrum of Bentonite. The Inset in the Figure Gives the IR Spectrum of Pure Montmorillonite 63

4.5: ToF-SIMS Spectra of; (a)Bentonite, (b)Chlorite-Illite, and (c)Kaolinite 67

4.6: XPS Spectra of; (a) Kaolinite, (b) Chlorite-Illite, and (c) Bentonite 68

4.7: Variation of R_d (mL/g) with Shaking Time for Cs^+ Sorption on; (a) Kaolinite, (b) Chlorite-Illite, and (c) Bentonite 71

4.8: Variation of R_d (mL/g) with Shaking Time for Ba^{2+} Sorption on; (a) Kaolinite, (b) Chlorite-Illite, and (c) Bentonite 72

4.9: Variation of R_d (mL/g) with Shaking Time for Co^{2+} Sorption on; (a) Kaolinite, (b) Chlorite-Illite, and (c) Bentonite 73

4.10: The Loading Curves Corresponding to Sorption of (a) Cs^+, (b) Ba^{2+}, and (c) Co^{2+} on Kaolinite 77

4.11: The Loading Curves Corresponding to Sorption of (a) Cs^+, (b) Ba^{2+}, and (c) Co^{2+} on Chlorite-Illite 78

4.12: The Loading Curves Corresponding to Sorption of (a) Cs^+, (b) Ba^{2+}, and (c) Co^{2+} on Bentonite 79

4.13: Freundlich Isotherm Plots Corresponding to Sorption of (a) Cs^+, (b) Ba^{2+}, and (c) Co^{2+} on Kaolinite 83

4.14: Freundlich Isotherm Plots Corresponding to Sorption of (a) Cs^+, (b) Ba^{2+}, and (c) Co^{2+} on Chlorite-Illite 84

4.15: Freundlich Isotherm Plots Corresponding to Sorption of (a) Cs^+, (b) Ba^{2+}, and (c) Co^{2+} on Bentonite 85

4.16: D-R Isotherm Plots Corresponding to Sorption of (a) Cs^+, (b) Ba^{2+}, and (c) Co^{2+} on Kaolinite 89

4.17: D-R Isotherm Plots Corresponding to Sorption of (a) Cs^+, (b) Ba^{2+}, and (c) Co^{2+} on Chlorite-Illite 90

4.18: D-R Isotherm Plots Corresponding to Sorption of (a) Cs^+, (b) Ba^{2+}, and (c) Co^{2+} on Bentonite 91

4.19: Langmuir Isotherm Plots Corresponding to Sorption of (a) Cs^+, (b) Ba^{2+}, and (c) Co^{2+} on Kaolinite 93

4.20: Langmuir Isotherm Plots Corresponding to Sorption of (a) Cs^+, (b) Ba^{2+}, and (c) Co^{2+} on Chlorite-Illite 94

4.21: Langmuir Isotherm Plots Corresponding to Sorption of (a) Cs^+, (b) Ba^{2+}, and (c) Co^{2+} on Bentonite 95

4.22: Arrhenius Plots for Sorption of; (a) Cs^+, (b) Ba^{2+}, and (c) Co^{2+} Sorption on Kaolinite 102

4.23: Arrhenius Plots for Sorption of; (a) Cs^+, (b) Ba^{2+}, and (c) Co^{2+} Sorption on Chlorite-Illite 103

4.24: Arrhenius Plots for Sorption of; (a) Cs^+, (b) Ba^{2+}, and (c) Co^{2+} Sorption on Bentonite 104

4.25: Variation of DF Values of; (a) K^+, (b) Mg^{2+}, and (c) Ca^{2+} as a Function of Depth in Kaolinite Matrix for Sorption of Cs^+, Ba^{2+}, and Co^{2+} 111

4.26: Variation of DF Values of; (a) K^+, (b) Mg^{2+}, and (c) Ca^{2+} as a Function of Depth in Chlorite-Illite Matrix for Sorption of Cs^+, Ba^{2+}, and Co^{2+} 112

4.27: Variation of DF Values of; (a) Na^+, and (c) Mg^{2+} as a Function of Depth in Bentonite Matrix for Sorption of Cs^+, Ba^{2+}, and Co^{2+} 113

4.28: A typical ToF-SIMS Spectrum of Kaolinite. The Inset in the Figure Shows the Variation of Cs^+, Ba^{2+}, and Co^{2+} Signal Intensity with Depth 124

4.29: A typical ToF-SIMS Spectrum of Chlorite-Illite. The Inset in the Figure Shows the Variation of Cs^+, Ba^{2+}, and Co^{2+} Signal Intensity with Depth 125

4.30: A typical ToF-SIMS Spectrum of Bentonite. The Inset in the Figure Shows the Variation of Cs^+, Ba^{2+}, and Co^{2+} Signal Intensity with Depth 126

4.31: Variation of the Sorbed Amounts of Cs^+, Ba^{2+}, and Co^{2+} with Depth in Kaolinite Matrix..... 127

4.32: Variation of the Sorbed Amounts of Cs^+, Ba^{2+}, and Co^{2+} with Depth in Chlorite-Illite Matrix 128

4.33: Variation of the Sorbed Amounts of Cs^+, Ba^{2+}, and Co^{2+} with Depth in Bentonite Matrix 129

4.34: XPS Spectra of; (a) Natural Kaolinite, (b) Cs-Sorbed Kaolinite, and (c) Ba-Sorbed Kaolinite 134

4.35: XPS Spectra of; (a) Natural Chlorite-Illite, (b) Cs-Sorbed Chlorite-Illite, and (c) Ba- Sorbed Chlorite-Illite 135

4.36: XPS Spectra of; (a) Natural Bentonite, (b) Cs-Sorbed Bentonite, and (c) Ba-Sorbed Bentonite 136

4.37: XRD Spectra of; (a) Natural Kaolinite (b) Cs-Sorbed Kaolinite, (c) Ba-Sorbed Kaolinite, and (d) Co-Sorbed Kaolinite 139

4.38: XRD Spectra of; (a) Natural Chlorite-Illite, (b) Cs-Sorbed Chlorite-Illite, (c) Ba-Sorbed Chlorite-Illite, and (d) Co-Sorbed Chlorite-Illite 140

4.39: XRD Spectra of; (a) Natural Bentonite, (b) Cs-Sorbed Bentonite, (c) Ba-Sorbed Bentonite, and (d) Co-Sorbed Bentonite 141

4.40: The Variation of Freundlich Parameter, k, with Temperature for the Sorption of (a) Cs^+, (b) Ba^{2+}, and (c) Co^{2+} on Kaolinite, Chlorite-Illite, and Bentonite 145

4.41: Variation of the R_d Values with Equilibrium Aqueous Concentration, $[C]_l$ (meq/ml), and Temperature (K) as Predicted by the Empirical Equations Corresponding to Cs^+ Sorption on Bentonite 146

4.42: Variation of ln C with x^2 for Sorption Cases of Cs^+, Ba^{2+}, and Co^{2+} on; (a) Kaolinite, (b) Chlorite-Illite, and (c) Bentonite 149

LIST OF TABLES

1.1: Some Radionuclides of Importance in Radioactive Waste Considerations ..3

1.2: Classification of Radioactive Wastes 4

1.3: Summary of Properties of Clay Minerals of Interest in this Work 9

1.4: Cation Exchange Capacities for Clays of Interest in this Work 14

1.5: Iso-electric Points for Some Naturally Occuring Substances 16

3.1: Concentrations of Na, K, Ca and Mg in Bilkent Tapwater Used in our Sorption Studies 48

3.2: The Size Distribution of Kaolinite, Chlorite-Illite, and Bentonite Obtained Using Andreasen Pipette Method 49

4.1: The Percentage Elemental Composition of the Natural Clay Minerals Obtained by ToF-SIMS and XPS 66

4.2: Freundlich Isotherm Constants, n and k, Obtained From the Least Square Fits of the Sorption Data of Cs^{+}, Ba^{2+}, and Co^{2+} on Kaolinite, Chlorite-Illite, and Bentonite 82

4.3: D-R Isotherm Constants, K and C_m, Obtained From the Least Square Fits of the Sorption Data of Cs^+, Ba^{2+}, and Co^{2+} on Kaolinite, Chlorite-Illite, and Bentonite. The E Values Calculated using K Values are also Given 88

4.4: Values of Enthalpy Change, ΔH^o (kJ/mol) and Entropy Change, ΔS^o (J/mol.K) Obtained From Arrhenius Plots of the Sorption Data of Cs^+, Ba^{2+}, and Co^{2+} on Kaolinite, Chlorite-Illite, and Bentonite 100

4.5: The Average Values of Enthalpy Change, ΔH_{av}^o (kJ/mol), Entropy Change, ΔS_{av}^o (J/mol.K), and the Calculated Gibbs Free Energy Change, ΔG^o (kJ/mol) for Cs^+, Ba^{2+}, and Co^{2+} Sorption on Kaolinite, Chlorite-Illite, and Bentonite 101

4.6: The Elements Considered in ToF-SIMS Calculations, their Relative Sensitivity Factors and Natural Isotopes 109

4.7: The Initial and Final Ratios (Cation/Al+Si), R_i and R_f, the Equivalent Depleted Amounts (EDA), and the Percentage Contribution to Total Depletion, D_x, as a Function of Depth for the Sorption of Cs^+, Ba^{2+}, and Co^{2+} on Kaolinite. All Calculations are Based on ToF-SIMS Measurements .. 116

4.8: The Initial and Final Ratios (Cation/Al+Si), R_i and R_f, the Equivalent Depleted Amounts (EDA), and the Percentage Contribution to Total Depletion, D_x, as a Function of Depth for the Sorption of Cs^+, Ba^{2+}, and Co^{2+} on Chlorite-Illite. All Calculations are Based on ToF-SIMS Measurements 117

4.9: The Initial and Final Ratios (Cation/Al+Si), R_i and R_f, the Equivalent Depleted Amounts (EDA), and the Percentage Contribution to Total

Depletion, D_x, as a Function of Depth for the Sorption of Cs^+, Ba^{2+}, and Co^{2+} on Bentonite. All Calculations are Based on ToF-SIMS Measurements 118

4.10 The Amounts of Sorbed Cs^+, Ba^{2+}, and Co^{2+} (relative to Al+Si) as a Function of Depth in Kaolinite, Chlorite-Illite, and Bentonite Matrices Obtained from ToF-SIMS measurements 120

4.11: The Total Equivalent Sorbed Amounts, (ΣESA), of Cs^+, Ba^{2+}, and Co^{2+} and the Total Equivalent Depleted Amounts, (ΣEDA), of Depleted Cations for Sorption on Kaolinite, Chlorite-Illite, and Bentonite Obtained from ToF-SIMS Measurements 123

4.12: The Elements Detected by XPS in the Clay Structure, their Binding Energies (eV), and their Sensitivity Factors 131

4.13: The Initial and Final Ratios (Cation/Al+Si), R_i and R_f, the Equivalent Depleted Amounts (EDA), and the Equivalent Sorbed Amounts (ESA) Obtained from XPS Measurements of Cs^+ and Ba^{2+} Sorption Kaolinite, Chlorite-Illite, and Bentonite 133

4.14: The Values of A, B, and N for the Sorption of Cs^+, Ba^{2+}, and Co^{2+} on Kaolinite, Chlorite-Illite, and Bentonite 144

4.15: The Values of the Constants C_o and D for Cs^+, Ba^{2+}, and Co^{2+} Sorption on Kaolinite, Chlorite-Illite, and Bentonite Obtained From the Diffusion Model Based on ToF-SIMS Data 148

1. INTRODUCTION

1.1- Radioactive Waste Management

The ongoing increase in the nuclear activities around the world necessitates finding out adequate ways to protect the biosphere against the threat of the resulting radioactive wastes. A wide range of radioactive elements are being introduced into the environment from the nuclear power plants, weapons testing, and applications in medicine, industry, and research. Table 1.1 gives a list of some important fission and activation-products that have potential threat to the environment [1].

The term waste management refers to the complete spectrum of background policy and actual practices which define the classification, control, movement, conditioning, storage, and disposal of wastes. The overall objective of radioactive waste management is to isolate the wastes in a manner that ensures there is no unacceptable detriment to man and to the biological environment, as a whole at

present and in the future. The two fundamental options available for disposal of any material are either to endeavor to keep it in the same place for as long as necessary , or to allow natural processes to mobilize and disperse it, harmlessly. The first concept is known as *containment*, whereas the second is commonly referred to as *dilution and dispersion*. From radioactive waste view point, there is an increasingly widespread move towards adopting both concepts in any single waste disposal system. The way this is usually envisaged is that short lived radionuclides are contained until a sufficient number of half-lives have passed that their concentration in the waste is extremely low. Since containment of very much longer-lived radionuclides for any equivalent number of half-lives is impossible to achieve, the system is also designed to allow for their eventual slow mobilization and dispersal. The definition of how long the initial containment period should last depends very much on the waste type and the predicted behavior of the environment chosen for disposal [2] .

1.1.1- Categories of Radioactive Waste

Radioactive wastes can be divided into three main categories each having different characteristics. The radioactivity levels for different categories are given in Table 1.2 [3]. Unreprocessed spent fuel contains fissile actinides and fission products that are extremely hazardous and must be kept under strictly controlled conditions.

Table 1.1: Some radionuclides of importance in radioactive waste considerations

Radionuclide	Half Life	Source	Fission Yield (%)
^{135}Cs	3.0×10^{6} y	Nuclear Fission	6.54
^{137}Cs	30.0 y	Nuclear Fission	6.18
^{89}Sr	50.5 d	Nuclear Fission	4.82
^{90}Sr	28.5 y	Nuclear Fission	5.77
^{140}Ba	12.75 d	Nuclear Fission	6.21
^{132}Te	3.62 d	Nuclear Fission	4.31
^{133}Xe	5.24 d	Nuclear Fission	6.70
^{129}I	1.57×10^{7} y	Nuclear Fission	0.76
^{140}La	1.68 d	Nuclear Fission	6.21
^{144}Ce	284.9 d	Nuclear Fission	5.49
^{143}Pr	13.58 d	Nuclear Fission	5.96
^{147}Nd	10.98 d	Nuclear Fission	2.27
^{147}Pm	2.623 y	Nuclear Fission	2.27
^{93}Zr	1.5×10^{6} y	Fission+Activation	6.38
^{99}Mo	2.748 d	Nuclear Fission	6.07
^{99}Tc	2.13×10^{5} y	Nuclear Fission	6.07
^{55}Fe	2.73 y	Activation	-
^{60}Co	5.271 y	Activation	-
^{59}Ni	7.5×10^{4} y	Activation	-

The spent fuel after being converted into a dry stable solid is referred to as 'high level waste'. As an alternative to disposal, this material may be stored under controlled conditions for a period of several decades until the activity and heat production have sufficiently decayed. At the end of this period, the term 'intermediate level waste' is applied. The term 'low level waste' is used to encompass a range of materials which are contaminated with radionuclides from various sources.

In the nuclear industry, low level wastes comprise filters, ion exchange resins, laboratory wastes, etc. Other sources include hospitals and industry. The disposal of low level wastes is generally by shallow burial. High and intermediate level wastes, however, require special disposal considerations.

Table 1.2: Classification of radioactive wastes

Category		Gas (Bq/L)	Liquid (Bq/L)	Solid (Bq/m^3)
Low Level	α	$< 3.7\times10^{-6}$	$< 3.7\times10^{7}$	$< 10^{10}$
	β, photon	$< 3.7\times10^{-3}$	$< 3.7\times10^{7}$	$< 10^{10}$
Intermediate Level	α	$> 3.7\times10^{-6}$ - 3.7	3.7×10^{7}-3.7×10^{10}	10^{10} - 10^{12}
	β, photon	3.7×10^{-3}-3.7×10^{3}	3.7×10^{7}-3.7×10^{10}	10^{10} - 10^{12}
High Level	α	> 3.7	$> 3.7\times10^{10}$	$> 10^{12}$
	β, photon	$> 3.7\times10^{3}$	$> 3.7\times10^{10}$	$> 10^{12}$

1.1.2- Disposal Options of Radioactive Waste

According to the International Atomic Energy Agency, IAEA, [4] the major options valid for geological underground disposal of radioactive wastes are:

1- Disposal in shallow ground

2- Disposal in deep geological formations

3- Disposal in rock cavities

In general safe disposal of radioactive wastes is achieved by:

1- Confinement of the waste in one or more natural or man-made barriers and thus its adequate isolation from the human environment, in particular from ground water.

2- Retardation of radionuclide migration if the waste is, or will be, in contact with ground water or subject to other migration mechanisms.

3- Disposal of the waste at a depth or location where future natural or man made disruptive events are extremely unlikely [5].

1.1.3- Nuclear Waste Repository

The nuclear waste repository refers to a system of engineered structures placed within a well characterized natural setting that will provide safe isolation and permanent disposal of nuclear waste. The uncertainty inherent in the properties and performance of natural systems makes it necessary to design a repository with multiple retardation barriers formed of both engineered and natural ones. Each of these barriers by itself should be capable of ensuring safe isolation of nuclear waste.

A conceptual set of multiple barriers for a repository is given in Figure 1.1. Starting from the innermost set of barriers, these include the solidified waste form or matrix, a container or canister, a backfill or buffer and finally the encompassing geological formation as a host rock [6].

For practical purposes, the repository system is thought to be composed of two main zones; the near-field and the far-field zones. The near-field includes all engineered barriers (i.e. solid matrix, buffering material, canister) plus a region of the surrounding rock which is significantly altered by heat (for HLW) or chemical releases from the waste package. The far-field zone, however, is the undisturbed natural geological system. It is very much larger physically and may have quite complex geological structure, but compared with the near-field, it is in a relatively steady state with regard to chemistry, hydrology and temperature. Overall, this

region controls the rate at which water can enter the near-field and also retards the transport and dilutes the concentration of radionuclides released from the near field. The output from the far field goes into the biosphere and is the source for calculation of radiation doses to man [2].

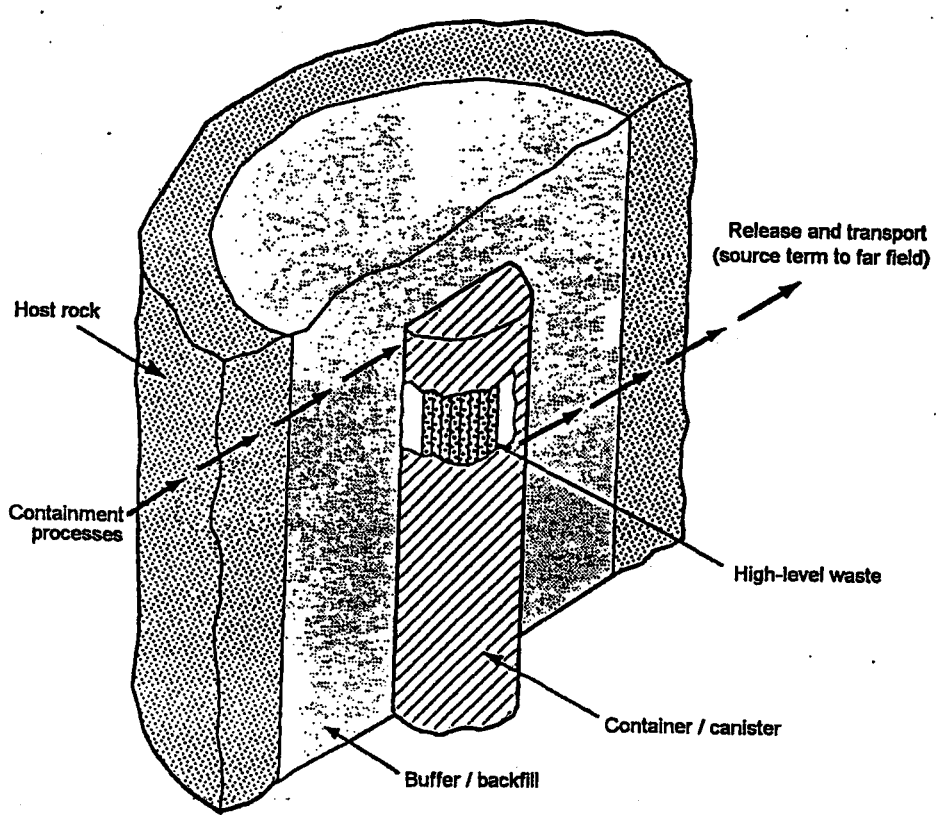

Fig. 1.1: Diagram of a radioactive waste repository (engineered barrier system)

1.2- Clay Minerals

1.2.1- General Description

Clay minerals are essentially hydrous aluminum silicates of very small particle size (< 2 μm). In some, Mg and Fe substitute in part for aluminum and alkali or alkaline earths may be present as essential constituents. The structure of a pure clay mineral is made up of two basic blocks. The first is the sheet formed of silicon terahedral units and the second is another sheet composed of aluminum octahedral units. The stacking of these sheets into layers, the bonding between layers, and the substiution of other ions for Al and Si determines the type of the clay minerals. Among the properties of clay minerals are their plasticity, when mixed with a small amount of water, their low permeability, thermal stability, and wide availability. Although a clay may be made up of a single clay mineral, there are usually several mixed with other minerals such as feldspars, quartz, carbonates and micas [7].

1.2.2- Structural Features of Some Clay Minerals

The main structural features of the clays used in this study; kaolinite, illite, chlorite, and montmorillonite are summarized in Table 1.3 and are discussed as

Table 1.3: Summary of properties of clay minerals of interest in this work

Clay Mineral	Type	Interlayer bond Strength	Surface Area (m^2/g)	Basal Spacing(Å)
Kaolinite	1:1	strong	5-20	7
Illite	2:1	strong	50-200	10
Chlorite	2:1:1	moderate-strong		14
Montmorillonite	2:1	weak	700-800	9.8-18

- ***Kaolinite:*** It consists of an octahedrally coordinated sheet of aluminum ions and a tetrahedrally coordinated sheet of silicon ions (Fig. 1.2). The silicon ion is so small relative to oxygen and hydroxyl ions that it fits in the tetrahedral sites. Oxygen and hydroxyl ions have essentially the same size so that interchanging them makes no difference to the geometry provided that the electric charges are balanced in the structure as a whole. The ideal formula of kaolinite is $Al_2Si_2O_5(OH)_4$ and most minerals of the kaolinite group appear to be close to ideal in composition. Because each structural unit contains one octahedral and one tetrahedral sheet, kaolinite is referred to as a 1:1 clay. When these sheets stack, the OH^- ions on one sheet lie next to and in close contact to the O^{2-} layer of its neighbour sheet. As a result the structure becomes tightly bound via hydrogen bonding. Kaolinite is a non-expanding clay, hence it is unable to absorb water into the interlayer position. The nonexpanding nature of kaolinite explains the failure of soils high in this clay to swell or shrink much on wetting or drying. The unit layer of kaolinite is about 7Å

thick which gives rise to a characteristic x-ray diffraction peak corresponding to about 7Å.

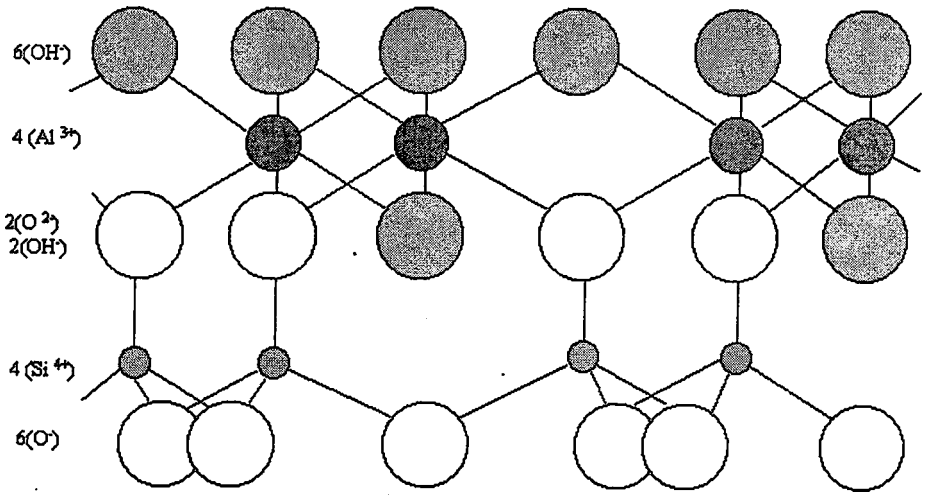

Fig. 1.2: Structure of Kaolinite

- *Illite*: It is a member of the mica family and is generally known as hydrous mica. It is a (2:1) type mineral, i.e. two tetrahedral, one octahedral sheets involved per structural unit (Fig. 1.3). The layers in the micas are held together by relatively strong electrostatic forces between the negatively charged silicate layers and the K^+ ions between them, Thus, no water is present in the entire layer space, and the K^+ ions are not exchangeable under normal conditions. When the K^+ content in hydrous mica is not enough to neutralize the negative charge on the layers, other cations may

be adsorbed in the interlayer position to counter this. The basal spacing of the micas is about 10 Å and the term illite is used to cover all clay-sized minerals belonging to the mica group, that is, clay minerals that show a 10 Å basal spacing in x-ray diffraction.

- *Chlorite*: The chlorite structure have a basic 2:1 layer structure which is nonexpanding. Chlorite differ from other 2:1 layer minerals in one unique respect; i.e. it contains a stable positively charged octahedral sheet rather than adsorbed cations in the interlayer space. The octahedral sheet consists of two layers of OH^- ions that enclose either Mg^{2+}, Fe^{2+}, or Al^{3+} as the central cations and leads to a positive charge on the sheet (Fig. 1.4). By virtue of the positive charge, the interlayer sheet neutralize the negative charge of the 2:1 sheets. Because of its unique structure, chlorite is sometimes called a 2:1:1 layer mineral. Occasionally, the interlayer octahedral sheet neither fill the interlayer space nor completely neutralize the negative charge of the 2:1 sheets. The unsatisfied charge is then neutralized by various adsorbed cations. The basal spacing is about 14 Å. Natural chlorites have variable amounts of Al, Fe^{2+}, and Fe^{3+} substituting for Mg^{2+}, and Al substituting for Si. The ideal formula is $(Mg, Fe, Al)_6 (Si, Al)_4 O_{10} (OH)_8$.

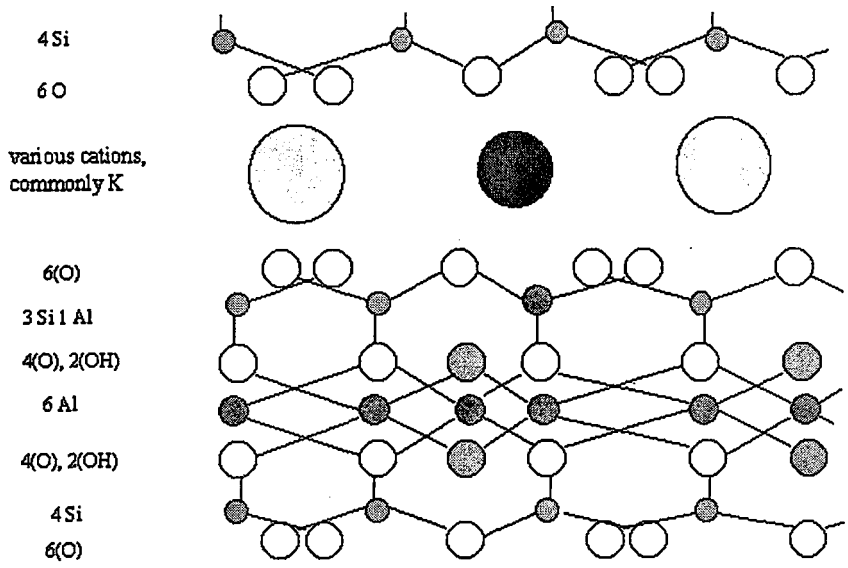

Fig. 1.3: Structure of Hydeous Mica (Illite)

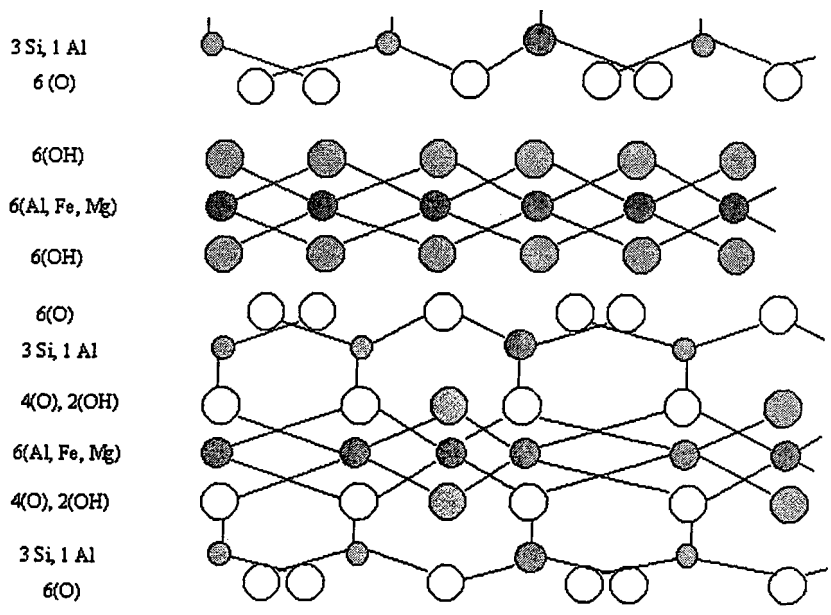

Fig. 1.4: Structure of Chlorite

- *Montmorillonite (Smectite)*: The smectite group comprises a number of clay minerals composed of 2:1 layer structurs. The term smectite is used to describe the clay whose spacing expands up to 17 Å on treatment with ethylene glycol. Montmorillonite, a member of this group, is the dominant clay mineral in the bentonite rocks. It has the unusual property of expanding several times its original volume when placed in water [7]. The structure of montmorillonite is considered to be analogous to that of pyriphyllite with the structural formula $Na_x\{Mg_xAl_{2-x}(OH)_2[Si_4O_{10}]\}.nH_2O$. In montmorillonite, the charge is developed by substitution of Mg^{2+} for Al^{3+} in the octahedral layers (Fig. 1.5). This isomorphous substitution leads to the development of a permanent negative charge on the clay structure. The developed negative charge is balance by hosting various exchangeable cations like Na^+, K^+, and Ca^{2+} in the interlayer spacing [9].

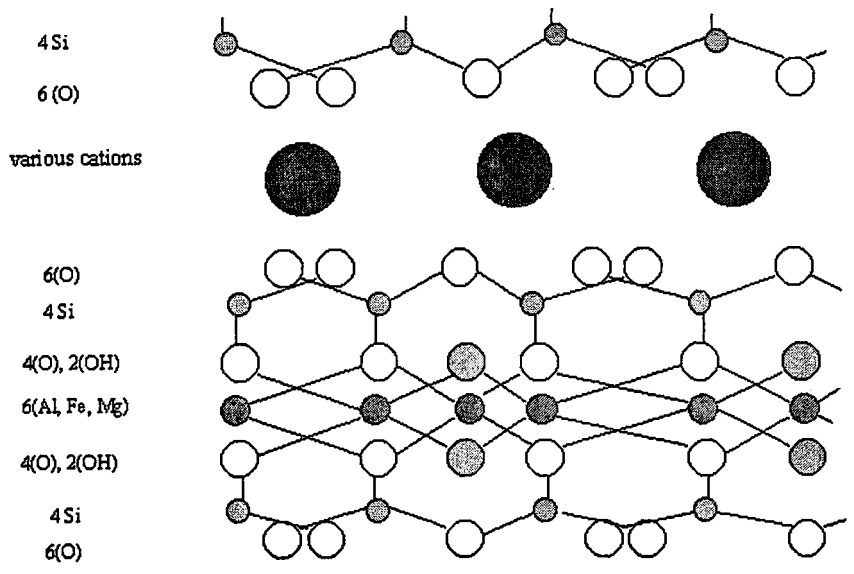

Fig. 1.5: Structure of Montmorillonite

1.2.3- Cation Exchange Capacity

Cation exchange is one of the most important forms of sorption on clays and refers to the process in which cations from natural waters are sorbed by mineral particles with the concurrent release of an equivalent amount of cations. The cation exchange capacity, CEC, of a clay represents the total of all exchangeable cations. It is reported as milliequivalents of cation per 100 g of mineral. Different methods are proposed for the measurement of CEC of various minerals [10,11,12]. One of the most widely used method is to measure the uptake of ammonium ions from 1M ammonium acetate solution at pH 7 by an air-dried clay. Table 1.4 gives CEC values for a number of clay minerals of interest in this work [13].

Table 1.4: Cation Exchange Capacities for Clays of Interest in this Work

Material	Montmorillonite	Kaolinite	Illite	Chlorite
CEC(meq/100g)	70-100	3-15	10-40	10-40

As far as the adsorption properties are concerned, aluminosilicate minerals may be divided into three general groups [14]:

1- Expanding layer structures, such as smectites, which can greatly increase their surface area on solvation and which generally carry a negative charge over a

very wide range of pH's.

2- Cage structures, such as zeolites, which have internal surfaces accessible only to ions or molecules below a certain size.

3- Structures whose adsorption properties are determined solely by the chemical natures of their surfaces.

The surface charge of aluminosilicate minerals may arise either from isomorphous cation substitution within the structure, which is pH independent, or by protonation / deprotonation reactions at oxide or hydroxide surface groups which is pH dependent. The former mechanism is generally considered to dominate in smectite minerals. Clay minerals with layer structure (e.g. smectite and vermiculite) are able to exchange cations (mainly Na^+, K^+, Mg^{2+}, and Ca^{2+}) in positions between the layers. In those clays, the high specific surface area and the large number of exchange sites result in significant exchange capacity [1].

A pH-dependent surface charge can be formed as a result of chemical reactions on the surface or by ionization of some surface components of the clay. This mechanism will depend on the basicity of the O^{2-} ions (i.e. their coordinative unsaturation) and the acidity of the OH groups. This type of processes is important in the sorption studies of the clays since it determines which species and in what

form will be sorbed at a certain pH. The net charge on a surface containing hydroxyl groups is a strong function of pH. In acidic solutions the surface will be positively charged, its cation sorption capacity will be small, and it will have a finite anion sorption capacity. In basic solutions, the surface will be negatively charged and the cation sorption capacity will be significant. The pH at which the net charge is zero is called the 'Iso-Electric Point' (IEP). Below the IEP, the surface is positively charged, and above it it is negatively charged. Table 1.5 lists IEP values for some naturally occurring substances [8].

Table 1.5: Iso-electric point for some naturally occurring substances

Substance	IEP
SiO_2 (quartz)	2.0
SiO_2 (gel)	1.0-2.5
Al_2O_3 (condurum)	9.1
$Al(OH)_3$ (gibbsite)	~9
TiO_2 (anatase)	7.2
Fe_3O_4 (magnetite)	6.5
Fe_2O_3 (hematite)	5-9
FeO(OH) (geothite)	6-7
$Fe_2O_3.nH_2O$	6-9
MnO_2 (various forms)	2
Kaolinite	~3.5
Montmorillonite	<2.5

1.2.4- Clay-Solution Interactions and Sorption Affinity

When a clay particle is suspended in an aqueous phase, an electric charge developes on the clay surface as a result of passage of interlayer cations into solution and protonation/deprotonation of the Si-OH and Al-OH groups present at the clay surface and edges. As mentioned in the previous section, deprotonation is pH-dependent and occurs when the operating pH exceeds the IEP of the clay surface. The charged surface and the diffuse cloud of oppositely charged ions are called the double layer. In general the double layer consists of ions more or less attached to the clay surface (the fixed or Stern layer) and outside that there is a diffuse (or Gouy) layer in which the ions are free to move (Fig. 1.6). In the Gouy layer, the concentration of cations not balanced by anions decreases exponentially away from the boundary of the fixed layer. The ions in the fixed layer may be held by purely electrostatic forces, or by formation of complexes with groups on the surface of the solid [8].

The affinity of the negatively charged surface towards ions in solution refers to the extent to which that surface would favor sorbing those ions. In ion exchange equilibria, the affinity differs depending on (i) Coulombic interactions between the counter ion (in various states of hydration) and the fixed groups of the exchanger, and (ii) ion-dipole and ion-induced dipole interactions between the counter ions and water molecules (ionic hydration). Where (i) is weak compared with (ii), the

following affinity sequence is observed (Hofmeister series):

$$Cs^+ > K^+ > Na^+ > Li^+$$

$$Ba^{2+} > Sr^{2+} > Ca^{2+} > Mg^{2+}$$

This means that the ion with larger hydrated radius tends to be displaced by the ions of smaller hydrated radius. As interactions of the first type predominate over those of the second, the selectivity may be reversed. For most clays the normal series prevails, while for some zeolites and glasses, the reversed affinity may be observed [15]. Affinity is reported to be dependent as well on concentration and oxidation state of the sorbate. As the concentration of the sorbate ions in solution increases, an increasing number of ions show tendency to migrate to the solid surface as a result of internal repulsions leading to an increase in surface coverage. Also as the oxidation state of the sorbate ions increase, the solid surface affinity towards them increases [16].

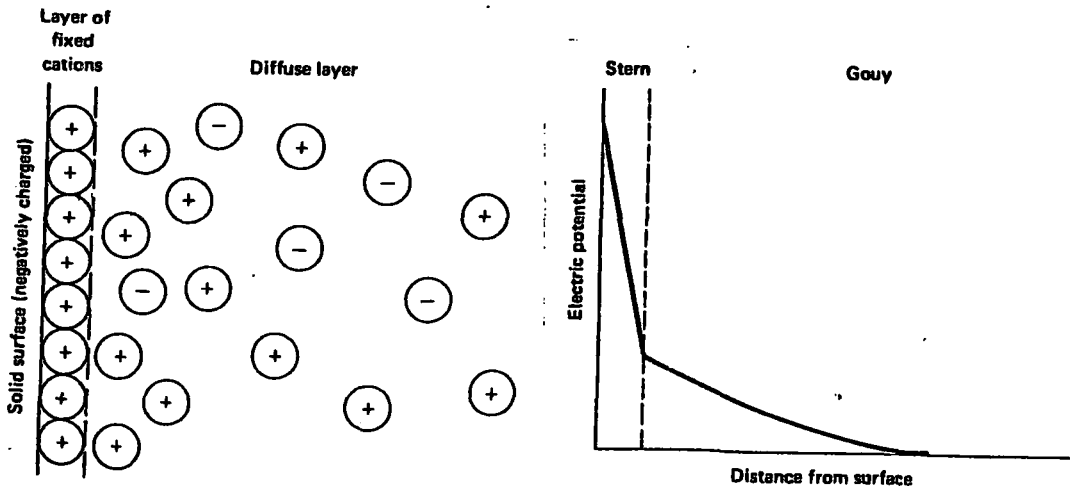

Fig. 1.6: Schematic picture of the fixed (Stern) and diffuse (Gouy) layers

1.3- Groundwater and Radionuclide Migration

The most reasonable scenario through which radionuclides could be transported from the repository to the biosphere is by groundwater flowing through a network of fractures in the surrounding rocks. The extent of release of radionuclides to the biosphere is minimized if the travel times of water are sufficiently long in comparison with the half-lives of the radionuclides [17].

The migration process of the radionuclides by groundwater is affected much by various parameters. Among these parameters are; the pH, the radox potential, Eh, the total salinity of water and the concentration of potential complexing agents. pH determines the degree of hydrolysis and the ion-exchange. Eh determines the valence state for multivalent waste elements. The pH of groundwater is influenced mainly by the presence of carbonates in the system. In the absence of air, Eh is largely determined by the presence of minerals containing natural metal redox systems [18].

An important fact about deep groundwaters is that they are nearly always reducing. Therefore, a canister made of a noble material like copper (proposed because of its large thermodynamic stability against water corrosion) should have a long durability. The stability field of copper decreases with increasing chloride concentration, hence concentrations of chloride larger than 10-20 g/L should be

avoided [19].

The vast majority of radionuclides that could be transported in underground water exist in the cationic form. These radionuclides might undergo reactions in the aqueous medium that could affect their chemical form and thus their sorption characteristics. Such reactions can include [1]:

a- Hydration: the formation of aqua complexes by ion-dipole interactions. The energy of hydration increases with decreasing ionic radius and with increasing positive charge of the cation. Thus the energy of hydration is low for Cs^{+} and high for Th^{4+}.

b- Hydrolysis: if the charge of the cations is high, the repulsion of the protons by the cations may lead to the formation of hydroxo complexes. Hydrolysis depends strongly on pH and increases with increasing charge and decreasing ionic radius of the cation.

c- Condensation: polynuclear complexes are formed by condensation reactions where additional water molecules are removed. The driving force for this kind of reaction is the formation of the predominantly covalent M-O-M bonds and of one molecule of water.

The species of radionuclides present in natural waters can be characterized by the chemical nature and physico-chemical state. A better understanding of the sorption behavior of different radionuclides calls for a better knowledge of their speciation in aqueous media.

1.4- Retardation Mechanisms of Radionuclide Migration

The interaction of radionuclides in aqueous medium with the surrounding solids in near- and far-field zones influences strongly their migration behavior through the geosphere. The transport of these radionuclides could be largely retarded if the interaction is strong, particularly if the radionuclides are incorporated in the solids.

In general, retardation mechanisms considered in evaluating migration from geological repositories are schematically shown in Fig. 1.6. These mechanisms can be classified into the following groups [2]:

a- Purely physical processes such as molecular filtration, ion exclusion, and diffusion into dead-end pores.

b- Direct interactions with solid surfaces by physical adsorption, chemical adsorption or direct incorporation (mineralization) into the solid structure.

c- Indirect chemical reactions; e.g. precipitation caused by enhanced concentration on the solid surface.

Among those mechanisms sorption and precipitation are usually considered the most important ones. Sorption can be loosely defined as any process that results in the removal of a solute from a solution by attachment of that solute to the surface of a solid phase. Sorption reactions are means of satisfying the forces of attack, both physical and chemical, which exist at the surface of the solid phase. It includes processes as ion exchange, surface complexation, and physical sorption [6]. In all cases, the surface and exchange properties of the solids, in particular the type of the sorption sites, are important as well as the knowledge of the chemical nature of the radionuclides in the aqueous systems, in the understanding of the migration behavior of radionuclides. Together with precipitation, the following *main groups* of sorption of radionuclides on solids matrices can be catagorized [1]:

a- Exchange of non hydrolyzed cationic species at the outer surface or within the layer structure of solids. This type of reaction plays an important role in case of ions like Cs^{+}, Sr^{2+}, and Ra^{2+}, and is very effective in clay minerals with high exchange capacities. The predominant type of interaction is ion exchange.

b- Reactions of hydroxo complexes or anionic forms of radionuclides with hydroxyl groups at the surface of solids. This type of reaction has been characterized by the term 'Hydrolytic Sorption' in the literature. By this group of interactions, bonds of predominantly covalent nature are formed. This reaction can be described as an ion exchange reaction if an unhydrolyzed cation

exchanges with the protons in the surface hydroxyl groups and is consequently attached to the surface through an O bridge.

c- Adsorption of complexes of radionuclides with various inorganic or organic ligands and adsorption of their colloidal species. Adsorption of organic complexes of radionuclides, particularly complexes with humic acids is an important example. The predominant type of interaction is physical adsorption with formation of relatively weak bonds.

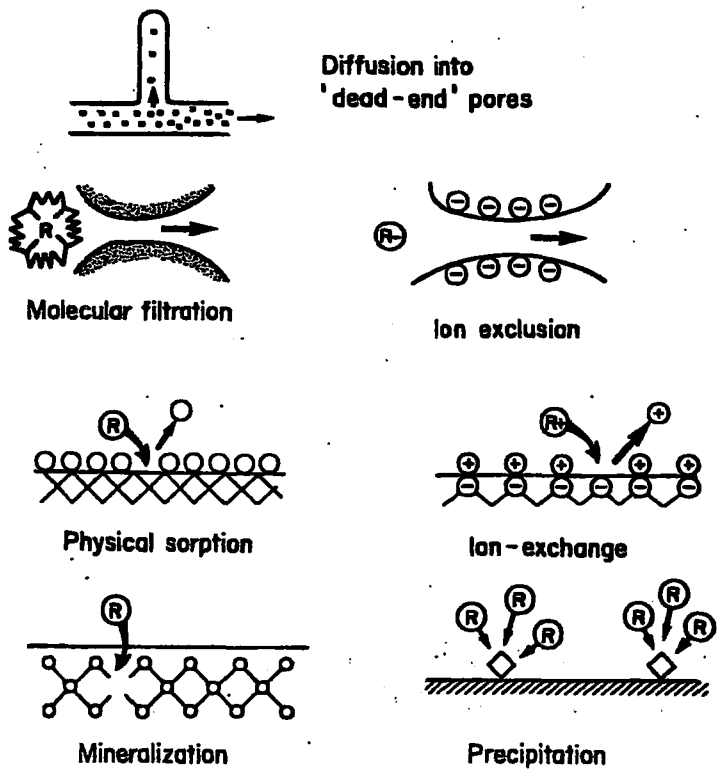

1.7: Retardation mechanisms in migration considerations through geological media

1.5- The Batch Method

The batch method is a widely used method in sorption studies aiming at examining the effects of different parameters on sorption. In this technique, the clay is placed in a polyethylene tube in contact with a solution containing the cation. The samples are then shaken on a lateral shaker for certain time intervals. Following shaking, the phases are seperated by centrifuging or filtering and the cation concentration in the liquid phase is determined. This method was applied in all our radiochemical studies.

In batch operations, the solid adsorbent is usually applied in powdered form to increase the surface area and reduce the diffusional resistence inside the pores. Shaking of the suspension improves contact of particles with liquid and decrease the mass transfer resistence at the surface [20].

The batch technique can alternatively be operated using a magnetic stirrer in place of the lateral shaker. This has the advantage of providing better mixing, thus minimizing the diffusion resistence of the sorbing ions This method was applied in the preparation of samples to be analyzed using ToF-SIMS, XPS, and XRD where high concentrations of sorbing ions were used aiming to saturate the clay surface (more datails are given in chapter 3).

1.6- Literature Review

The reliable prediction of radionuclide transport from a radioactive waste burial site into the biological environment requires a thorough knowledge of the parameters which influence the migration behavior of those radionuclides. Those parameters are mostly related with the properties of liquid and solid phases in contact. Among the properties of the liquid phase are pH, Eh, ionic strength, and temperature. The properties of the solid phase, however, are determined by factors like the cation exchange capacity and the particle size. Other parameters of significance are the liquid to solid ratio (V/M) and the rate of mixing.

A large number of laboratory and field studies have been carried out internationally in order to understand the effect of such factors on the sorption process of various radionuclides on different clays and soil fractions. Most of those studies were performed using radiochemical methods and there is a scarcity, in this field, in studies performed using spectroscopic techniques. Surveying literature, it was found that a variety of studies were performed to examine different sorption aspects of Cs^{+}, Ba^{2+}, and Co^{2+} on clays and soil fractions [21-37,49-52,59,63,70-73]. Investigations of the effect of loading on the sorption of those cations showed that sorption is nonlinear and that the most adequate isotherm model for describing the sorption data over different concentration ranges is Freundlich isotherm [21-23,28,32,34,59,60]. The validity of Dubinin-Radushkevich isotherm model was also

reported but to a lesser extent [21-23,32,49,59,60,62]. The applicability of Langmuir isotherm model was reported for Co^{2+} sorption at very small concentrations on various clay and oxide surfaces [35,59,62]. Based on the loading studies, sorption nonlinearity was reported to be more pronounced for sorption on chlorite and illite than on montmorillonite [27,51]. Studies previously carried out at our laboratories to investigate the effect of contact time on the sorption of Cs^+, Ba^{2+}, and Co^{2+} on kaolinite, chlorite-illite, and bentonite have shown that equilibrium was achieved after several days of contact and that sorption occurred via first order kinetics [21-23]. While sorption of Cs^+ and Co^{2+} is reported to be largely irreversible, that of Ba^{2+} have significant reversibility [26,27,51,33].

Another parameter that is widely investigated in sorption studies is the ionic strength of aqueous media. According to those studies, sorption increases as ionic strength is decreased. While sorption of monovalent cations like Cs^+ is competed with that of ions like K^+, Na^+, and sometimes H^+ (depending on the pH), sorption of divalent cations like Ba^{2+} and Co^{2+} is -to a certain extent- competed with that of Ca^{2+}, and Mg^{2+} ions [25-28,31,32,37,51].

Studies of the pH effect on sorption of Cs^+ on illite and some fresh water solids (containing partially some clays) reported an essentially pH-independent sorption of Cs^+ around neutral pH values. In another study, however, it is reported that sorption of Cs^+ on illite and montmorillonite increased with increasing pH in the

range 5-8.5 [28]. Whereas sorption of Ba^{2+} on kaolinite and chlorite-illite was found to be almost pH-independent, sorption of Ba^{2+} on montmorillonite was strongly pH-dependent [21]. Co^{2+} sorption on soil minerals was reported to be pH-independent on minerals but a strong function of pH on oxides [33,35].

Investigation of the effect of V/M ratio on sorption of Ba^{2+} and Co^{2+} on kaolinite and some soil oxides showed that the sorbed amounts of those cations increased upon increasing the V/M ratio [23]. The same behavior was reported for Cs^{+} sorption on fresh water solids [29].

Compared with the other parameters, a limited number of studies were performed to examine the effect of temperature on the sorption behavior of Cs^{+}, Ba^{2+}, and Co^{2+} on clay minerals. The effect of temperature is expected to be significant for intermediate and high level radioactive wastes were heat is continuously generated as a result of the decay processes of radionuclides. Moreover, radioactive wastes deposited in deep geological repositories would be subject to the action of underground water that is at a higher temperature than that of surface water. According to literature resources, an exothermic sorption behavior of Cs^{+} on alumina [59], and on illite and montmorillonite [28], and an endothermic behavior of Co^{2+} on bentonite [62], were reported In an earlier study, we have reported the exothermic behavior of Cs^{+} and Ba^{2+} on magnesite [60].

With regard to sorption mechanism, it is stated that for Cs^+ and Ba^{2+} sorption on clays, ion exchange is the primary sorption mechanism [27,33,29,51]. Co^{2+} sorption, on the other hand, is reported to take place via complexation reactions with surface hydroxyl groups as a complementary mechanism to ion exchange [26,33].

1.7- The Present Study

1.7.1- General Objectives

In this study radiochemical, spectroscopic (ToF-SIMS, XPS), and X-ray diffraction (XRD) techniques were applied to examine different aspects of the sorption behavior of Cs^+, Ba^{2+}, and Co^{2+} on three natural samples of clays containing primarily kaolinite, illite-chlorite, and bentonite. An important part of this study is devoted to investigate the effect of temperature on the interaction of Cs^+, Ba^{2+}, and Co^{2+} at different initial concentrations with the clay samples using the radiotracer method to obtain some thermodynamic parameters of sorption. Moreover, surface spectroscopic studies were carried out using ToF-SIMS and XPS in addition to applying XRD. The application of these techniques as quantitative tools in sorption studies has been very limited and the contribution given here, in particular, that of ToF-SIMS forms an original one as will be discussed below.

Cesium is an alkali element (Z=55) that has high solubility in water. It has several radioactive isotopes the most important of which are ^{134}Cs ($t_{1/2}$= 2.06 years), ^{135}Cs ($t_{1/2}$= 3.0×10^{6} years), and ^{137}Cs ($t_{1/2}$= 30.17 years) produced in nuclear fission. The fission yields of ^{135}Cs and ^{137}Cs are relatively high; 6.54 % and 6.18 %, respectively. Due to their long half life, both of ^{135}Cs and ^{137}Cs are principal radiocontaminants. ^{137}Cs was used as a tracer in our sorption experiments because of its suitable half life. It emits a strong γ-ray (662 keV) making its measurement in environmental samples relatively simple and accurate.

Barium is an alkaline earth element (Z=56), its radioactive isotope ^{140}Ba ($t_{1/2}$= 12.79 day) is a fission product with a high yield (6.21 %). This radionuclide is a serious radiocontaminant during the first 100 days when discharged into the environment. Furthermore, Ba being a homologue of Ra is a suitable cation for the radiochemical study of Ra, which have several radioisotopes that are important in waste considerations. ^{133}Ba was chosen as a suitable tracer in our studies because of its long half life (10.7 years) and a strong γ-ray at 361 keV energy.

Cobalt belongs to the first period of transition metals (Z=27). It exists in aqueous medium as a tetra- or hexa-aqua complex. In radiochemical waste considerations, ^{60}Co ($t_{1/2}$=5.3 y) is an important radionuclide that is formed by activation of ^{59}Co, present as a component in steel used in nuclear facilities. ^{60}Co is also widely used in medicine to sterilize medical equipment and treat cancer. Due to

its wide applications, relatively long half life and intense γ-radiation (1332 keV), ^{60}Co is a radionuclide which requires safe storage and eventual disposal.

The natural clay samples that were used in this study were obtained from the Turkish Mining Institute (MTA). The clays, which exist in high abundance, originated from natural mineralogical beds at Sindirgi, Afyon, and Giresun regions in Turkey. The characterization of these clay samples -which is discussed in detail in Chapter 4- showed that the primary clay minerals were kaolinite in Sindirgi clay, chlorite and illite in Afyon clay, and montmorillonite in Giresun clay. The main properties and structural features of these clays in their pure forms were given in section 1.2

Radiochemical batch experiments were carried out to examine the effects of time, concentration, and temperature on the sorption of Cs^+, Ba^{2+}, and Co^{2+} on clays. Solutions of these cations spiked with several microliters of the radionuclides ^{137}Cs ($t_{1/2}$=30.1 y), ^{133}Ba($t_{1/2}$=10.7 y), and ^{60}Co($t_{1/2}$=5.3 y) were monitored using γ-ray spectroscopy prior to and after each sorption experiment. These experiments provided information about the kinetics, sorption isotherms, and the thermodynamic parameters such as enthalpy change, ΔH^o, entropy change, ΔS^o, and Gibbs free energy change, ΔG^o, in sorption. These parameters were obtained using an Arrhenius type equation, the derivation of which for a batch system is given in the next chapter.

Since sorption is mainly a surface phenomenon, part of our sorption studies were carried out using surface sensitive techniques; Time of Flight- Secondary Ion Mass Spectrometry (ToF-SIMS) and X-ray Photoelectron Spectroscopy (XPS). In addition, depth profiling up to 70 Å was done using ToF-SIMS to investigate Cs^{+}, Ba^{2+}, and Co^{2+} concentrations through the clay surface. These experiments were performed in cooperation with the Interface Analysis Centre at Bristol University. ToF-SIMS and XPS studies were helpful in figuring out the surface composition of different clays prior to and after sorption. As a result, quantification of the depletion of different elements initially contained within the analyzed clay surface enabled the evaluation of the role of ion exchange in the sorption process. The type of analysis we followed using ToF-SIMS is -to our knowledge- the first in this field of research. X-Ray Diffraction (XRD) technique was applied to figure out the mineralogical composition of the clay minerals used. These experiments were performed in cooperation with the Interface Analysis Centre at Bristol University. XRD spectra of the clay samples after sorption provided information about the possible structural changes taking place in the clay lattice.

1.7.2- Techniques Used

1.7.2.1- The Radiotracer Method

The radiotracer method is widely used in sorption studies involving

radioactive wastes. The experimental procedure consists of spiking a solution containing a stable isotope of an element with its radionuclide, then mixing the solution and the clay mineral. The radionuclide concentration in an aliquot of the solution is monitored periodically during the sorption study. The decrease in the radionuclide concentration in solution is attributed to its sorption by the mineral. The implicit assumption here is that the stable and radioactive isotopes of the element under investigation exhibit the same chemical behavior.

1.7.2.2- Time of Flight-Secondary Ion Mass Spectroscopy (ToF-SIMS)

ToF-SIMS is a form of Secondary Ion Mass Spectroscopy (SIMS) with a Time of Flight analyzer replacing the traditional Quadropole analyzer. It is one of the most sensitive of all commonly employed surface analytical techniques. One of the advantages that ToF-SIMS offers over other surface sensitive techniques is its sensitivity up to very low concentrations (~ ppm) of elements. In ToF-SIMS, the surface of the sample is bombarded by high energy ions (1-30 MeV). The most commonly employed bombarding ions are Ar^+ ions in addition to alkali metal ions and Ga^+. This leads to sputtering of charged or neutral species from the surface in the form of atoms, ions, clusters of atoms or molecular fragments. SIMS generally have a number of different variants like Static SIMS, Dynamic SIMS, and Imaging SIMS. Whereas Static SIMS is used for sub-monolayer analysis, Dynamic SIMS is useful in obtaining compositional information as a function of depth below the

surface. Imaging SIMS, however, is used for spatially resolved elemental analysis.

Time of Flight (ToF) mass analyzers are employed to provide substantially higher sensitivity and a much greater mass range compared with a typical quadrupole MS analyzer. In order to obtain compositional informations with minimum possible damage to the surface, it is important to ensure that a sufficient signal is obtained at the desired spatial resolution whilst minimizing the ion flux incident on any part of the surface. This can be achieved by switching from the traditional instrumental approach of using continuous-flux ion guns and quadrupole analyzers to using pulsed ion sources and ToF mass analyzers. The latter is a much more efficient way of acquiring spectral data and providing good resolution and sensitivity up to very low masses.

Depth profiling is employed to obtain information about compositional variations with depth below the initial surface. Since the SIMS technique itself relies upon the removal of atoms from the surface it is by nature a destructive technique, but also, ideally suited for depth profiling. Thus a depth profile of a sample can be obtained by recording sequential SIMS spectra as the surface is gradually eroded away by the incident ion beam probe. The achievable depth resolution is dependent upon the uniformity of etching by incident ion beam, the absolute depth of the original surface to which etching has already been carried out, as well as the nature of the ion beam utilized (i.e. the mass and energy of the ions).

1.7.2.3- X-ray Photoelectron Spectroscopy

X-ray photoelectron spectroscopy (XPS), is one of the most widely used surface sensitive technique. It comprises a group of techniques in which photoelectrons emitted from a sample, which is irradiated by electromagnetic radiation of a suitable wavelength, are separated on the basis of their kinetic energies and detected by a photomultiplier device which is then recorded in the form of electron yield against the electron energy. In XPS, the irradiating source is an x-ray beam and the photoelectrons are emitted from the core and valence levels of the constituent atoms of the sample.

Although originally conceived as an analytical technique, XPS can also give information on the 'chemical environment' of constituent atoms. The information content of the XPS spectrum may be considered in two parts; Elemental composition and chemical speciation. XPS is basically a form of atomic spectroscopy and, as such, it has a clear and well-defined analytical role based on the positions and sizes of peaks within the spectrum. However, the exact energy levels of the core and valence electrons respond to their electronic environment and additional structural or chemical information, may be obtained from binding energy shifts and spectral fine structure [38].

Application of XPS to sorption studies has shown an increase in the last

decade. A number of studies in which XPS was used for obtaining qualitative and quantitative analytical information and/or chemical and structural information are available in literature [39 - 45]. XPS technique is suitable for the study of sorption reactions for a number of reasons. First and foremost is that it is inherently surface sensitive. It is particularly versatile because it can detect any element of geochemical interest except hydrogen, it can be used to estimate surface coverage of sorbed species or thickness of their precipitate films, and it can provide important information on the chemical state of the substrate surface before reaction, and both the substrate and sorbed species after reaction [46].

1.7.2.4- X-ray Diffraction (XRD)

The principal tool for the identification of crystalline soil minerals is x-ray diffraction. X-rays are produced by bombarding metal foil (most commonly Cu foil) with electrons to emit polychromatic radiation. This radiation is filtered by another metal foil (Ni foil in the case of Cu source) to produce monochromatic radiation (Cu $K_{\alpha 1,2}$ doublet, λ=1.54Å). The wavelengths of x-rays are of the same order of magnitude as distances between atoms or ions in a molecule or crystal (Å, 10^{-10}m). Once produced, x-rays are focused on a sample. Some of the x-rays pass through the sample while others are reflected (diffracted) by the planes of atoms in the various minerals. A crystal diffracts an x-ray beam passing through it to produce beams at specific angles depending on the x-ray wavelength, the crystal orientation, and the

structure of the crystal. The diffraction pattern of a pure substance is like a finger print of the substance. This means that the same substance always give the same pattern, and in a mixture of substances, each produces its pattern independently of the others.

Powders of crystalline materials diffract x-rays. Powder x-ray diffraction provides less information than single crystal diffraction. However, it is much faster and simpler. Powder diffraction is useful for confirming the identity of the clay fraction and determining crystallinity and phase purity. The identification is facilitated by the availability of standard patterns of different minerals, hence identification can be carried out by a search /match procedure. Furthermore, the area under the peak can be related to the amount of each phase present in the analyzed sample.

2. MATHEMATICAL RELATIONS

2.1- The Distribution Ratio

The distribution ratio, R_d, is an empirical value that is used to quantify sorption. In this concept, it is assumed that the migration of radionuclides can be calculated and modeled on the basis of distribution ratios which are characteristic for each element in solution and a certain solid. R_d, as used in sorption studies, is a measure of the ratio of the amount of the element bound to the solid phase relative to the amount of the same element in liquid phase:

$$R_d = \frac{m_s / M}{m_l / V} \qquad (2.1)$$

where m_s, m_l are the masses of the nuclide (meq) at the solid phase and in the solution respectively, M is the mass of the solid phase (g) and V is the volume of the solution (mL).

In sorption studies, R_d aids in quantifying the extent of retardation of a certain trace element transport via the aqueous phase by a solid phase. In the experimental determination of R_d, the behavior of a chemical species is monitored periodically by measuring the activity of its radioactive isotope in the liquid phase. It is assumed that the chemical properties of the stable isotope do not differ significantly from that of a radioactive tracer isotope.

The distribution ratio for a component C can be expressed in terms of concentration as:

$$R_d = \frac{[C]_s}{[C]_l} \qquad (2.2)$$

Where $[C]_s$ (meq/g) and $[C]_l$ (meq/mL) are the concentrations of species C in the solid and liquid phases respectively. At the beginning of the sorption step, V (mL) of solution with initial concentration $[C]^\circ$ (meq/mL) is used, and at the end of sorption step $V+\Delta W_{pt}$ (mL) (ΔW_{pt} refers to the amount of water remaining after the pretreatment step (see 3.1.2)) of solution with concentration $[C]_l$ are present, hence the concentration of C in the solid phase after sorption can be expressed as :

$$[C]_s = \frac{V[C]^\circ - (V + \Delta W_{pt})[C]_l}{W_s} \qquad (2.3)$$

In terms of activity, $[C]_l$ can be written as :

$$[C]_l = \frac{A_l}{A^\circ}[C]^\circ \qquad (2.4)$$

From (2.2), (2.3) and (2.4), the following equation is obtained :

$$R_d = \frac{VA^\circ - (V + \Delta W_{pt})A_l}{A_l W_s} \qquad (2.5)$$

Where:

A° = initial count rate of solution added for sorption (cps)/mL

A_l = count rate of solution after sorption (cps)/mL

W_s = weight of solid material (g)

ΔW_{pt}= amount of liquid remaining in the tube after pretreatment, before sorption (g)

2.2- Adsorption Isotherm Models

The equilibrium sorption data at a given temperature is usually represented by an adsorption isotherm, which is a relationship between the quantity sorbed per unit mass of solid and the concentration of the sorbate in solution. Many theoretical and empirical models have been developed to represent the various types of adsorption isotherms. Langmuir, Freundlich and Dubinin-Radushkevich are among the most frequent isotherm models used for this purpose.

2.2.1- Langmuir Isotherm Model

A simple model of the solid surface is used to derive the equation of this isotherm. In this model, the solid is assumed to have a uniform surface at which there are no interaction between one sorbed molecule and another, the sorbed

molecules are localized at specific sites and only a monolayer can be sorbed. Langmuir isotherm is given as:

$$[C]_s = \frac{K.C_m.[C]_l}{1+K[C]_l} \tag{2.6}$$

Where:

$[C]_s$: Amount of solute per unit mass of solid phase (meq/g)

C_m : Maximum amount of solute that can be sorbed by solid phase (meq/g)

$[C]_l$: Equilibrium concentration of solute in solution (meq/mL)

K : A constant related to the energy of sorption

The equation above may be rearranged to lead to the linear form:

$$[C]_s = C_m - \frac{[C]_s}{K[C]_l} \tag{2.7}$$

By plotting $[C]_s$ versus $[C]_s/[C]_l$, a straight line is obtained. The slope of that line gives 1/K and the intercept gives C_m. The distribution ratio, R_d, can be obtained by rearranging the above equation to give:

$$R_d = \frac{KC_m}{1+K[C]_l} \tag{2.8}$$

2.2.2- Freundlich Isotherm Model

It is the most widely used non-linear model for describing the dependence of sorption on adsorbate concentration. The general expression of Freundlich isotherm

is given as:

$$[C]_s = k\,[C]_l^{\,n} \qquad (2.9)$$

Where;

$[C]_s$: the amount of ions adsorbed on the solid matrix at equilibrium (meq/g),

$[C]_l$: the concentration of the cation in solution at equilibrium (meq/mL),

k and n : Freundlich constants that refers to sorption affinity and sorption linearity

This expression can be linearized as:

$$\log [C]_s = \log k + n \log [C]_l \qquad (2.10)$$

Plotting $\log[C]_s$ versus $\log[C]_l$ yields n as the slope and log k as the intercept.

Freundlich isotherm model allows for several kinds of adsorption sites on the solid, each kind having a different heat of adsorption. The Freundlich isotherm represents well the data at low and intermediate concentrations and is a good model for heterogeneous surfaces. When the value of Freundlich constant n is equal to unity, Freundlich equation becomes linear and the Freundlich constant k becomes equivalent to the distribution ratio, R_d. Equation (2.10) can be rearranged to give the distribution ratio, R_d :

$$R_d = k\,[C]_l^{\,n-1} \qquad (2.11)$$

2.2.3- Dubinin-Radushkevich (D-R) Isotherm Model

The D-R isotherm model is applicable at low concentration ranges and can be used to describe sorption on both homogeneous and heterogeneous surfaces. It

can be represented by the general expression:

$$[C]_s = C_m \exp\text{-}(K\varepsilon^2) \qquad (2.12)$$

$[C]_s$ and $[C]_l$ were defined earlier and the other terms represent:

ε : $RT \ln(1+1/[C]_l)$,

R : the ideal gas constant (8.3145 J /mol. K),

T : the absolute temperature (K),

K : a constant related to the energy of sorption,

C_m : the sorption capacity of adsorbent per unit weight (meq/g),

The linear form of the equation above may be obtained by rearranging it to give:

$$\ln [C]_s = \ln C_m - K\varepsilon^2 \qquad (2.13)$$

If $\ln [C]_s$ is plotted against ε^2, K and $\ln C_m$ will be obtained from the slope and the intercept, respectively.

Equation (2.12) may be written in a form that gives R_d :

$$R_d = (1/[C]_l)C_m \exp\text{-}(K\varepsilon^2) \qquad (2.14)$$

The value of K $(mol/kJ)^2$ is related to the 'Adsorption Mean Free Energy', E (kJ/mol), defined as the free energy change required to transfer one mole of ions from infinity in solution to the solid surface[47]. The relation is given as:

$$E = (2K)^{-0.5} \qquad (2.15)$$

2.3- Thermodynamic Relations

In a batch adsorption process, the adsorption reaction can be written as:

$$C_l + \underline{S}_{(s)} \Leftrightarrow C_s \qquad (2.16)$$

Where C_l stands for the solute particles in solution, $\underline{S}$ for the sorption sites on the surface of the adsorbent and C_s for the solute particles adsorbed on the adsorbent. The equilibrium constant for the reaction above can be written in terms of the activities as:

$$K = \frac{a_{C_s}}{a_{\underline{s}} . a_{C_l}} \qquad (2.17)$$

The activity of the solid phase can be taken as unity at the reference state, then the above expression can be written in terms of the concentrations and the activity coefficients 'γ' as:

$$K = \frac{[C]_s}{[C]_l} . \frac{\gamma_{C_s}}{\gamma_{C_l}} \qquad (2.18)$$

For dilute solutions the activity coefficients can be taken as unity, so that the equilibrium constant becomes equivalent to the distribution coefficient 'R_d' defined as the ratio of the solute concentration on the solid phase to that on the liquid phase.

In line with the above derivation, the distribution coefficient may be related to the change in Gibbs free energy, ΔG, by the following equation:

$$\Delta G = \Delta G^o + RT\ln R_d \qquad (2.19)$$

Where ΔG^o is the standard Gibbs free energy change, R is the ideal gas constant,

and T is the absolute temperature.

At equilibrium no change in Gibbs free energy occurs and the above equation reduces to:

$$\Delta G^o = - RT\ln R_d \qquad (2.20)$$

So using equation (2.20), it is possible to determine ΔG^o of sorption directly from the R_d values at different temperatures.

Gibbs free energy change can also be written in terms of the enthalpy change, ΔH^o , and the entropy change, ΔS^o , as given below:

$$\Delta G^o = \Delta H^o - T\Delta S^o \qquad (2.21)$$

Combining equation (2.20) and (2.21) the following expression results

$$\ln R_d = \frac{\Delta S^o}{R} - \frac{\Delta H^o}{RT} \qquad (2.22)$$

By plotting ln R_d versus 1/T, it is possible to determine the value of ΔH^o of sorption from the slope and ΔS^o of sorption from the intercept of the linear fits.

2.4- ToF-SIMS Calculations

ToF-SIMS data were obtained as counts of analyzed element per unit area of

surface. Those counts were corrected using the relative sensitivity factors corresponding to each element. For elements with more than one isotope, the major isotope's data were considered and correction to 100% abundance was done. The sensitivity corrected data were normalized to (Al+Si) contents, assuming that Al and Si contents remained unchanged following sorption. Ratios of the elements were calculated also relative to Si and Al separately, but the ratios relative to Al+Si gave the best results. These ratios were multiplied with a correction factor equal to the ratio of Si/Al before sorption to that after sorption to overcome errors caused by fluctuations in Al and Si amounts. This allowed meaningful comparisons in examining the elemental changes that the clay undergoes following sorption.

In order to compare the affinity of exchange of the cations in the clay surface towards the adsorbate, a 'Depletion Factor', DF, for a particular cation x in the solid matrix is defined as:

$$(DF)_x = \frac{(R_i)_x - (R_f)_x}{(R_i)_x} \tag{2.23}$$

Here, $(R_i)_x$: is the corrected ratio of cation x in the original sample

$(R_f)_x$: is the corrected ratio of cation x in the sample following sorption

In this sense, DF is some sort of affinity of the cation x to migrate from the solid phase to the aqueous phase upon sorption of a particular ion. Its highest possible value of unity indicates complete exchange, and its lowest value of zero indicates no exchange.

The depleted amount (D_x) of cation x in equivalents is calculated by multiplying the difference $[(R_i)_x-(R_f)_x]$ by z_x, the charge of cation x. This may be defined as the Equivalent Depleted Amount (EDA). The percentage contribution of cation x to the total depletion of all cations at a given depth is then given as:

$$D_x = \frac{[(R_i)_x - (R_f)_x].z_x}{\sum_x^n \{[(R_i)_x - (R_f)_x].z_x\}_n} \times 100 \qquad (2.24)$$

3. EXPERIMENTAL

3.1- Experiments Using the Radiotracer Method

3.1.1- Analysis of Bilkent Tapwater

Bilkent tapwater -as a substitute for groundwater- was used in the radiotracer studies. Samples of tapwater were collected over a period of three months and were then analyzed for their elemental content by Flame Atomic Absorption/Emission Spectroscopy. The instrument used in analysis was a Perkin Elmer 1100 B model spectrometer located in the Environmental Engineering laboratories at Middle East Technical University. The concentrations of each of the primary elements Na, K, Ca and Mg in Bilkent tapwater did not show significant changes with time. The average

concentrations of those elements are given in Table 3.1. The measurements were performed at the wavelengths (nm) 589.1, 766.5, 422.7, and 285.2 for the elements Na, K, Ca, and Mg, respectively.

Table 3.1: Concentrations of Na, K, Ca, and Mg in Bilkent Tapwater Used in Sorption Studies

Element	Concentration (meq/mL)
Na	3.92×10^{-4}
K	1.04×10^{-4}
Ca	3.24×10^{-4}
Mg	4.30×10^{-4}
PH	6.89-7.25

3.1.2- Pretreatment of the Clay Samples

The pretreatment step aimed to mimic the equilibrium situation of the clay minerals with groundwater prior to sorption experiments. In all experiments, the particle size of kaolinite, chlorite-illite, and bentonite was < 38 μm. The size distribution of those clays is given in Table 3.2 [21].

Sorption experiments were performed in polyethylene tubes. The tubes were first cleaned, dried at 60°C overnight, cooled and weighed. 30 mg of clay and 3 mL of laboratory tapwater were added into each tube that were then shaken at room temperature for 4 days with a lateral shaker at 125 rpm. Samples were then centrifuged at 6000 rpm for 30 minutes and the aqueous phases were discarded.

Each tube was reweighed, and the amount of water left after pretreatment (ΔW_{pt}) was determined. The pretreated clays were used in the sorption experiments carried out using the radiotracer method.

Table 3.2: The size distribution of kaolinite, chlorite-illite, and bentonite obtained using Andreasen pipette method*

	Percent by Weight		
Particle Size (μm)	**Kaolinite**	**Chlorite-Illite**	**Bentonite**
>2	45	24	-
2-4	12	16	16
4-8	15	16	18
8-16	14	19	32
19-24	9	12	18
24-38	5	13	16

* Ref. [21]

3.1.3- Isotopic Tracers

The tracers used in the sorption experiments were ^{137}Cs ($t_{1/2}$=30.1 y), ^{133}Ba($t_{1/2}$=10.7 y), and ^{60}Co($t_{1/2}$=5.3 y). Appropriate amounts of stable isotopes solutions were spiked with few microliters of the corresponding radionuclides solutions used in the different experiments. The initial count rates were measured as

46145 ± 215, 19136 ± 138, and 3978 ± 63 cpm for 3 mL aliquots of cesium, barium, and cobalt solutions, using the prominent γ rays of 662, 361, and 1332 keV, respectively.

Spectrum 88 type instrument was used in activity measurement equipped with a High Purity Germanium Coaxial Detector connected to a Multichannel Analyzer. A drawing of the detector is given in Fig. 3.1. Detector was a p-type Ge detector with Al end cup and its useful energy range was 40 keV to 10 MeV. The outside diameter of the end cup is 76 mm and its thickness is 1 mm. The front window of end cup have a 0.5 mm thickness. The characteristics of the Ge crystal are listed below:

Diameter:	50 mm
Length	48 mm
Active Volume	9200 mm^3
Ge head Layer Thickness	600 μm
Detector to Window thickness	≤ 5 mm

The multichannel analyzer was a microprocessor based stand alone analyzer with 4096 channels. It provides complete data acquisition, storage, display, manipulation and input/output capabilities. In order to minimize the background activity, the detector is shielded with a lead cylinder with a length of 420 mm, thickness of 90 mm, and a diameter of 210 mm [48].

All the experiments were performed in duplicates. In order to estimate any loss in activity originating from adsorption on the inside wall of the tubes, blank experiments were performed using solutions of stable isotope of the elements. The results showed that the relative error in activity stemming from adsorption by inside tubes surfaces was always less than ± 0.05. During the experiments the solution condensed on the inside surfaces and covers of the tubes. Tubes were shaken vigorously prior to centrifugation to collect any liquid drops or clay particles adhering to the inside surface/cover of the tube. The uncertainties associated with the measurements stemmed principally from those of activity, where the uncertainty is equal to the square root of the measured activity value. Other error sources were those originating from weight and volume measurements with relative errors of ± 0.003 and ± 0.033, respectively.

Based on these errors, the relative error in the R_d values was calculated to be in the range ± 0.040- 0.10 depending on the measured activities.

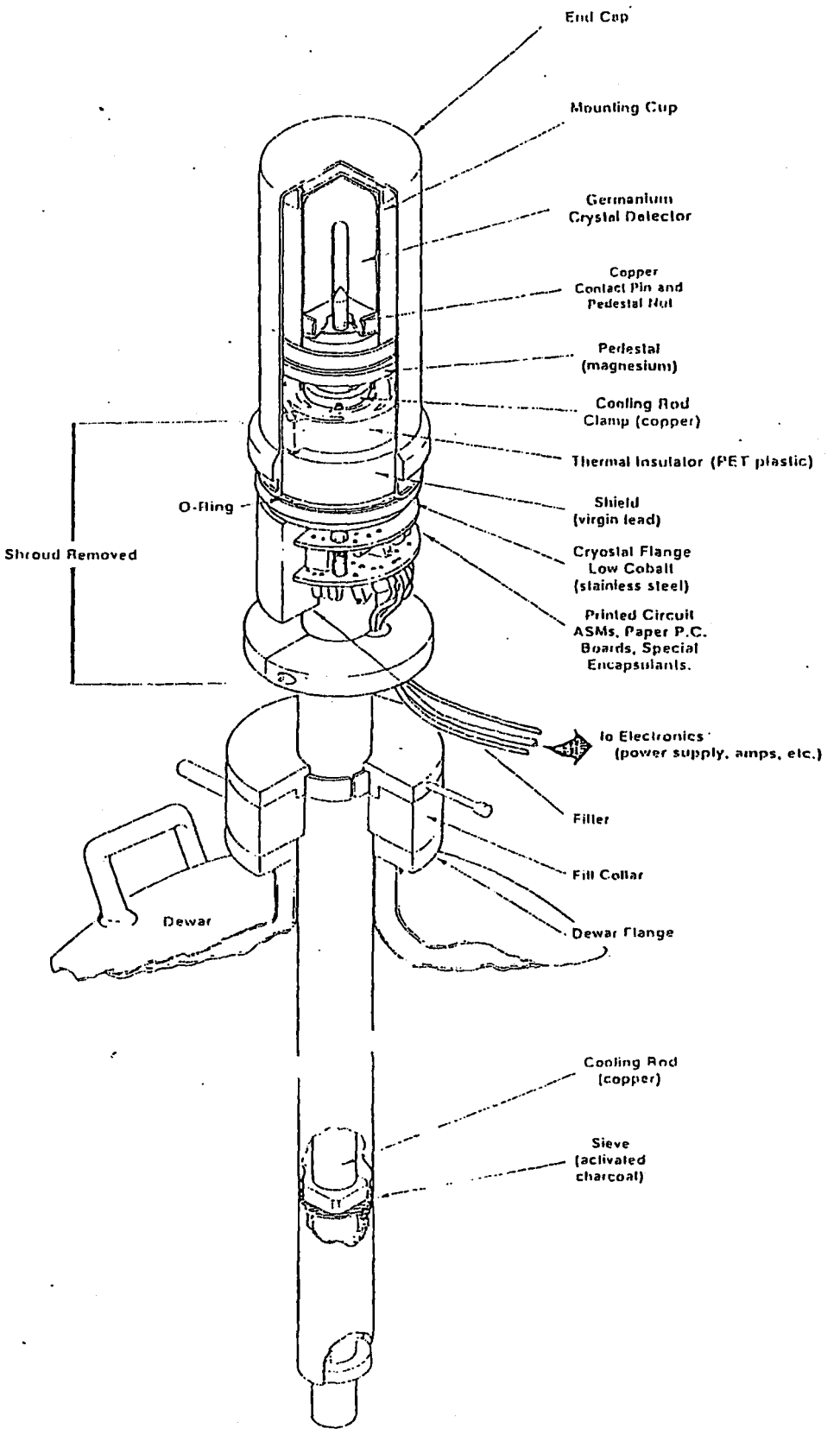

Fig. 3.1: A schematic draw of the Ge detector

3.1.4- Kinetic Studies

To each of the clay samples, 3 mL portions of Cs^+, or Ba^{2+}, or Co^{2+} solutions were added. The initial concentration of each solution was 1×10^{-3} meq/mL prepared from CsCl, $BaCl_2$, and $Co(NO_3)_2$ salts, spiked with appropriate amounts of ^{137}Cs, ^{133}Ba, and ^{60}Co radiotracers. Samples were shaken at room temperature for periods ranging from half an hour to seven days. They were then centrifuged and 2 mL portions of the liquid phases were counted to determine their activities.

3.1.5- Effect of Loading and Temperature :

Loading experiments were carried out to investigate the effect of initial cesium, barium, and cobalt ion concentrations on sorption at different temperatures. The experiments were performed at the initial concentrations of 1×10^{-3} , 1×10^{-4} , 1×10^{-5}, and 1×10^{-6} (meq/mL) at four different temperatures; 30, 40, 50 and 60°C. Three mL portions of solutions containing an appropriate amount of radiotracers were added to each sample tube containing 30 mg of clay at the desired temperature. Prior to mixing the sorbate solutions with the clays, these solutions were heated to the temperature at which the experiment was conducted. The samples were shaken for two days, centrifuged and 2 ml portions of the liquid phase were counted. Shaking was done in a temperature-controlled environment using a Nuve ST 402 water bath shaker equipped with a microprocessor thermostat. The fluctuation in controlled temperature was ± 0.5 °C. Water level inside the water bath was

controlled periodically and any water loss was compensated.

3.2- Experiments Using Time of Flight-Secondary Ion Mass Spectroscopy (ToF-SIMS), X-ray Photoelectron Spectroscopy (XPS), X-ray Diffraction (XRD), and FT-Infrared Spectroscopy (FTIR)

3.2.1- Sorption Experiments

The batch method was applied in these experiments, but instead of the lateral shaker -like in the radiochemical experiments-, a magnetic stirrer was used. Relatively higher concentrations of sorbate concentration were used here to achieve saturation of the clays, and this necessitated more efficient mixing to minimize the diffusional resistance of the sorbates. No pretreatment of the clays was carried out. The aim behind this was to determine the alkali and alkaline earth metals amounts in natural clays and figure out their contribution to ion-exchange with the sorbate ions. Furthermore, the sorbate solutions were prepared using distilled water for the same purpose.

Clay samples weighing 4.0 g each were exposed to 400.0 mL aliquots of solutions of 0.010M CsCl, or 0.010M $BaCl_2$, or 0.010M of $Co(NO_3)_2$ and mixed for 48 hours using a magnetic stirrer. Samples were then filtrated and dried overnight at 90°C. The measured pH range of the experiments was 6.97-8.23 and no external pH control was done. Following sorption, the aqueous phase concentrations of the elements; Na, K, Ca, Mg, Fe, and Al at the corresponding wavelengths (nm) 589.1, 766.5, 422.7, 285.2, 248.2, and 309.2, were measured in order to determine the extent of their depletion upon sorption. The measurements were performed using a Perkin Elmer 1100B Model atomic absorption spectrometer located at the Department of Environmental Engineering laboratories at Middle East Technical University.

3.2.2- ToF-SIMS Analysis of Clay Samples Before and After Sorption:

`ToF-SIMS analysis of the solid phases before and after Cs^+, Ba^{2+}, and Co^{2+} sorption were performed using a Vacuum Generator ToF-SIMS instrument located at the University of Bristol Interface Surface Analysis Centre. Powder samples were pressed lightly onto a sample stub using a carbon dag and then left to dry prior to analysis. During analysis, the vacuum in the analysis chamber was kept at approximately 10^{-9} mbar. Spectra were recorded over fifty accumulations, at x5000 magnification, i.e. an area of 64x48 mm. The ion beam pulse length was 30 ns with a repetition rate of 10 kHz. The Ga^+ ion gun used to produce the ions was operated

at 1nA current and 20 keV energy. The electron flood gun was used as required for neutralization. The above conditions resulted in an etching rate of approximately 10 Å per 50 second etch. The samples were etched and analysis performed at successive depths of 10, 20, 30, 40, 50, and 70 Å.

4.2.3- XPS Analysis of Clay Samples Before and After Sorption:

X-ray photoelectron spectra were recorded using a VG Scientific Escascope instrument with MgK_{α} x-rays ($h\nu$=1253.6 eV). Wide and regional spectra were recorded with step scans of 40 eV, 30 eV and step sizes of 1.0 and 0.1 eV, respectively. Samples were mounted as freshly ground powders pressed onto adhesive copper tape. Pressure was kept below 1×10^{-8} mbar during analysis. C 1s line (B.E=284.8 eV) originating from the adventitious hydrocarbons at the surface of the samples was used as the reference line. Sensitivity corrections were done using Wagner sensitivity factors and quantification was performed via a VG Scientific VGS5250 software.

3.2.4- XRD Analysis of Clay Samples Before and After Sorption:

Samples of natural-, Cs-, Ba-, and Co-sorbed clays were ground prior to mounting on single crystal silicon wafers for x-ray diffraction analysis. Methanol

was used to disperse the powder samples evenly over the holder. A Bruker AXS D500 x-ray diffractometer was used. The source consisted of unfiltered Cu. Kα radiation, generated in a tube operating at 40 kV and 30 mA. Spectra were recorded with 2 theta values ranging from 3 to 35 degrees in steps of 0.02 degree and dwell times of 10 s per step. The samples were rotated during analysis, which was performed at ambient temperature. Bruker AXS DIFFRAC-AT software was used to process the results and compare them with the Joint Committee on Powder Diffraction Standards (JCPDS) database.

3.2.5- FTIR Analysis of Natural Clay Samples:

The FTIR analysis of kaolinite, chlorite-illite, and bentonite was carried out using a Bomem MB-Series instrument. The samples were introduced using KBr pellets and spectra were recorded in the range 400-4000 cm^{-1}. The scan rate was 22 scans/minute, the resolution 4 cm^{-1} and a total of 64 scans were recorded for each spectrum. A Win Bomem Easy software was used to process the results.

4. RESULTS AND DISCUSSIONS

4.1- Characterization of the Clay Minerals

The natural clay minerals used in this work were characterized using X-ray diffraction (XRD) and Infrared Spectroscopy (IR). The elemental contents of the surface of the clays were determined using Time of Flight-Secondary Ion Mass Spectroscopy (ToF-SIMS) and X-ray Photoelectron Spectroscopy (XPS).

XRD was used to study the mineralogical composition of the natural clay minerals used in this work. The analysis showed that Sindirgi clay was composed mainly of kaolinite in addition to quartz as shown in Fig. 4.1(a). Afyon clay was composed mainly of chlorite, illite, and quartz in addition to minor quantities of calcite. Fig. 4.1 (b) gives the XRD spectrum of Afyon clay which is referred to as chlorite-illite clay in this study. The XRD analysis of Giresun clay showed that the

main components were montmorillonite in addition to quartz, feldspars and some calcite as shown in Fig. 4.1(c). The term bentonite, usually used to refer to the clay rock rich in montmorillonite, is used throughout this study to represent Giresun clay.

Various clay minerals can be identified using IR analysis based on their characteristic absorption features in the IR spectra. Although the identification of the clays by IR is usually not easy, IR spectra may still provide some clues about the composition of clays. The identification was carried out through a comparison between the spectra of pure clays provided in literature, and those of the clays used in this study. The IR spectra of kaolinite, chlorite-illite, and bentonite are given in Figs. 4.2, 4.3, and 4.4 respectively. The inset in each of those figures shows the IR spectrum of the pure clay [38]. The OH stretchings occurring around the 3700-3620 cm^{-1} doublet are characteristic for kaolinite (Fig. 4.2). The OH deformation bands near 938-916 cm^{-1} are also typical for kaolinite. IR was not much useful in the identification of chlorite-illite clay (Fig 4.3). The mixed nature of the clay might be behind that. However, the presence of the broad OH stretching band near 3625 cm^{-1}, ranging down to 3620 cm^{-1} (3623 cm^{-1} in our sample) can be indicative for illite presence. Chlorite is usually identified by the broad OH stretching doublet at 3625, 3485 cm^{-1}, but this feature is usually masked by the stretching bands of adsorbed water. Montmorillonite, the major component of bentonite, can be identified by the typical broad OH stretching at 3622 cm^{-1}. This band occurs close to that of inner OH groups in kaolinite but can be identified by its much greater breadth.

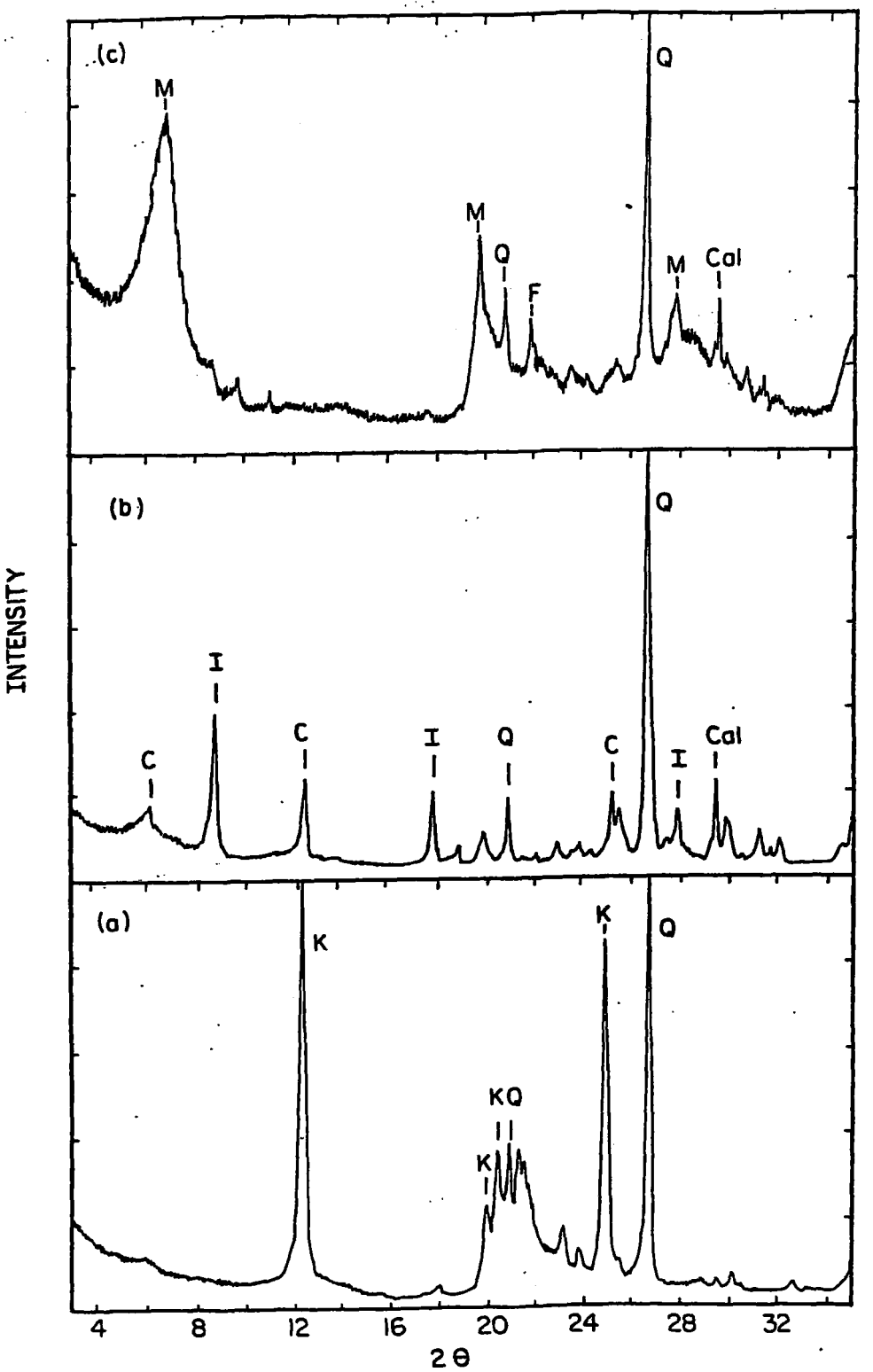

Fig. 4.1: XRD Spectra of; (a) Kaolinite, (b) Chlorite-Illite, and (c) Bentonite
K: Kaolinite, Q: Quartz, C: Chlorite, I: Illite, Cal: Calcite,
M: Montmorillinite, F: Feldspar

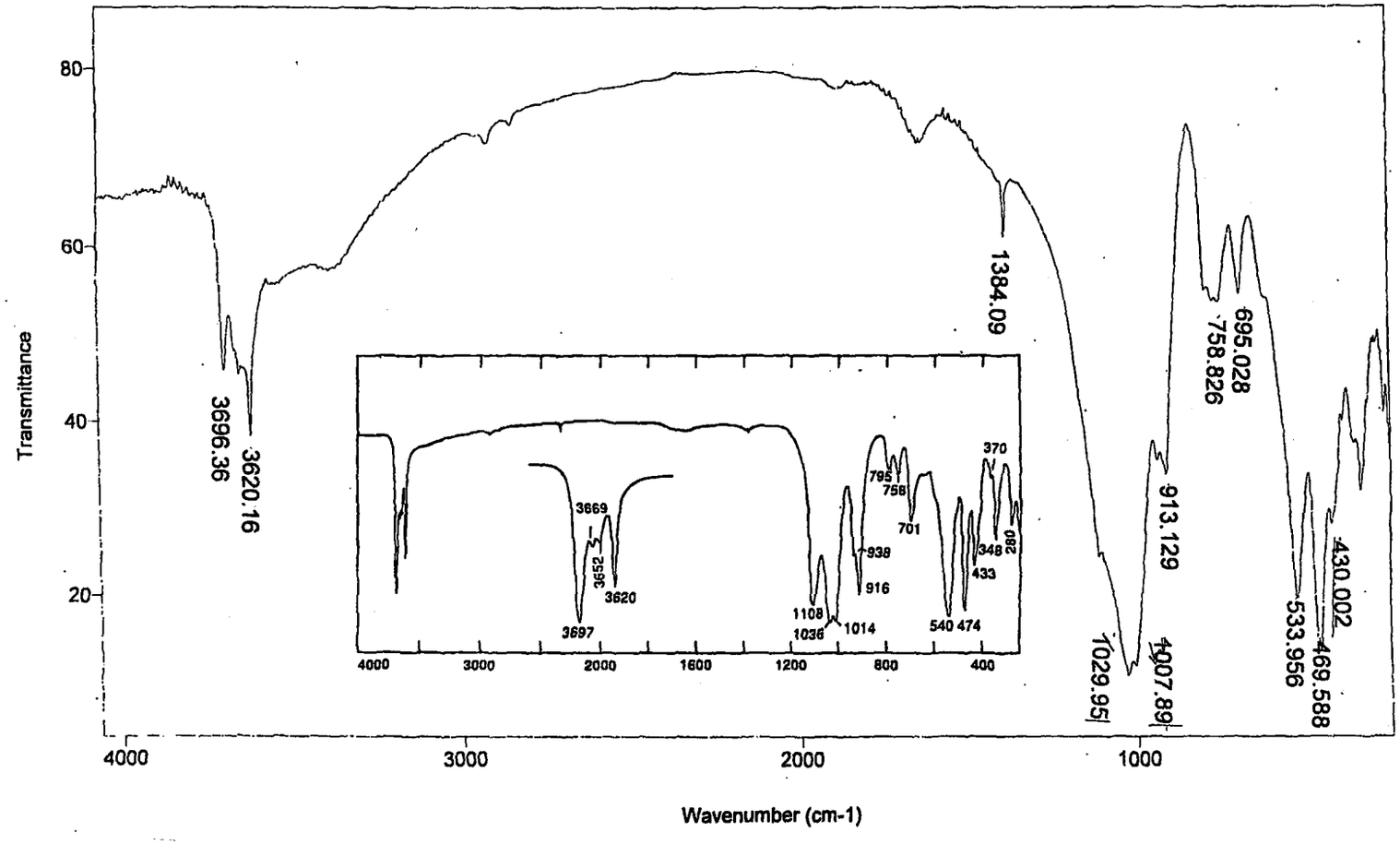

Fig. 4.2: IR Spectrum of Kaolinite. The Inset in the Figure Gives the IR Spectrum of Pure Kaolinite

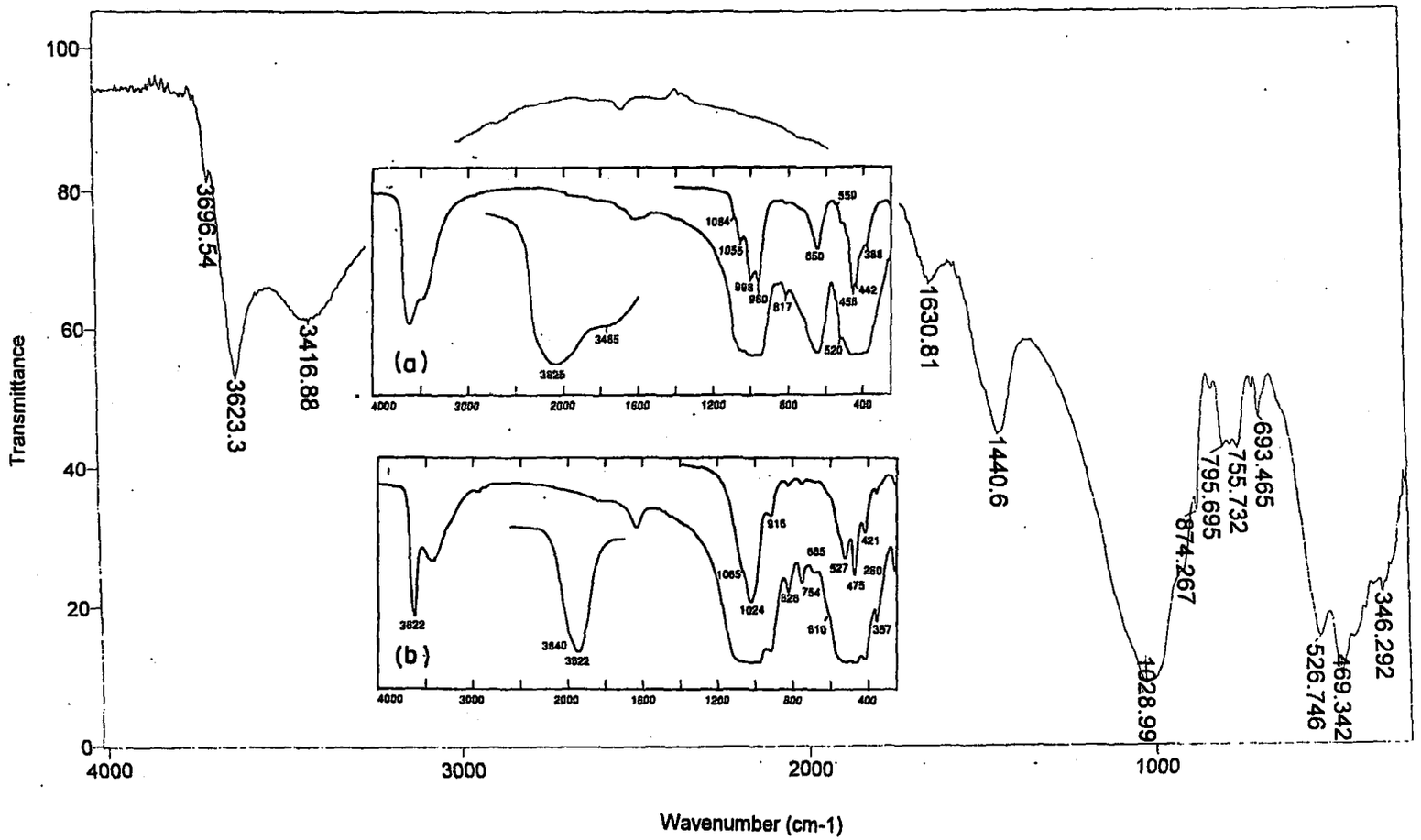

Fig. 4.3: IR Spectrum of Chlorite-Illite. The Insets in the Figure Gives the IR Spectra of (a) Pure Chlorite and (b) Pure Illite

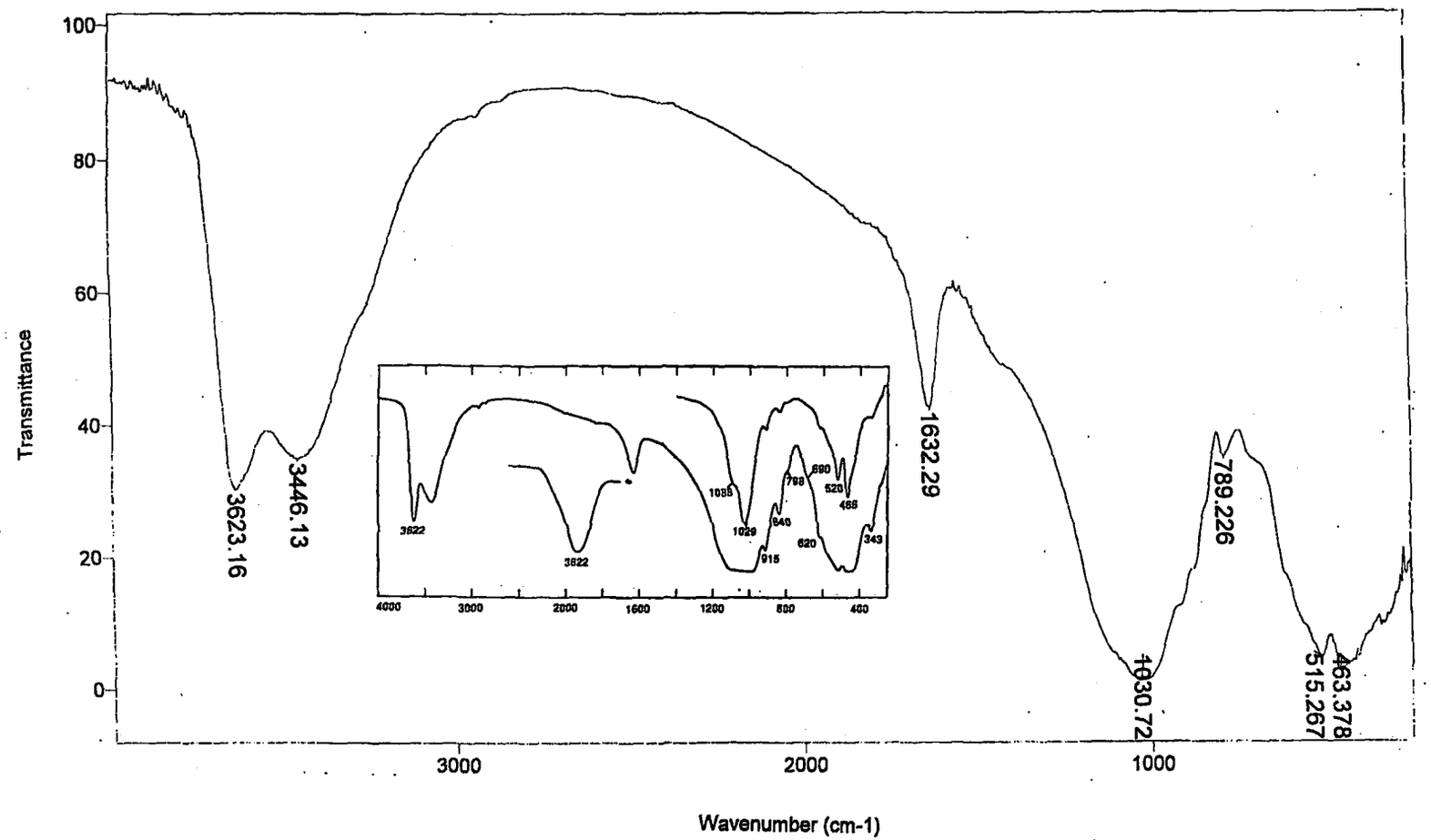

Fig. 4.4: IR Spectrum of Bentonite. The Inset in the Figure Gives the IR Spectrum of Pure Montmorillonite

The elemental composition of the clay surfaces was determined using Time of Flight-Secondary Ion Mass Spectroscopy (ToF-SIMS) and X-ray Photoelectron Spectroscopy (XPS). ToF-SIMS and XPS spectra of bentonite, chlorite-illite, and kaolinite are given in Fig. 4.5 and Fig. 4.6, respectively. The measured contents of the elements were corrected using the corresponding relative sensitivity factors. Based on the total amounts throughout the analyzed clay depth, the percentage elemental compositions of the three clays are given in Table 4.1. The same table gives the XPS results as well. It must be noted that some of the elements with very small contents could not be detected using XPS, due to the poorer detection limit of this technique compared to ToF-SIMS. The differences observed in percentages of the detected elements between ToF-SIMS and XPS result from the differences in the natures of each technique; i.e. escape depth, detection limits, cross sections, etc. While in ToF-SIMS studies, the total etched depth was 70 Å, no etching was performed in XPS studies were the escape depth is estimated [38] to be around 30 Å for clays. On the other hand, in the XPS results iron content of the clays - particularly the chlorite-illite- appears to be extremely small. This is not confirmed by ToF-SIMS data which showed much larger iron quantities. The XRD features of chlorite fractions where the (001)/(002) (2θ= 6.3/12.5) peak ratio appears to be small as in the case of iron-rich chlorite confirms the ToF-SIMS findings.

Compared with their ratio in natural clays, Si/Al ratios in the clays used in this work are relatively larger. In pure kaolinite, chlorite, illite, and bentonite the Si/Al ratios are 1, 1, 2, and 2 respectively. In our samples, however, the ratios (based

on 70 Å depth) are 1.6, 2.5, 3.2 for kaolinite, chlorite-illite, and bentonite, respectively. This could be originating from the presence of quartz in significant amounts, thus leading to high amount of Si. Another possible reason might be the isomorphous substitution of Fe and Mg for Al resulting in lower Al amounts.

The Si and Al contents at the clay surface can aid in the determination of the iso electric point (IEP) of each clay on the basis of the number of SiOH and AlOH groups making up the surface. When the Al is octahedrally coordinated, AlOH groups have an IEP of 9.2; when the Al is tetrahedrally coordinated the IEP is 6.8. SiOH groups have an IEP of 1.8. An aluminosilicate surface with mostly SiOH groups will thus have a low IEP, and a surface with mostly AlOH groups will have a high IEP [8]. If it is assumed that the Si and Al contents of the surface of natural clays provided by ToF-SIMS and XPS measurements are good representatives of the SiOH and AlOH groups and that all Al is octahedrally coordinated, then an estimation of the IEP can be made for each of the natural clays. Calculation of the IEP for each clay is carried out by multiplying the amount of surface Al with the IEP of AlOH and that of Si with the IEP of SiOH (both of which is given above) and finally dividing the sum by the amount of Al+Si. Based on ToF-SIMS data, the IEP of bentonite, chlorite-illite, and kaolinite are calculated as 2.9, 3.7, and 3.8, respectively. Alternatively, the calculated IEP's using the XPS data were 3.5, 4.2, and 4.1, respectively. Those values correspond to an ideal case where all surface Al is octahedrally coordinated. When part of the Al is tetrahedrally coordinated - as it is usually the case in natural clays-, the values are expected to decrease since the IEP

of tetrahedrally coordinated Al is less than that of the octahedrally coordinated Al (see the values above). The significance of IEP in sorption was discussed in section 1.2.3. and will be considered further when discussing the sorption mechanism later in this chapter.

Table 4.1: The Percentage Elemental Composition of the Natural Clay Minerals Obtained by ToF-SIMS and XPS Techniques.

	Kaolinite		**Chlorite-Illite**		**Bentonite**	
Element	**ToF-SIMS**	**XPS**	**ToF-SIMS**	**XPS**	**ToF-SIMS**	**XPS**
Si	56.76	67.30	51.86	60.36	60.44	70.34
Al	34.57	30.34	21.07	27.78	18.77	21.08
Fe	3.94	-	19.39	1.56	14.36	-
Ca	0.86	1.49	3.02	8.87	0.44	-
Mg	1.33	-	2.99	-	4.08	-
K	2.50	0.87	1.57	1.24	0.34	-
Na	0.03	-	0.09	-	1.56	8.48
Others	0.01	-	0.01	-	0.01	-

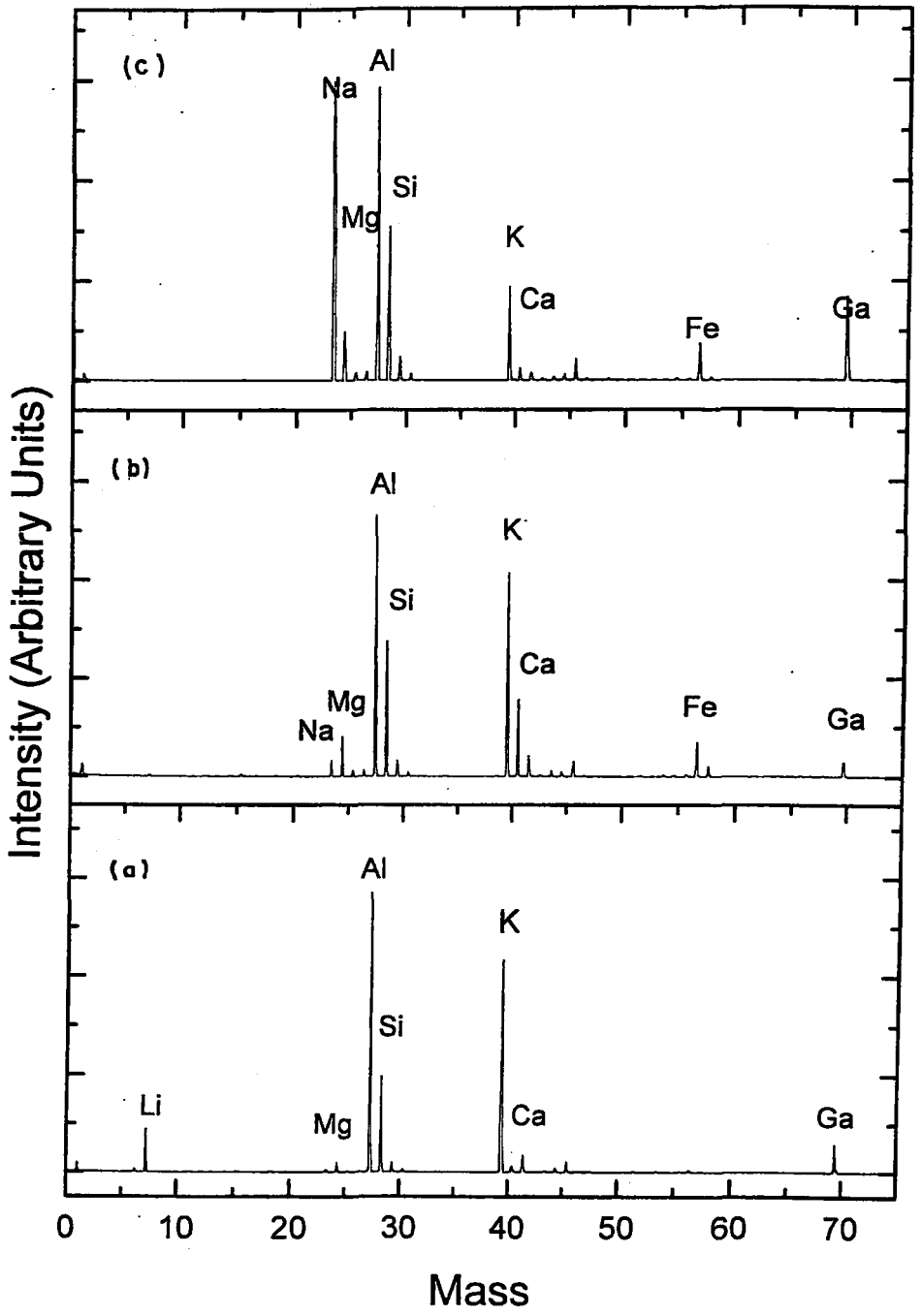

Fig. 4.5: ToF-SIMS Spectra of; (a) Kaolinite, (b) Chlorite-Illite, and (c) Bentonite

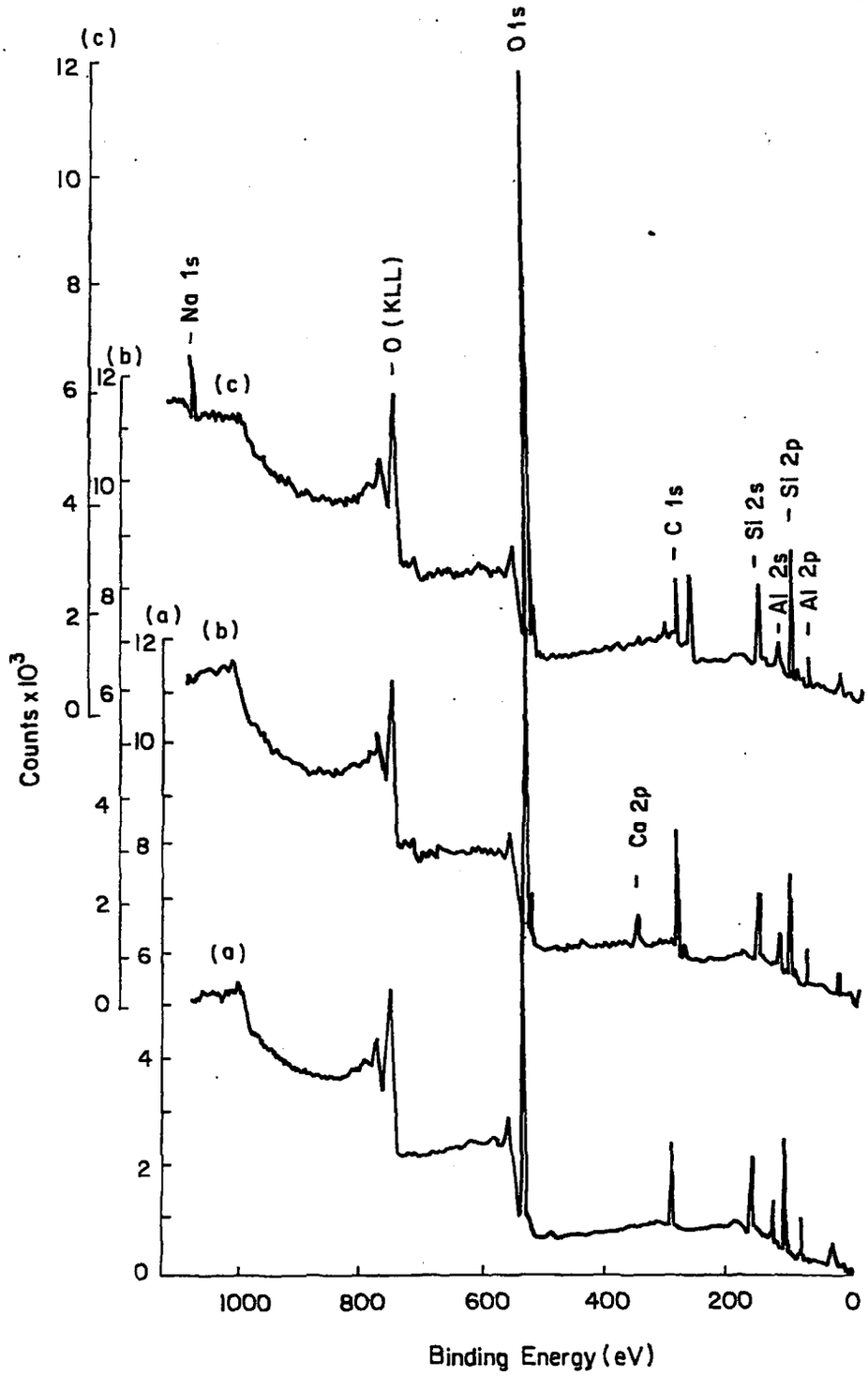

Fig. 4.6: XPS Spectra of; (a) Kaolinite, (b) Chlorite-Illite, and (c) Bentonite

4.2- Radiochemical Sorption Studies

4.2.1- Effect of Time on Sorption

The sorption studies of Cs^+, Ba^{2+} and Co^{2+} ions on kaolinite, chlorite-illite, and bentonite as a function of time were performed for time intervals ranging between one hour up to seven days. In all cases, the initial concentration of the sorbed ion was 1.0×10^{-3} meq/ml and the experiments were carried out at room temperature. The change of the R_d values for the sorption of Cs^+, Ba^{2+}, and Co^{2+} on kaolinite, chlorite-illite, and bentonite as a function of time are given in Appendix A (Tables A1, A2, A3, respectively). Plots of the variation of R_d as a function of time for the sorption cases of each cation on the three clays are given in Figs. 4.7, 4.8, and 4.9. In general, the results show that equilibrium is approached after several hours of contact. Such a rapid attainment of equilibrium is indicative that sorption is primarily a surface phenomena where the clay surface is readily accessible to ions in solution. On the basis of the obtained results an equilibrium period of 2 days was selected as a fixed parameter in the further experiments, where the effects of loading and temperature, were examined.

It is reported that the sorption rate is faster when the initial sorbed ion concentration is smaller [49]. This fact indicates that applying the same shaking period in further experiments where the initial concentration is smaller than the one used in these experiments (as was the case in most of the experiments carried out to

study the effects of loading and temperature) would insure the attainment of equilibrium. The R_d values of each of the sorbed cations on the three clays indicate that the sorption order is bentonite > chlorite-illite > kaolinite, the thing in line with the CEC values of those clays.

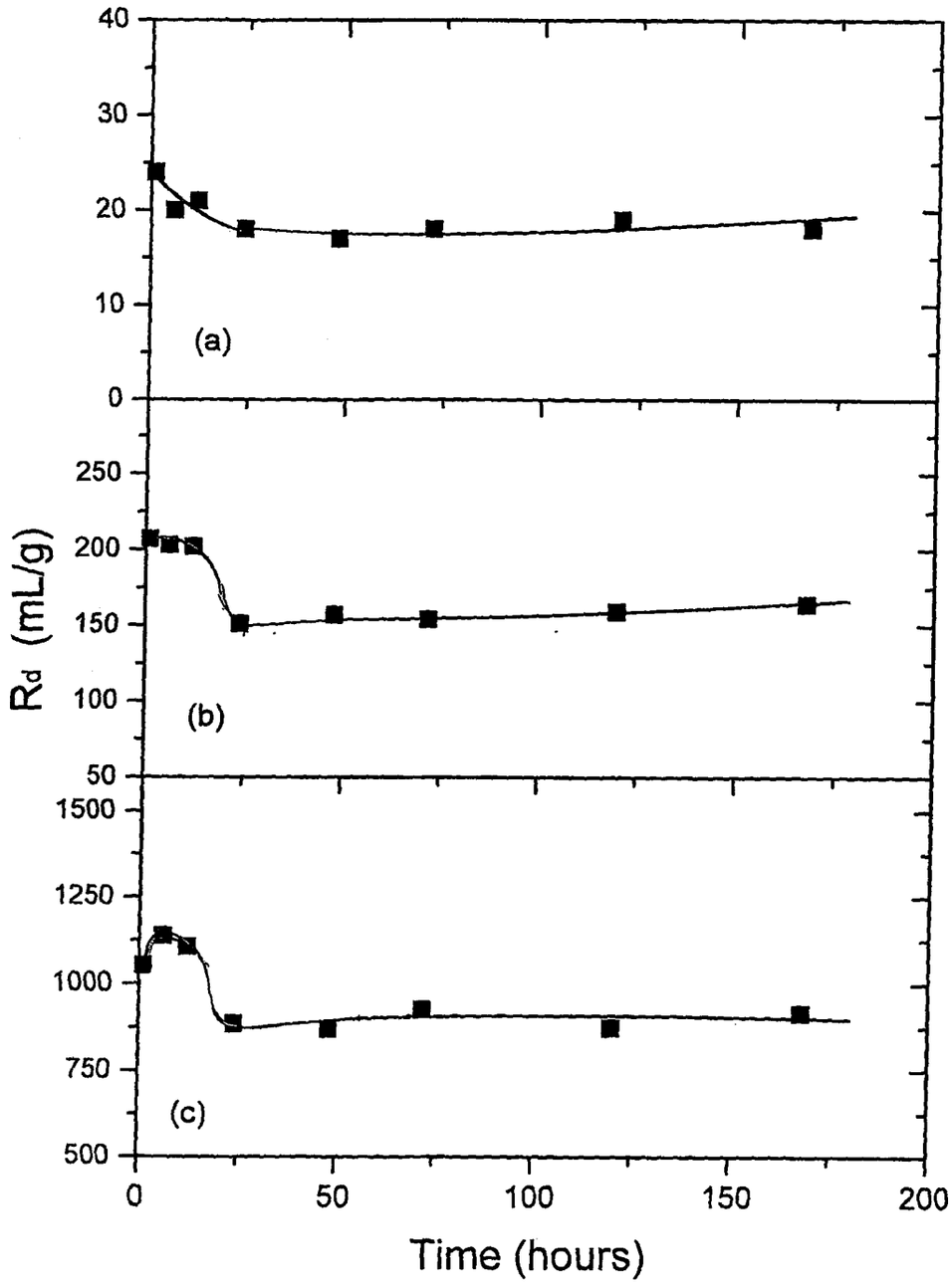

Fig. 4.7: Variation of R_d Values with Shaking Time for Cs^+ Sorption on; (a) Kaolinite, (b) Chlorite-Illite, and (c) Bentonite

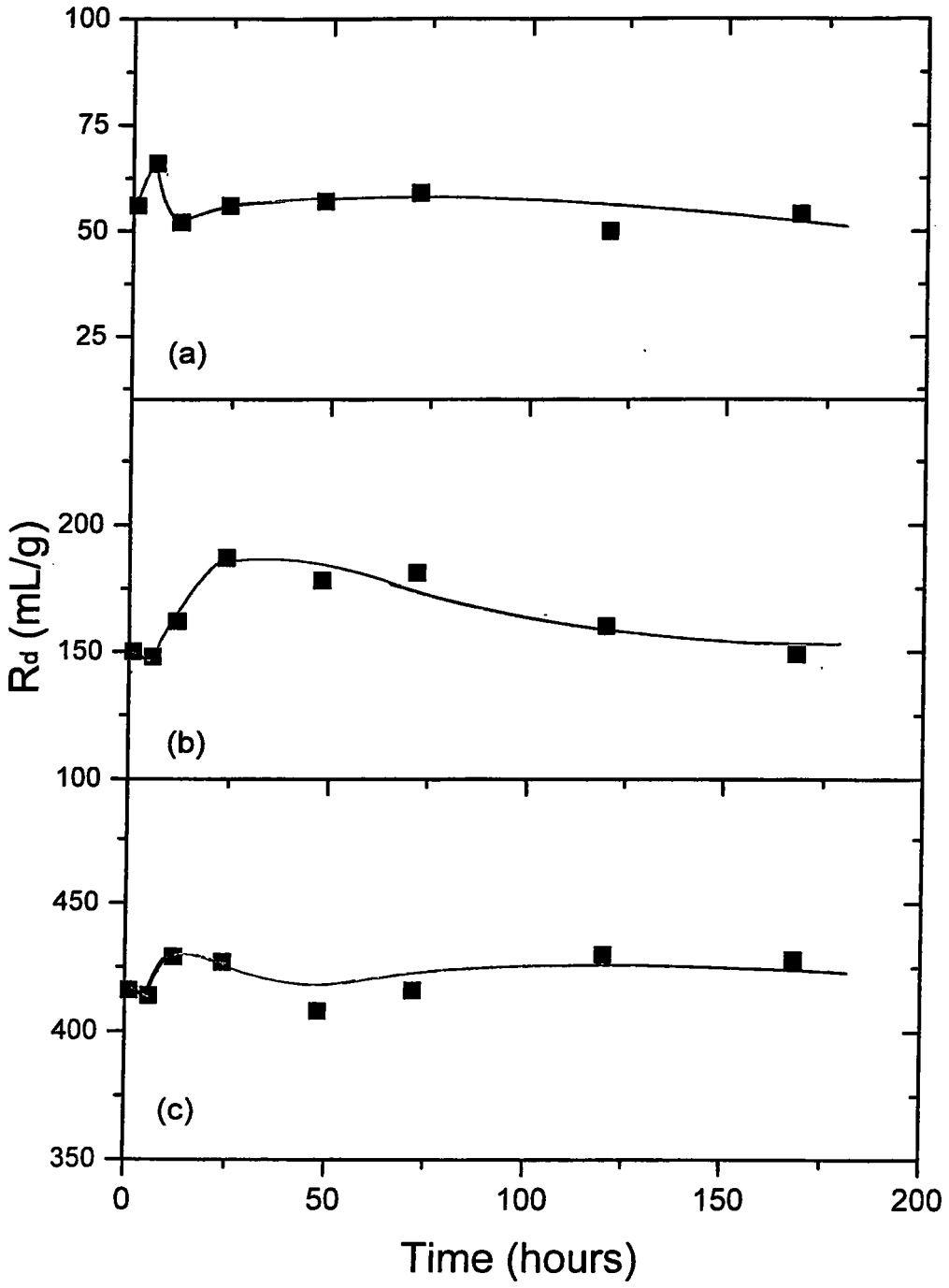

Fig. 4.8: Variation of R_d Values with Shaking Time for Ba^{2+} Sorption on; (a) Kaolinite, (b) Chlorite-Illite, and (c) Bentonite

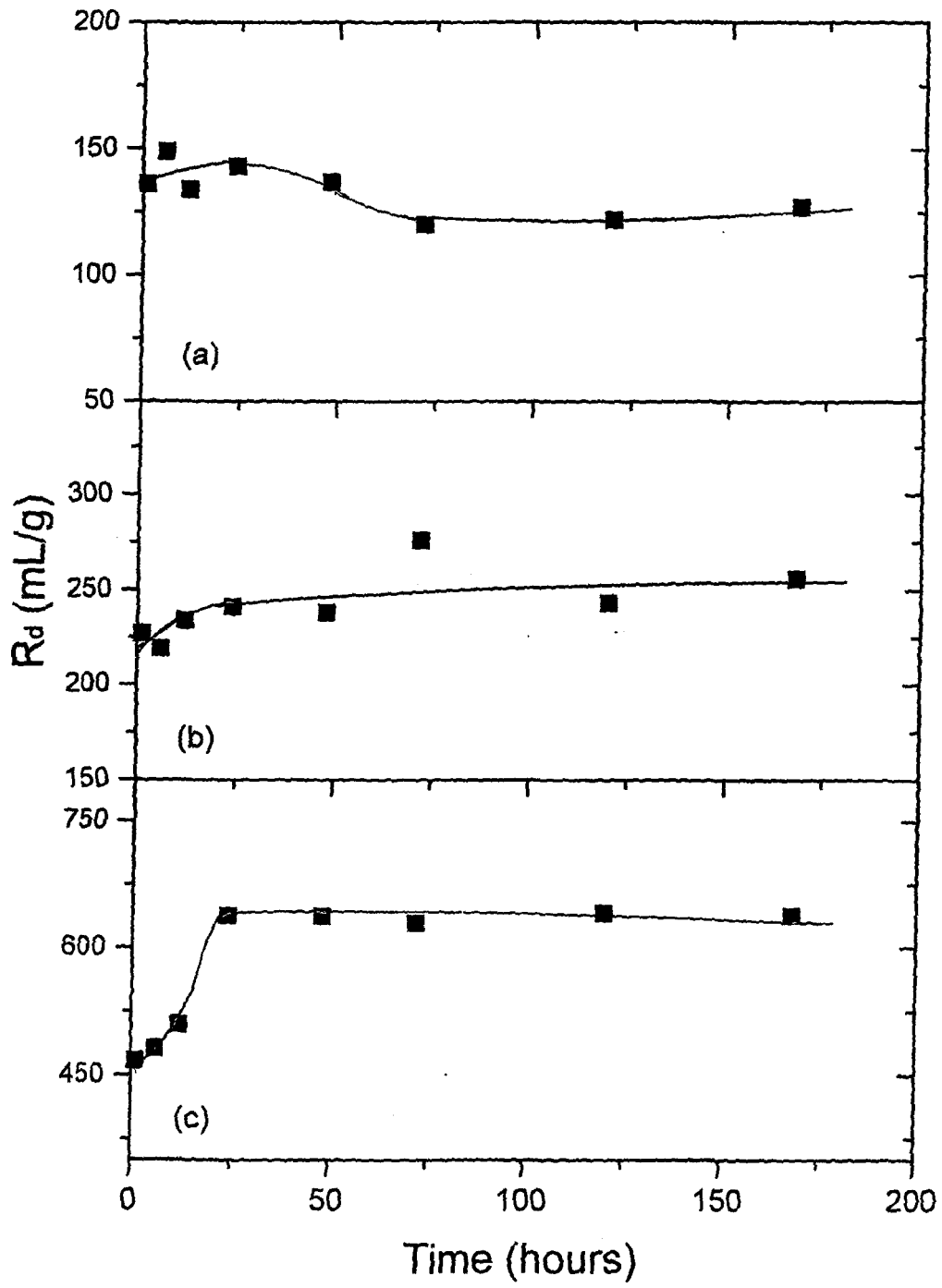

Fig. 4.9: Variation of R_d Values with Shaking Time for Co^{2+} Sorption on; (a) Kaolinite, (b) Chlorite-Illite, and (c) Bentonite

4.2.2- Loading and Temperature Studies

The experimental results of the distribution ratio, R_d, for the sorption of Cs^+, Ba^{2+}, and Co^{2+} on kaolinite, chlorite-illite, and bentonite at different loadings and temperatures are given in Appendix B (Tables B1, B2, and B3). The tables give the initial concentrations, $[C]^o$ (meq/ml), the equilibrium aqueous concentrations, $[C]_l$ (meq/ml), the equilibrium concentrations on the solid, $[C]_s$ (meq/g), and R_d values (ml/g) for sorption of the three cations on each natural clay. Data presented by these tables were used in the construction of the loading curves, sorption isotherms and Arrhenius plots used to determine some thermodynamic parameters as shown in the following sections.

The tables show that as the initial concentration increases, the R_d values decrease. This stems from the fact that as the initial concentration of the sorbate cation is increased, the ratio of the ions that are accommodated by the solid surface to those remaining in solution decreases, since a limited number of sites on the clay are available for sorption. This is reflected by the equilibrium concentrations on both aqueous and solid phases, where the former show larger increase upon increase in initial concentration compared to a smaller increase of the latter.

It is interesting to note that, particularly for Cs^+ and Ba^{2+} sorption, at higher loadings the highest R_d values were obtained for bentonite, whereas at lower loadings, chlorite-illite mixed clay had the highest R_d values. This might suggest the

existence of energetically more favorable sites in chlorite-illite clay which have limited sorption capacity. The larger sorption capacity of bentonite at higher loadings originates probably from the large interlayer space available for sorption, compared with both of chlorite and illite where interlayer sorption is limited. Kaolinite, on the other hand showed relatively small R_d values indicating a poorer sorption capacity. It is important to realize that comparing the sorption capacities of different clays based on the R_d values could be misleading unless one is making the comparison based on the same initial concentration of the sorbate ion.

4.2.2.1- Loading Curves

The loading curves were constructed by plotting the R_d values against log $[C]_s$, the equilibrium concentration (meq/g) of sorbed cations on kaolinite, chlorite-illite, and bentonite as shown in Figs. 4.10, 4.11, and 4.12. The fits in the figures are to guide the eye.

- **Loading curves for sorption on kaolinite:** The R_d values show a smooth decrease as loading of Cs^+ increases (Fig. 4.10(a)) and a somewhat inverse S shape is observed. For Ba^{2+} sorption, however, the distribution ratio decreases significantly as the Ba^{2+} loading increases (Fig. 4.10 (b)) The loading curves of Co^{2+} (Fig. 4.10 (c)) resemble those of Cs^+ and indicate that saturation is not approached within the concentration range. This might indicate that while a single sorption site is involved

in sorption of Ba^{2+}, two sorption sites of close energies exist in the cases of Cs^{+} and Co^{2+}. Kaolinite is a clay where layers are tightly bound via hydrogen bonding and as a result interlayer sorption is difficult. Thus sorption takes place primarily on the surface and the edges of the clay.

- Loading curves for sorption on chlorite-illite: The loading curves at different temperatures are given in Fig. 4.11. The distribution ratio decreases significantly as loading of Cs^{+} and Ba^{2+} (Figs. 4.11 (a,b)) is increased and the curves indicate the presence of multi sorption sites provided by chlorite and illite components of the clay. In the case of Co^{2+} sorption (Fig. 4.11 (c)), however, a single site seems to dominate, within the concentration range, until saturation is reached.

- Loading curves of sorption on bentonite: the curves show characteristic inverse S shape in all cases as shown in Fig. 4.12 indicating that sorption occurs on two sites, one at low loadings and the other at high loadings within the concentration range of the experiments. Montmorillonite, the major component of bentonite, is known to sorb different cations at surface sites as well as in the interlayer positions.

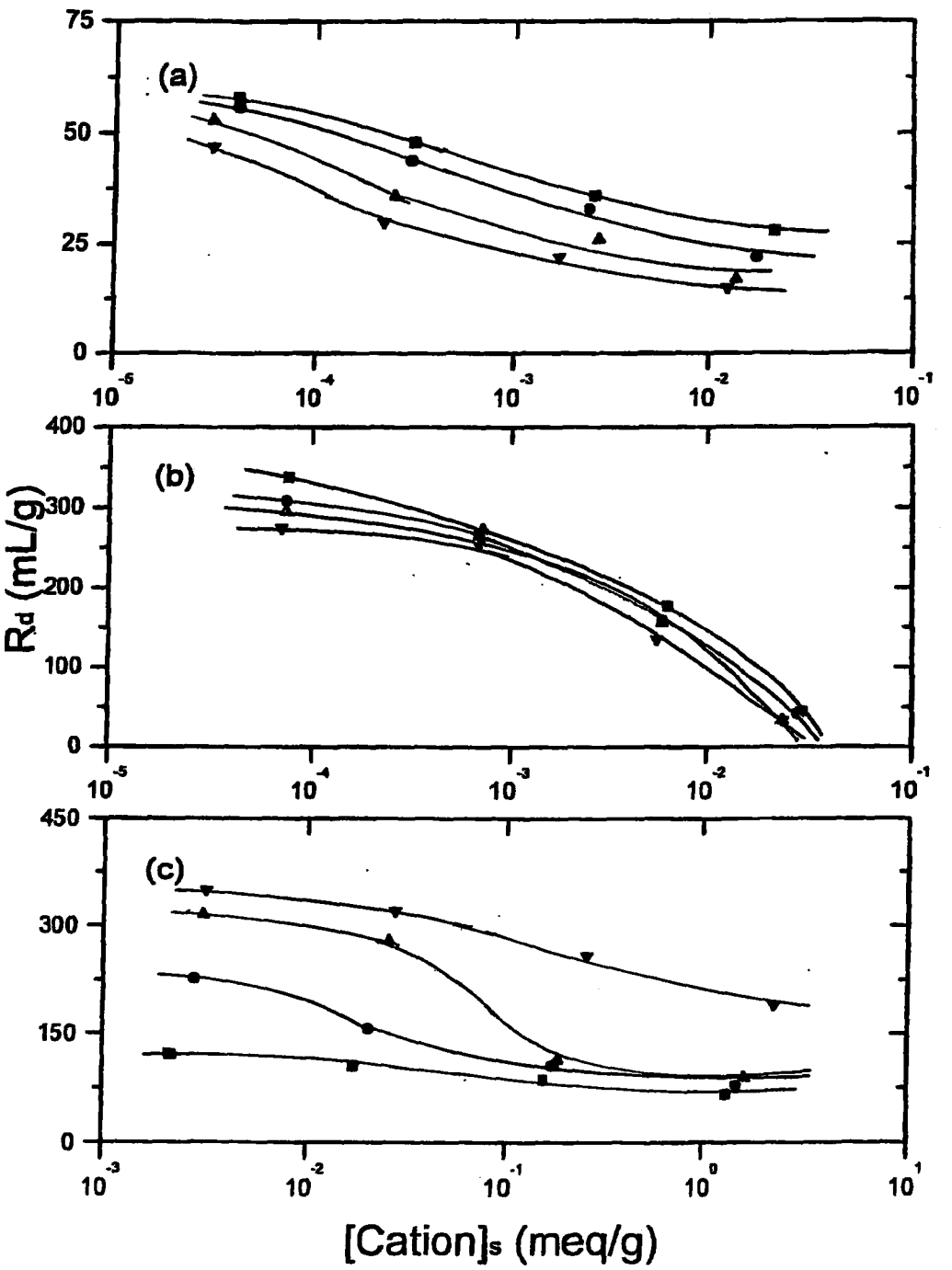

Fig. 4.10: The Loading Curves for Sorption of (a) Cs^+, (b) Ba^{2+}, and (c) Co^{2+} on Kaolinite ■:303 K ●:313 K ▲:323 K ▼:333 K

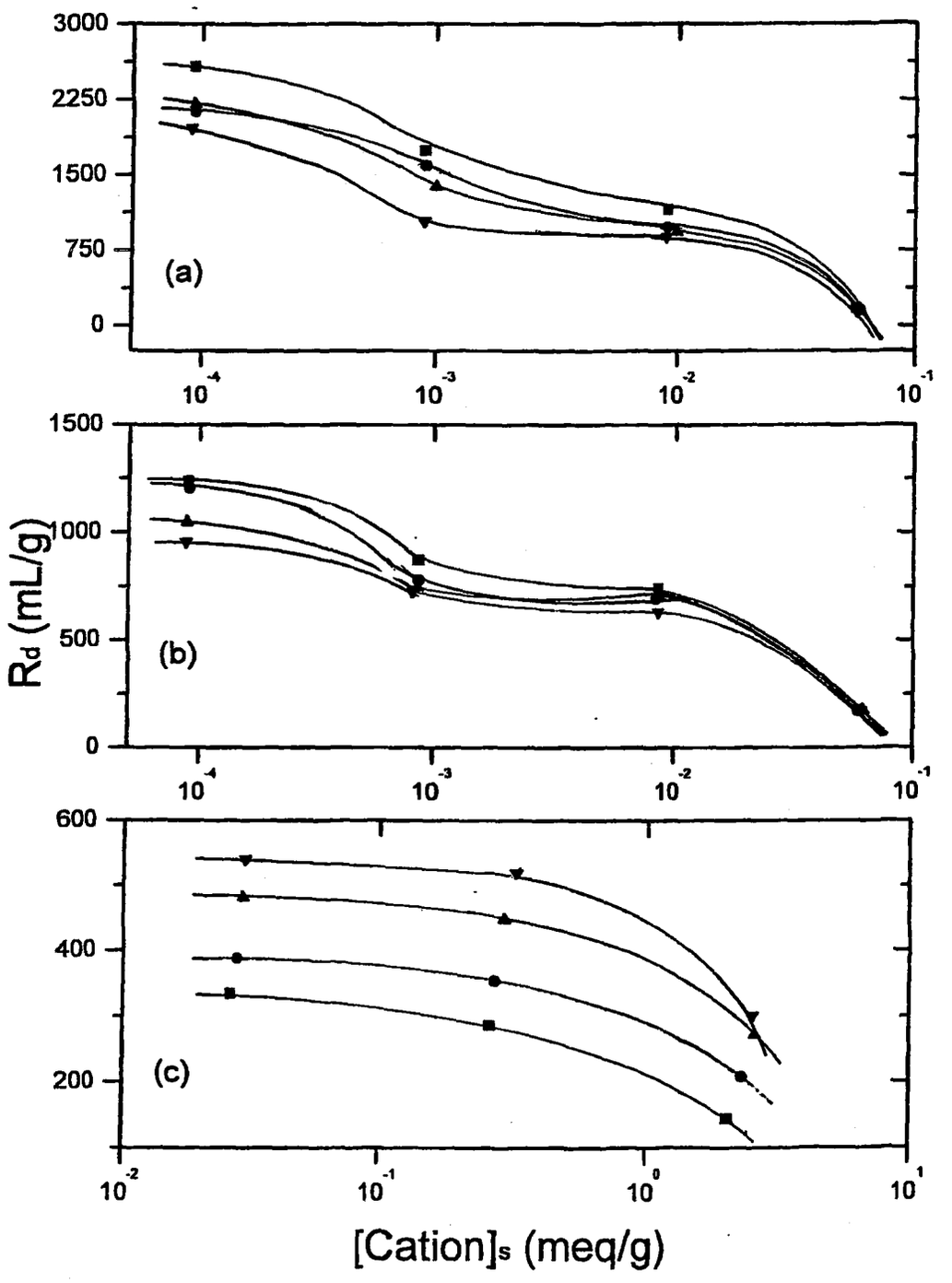

Fig. 4.11: The Loading Curves for Sorption of (a) Cs^+, (b) Ba^{2+}, and (c) Co^{2+} on Chlorite-Illite ■:303 K ●:313 K ▲:323 K ▼:333 K

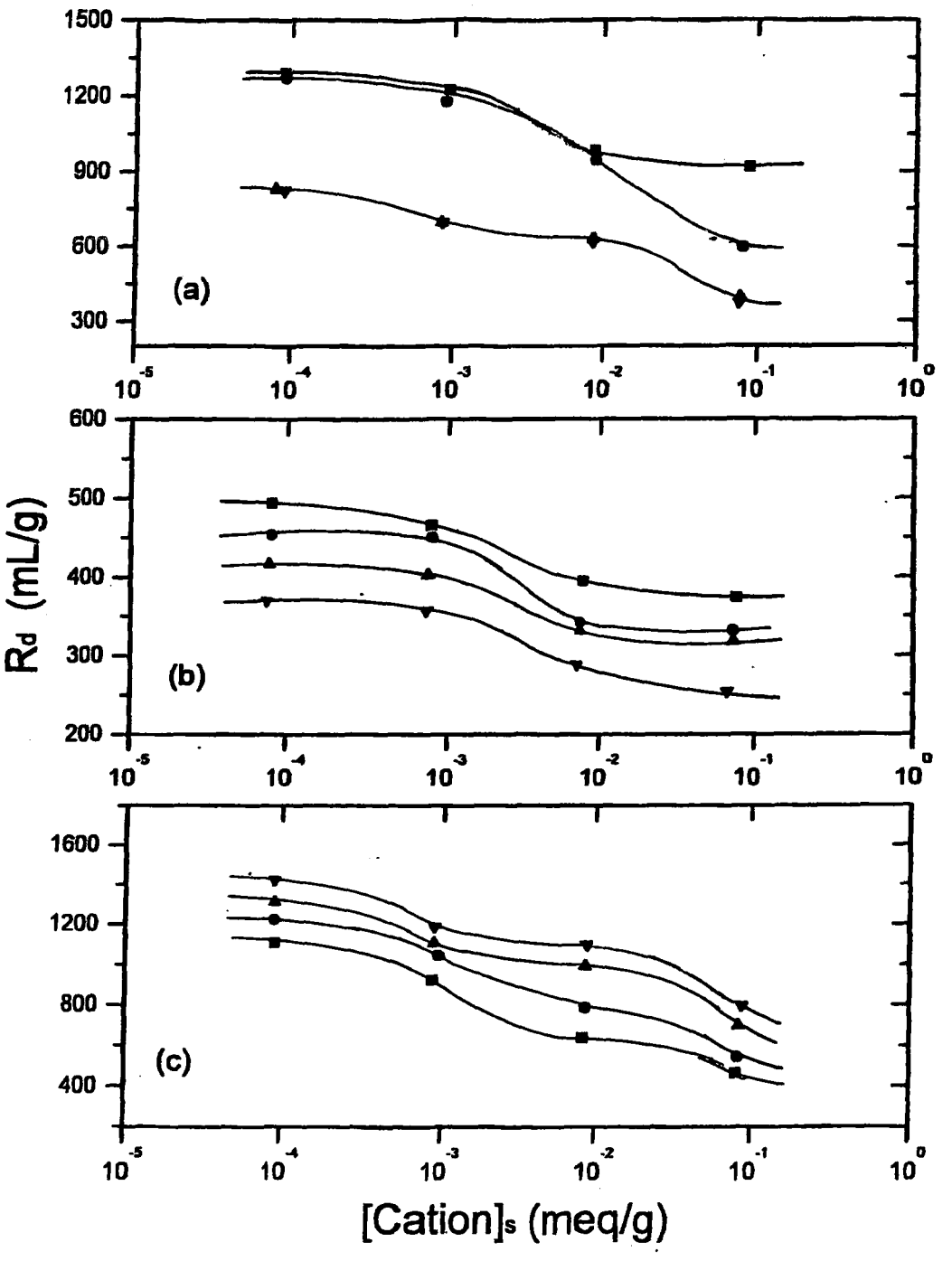

Fig. 4.12: The Loading Curves for Sorption of (a) Cs^{+}, (b) Ba^{2+}, and (c) Co^{2+} on Bentonite ■:303 K ●:313 K ▲:323 K ▼:333 K

4.2.2.2- The Sorption Isotherms

I- Freundlich Isotherms

Freundlich isotherm model was the most adequate model in the description of the sorption data of Cs^+, Ba^{2+}, and Co^{2+} on the three clays. The isotherm plots for the three cations at different loadings and temperatures on kaolinite, chlorite-illite, and bentonite are given in Figs. 4.13, 4.14, 4.15 respectively. The Freundlich constants, n and k, obtained for different sorption cases from the least square fits of equation 2.10 are given in Table 4.2.

The values of n being less than 1.0 in all cases indicate a non-linear sorption that takes place on a heterogeneous surface [50]. The nonlinearity suggests that the

sorption barrier increases exponentially as loading is increased leading to smaller R_d values. In general, the n values are not significantly affected by the temperature within the range 303-333 K. Among different cases, the n values in the case of bentonite are closer to unity compared to other clays , particularly chlorite-illite clay. The same was observed in previous studies [51, 52] and was referred to the presence of sites whose sorption energies are largely different in chlorite and illite clays compared to those of montmorillonite. Except for the case of Ba^{2+} sorption, kaolinite possessed high n values, somewhat close to those of bentonite.

The k values indicate that kaolinite and chlorite-illite clays possess the

highest affinity towards Co^{2+} sorption. Whereas bentonite has higher affinity towards Cs^{+} sorption at lower temperatures, the affinity towards Co^{2+} becomes higher as temperature increases. The high affinity towards Co^{2+} stems probably from its relatively higher charge density compared with Ba^{2+} and Cs^{+} ions. The higher affinity of a certain clay towards a particular cation does not necessarily result in higher R_d values (higher sorption) for that cation. This is because other factors should be considered. One important factor is the aqueous chemistry of that cation, i.e. the ability of cations with high hydration energies to overcome the hydration sheath attraction and reach the sorption site. It is reported that cation selectivity and fixation by a clay result from the interplay of two factors [53]: (i) the force of attraction of a cation for its hydration shell, and (ii) the force of attraction of the cation for clay surface (affinity of the clay towards sorption of that cation). Selectivity arises because these forces differ for different cations and sorption occurs when the second force exceeds the first. Since Co^{2+} ion exist in water as an aqua-hydrated ion (tetra- or hexa-) [54], its mobility is as a result more restricted compared with Cs^{+} and Ba^{2+} ions, particularly with Cs^{+} which exists as a 'naked' ion [55]. While the affinity of Co^{2+} sorption on the three clays increased with increasing temperature, it decreased for Ba^{2+} and Cs^{+} sorption on kaolinite and bentonite, or remained almost unchanged in the case of chlorite-illite. This is related to the endothermic/exothermic sorption behavior of those ions, the issue to be discussed in a following section.

Table 4.2: Fruendlich constants, n and k, obtained from the least square fits of the sorption data of Cs^+, Ba^{2+}, and Co^{2+} on kaolinite, chlorite-illite, and bentonite (The Linear Correlation Coefficients were all greater than 0.998)

Clay Type	Sorbed Cation	Freu. Constant	Temperature (K)			
			303	313	323	333
Kaolinite	Cs^+	n	0.90	0.87	0.86	0.84
		k	13.4	9.1	7.1	4.9
	Ba^{2+}	n	0.73	0.75	0.73	0.73
		k	7.0	8.9	6.5	6.3
	Co^{2+}	n	0.91	0.85	0.81	0.89
		k	48.1	43.7	41.2	48.7
Chlorite-Illite	Cs^+	n	0.71	0.71	0.71	0.72
		k	23.1	22.5	21.6	22.2
	Ba^{2+}	n	0.78	0.78	0.77	0.80
		k	36.4	34.6	36.4	40.2
	Co^{2+}	n	0.84	0.88	0.88	0.88
		k	77.6	127.6	168.3	185.4
Bentonite	Cs^+	n	0.95	0.90	0.91	0.90
		k	617	282	209	174
	Ba^{2+}	n	0.95	0.95	0.95	0.94
		k	249	209	204	160
	Co^{2+}	n	0.89	0.91	0.92	0.92
		k	189	251	331	389

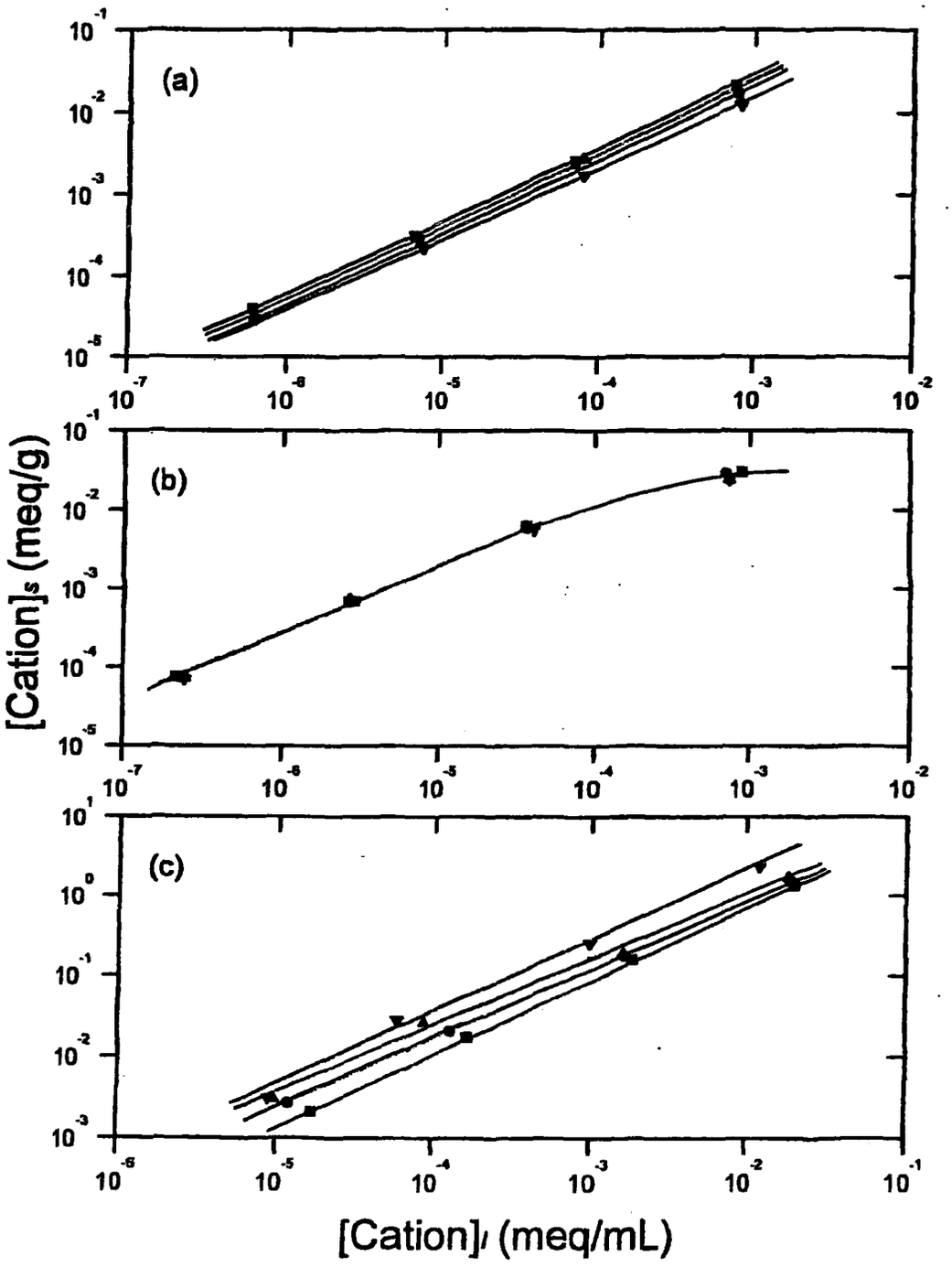

Fig. 4.13: Freundlich Isotherm Plots for Sorption of (a) Cs^+, (b) Ba^{2+}, and (c) Co^{2+} on Kaolinite ■:303 K ●:313 K ▲:323 K ▼:333 K

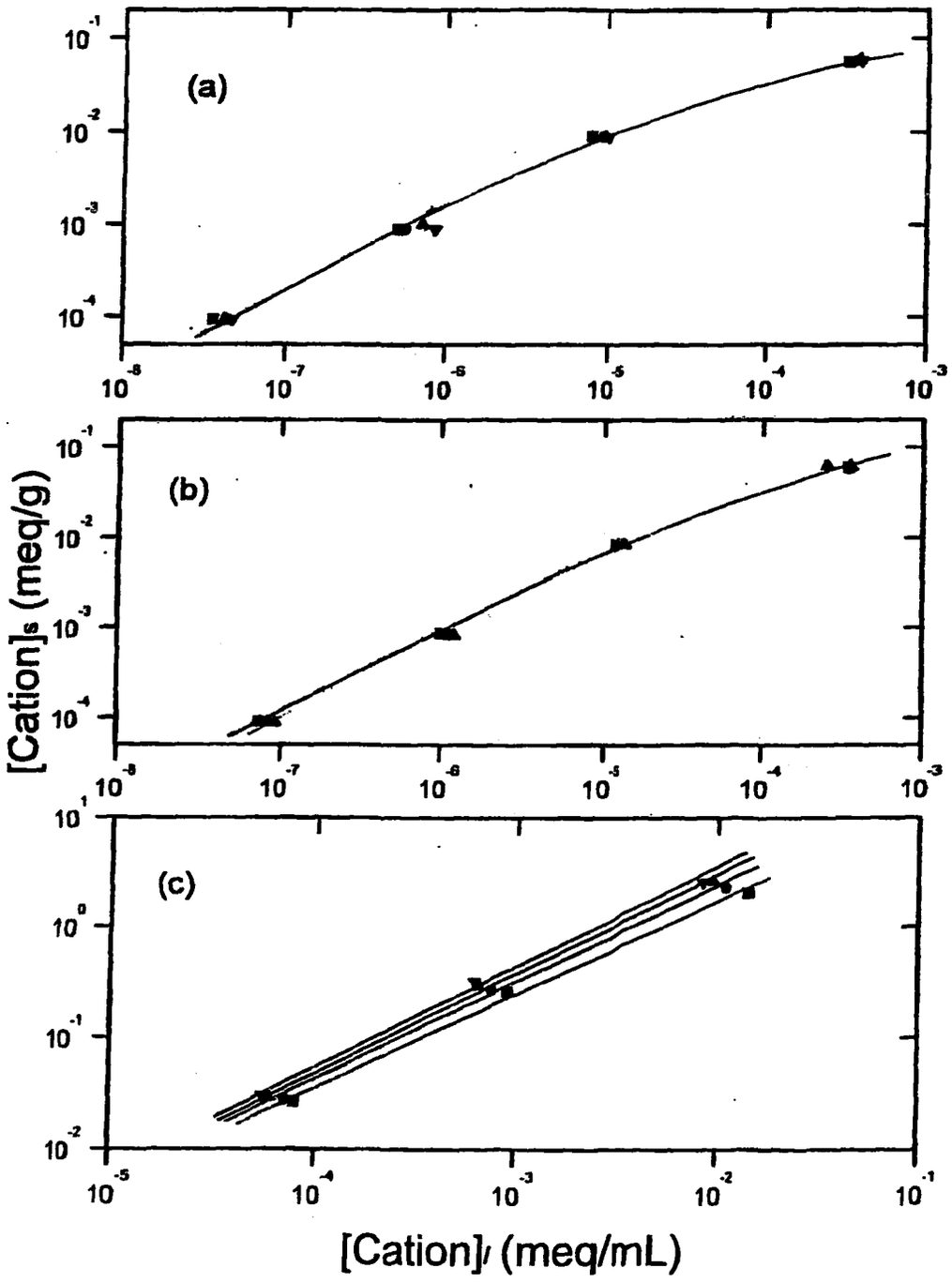

Fig. 4.14: Freundlich Isotherm Plots for Sorption of (a) Cs^+, (b) Ba^{2+}, and (c) Co^{2+} on Chlorite- Illite ■:303 K ●:313 K ▲:323 K ▼:333 K

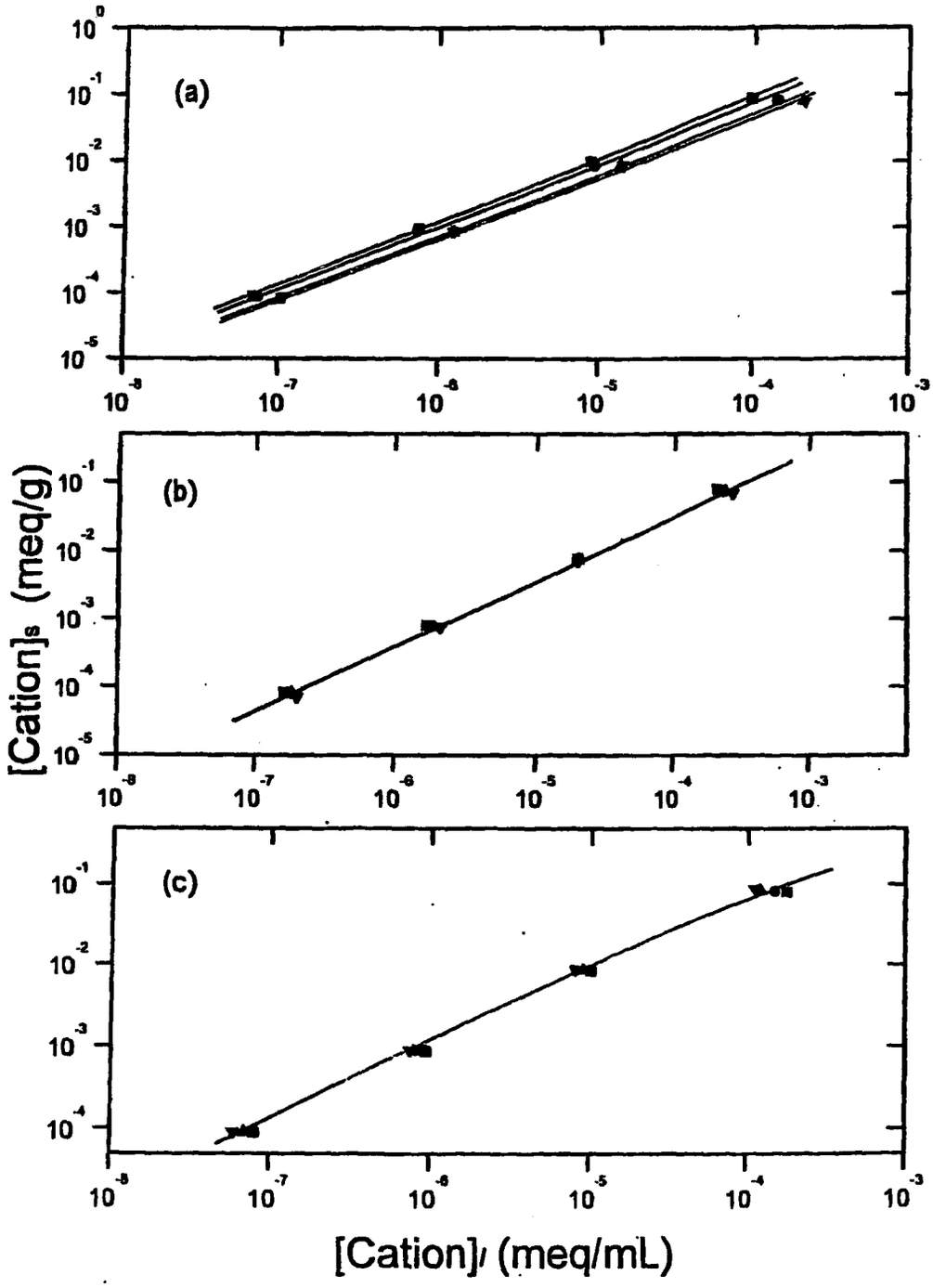

Fig. 4.15: Freundlich Isotherm Plots for Sorption of (a) Cs^+, (b) Ba^{2+}, and (c) Co^{2+} on Bentonite ■:303 K ●:313 K ▲:323 K ▼:333 K

II- Dubinin-Radushkevich (D-R) Isotherms

The D-R isotherm plots were constructed using equation 2.13. The sorption data of Cs^+, Ba^{2+} and Co^{2+} followed well the D-R model as shown in Figs 4.16, 4.17, and 4.18 for sorption on kaolinite, chlorite-illite, and bentonite, respectively The isotherm parameters K, C_m were obtained from the least square fits of the plots. K is a constant related to the sorption energy, while C_m is related to the sorption capacity of the solid. The mean free energy, E, values were calculated using K values as given in equation 2.15. E refers to the amount of energy required to transfer one mole of sorbed ions from infinity in solution to the solid surface [47]. The values of C_m, K and E are given in Table 4.3.

According to the C_m values, bentonite is the clay with highest sorption capacity towards all three cations followed by chlorite-illite and then by kaolinite. This is inline with the CEC capacities reported earlier (Table 1.4) It is interesting that the order of sorption capacity of each sorbed cation on the three clays follows that of the sorption affinity estimated based on the value of Freundlich constant, k (Table 4.2). The C_m values suggest that kaolinite possesses higher sorption capacity towards Co^{2+}. While the C_m values decrease as temperature is increased in the cases of Cs^+ and Ba^{2+} sorption, it increases in the case of Co^{2+} sorption. Chlorite-illite like kaolinite possesses higher sorption capacity towards Co^{2+}. The C_m values remains almost unchanged in Cs^+ and Ba^{2+} sorption but increase significantly with increased temperature in Co^{2+} sorption case. In the bentonite case, the C_m values indicate that

the sorption capacity at lower temperatures is the largest for Cs^{+} and is comparable for Co^{2+} and Ba^{2+}. At higher temperatures the sorption capacity of bentonite becomes the highest towards Co^{2+}. In all cases, the mean free energy of sorption, E, on different clays is in the 8-16 kJ/moL energy range corresponding to ion-exchange type of sorption [56].

Table 4.3: The D-R Isotherm constants, K $(mol/kJ)^2$, C_m (meq/100g), and E (kJ/mol)obtained from the least square fits for the sorption data of Cs^+, Ba^{2+}, and Co^{2+} on kaolinite, chlorite-illite, and bentonite. (The Linear Correlation Coefficients were all greater than 0.997)

Clay Type	Sorbate Ion	D-R Constant	Temperature (K)			
			303	313	323	333
Kaolinite	Cs^+	C_m	13.9	11.0	9.4	6.9
		K	0.0065	0.0059	0.0055	0.0051
		E	8.8	9.2	9.5	9.9
	Ba^{2+}	C_m	17.0	17.9	14.9	14.4
		K	0.0052	0.0050	0.0045	0.0043
		E	9.8	10.0	10.5	10.8
	Co^{2+}	C_m	23.3	20.0	29.5	52.1
		K	0.0095	0.0075	0.0073	0.0072
		E	7.3	8.2	8.2	8.3
Chlorite-Illite	Cs^+	C_m	37.9	38.3	36.8	35.7
		K	0.0045	0.0043	0.0040	0.0038
		E	10.5	10.8	11.2	11.5
	Ba^{2+}	C_m	45.8	44.3	49.4	48.9
		K	0.0050	0.0047	0.0046	0.0043
		E	10.0	10.3	10.5	10.4
	Co^{2+}	C_m	58.7	76.4	91.9	96.5
		K	0.0097	0.0092	0.0085	0.0079
		E	7.2	7.4	7.7	8.0
Bentonite	Cs^+	C_m	158.1	116.0	94.6	91.6
		K	0.0057	0.0052	0.0051	0.0048
		E	9.4	9.8	9.9	10.2
	Ba^{2+}	C_m	101.8	90.1	93.9	78.9
		K	0.0062	0.0058	0.0055	0.0052
		E	9.0	9.3	9.5	9.8
	Co^{2+}	C_m	100.1	118.2	115.6	136.5
		K	0.0056	0.0053	0.0049	0.0046
		E	9.4	9.7	10.1	10.4

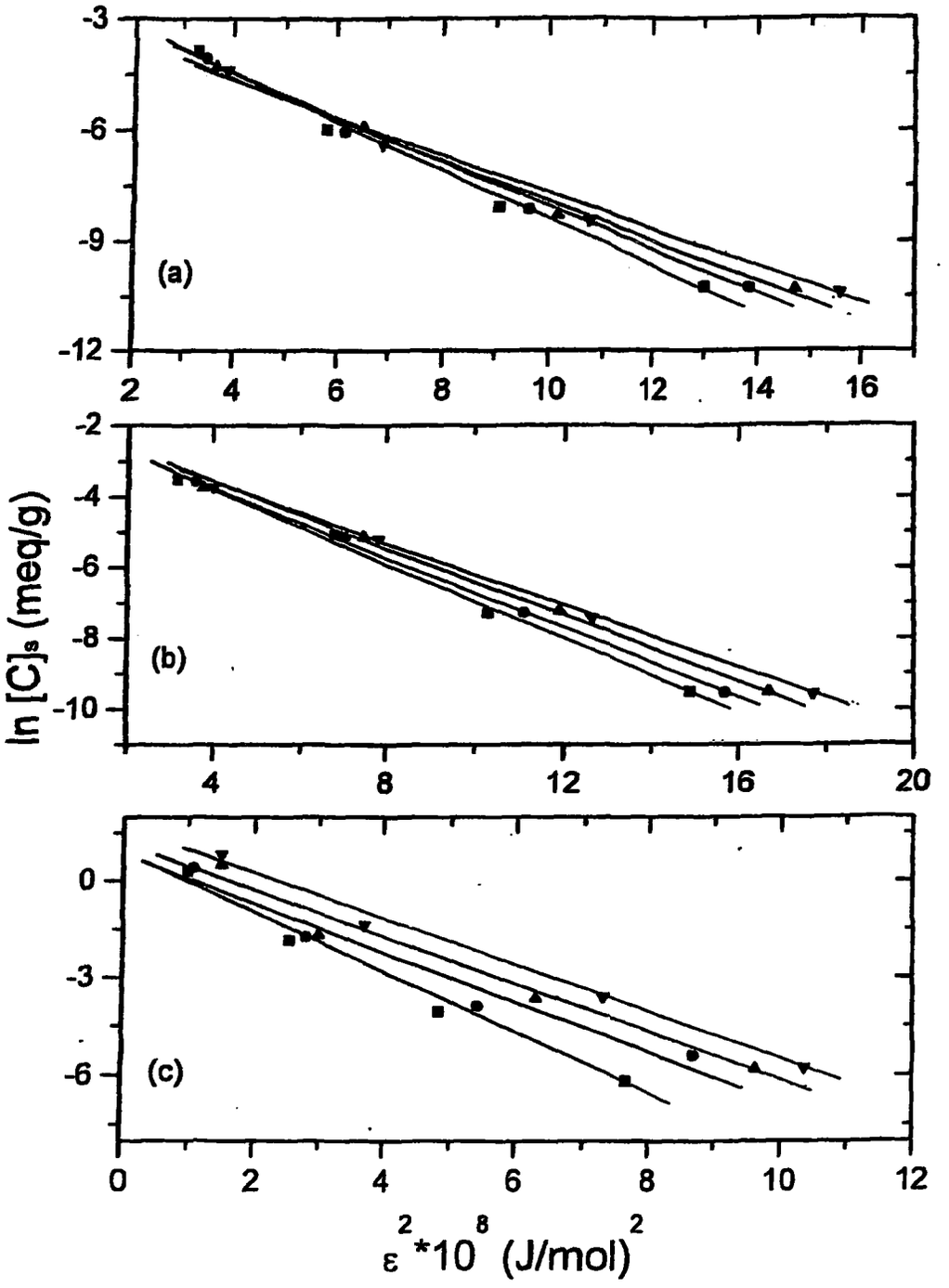

Fig. 4.16: D-R Isotherm Plots for Sorption of (a) Cs^{+}, (b) Ba^{2+}, and (c) Co^{2+} on Kaolinite ■:303 K ●:313 K ▲:323 K ▼:333 K

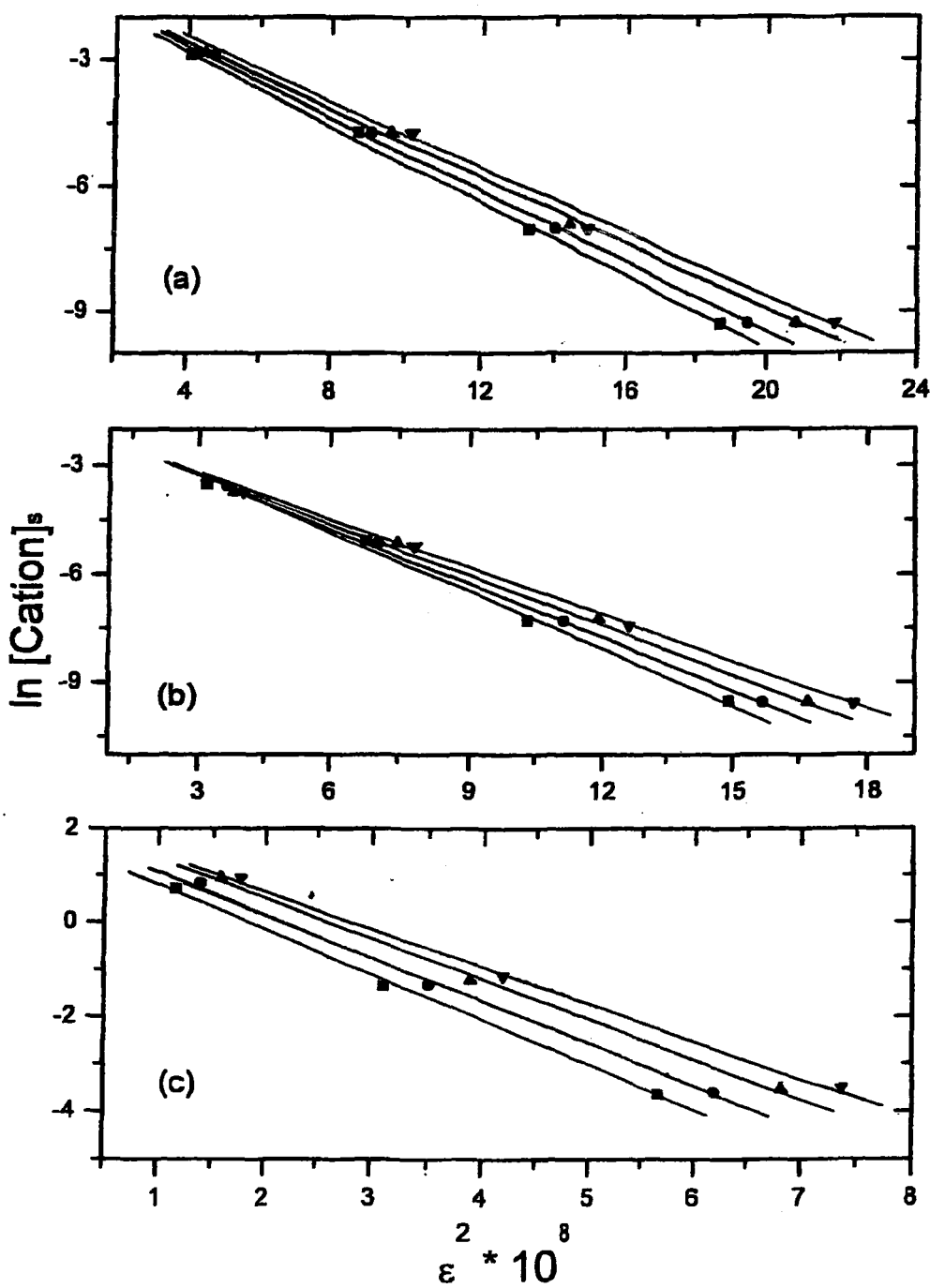

Fig. 4.17: D-R Isotherm Plots for Sorption of (a) Cs^{+}, (b) Ba^{2+}, and (c) Co^{2+} on Chlorite-Illite ■:303 K ●:313 K ▲:323 K ▼:333 K

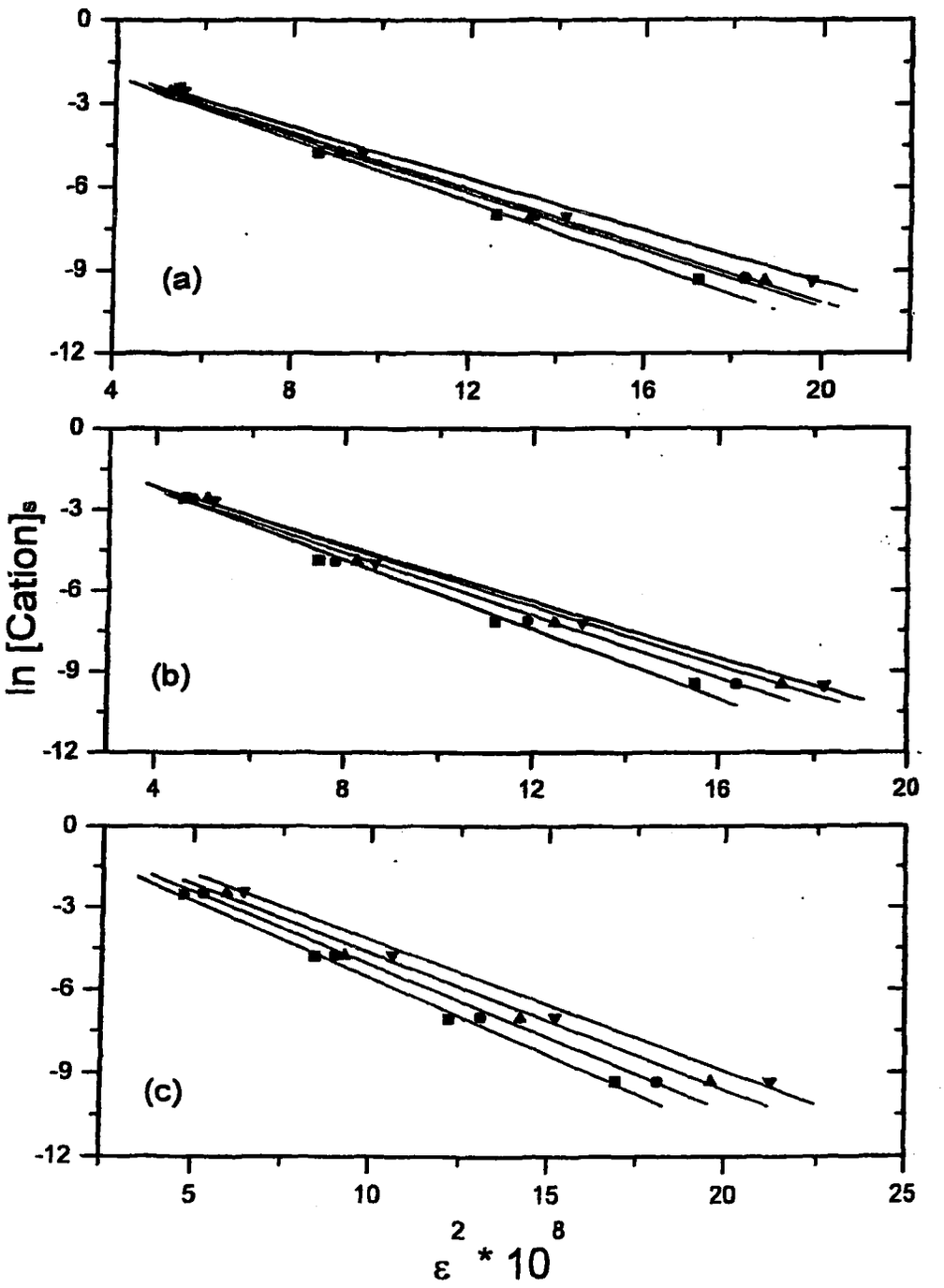

Fig. 4.18: D-R Isotherm Plots for Sorption of (a) Cs^{+}, (b) Ba^{2+}, and (b) Co^{2+} on Bentonite ■:303 K ●:313 K ▲:323 K ▼:333 K

III- Langmuir Isotherms

The linearized form of Langmuir isotherm equation (2.7) did not yield a linear behavior of the sorption data of the Cs^{+}, Ba^{2+}, and Co^{2+} on the clays as shown in Figs. 4.19, 4.20, and 4.21 for kaolinite, chlorite-illite, and bentonite respectively. The obtained plots show exponential behavior rather than a linear one indicating that this model is inadquate for describing the sorption data within the whole concentration range of studies.

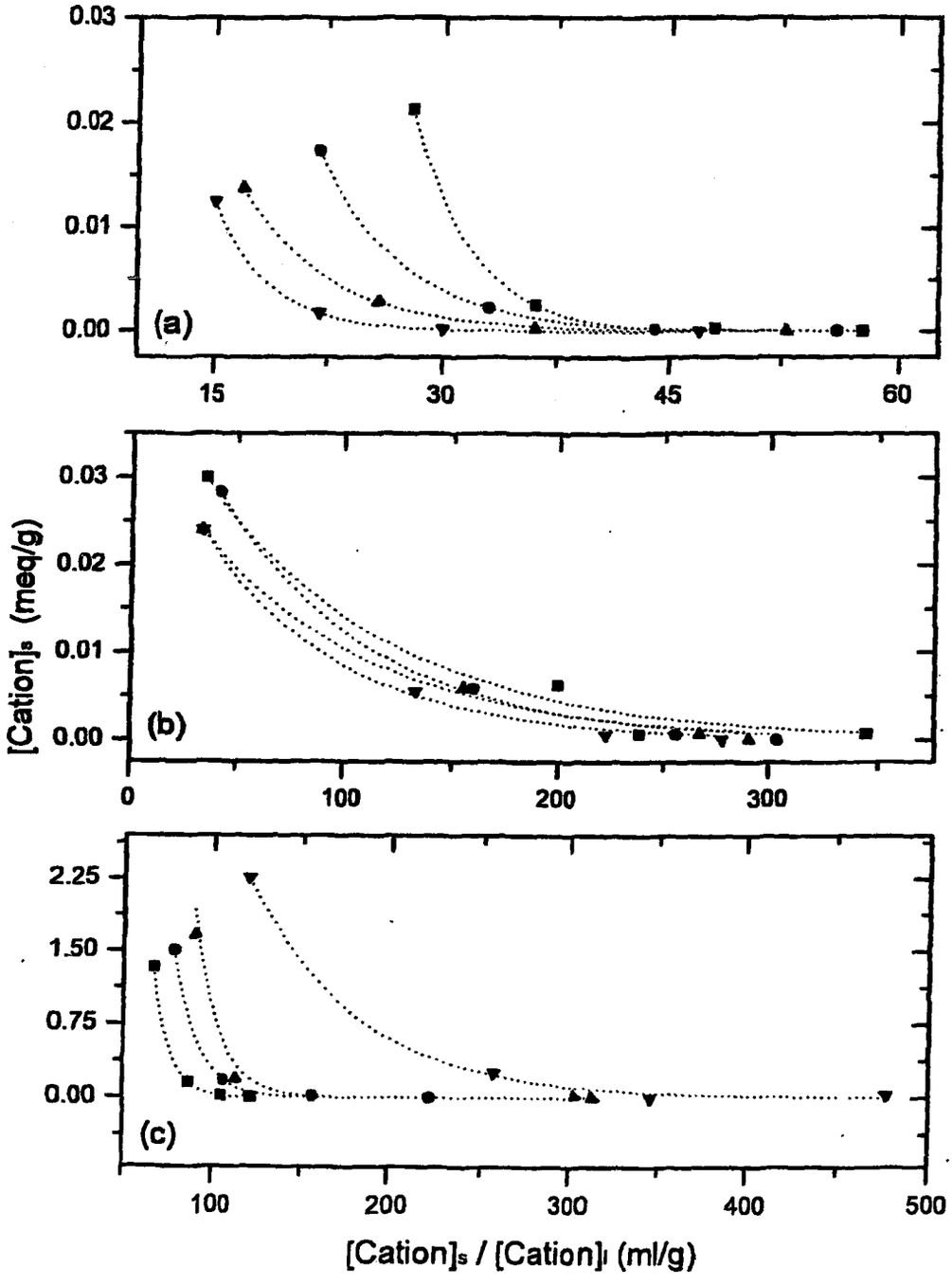

Fig. 4.19: Langmuir Isotherm Plots for Sorption of (a) Cs^+, (b) Ba^{2+}, and (c) Co^{2+} on Kaolinite ■:303 K ●:313 K ▲:323 K ▼:333 K

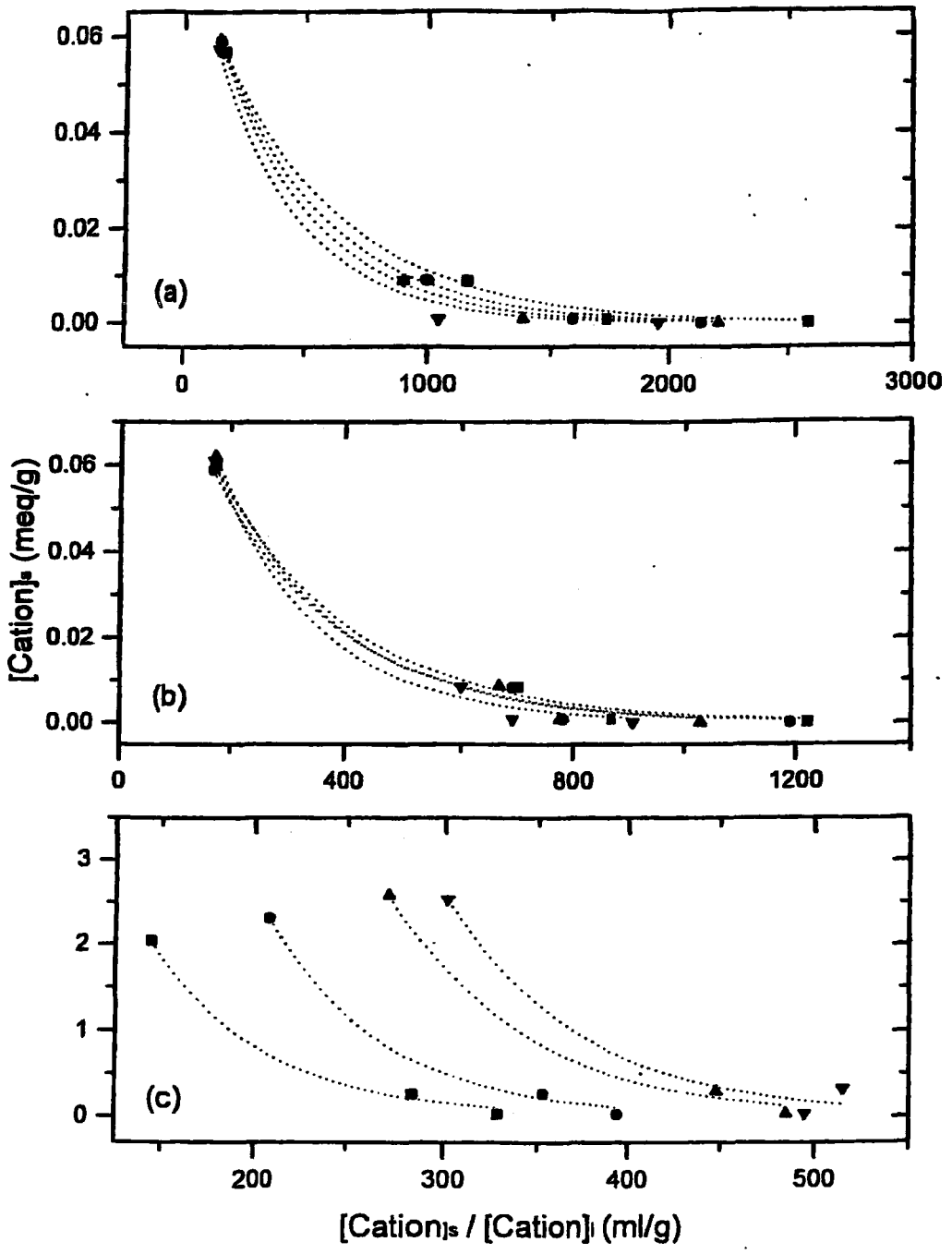

Fig. 4.20: Langmuir Isotherm Plots for Sorption of (a) Cs^{+}, (b) Ba^{2+}, and (c) Co^{2+} on Chlorite-Illite ■:303 K ●:313 K ▲:323 K ▼:333 K

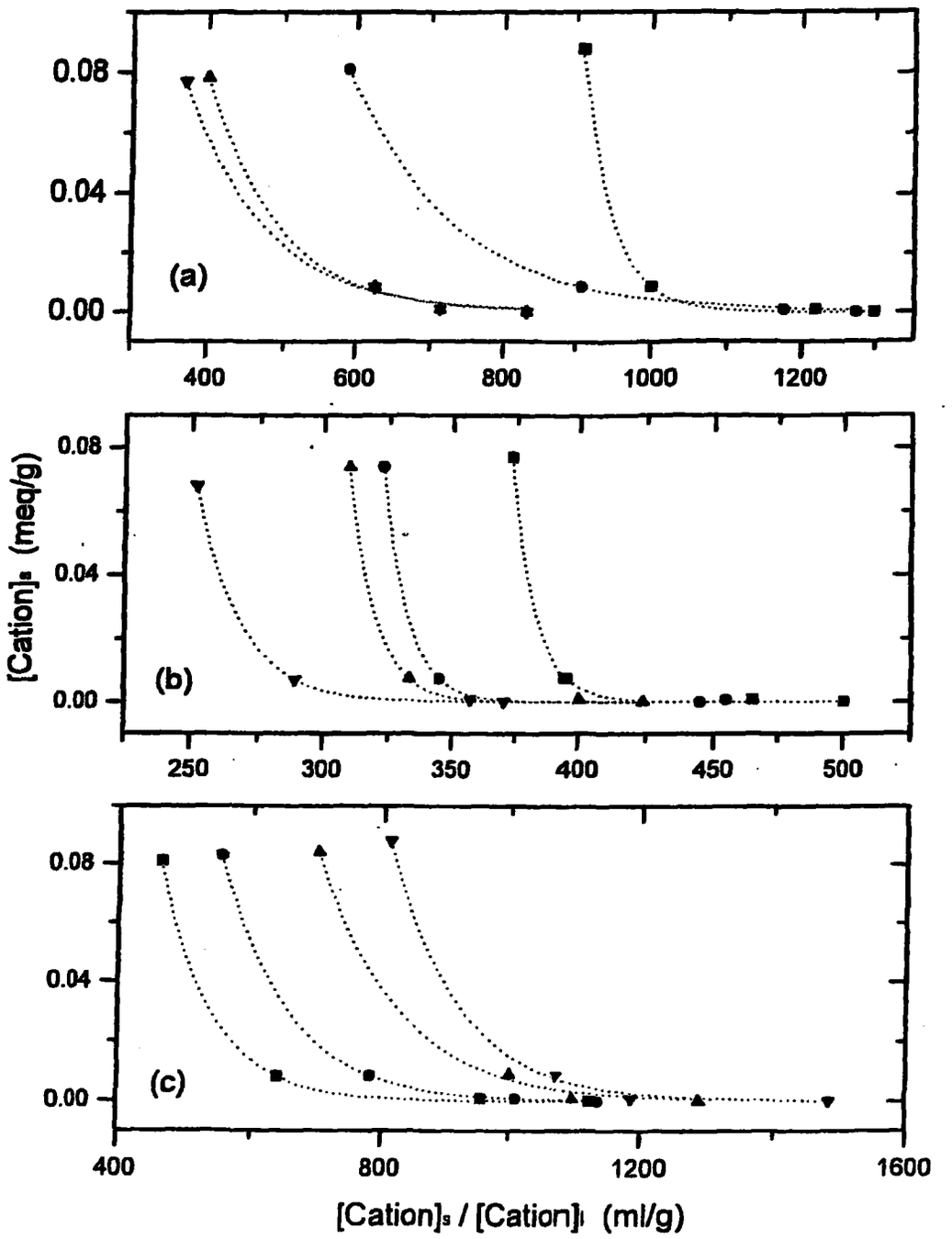

Fig. 4.21: Langmuir Isotherm Plots for Sorption of (a) Cs^{+}, (b) Ba^{2+}, and (c) Co^{2+} on Bentonite ■:303 K ●:313 K ▲:323 K ▼:333 K

4.2.2.3- The Thermodynamic Parameters

Utilizing the sorption data at different temperatures, the thermodynamic parameters; the enthalpy change, ΔH^o, the entropy change, ΔS^o, and the Gibbs free energy change, ΔG^o, were calculated. These parameters are helpful in determining the endothermicity/exothermicity, stability and the spontaneity of the sorption process. In exothermic sorption, denoted by negative ΔH^o values (kJ/mol), low temperatures are favored. On the other hand, positive ΔH^o values denotes endothermic processes, where increasing temperatures favors sorption. Magnitudes of enthalpy change are related to the type of sorption. Typical values of ΔH^o for physical sorption lie in the range of 4 - 40 kJ/mol. Such values are small and correspond to weak electrostatic and van der Waals forces as compared to chemisorption where chemical bond formation is involved and ΔH^o values can go up to 800 kJ/mol [57].

of least square fits of Arrhenius plots (equation 2.22) given as:

$$\ln R_d = \frac{\Delta S^o}{R} - \frac{\Delta H^o}{RT}$$

By plotting ln R_d versus the reciprocal of absolute sorption temperature, ΔH^o is obtained from the slope and ΔS^o is obtained from the intercept of the plot. The least square fits of the sorption of Cs^+, Ba^{2+}, and Co^{2+} ions on kaolinite, chlorite-illite, and bentonite are shown in Figs. 4.22, 4.23, and 4.24 respectively. Values of ΔH^o and

$\Delta S°$ were calculated for different initial concentrations as shown in Table 4.4.

As Table 4.4 shows, values of $\Delta H°$ and $\Delta S°$ changes as the initial concentration is changed. This change occurs randomly in most cases. Actually both $\Delta H°$ and $\Delta S°$ are functions of temperature and pressure only and as such no concentration dependence is expected. However, since those values were calculated depending on the assumption that R_d is a fully equilibrium constant - R_d is an equilibrium constant for a particular initial concentration only-, changes in R_d at different initial concentrations lead to changes in $\Delta H°$ and $\Delta S°$ values. In order to obtain values of $\Delta H°$ and $\Delta S°$ that are representative over the entire concentration ranges, averaged $\Delta H°$ and $\Delta S°$ of different sorption cases were calculated. Here it is implicitly assumed that the fluctuations in the $\Delta H°$ and $\Delta S°$ values at various concentrations are small enough to allow calculating an average. The averaged enthalpy and entropy changes, $\Delta H_{av}°$ and $\Delta S_{av}°$ were used in calculating $\Delta G°$ values at different temperatures according to equation 2.21, given as:

$$\Delta G^o = \Delta H^o - T\Delta S^o$$

The values of $\Delta H_{av}°$, $\Delta S_{av}°$, and ΔG^o values are given in Table 4.5.

In all cases, $\Delta H°$ values came out to be negative for Cs^+ and Ba^{2+} sorption and positive for Co^{2+} sorption indicating an exothermic nature of sorption in the former case and an endothermic nature in the latter case. Thus, while a decrease in temperature would favor sorption of Cs^+ and Ba^{2+}, an increase in temperature is

required for more Co^{2+} to be sorbed. For both of Cs^{+} and Ba^{2+}, the order of enthalpy changes were bentonite > kaolinite > chlorite-illite For Co^{2+} sorption, however, the order of enthalpy change was kaolinite > chlorite-illite > bentonite.

The decrease in sorption of Cs^{+} and Ba^{2+} ions with the increase in temperature may be attributed to the increased desorption caused by an increase in the thermal energy of the sorbates [58]. It can result also from the increase in solubility of both ions in liquid phase as temperature is increased. Exothermic behavior of Cs^{+} was reported on a number of solids [28,59,60]. The endothermic behavior of Co^{2+} on some solids was also reported by other studies [59,61,62]. Co^{2+} ions have high hydration energies and are well known for making aqua-hydrated cations in water. For cations that are solvated well in water, adsorption requires that such ions to a certain extent be denuded of their hydration sheath so that their migration toward the sorption interface is facilitated. The dehydration process of ions requires energy and this energy is assumed to exceed the exothermicity of the ions attacking the surface. The implicit assumption here is that after sorption, the environment of the metal ions is less aqueous than it was in the solution state. The removal of water from ions is essentially an endothermic process, and as more heat is supplied by increasing the temperature of adsorption more dehydrated cations will be available and thus the extent of sorption is expected to increase [63].

Whereas negative $\Delta S°$ values for Cs^{+} sorption on kaolinite and bentonite, positive ones are found in the case of Cs^{+} sorption on chlorite-illite. In all cases,

positive $\Delta S°$ values were obtained upon Ba^{2+} and Co^{2+} sorption. Positive $\Delta S°$ values are usually associated with a spontaneous process where the system shows an endothermic behavior or even a weak exothermic behavior. As the exothermic behavior becomes more pronounced negative $\Delta S°$ values are obtained. In literature, it is reported that the positive values of $\Delta S°$ resulting from sorption of divalent cations (Ba^{2+} and Co^{2+} in this case) on solid surfaces might suggest that ions displaced from the solid surface are greater in number than the sorbed Ba^{2+} or Co^{2+} ions, which means that two monovalent ions may be exchanged for a single Ba^{2+} or Co^{2+} ion [59]. The calculated negative values of $\Delta G°$ for all cases (Table 4.5) indicate that the sorption process of each is spontaneous. Whereas temperature has no significant effect on $\Delta G°$ values corresponding to Cs^{+} and Ba^{2+} sorption, those corresponding to Co^{2+} sorption increases slowly with temperature. In all cases, $\Delta G°$ magnitudes are roughly in the 8-16 kJ/mol energy range which corresponds to ion exchange type sorption mechanism [56].

Table 4.4: Values of the Enthalpy Change, $\Delta H°$ (kJ/mol), and the Entropy Change, $\Delta S°$(J/mol.K) obtained from the Arrhenius plots of the sorption data of Cs^+, Ba^{2+}, and Co^{2+} on kaolinite, chlorite-illite (CI), and bentonite

Cation-clay	Initial Conc., meq/ml	$\Delta H°$ (kJ/mol)	$\Delta S°$ (J/mol.K)
Cs-kaolinite	1.0×10^{-6}	-18	-31
	1.0×10^{-5}	-14	-17
	1.0×10^{-4}	-13	-12
	1.0×10^{-3}	-6	15
Ba-kaolinite	1.0×10^{-6}	-5	31
	1.0×10^{-5}	-5	32
	1.0×10^{-4}	-7	20
	1.0×10^{-3}	-9	2
Co-kaolinite	3.6×10^{-5}	29	137
	3.6×10^{-4}	43	179
	3.6×10^{-3}	28	129
	3.6×10^{-2}	30	132
Cs-CI	1.0×10^{-6}	-7	43
	1.0×10^{-5}	-14	17
	1.0×10^{-4}	-7	34
	1.0×10^{-3}	-5	27
Ba-CI	1.0×10^{-6}	-8	34
	1.0×10^{-5}	-5	40
	1.0×10^{-4}	-4	42
	1.0×10^{-3}	-1	40
Co-CI	3.6×10^{-4}	14	94
	3.6×10^{-3}	17	103
	3.6×10^{-2}	21	110
Cs-bentonite	1.0×10^{-6}	-15	11
	1.0×10^{-5}	-18	-10
	1.0×10^{-4}	-15	11
	1.0×10^{-3}	-26	-25
Ba-bentonite	1.0×10^{-6}	-8	25
	1.0×10^{-5}	-7	27
	1.0×10^{-4}	-8	23
	1.0×10^{-3}	-10	17
Co-bentonite	1.0×10^{-6}	7	81
	1.0×10^{-5}	7	79
	1.0×10^{-4}	15	104
	1.0×10^{-3}	16	103

Table 4.5: The average values of the enthalpy change, $\Delta H_{av}°$(kJ/mol), entropy change, $\Delta S_{av}°$(J/mol.K) and the calculated values of the Gibbs Free Energy change, $\Delta G°$ (kJ/mol), obtained at different temperatures for the sorption cases of Cs^+, Ba^{2+}, and Co^{2+} on kaolinite, chlorite-illite (CI), and bentonite.

			ΔG° (kJ/mol) at Different Temperatures (K)			
Cation-clay	**$\Delta H_{av}°$ (kJ/mol)**	**$\Delta S_{av}°$ (J/mol.K)**	**303**	**313**	**323**	**333**
Cs-kaolinite	-13 ± 4	-15 ± 9	-9 ± 4	-8 ± 4	-8 ± 4	-8 ± 4
Ba-kaolinite	-7 ± 2	21 ± 5	-15 ± 2	-16 ± 2	-16 ± 2	-16 ± 2
Co-kaolinite	33 ± 6	144 ± 20	-11 ± 6	-12 ± 6	-14 ± 6	-15 ± 6
Cs-CI	-8 ± 3	31 ± 10	-17 ± 3	-18 ± 3	-18 ± 3	-18 ± 3
Ba-CI	-5 ± 3	39 ± 3	-17 ± 3	-17 ± 3	-18 ± 3	-18 ± 3
Co-CI	17 ± 3	102 ± 7	-14 ± 3	-15 ± 3	-16 ± 3	-17 ± 3
Cs-bentonite	-19 ± 4	-3 ± 13	-18 ± 4	-18 ± 4	-18 ± 4	-18 ± 4
Ba-bentonite	-8 ± 3	23 ± 4	-15 ± 3	-15 ± 3	-15 ± 3	-16 ± 3
Co-bentonite	11 ± 4	92 ± 11	-17 ± 4	-18 ± 4	-19 ± 4	-20 ± 4

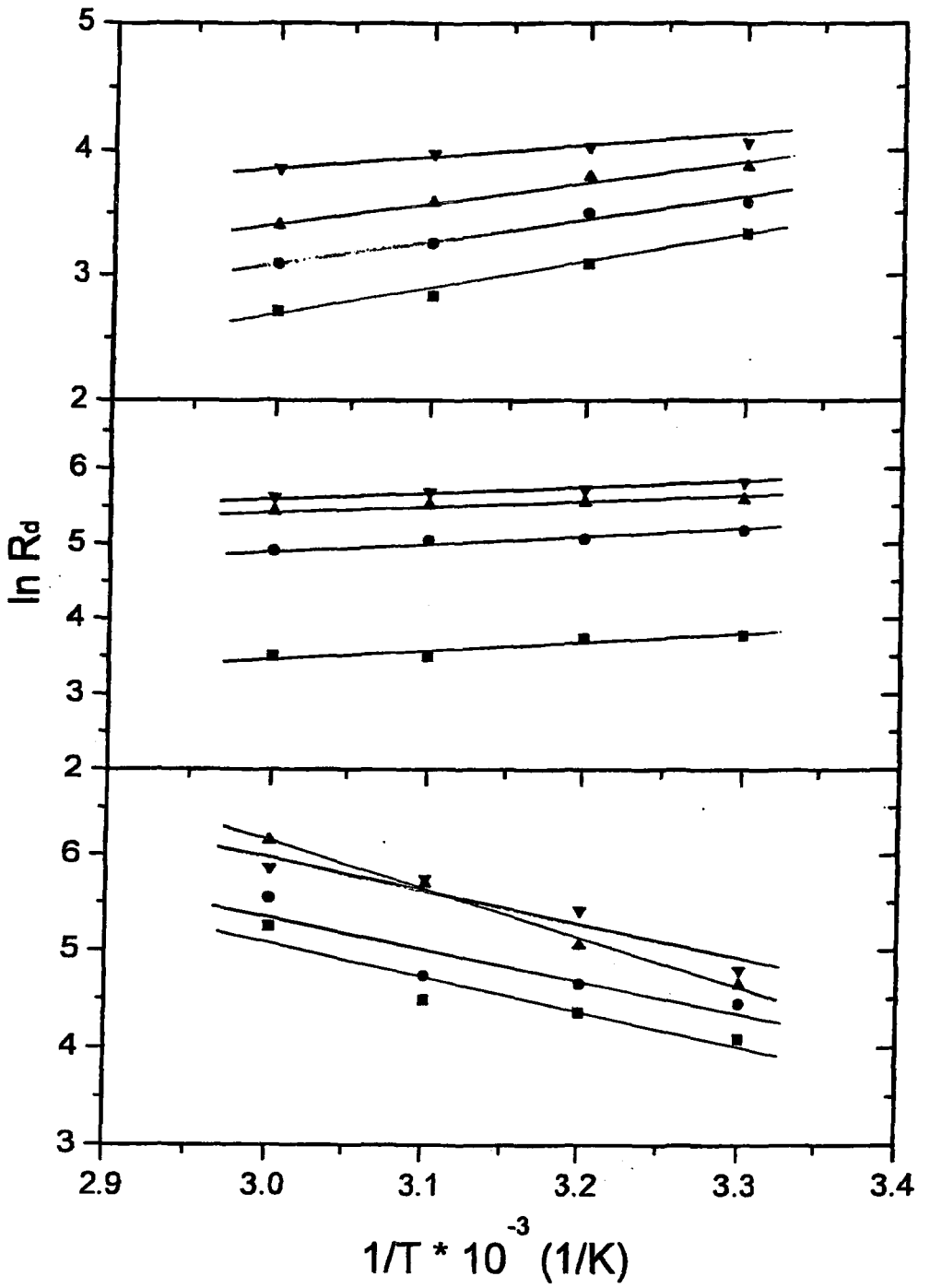

Fig. 4.22: Arrhenius Plots for Sorption of (a) Cs^+, (b) Ba^{2+}, and (c) Co^{2+} on Kaolinite

for Cs and Ba ■:1.0×10^{-3} (meq/ml) ●:1.0×10^{-4} (meq/ml) ▲:1.0×10^{-5} (meq/ml) ▼:1.0×10^{-6} (meq/ml)

for Co ■: 3.6×10^{-2} (meq/ml) ●:3.6×10^{-3} (meq/ml) ▲:3.6×10^{-4} (meq/ml) ▼:3.6×10^{-5} (meq/ml)

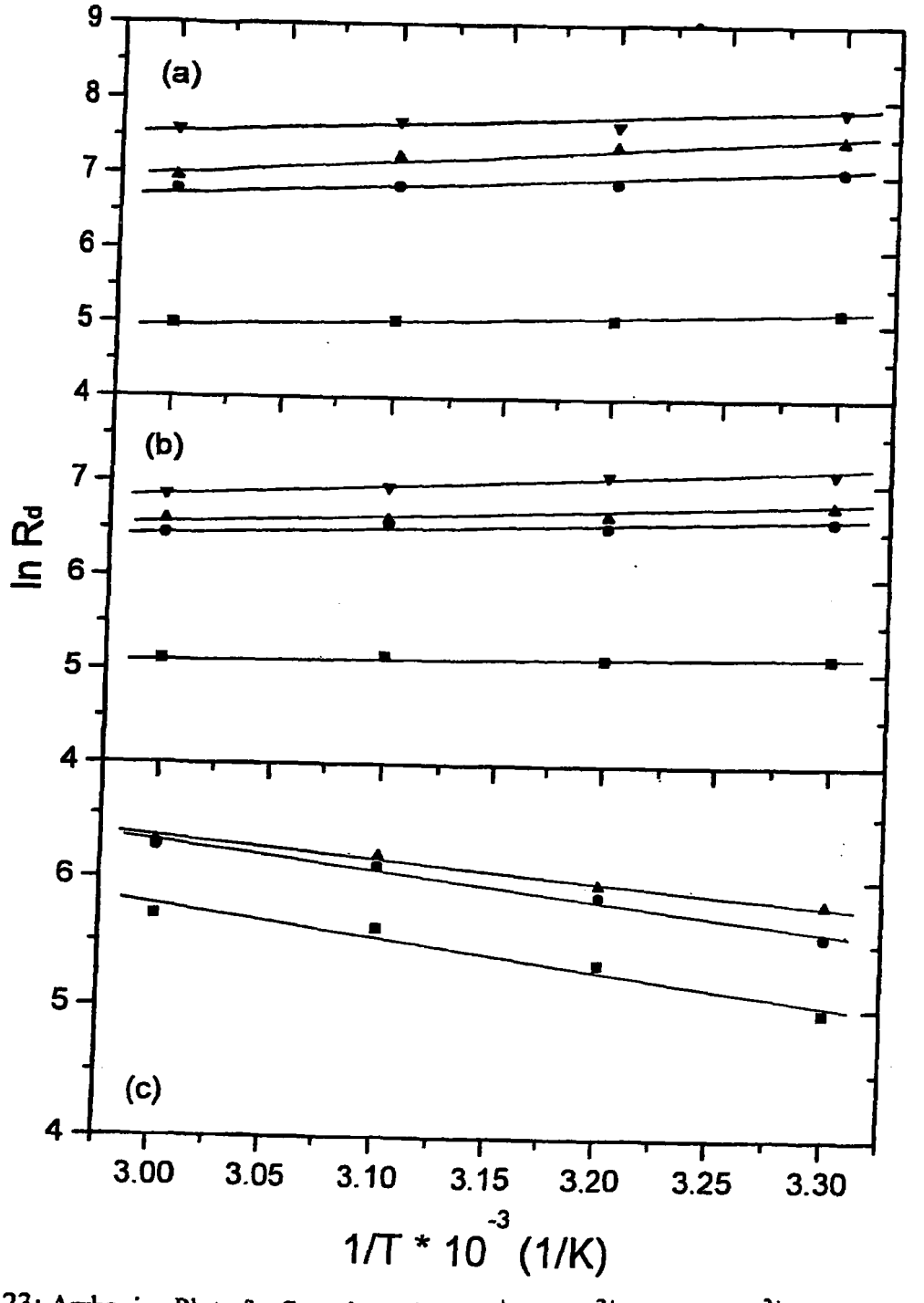

Fig. 4.23: Arrhenius Plots for Sorption of (a) Cs^+, (b) Ba^{2+}, and (c) Co^{2+} on Chlorite-Illite

for Cs and Ba ■:1.0×10^{-3} (meq/ml) ●:1.0×10^{-4} (meq/ml) ▲:1.0×10^{-5} (meq/ml) ▼:1.0×10^{-6} (meq/ml)

for Co ■: 3.6×10^{-2} (meq/ml) ●:3.6×10^{-3} (meq/ml) ▲:3.6×10^{-4} (meq/ml)

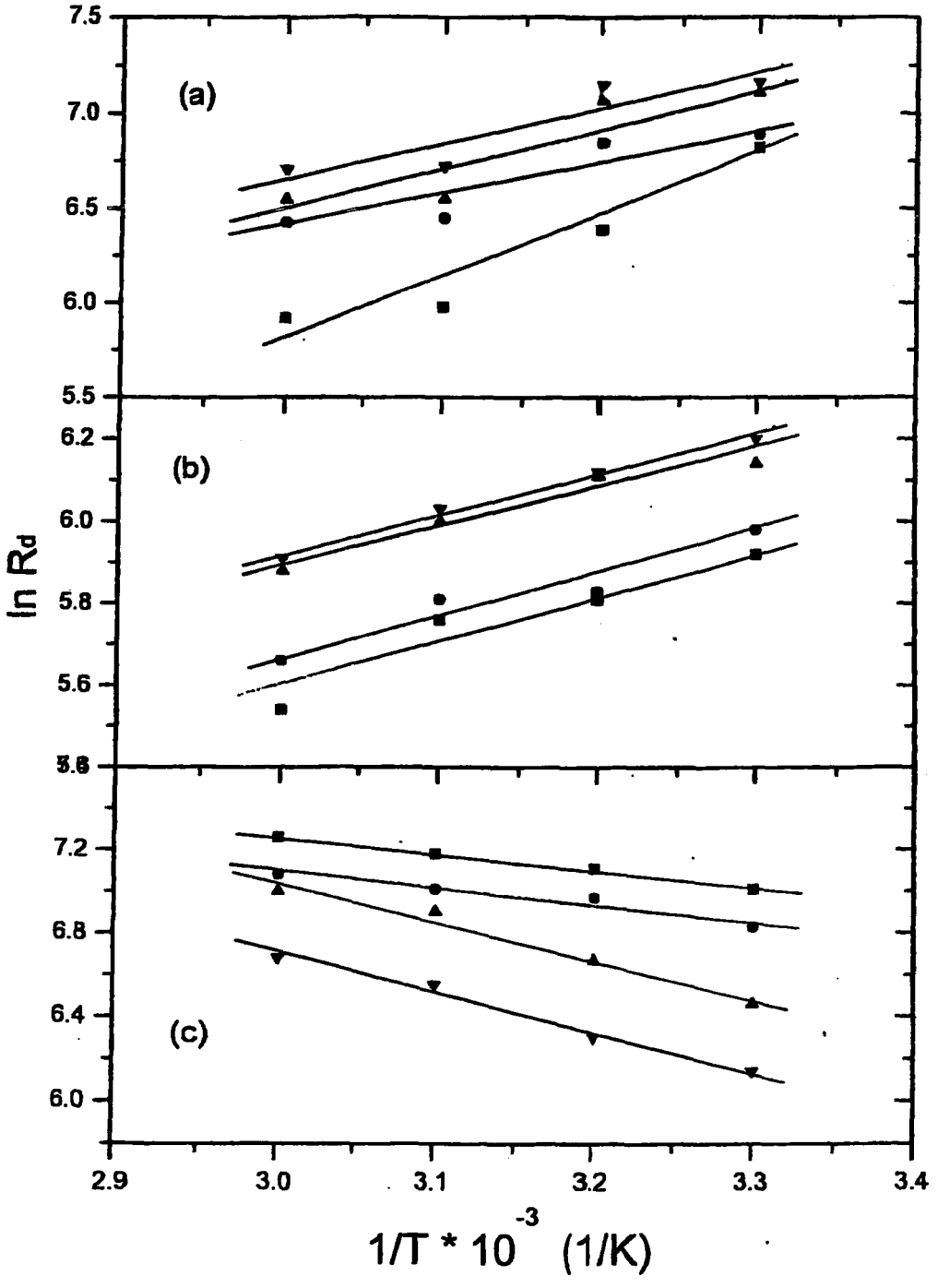

Fig. 4.24: Arrhenius Plots for Sorption of (a) Cs^+, (b) Ba^{2+}, and (c) Co^{2+} on Bentonite

■: 1.0×10^{-3} (meq/ml) ●: 1.0×10^{-4} (meq/ml)

▲: 1.0×10^{-5} (meq/ml) ▼: 1.0×10^{-6} (meq/ml)

4.3- Sorption Studies Using ToF-SIMS

ToF-SIMS is a surface sensitive technique that is applied to surface analysis of different kinds of materials. It is an ideal instrument for the characterization of complex molecular surfaces, the determination of surface composition and the detection of trace elements.

In our studies the aim was to quantify the surface composition prior to and following sorption of Cs^+, Ba^{2+}, and Co^{2+} on the natural clays. In addition to the uppermost surface, the analysis was extended to a total depth of 70 Å at intervals of 10, 20, 30, 40, 50, and 70 Å below surface using sputtering techniques. The quantitative analysis carried out in these studies enabled the determination of the depth profiles of the sorbed cations. In addition, the extent of depletion of various alkali and alkaline earth metals that are encountered in the clay structure were also determined.

An accurate quantitative analysis using ToF-SIMS requires both careful experiments and analysis of the experimental data. This stems from the fact that this technique could be subject to different instrumental and matrix effects that might affect the sensitivity of the measurements. Usually, the relative sensitivity corrections are believed to implicitly fold the errors created by instrumental effects (e.g. detector linearity, constancy of the spectrometer parameters) as long as the samples are analyzed under identical operating conditions. However, there are

situations were matrix effects are not fully compensated. Such situations arises, for example, in mixtures where the near surface concentration of oxygen and other chemically active elements which may be adsorbed from the environment or introduced by the primary ion beam may influence the secondary ion yield [64]. Incorporation of oxygen atoms in the sample surface is expected to enhance the yield of singly charged sputtered positive ions because of its electronegativity effects on ion-surface electron exchange [65]. Furthermore, the implantation of Ga_2^+ ions on the analyzed sample by the Ga^+ primary ion beam causes interference of Ga_2^+ (A=138) with the major isotope of Ba (71.7%) having the same mass number [66]. Furthermore, poorly conducting materials usually suffer from the problem of charging, i.e. the buildup of positive charge on the analyzed surface as a result of bombardment by the primary ion beam. Charge buildup during analysis can cause secondary ions with narrow energy distributions (e.g. alkali metals, alkaline earths) to shift outside the optimum transmittance window of the spectrometer thus lowering their yield [64]. In our experiments, the limitations arising from the charging effects were minimized by using an electron gun to flood the surface with low energy electrons thus compensating for the deposited positive charge. Sputtering was performed at several points to minimize the effect of any surface heterogeneity.

A careful methodology of analysis of the experimental data was followed in order to minimize the effect of any non-avoidable matrix error that could affect the sensitivity of the measurements. First, the peak intensities considered were the ones

corresponding to the major isotopes of different elements. For elements in which the major isotopes could be contaminated by foreign isotopes, the next major isotopes were considered in the calculations. Examples of such elements are Ba, Fe, Ca, and Mg. As stated previously, the major Ba isotope (^{138}Ba) is usually contaminated with Ga_2^+ originating from the primary ion beam of Ga^+ used for sputtering. This interference was confirmed by calculating the ratio of peak intensities of ^{138}Ba to those of other Ba isotopes and comparing with the natural isotopic ratios. Consequently other Ba isotopes were used in the calculations (^{137}Ba and ^{134}Ba) and correction to 100% abundance was performed. The same test was followed for other elements as well. Following this, the obtained intensities were corrected using the corresponding relative sensitivity factors (RSF). Table 4.6 gives the isotopes of different elements in the clays, together with the relative sensitivity factors of these elements. The RSF's used in the calculations were the ones presented by Sparrow, 1977 [67]. The Sparrow sensitivity factors takes into consideration many factors among which are the electronegativity, electron affinity, ionization potential, and mass of the secondary ions, mass and energy of primary ions. Following the RSF corrections the ratios of different elements relative to those of Al+Si were calculated. Both of Al and Si are 'skeletal' elements in the clay matrix that are not expected to take part in any exchange process with a sorbed cation. Ratios of the elements were calculated also relative to Si and Al separately, but the ratios relative to Al+Si gave the best results. By calculating those ratios, any differences arising from different count times of the samples were eliminated and a basis for comparing the elemental contents of the clays before and after sorption was established. The

Si/Al ratios before and after sorption for some clays have shown some serious fluctuations following sorption. This was most pronounced in the case of Co^{2+} sorption on chlorite-illite and bentonite, where the fluctuations were about 20% of the original ratio (that corresponding to unexchanged clays). This apparent increase of the Si/Al ratio in the exchanged clay would mean a depletion of some Al upon sorption. However, upon examining the aqueous phase of the mixtures following sorption, using Atomic Absorption Spectroscopy (AAS), no Al was detected. Similar anomalies were also observed for Fe, which is also believed to be a structural element of clays. The AAS measurements showed no Fe in the aqueous phase after sorption. This apparent depletion of Al and Fe after sorption probably indicates a decrease in the probability of both elements being ionized upon sputtering. The Al^{3+} and Fe^{n+} (n =2 or 3) ions could be shielded by the sorbed ions located in their vicinity. It is possible that the sorbed ions are held by the coordinatively unsaturated O^{2-} ions (exposed on the surface) that participate in the coordination sphere of Al and Fe so that the $-O_xM$ (M: sorbed ion) formed phase hinders the ionization of both elements. In literature, it is reported that there is a strong correlation between the amount of sorbed Cs^+ and areas of aluminosilicates where Al is prevalent [68,69]. If it is assumed that the same applies for Ba^{2+} and Co^{2+} as well, then the hinderance of Al ionization mentioned above is supported. In the case of alkali and alkaline earth metals, their depletions were confirmed by AAS measurements. In order to normalize with respect to Si/Al ratio variations, elemental values relative to Al+Si contents, were multiplied with correction factors found by taking the ratio of Si/Al before sorption to that after sorption for each measurements.

In the elemental content considerations only alkali and alkaline elements which are believed to be major exchanging cations were taken into account in sorption studies.

Table 4.6: The elements considered in ToF-SIMS calculations, their relative sensitivity factors and natural stable isotopes

Element	RSF	Natural Isotope(s)	% Abundance
Li	3500	^{6}Li, ^{7}Li	7.4, 92.6
Na	2000	^{23}Na	100
Mg	160	^{24}Mg, ^{25}Mg, ^{26}Mg	78.6, 10.1, 11.3
Al	120	^{27}Al	100
Si	27	^{28}Si, ^{29}Si, ^{30}Si	92.2, 4.7, 3.1
K	1800	^{39}K, ^{41}K	93.1, 6.9
Ca	250	^{40}Ca, ^{42}Ca, ^{43}Ca, ^{44}Ca, ^{46}Ca, ^{48}Ca	97.0, 0.6, 0.1, 2.1, 0.003, 0.2
Fe	21	^{54}Fe, ^{56}Fe, ^{57}Fe, ^{58}Fe	5.8, 91.7, 2.2, 0.3
Cs	600	^{113}Cs	100
Ba	90	^{132}Ba, ^{134}Ba, ^{135}Ba, ^{136}Ba, ^{137}Ba, ^{138}Ba	0.1, 2.4, 6.6, 7.8, 11.3, 71.7
Co	23	^{59}Co	100

4.3.1- Analysis of the Exchanged Ions Based on ToF-SIMS Measurements

The tendency of a certain cation initially present in the natural clay to exchange (or be depleted) upon sorption of Cs^+, Ba^{2+}, and Co^{2+} at a particular depth is represented by its corresponding depletion factor , DF, as was previously described by Equation 2.23. In this sense, the magnitude of DF is related to the affinity of a particular cation towards exchange with the sorbed ion. Its highest value of unity indicates complete exchange, and lowest value of zero indicates no exchange with the sorbed cation. ToF-SIMS analysis showed that upon sorption Cs^+, Ba^{2+}, and Co^{2+} ions on kaolinite and chlorite-illite, the major exchanging ions were K^+, Mg^{2+}, and Ca^{2+}. In the case of sorption on bentonite, however, the exchanging ions were mainly Na^+ and Mg^{2+}. The DF values of these ions are given in Appendix D (Tables D1, D2, and D3) and plotted in Figs. 4.25, 4.26, and 4.27 for sorption on kaolinite, chlorite-illite and bentonite, respectively. The fits in the figures are used to guide the eye. The data show that in kaolinite and chlorite-illite sorption cases while the DF values of Mg^{2+} and Ca^{2+} decrease as depth is increased, those of K^+ does not show a consistent behavior probably stemming from its higher mobility compared to Mg^{2+} and Ca^{2+} ions. Another trend that can be observed is that the depletion of the three cations is generally larger in the case of Co^{2+} sorption as compared with Cs^+ and Ba^{2+} sorption. Compared with Mg^{2+}, Na^+ seems to have larger exchange affinity with sorbed cations among which Co^{2+} appears to have the largest replacing ability in the case of bentonite sorption.

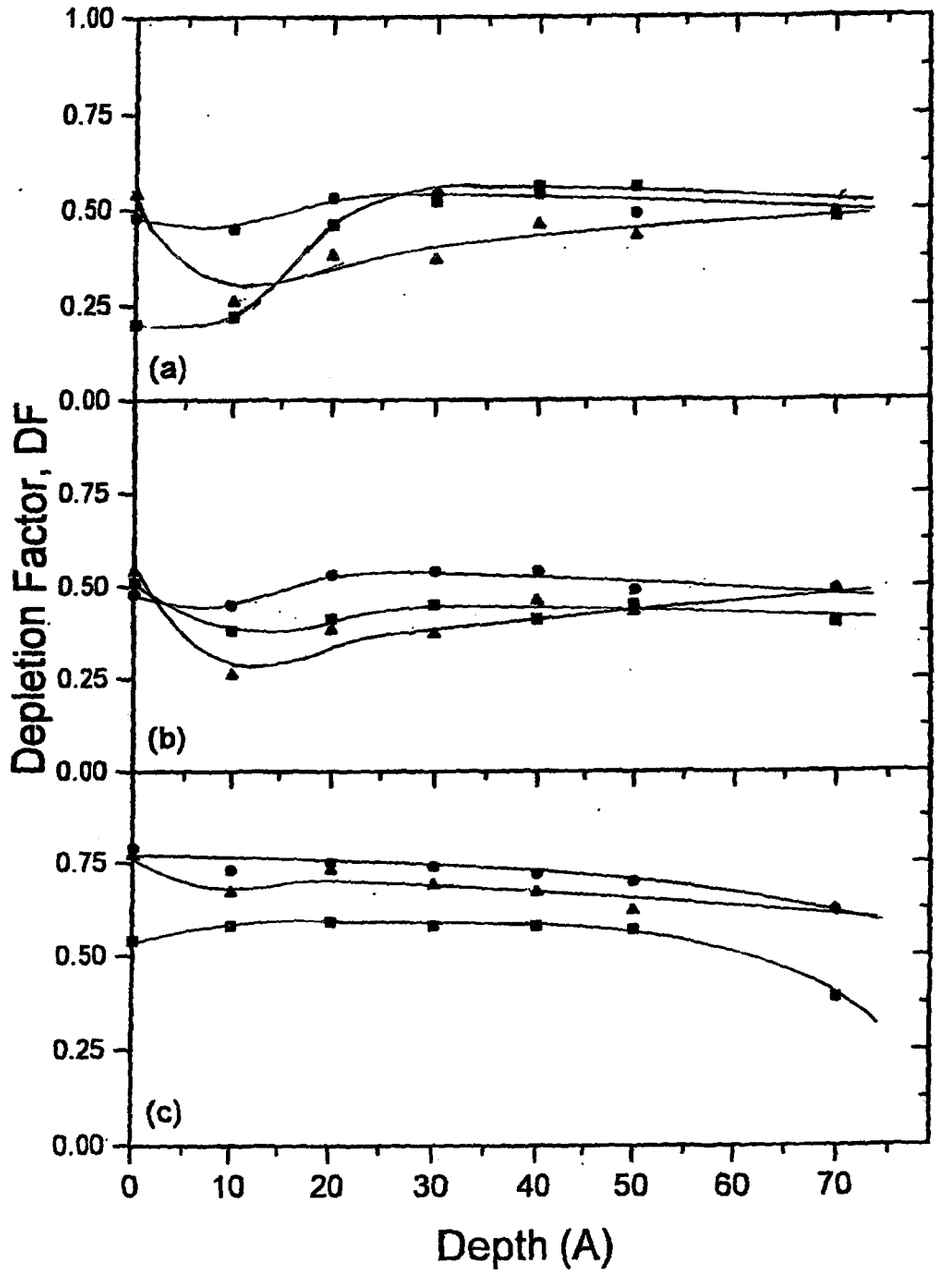

Fig. 4.25: Variation of DF values of (a) K^+, (b) Mg^{2+}, and (c) Ca^{2+} as a function of depth in kaolinite matrix for the sorption cases of;

■: Cs^+ ●: Ba^{2+} ▲:Co^{2+}

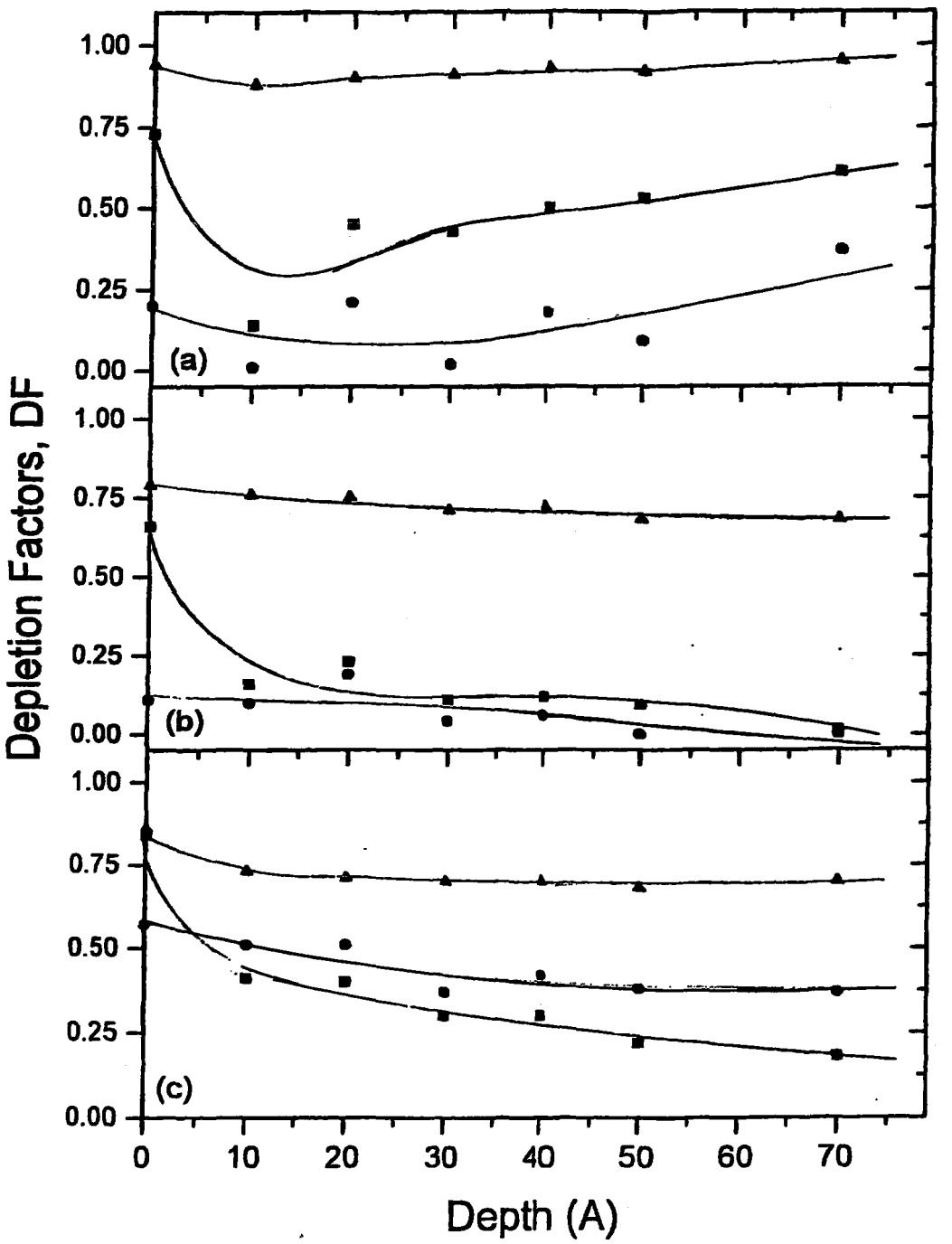

Fig. 4.26: Variation of DF values of (a) K^+, (b) Mg^{2+}, and (c) Ca^{2+} as a function of depth in chlorite-illite matrix for the sorption cases of;

■: Cs^+ ●: Ba^{2+} ▲: Co^{2+}

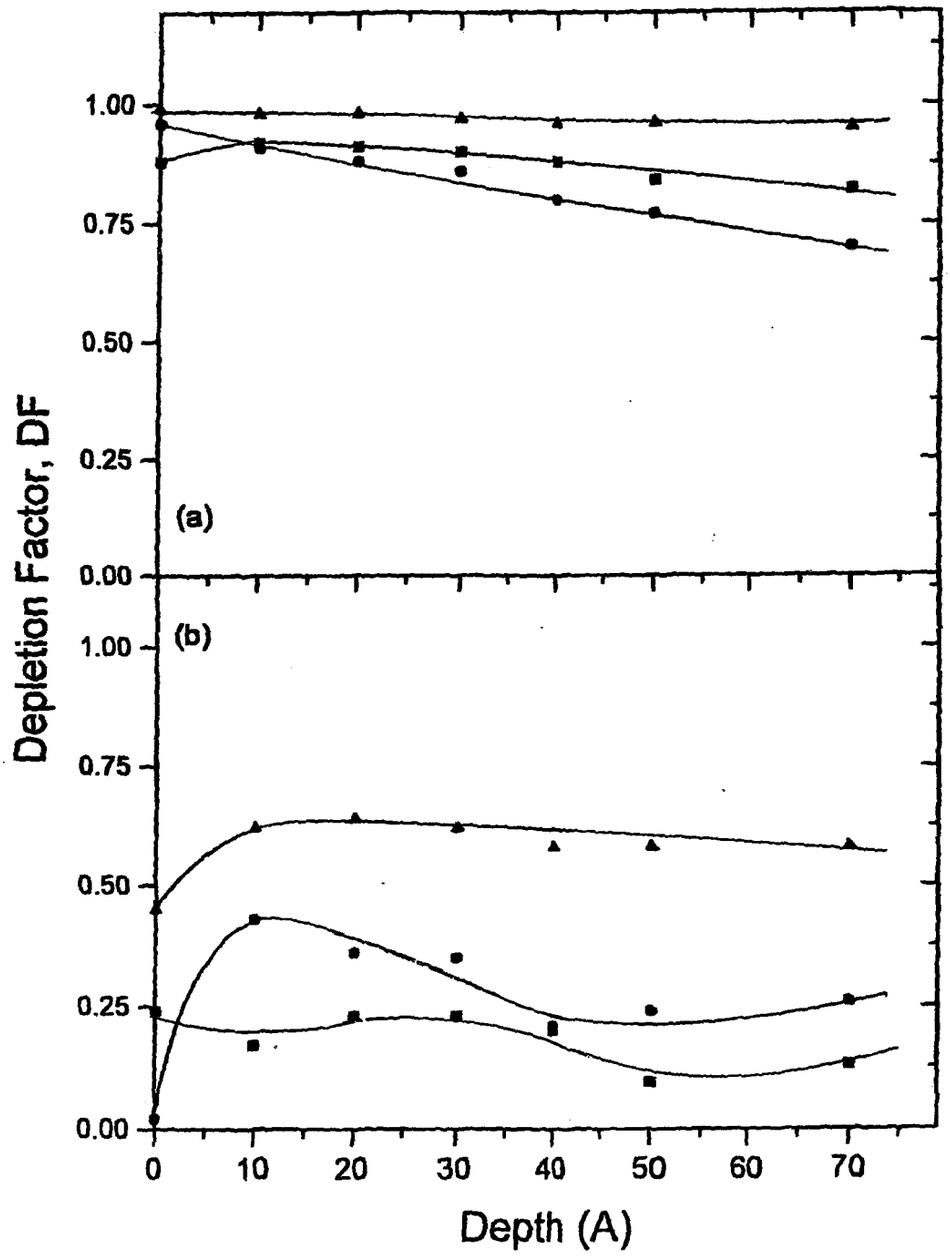

Fig. 4.27: Variation of DF values of (a) Na^+, and (b) Mg^{2+} as a function of depth in bentonite matrix for the sorption cases of;

■: Cs^+ ●: Ba^{2+} ▲:Co^{2+}

The initial and final contents of each depleted cation, its equivalent depleted amounts and its percentage contribution the total depletion (D_x) at each depth are given in Tables 4.7. 4.8, and 4.9 for sorption cases on kaolinite, chlorite-illite, and bentonite, respectively. The initial content of a particular cation refers to its content in the natural clay, (R_i), while the final content is that in the exchanged clay, R_f. The depleted amount of cation x in equivalents is calculated by multiplying the difference $[(R_i)_x-(R_f)_x]$ by z_x, the charge of cation x and is defined as the Equivalent Depleted Amount (EDA). As the name implies, the percentage contribution to the total depletion, D_x, for cation x at each depth is a value that quantitatively reflects the share of that cation in the total depletion (exchange) upon sorption. D_x for each cation was calculated using equation (2.24) which was given earlier.

In the case of kaolinite sorption, the D_x values for K^+, Mg^{2+}, and Ca^{2+} show that while Ca^{2+} contribution is higher near the uppermost surface, that of K^+ becomes more significant in the deeper sites. The behavior of Mg^{2+} tends -to a certain extent- to resemble that of Ca^{2+}. While K^+ shows higher contribution in the cases of Cs^+ and Ba^{2+} sorption, Mg^{2+} contributes most in Co^{2+} sorption case.

In chlorite-illite sorption, Ca^{2+} shows the highest contribution to total exchange in all cases. Like in the case of kaolinite, whereas the depletion of Ca^{2+} and Mg^{2+} decreases with increasing depth, that of K^+ shows a reversed order. This behavior may be related with the fact that in both natural clays while the initial

contents of Ca^{2+} and Mg^{2+} decrease with increasing depth that of K^{+} increases. It is important to note that the depletion of the three cations increases significantly in the case of Co^{2+} sorption indicating a poorer ability of those cations to compete with Co^{2+} for sorption sites compared with Cs^{+} and Ba^{2+}.

In bentonite, Na^{+} shows a higher contribution at the uppermost surface whereas the Mg^{2+} contribution becomes more significant towards the deeper sites. This behavior of Mg^{2+} is in line with the fact that whereas the initial Mg^{2+} content in kaolinite and chlorite illite natural clays decreases as depth is increased, it shows an increase in natural bentonite. On the average, Mg^{2+} ions contribute more to the total exchange than Na^{+} ions. While the contribution of both is comparable in Cs^{+} and Ba^{2+} ion sorption, that of Mg^{2+} highly surpasses the Na^{+} contribution in the case of Co^{2+} sorption.

Table 4.7: The initial and final ratios of cation/(Al+Si), R_i and R_f, the Equivalent Depleted Amounts (EDA), and the percentage contribution to total depletion, D_x, as a function of depth for the sorption of Cs^+, Ba^{2+}, and Co^{2+} on kaolinite. All calculations are based on ToF-SIMS measurements

			Cs-kaolinite			Ba-kaolinite			Co-kaolinite		
Cation	Depth(A)	R_I	R_f	EDA	D_x	R_f	EDA	D_x	R_f	EDA	D_x
K^+	0	0.0131	0.0105	0.0026	4.88	0.0068	0.0063	9.42	0.0061	0.0070	9.21
	10	0.0275	0.0215	0.0060	23.26	0.0151	0.0124	35.84	0.0202	0.0073	21.28
	20	0.0314	0.0169	0.0145	44.34	0.0148	0.0166	46.11	0.0195	0.0119	33.90
	30	0.0314	0.0152	0.0162	45.76	0.0145	0.0169	46.30	0.0199	0.0115	32.76
	40	0.0313	0.0137	0.0176	50.58	0.0144	0.0169	49.85	0.0168	0.0145	40.62
	50	0.0292	0.0172	0.0120	57.14	0.0149	0.0143	45.11	0.0165	0.0127	37.68
	70	0.0277	0.0143	0.0134	49.63	0.0141	0.0136	48.23	0.0141	0.0136	40.72
Total				0.0823			0.0970			0.0785	
Mg^{2+}	0	0.0239	0.0116	0.0246	46.25	0.0127	0.0224	33.48	0.0079	0.0320	42.11
	10	0.0143	0.0089	0.0108	41.86	0.0088	0.0110	31.79	0.0060	0.0166	48.40
	20	0.0124	0.0074	0.0100	30.58	0.0079	0.0090	25.00	0.0059	0.0130	37.04
	30	0.0126	0.0070	0.0112	31.64	0.0078	0.0096	26.30	0.0055	0.0142	40.46
	40	0.0120	0.0071	0.0098	28.16	0.0081	0.0078	23.01	0.0057	0.0126	35.29
	50	0.0128	0.0107	0.0042	20.00	0.0083	0.0090	28.39	0.0060	0.0136	40.36
	70	0.0125	0.0075	0.0100	37.04	0.0081	0.0088	31.21	0.0055	0.0140	41.91
Total				0.0806			0.0776			0.1160	
Ca^{2+}	0	0.0241	0.0111	0.0260	48.87	0.0050	0.0382	57.10	0.0056	0.0370	48.68
	10	0.0077	0.0032	0.0090	34.88	0.0021	0.0112	32.37	0.0025	0.0104	30.32
	20	0.0070	0.0029	0.0082	25.08	0.0018	0.0104	28.89	0.0019	0.0102	29.06
	30	0.0068	0.0028	0.0080	22.60	0.0018	0.0100	27.40	0.0021	0.0094	26.78
	40	0.0064	0.0027	0.0074	21.26	0.0018	0.0092	27.14	0.0021	0.0086	24.09
	50	0.0060	0.0036	0.0048	22.86	0.0018	0.0084	26.50	0.0023	0.0074	21.96
	70	0.0047	0.0029	0.0036	13.33	0.0018	0.0058	20.57	0.0018	0.0058	17.37
Total				0.0670			0.0932			0.0888	

Table 4.8: The initial and final ratios of cation/(Al+Si), R_i and R_f, the Equivalent Depleted Amounts (EDA), and the percentage contribution of each exchanging cation to total depletion, D_x, as a function of depth for the sorption of Cs^+, Ba^{2+}, and Co^{2+} ions on chlorite-illite (CI). All calculations are based on ToF-SIMS measurements

			Cs-CI			Ba-CI			Co-CI		
Cation	Depth(A)	R_I	R_f	EDA	D_x	R_f	EDA	D_x	R_f	EDA	D_x
K^+	0	0.0060	0.0016	0.0046	3.09	0.0048	0.0012	1.73	0.0004	0.0056	3.41
	10	0.0158	0.0135	0.0023	4.38	0.0157	0.0001	0.19	0.0019	0.0139	8.93
	20	0.0214	0.0117	0.0097	15.28	0.0168	0.0046	7.23	0.0022	0.0192	12.55
	30	0.0226	0.0130	0.0096	20.43	0.0221	0.0005	1.62	0.0020	0.0206	14.39
	40	0.0236	0.0118	0.0118	25.65	0.0192	0.0044	10.00	0.0017	0.0219	14.99
	50	0.0241	0.0113	0.0131	34.20	0.0220	0.0021	6.54	0.0019	0.0222	16.14
	70	0.0281	0.0109	0.0172	54.09	0.0176	0.0105	26.85	0.0015	0.0266	19.56
Total				0.0683			0.0234			0.1300	
Mg^{2+}	0	0.0446	0.0151	0.0590	39.65	0.0397	0.0098	14.12	0.0093	0.0706	43.05
	10	0.0463	0.0388	0.0150	28.57	0.0415	0.0096	18.15	0.0110	0.0706	45.34
	20	0.0442	0.0338	0.0202	32.75	0.0356	0.0172	27.04	0.0113	0.0658	43.01
	30	0.0402	0.0358	0.0088	18.72	0.0400	0.0004	1.29	0.0115	0.0574	40.08
	40	0.0408	0.0359	0.0098	21.30	0.0383	0.0050	11.36	0.0114	0.0588	40.25
	50	0.0390	0.0353	0.0074	19.32	0.0396	0	0	0.0124	0.0532	38.66
	70	0.0357	0.0352	0.0010	3.14	0.0350	0	0	0.0114	0.0486	35.44
Total				0.1218			0.0420			0.4250	
Ca^{2+}	0	0.0509	0.0083	0.0852	57.26	0.0217	0.0584	84.15	0.0070	0.0878	53.54
	10	0.0427	0.0251	0.0352	67.05	0.0211	0.0432	81.66	0.0071	0.0712	45.73
	20	0.0416	0.0251	0.0330	51.97	0.0207	0.0418	65.73	0.0076	0.0680	44.44
	30	0.0406	0.0263	0.0286	60.85	0.0256	0.0300	77.09	0.0080	0.0652	45.53
	40	0.0409	0.0287	0.0244	53.05	0.0236	0.0346	78.64	0.0082	0.0654	44.76
	50	0.0399	0.0310	0.0178	46.48	0.0249	0.0300	93.46	0.0088	0.0622	45.20
	70	0.0388	0.0320	0.0136	42.77	0.0245	0.0286	73.15	0.0084	0.0608	44.70
Total				0.2378			0.2668			0.4736	

Table 4.9: The initial and final ratios of cation/(Al+Si), R_i and R_f, the Equivalent Depleted Amounts (EDA), and the percentage contribution to total depletion, D_x, as a function of depth for the sorption of Cs^+, Ba^{2+}, and Co^{2+} on bentonite. All calculations are based on ToF-SIMS measurements

			Cs-bentonite			Ba-bentonite			Co-bentonite		
Cation	Depth(A)	R_I	R_f	EDA	D_x	R_f	EDA	D_x	R_f	EDA	D_x
Na^+	0	0.0419	0.0049	0.0370	62.29	0.0017	0.0402	96.17	0.0002	0.0417	50.67
	10	0.0309	0.0024	0.0285	60.51	0.0026	0.0283	37.88	0.0008	0.0301	30.87
	20	0.0221	0.0019	0.0202	44.49	0.0026	0.0195	32.77	0.0005	0.0216	23.18
	30	0.0165	0.0016	0.0149	37.16	0.0023	0.0142	42.77	0.0005	0.0161	19.24
	40	0.0125	0.0015	0.0110	35.71	0.0025	0.0100	82.26	0.0005	0.0120	17.00
	50	0.0102	0.0016	0.0086	47.78	0.0024	0.0078	24.68	0.0004	0.0098	14.89
	70	0.0016	0.0016	0.0070	34.65	0.0026	0.0060	18.40	0.0004	0.0082	12.46
Total				0.1272			0.1260			0.1395	
Mg^{2+}	0	0.0456	0.0344	0.0224	37.71	0.0448	0.0016	8.83	0.0253	0.0406	49.33
	10	0.0546	0.0453	0.0186	39.49	0.0314	0.0464	62.12	0.0209	0.0674	69.13
	20	0.0556	0.0430	0.0252	56.51	0.0356	0.0400	67.23	0.0198	0.0716	76.82
	30	0.0544	0.0418	0.0252	62.84	0.0354	0.0190	57.23	0.0206	0.0676	80.76
	40	0.0504	0.0405	0.0198	64.29	0.0399	0.0210	67.74	0.0211	0.0586	83.00
	50	0.0487	0.0440	0.0094	52.22	0.0368	0.0238	75.32	0.0207	0.0560	85.11
	70	0.0496	0.0430	0.0132	65.35	0.0363	0.0266	81.60	0.0208	0.0576	87.54
Total				0.1338			0.1784			0.4194	

4.3.2- Analysis of the Sorbed Cations Based on ToF-SIMS Measurements

Typical ToF-SIMS spectra of kaolinite, chlorite-illite, and bentonite are given in Figs 4.28, 4.29, 4.30, respectively. The inset in each figure shows the variation of Cs^+, Ba^{2+}, and Co^{2+} signals at different depths in clay structure. The amounts of sorbed cations as a function of depth in clays are given in Table 4.10 and drawn in Figs 4.31, 4.32, 4.33.

The amounts of the sorbed cations as a function of kaolinite matrix depth indicate higher sorption on the uppermost clay surface. The percentage of cation sorbed by the uppermost surface to its total sorbed amount is 43, 20, and 28 for Cs^+, Ba^{2+}, and Co^{2+} sorption, respectively. The sorbed amounts decreases with increasing depth and the sharpest decrease occur in the case of Cs^+ sorption.

Unlike the case of kaolinite sorption, the amounts of the sorbed cations as a function of chlorite-illite matrix depth show that only Ba^{2+} have a distinctly large fraction (22.1% of the total amount sorbed) sorbed on the uppermost clay surface.

The sorption profiles of Cs^+, Ba^{2+}, and Co^{2+} on bentonite resembles those of chlorite illite with the exception that the decrease in Cs^+ sorbed amounts across depth in bentonite is more pronounced. Like its depth profiles on kaolinite and chlorite-illite, large amounts of Ba^{2+} are fixed by uppermost surface sites (23.8% of the total sorbed amount). Based on the values given in Table 4.10 and Figs. 4.31,

4.32, and 4.33, the sorption order on the clays at room temperature is; $Co^{2+} \geq Ba^{2+} > Cs^{+}$ for sorption on kaolinite and chlorite-illite and $Ba^{2+} > Cs^{+} > Co^{2+}$ for sorption on bentonite.

Table 4.10: The amounts of sorbed Cs^{+}, Ba^{2+}, and Co^{2+} (relative to Al+Si) as a function of depth in kaolinite, chlorite-illite (CI), and bentonite matrices obtained from ToF-SIMS measurements

Sorbent Clay	Sorbed Cation	Amount of Cation/(Al+Si) at Different Depths (Å)						
		0	10	20	30	40	50	70
Kaolinite	Cs^{+}	0.073	0.021	0.016	0.014	0.012	0.011	0.012
	Ba^{2+}	0.075	0.055	0.047	0.049	0.047	0.051	0.048
	Co^{2+}	0.112	0.065	0.053	0.047	0.045	0.043	0.037
CI	Cs^{+}	0.033	0.059	0.045	0.045	0.038	0.035	0.033
	Ba^{2+}	0.088	0.056	0.048	0.054	0.053	0.050	0.050
	Co^{2+}	0.064	0.064	0.063	0.060	0.058	0.059	0.051
Bentonite	Cs^{+}	0.043	0.066	0.053	0.047	0.044	0.046	0.043
	Ba^{2+}	0.097	0.052	0.045	0.050	0.058	0.053	0.054
	Co^{2+}	0.055	0.043	0.036	0.034	0.034	0.034	0.031

Table 4.11 gives the total equivalent sorbed amounts (Σ ESA) of Cs^{+}, Ba^{2+}, and Co^{2+} -obtained by summing the sorbed amounts and multiplying the total with the corresponding charge of the ion- and the total equivalent depleted amounts, (Σ EDA) of exchanged cations in kaolinite, chlorite-illite, and bentonite. If these values are compared based on the assumption that the depletion in each sorption case takes place solely as a result of an ion exchange process with the sorbed ion, then a quantification of the share of the ion exchange mechanism in sorption can be made.

The ion exchange concept in general refers to the tendency of a surface to sorb a certain cation over another. A pH-independent ion exchange corresponds to the case where the sorbed ion exchanges with alkali and alkaline-earth ions present in the clay to balance the negative charge arising from isomorphous substitution. Table 4.11 shows that the total sorbed amounts distinctly exceeds the total depleted amounts in most of sorption cases indicating the existence of a sorption mechanism other than the pH-independent ion exchange. In some cases, however, the total depleted amounts exceeds the total sorbed amount leading to a positive deviation of about 25 percent. In terms of electrical neutrality, such a situation is puzzling and could probably be referred to experimental errors. In addition to pH-independent ion exchange, the sorption process is believed to occur via other complementary mechanisms among which is the pH-dependent ion exchange mechanism. The exchange of cations takes place when the operating pH is larger than the IEP of the clay surface. The IEP of the clays used in these studies (< 4.2) -which were discussed early in this chapter- are below the operating pH (6.97-8.23) of the experiments. Thus, it is expected that surfaces of the clays be negatively charged in the pH range, within which our sorption experiments were performed. Hence, sorption can occur as a result of interactions of sorbed ions with the AlO^- and SiO^- sites created as a result of the deprotonation of the acidic hydroxyl groups. The extent of such protonation is dependent on the acidity of the hydroxyl groups. This type of sorption is sometimes referred to as 'hydrolytic adsorption' and can be described by the following equation [1]:

$$\text{surface-OH} + M^{n+} \rightarrow \text{surface-O-}M^{(n-1)+} + H^+$$

The reaction could be figured out as an ion exchange reaction that takes place when the sorbed ion is in its unhydrolyzed form (either as a bare or hydrated ion). Of particular importance is also the kind of sorption that can occur on the coordinatively unsaturated O^{2-} groups that are exposed at the clay surface and that can complete their coordination sphere by holding the sorbed ion (M^{n+}) as $-O_xM$ groups.

To summarize, the sorption process can be viewed as an ion exchange process that is mainly pH-independent. The contribution of the pH-dependent ion exchange, or any other mechanism like precipitation, physical sorption, etc, varies with the operating pH and is in part related to the sorbed ion and the nature of the clay.

Table 4.11: The total equivalent sorbed amounts (ΣESA) of Cs^+, Ba^{2+}, and Co^{2+} and the total equivalent depleted amounts (Σ EDA) of depleted cations for sorption on kaolinite, chlorite-illite, and bentonite obtained from ToF-SIMS measurements

Sorbent Clay	Sorbed Ion	Σ ESA	Σ EDA
Kaolinite	Cs^+	0.16	0.230
	Ba^{2+}	0.74	0.268
	Co^{2+}	0.80	0.283
Chlorite-Illite	Cs^+	0.29	0.428
	Ba^{2+}	0.80	0.332
	Co^{2+}	0.84	1.029
Bentonite	Cs^+	0.34	0.261
	Ba^{2+}	0.82	0.304
	Co^{2+}	0.53	0.559

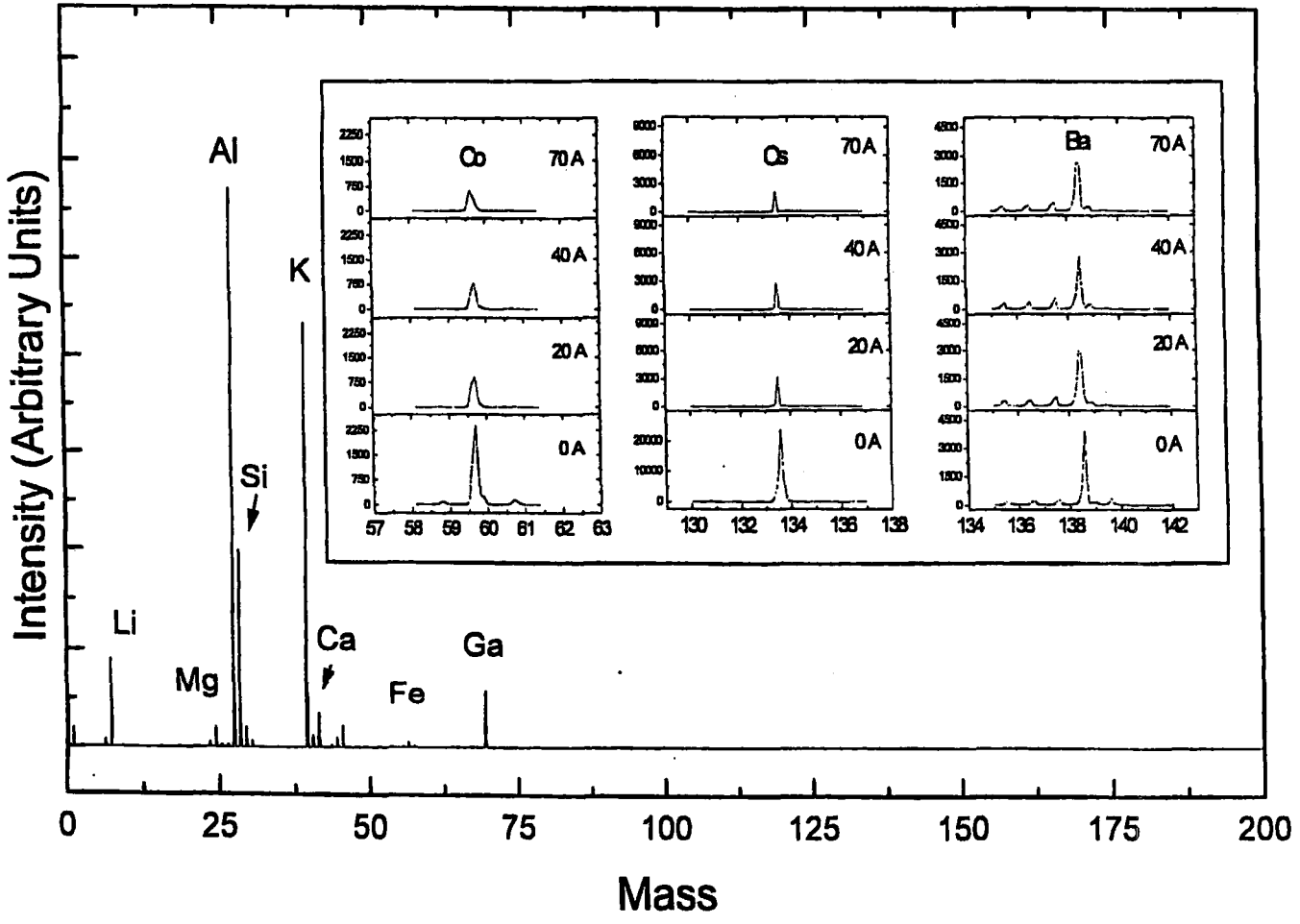

Fig. 4.28: A typical ToF-SIMS spectrum of kaolinite. The inset in the figure shows the variation of Cs^{+}, Ba^{2+}, and Co^{2+} signal intensity with depth

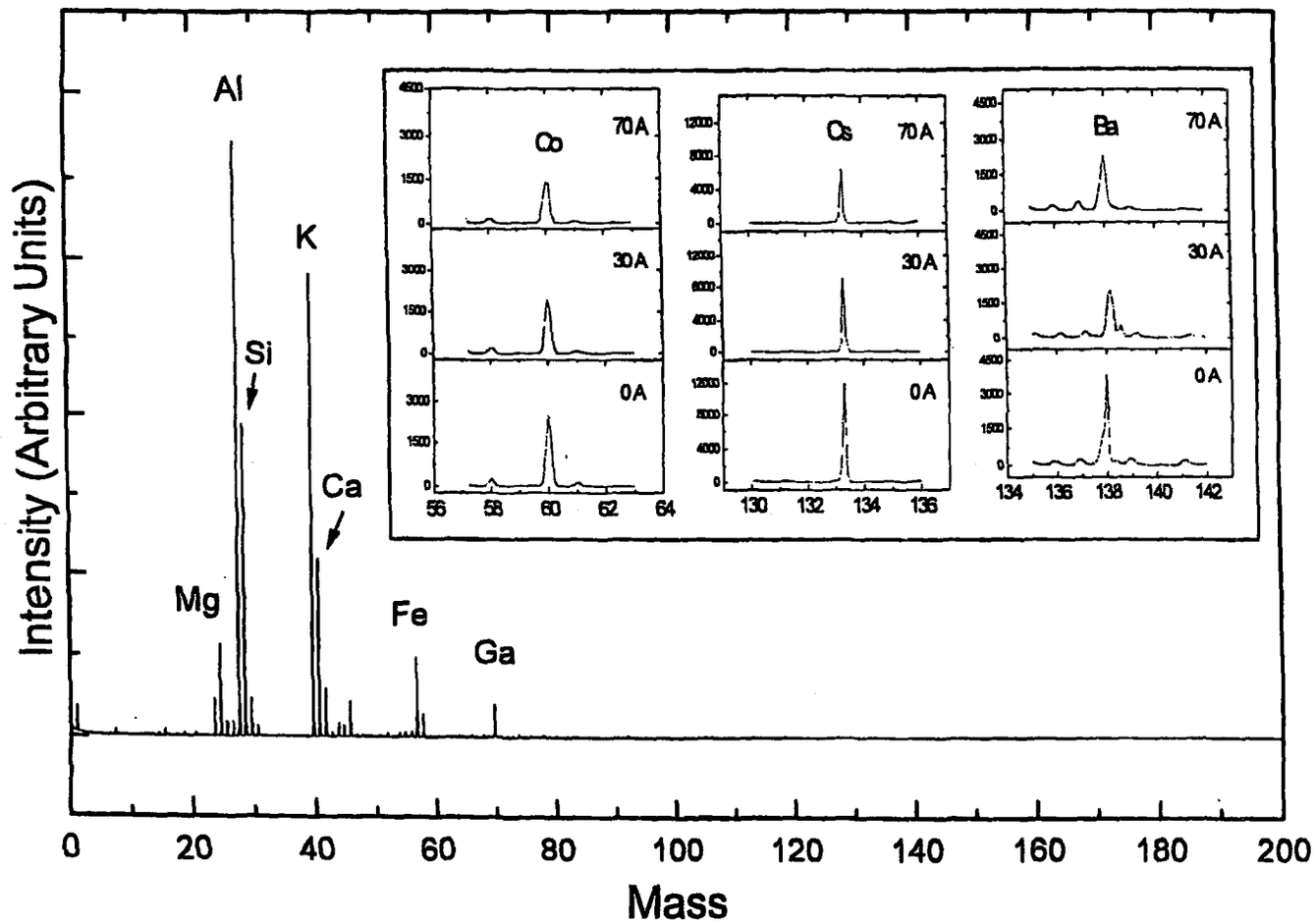

Fig. 4.29: A typical ToF-SIMS spectrum of chlorite-illite. The inset in the figure shows the variation of Cs^{+}, Ba^{2+}, and Co^{2+} signal intensity with depth

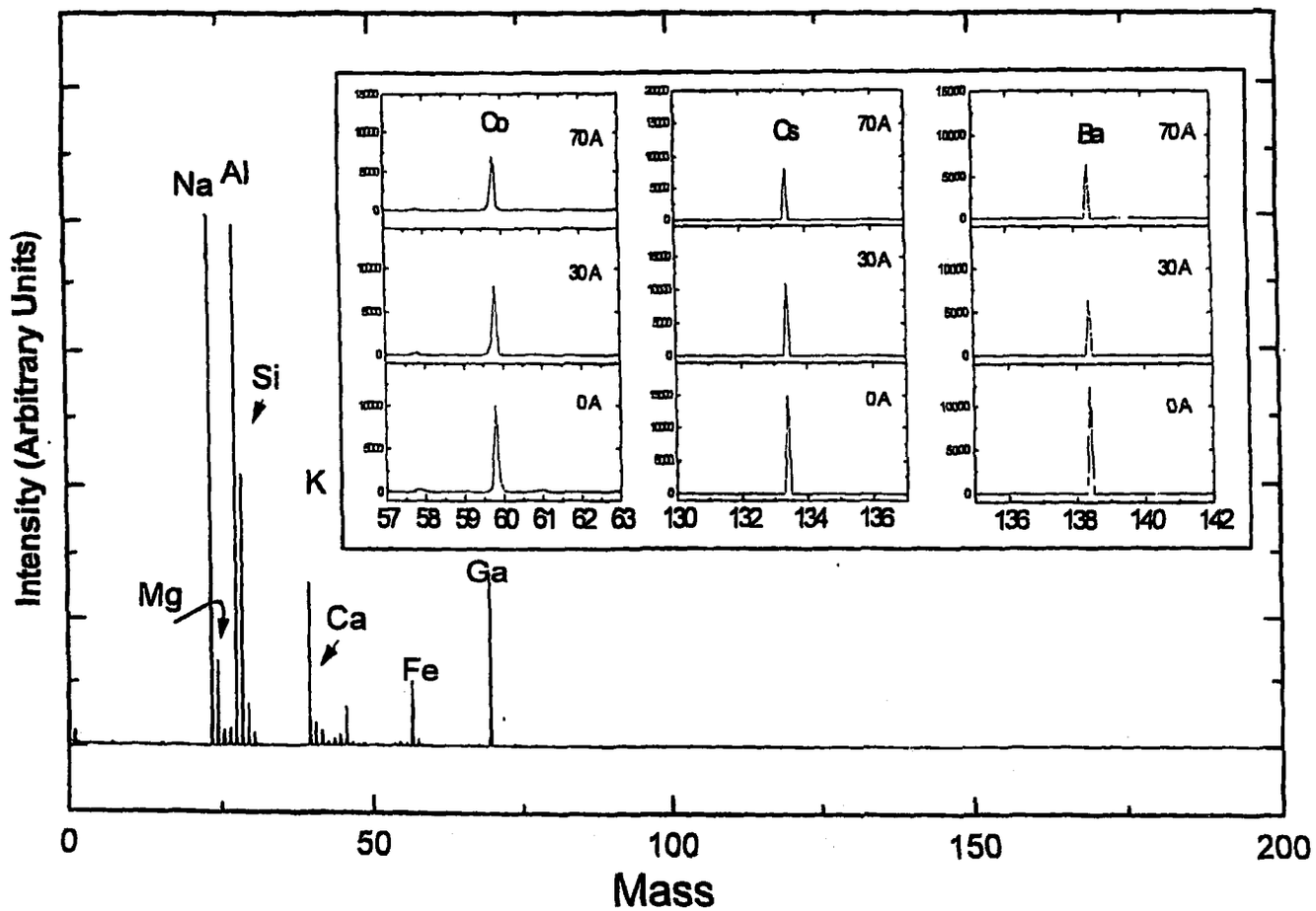

Fig. 4.30: A typical ToF-SIMS spectrum of bentonite. The inset in the figure shows the variation of Cs^+, Ba^{2+}, and Co^{2+} signal intensity with depth

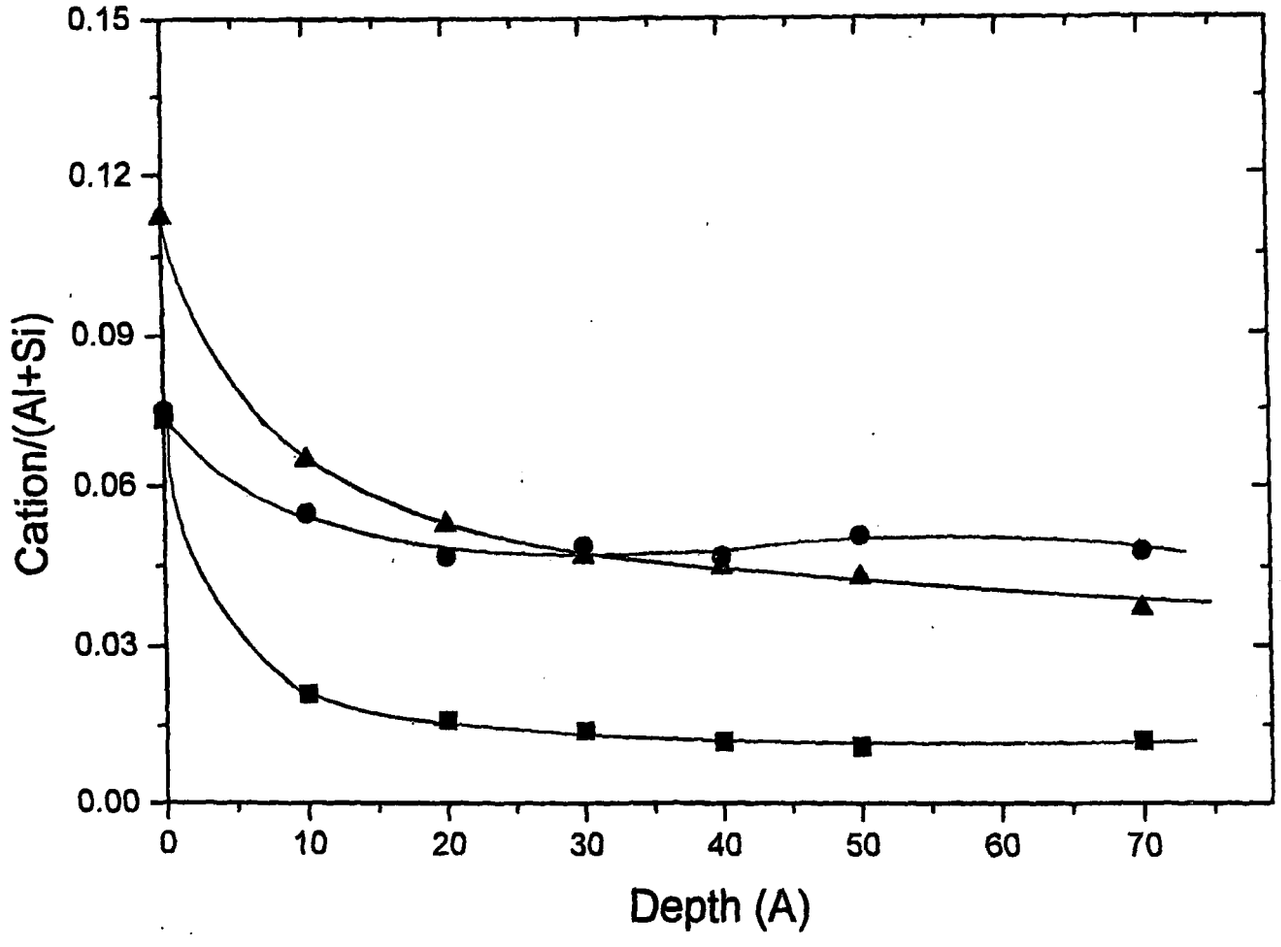

Fig. 4.31: The variation of sorbed amounts of Cs^+, Ba^{2+}, and Co^{2+} with depth in kaolinite matrix

■: Cs^+ :● Ba^{2+} ▲: Co^{2+}

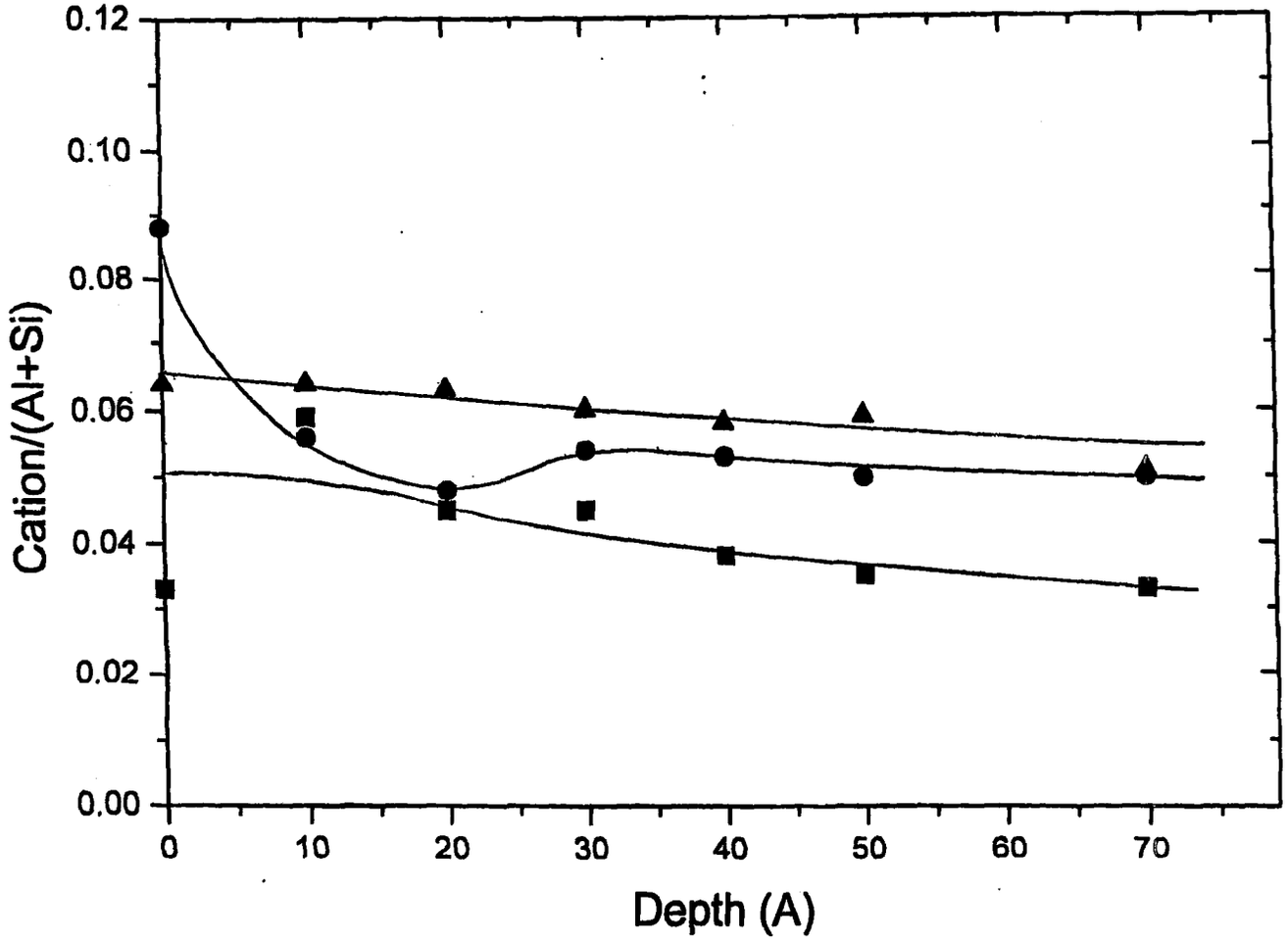

Fig. 4.32: The variation of sorbed amounts of Cs^+, Ba^{2+}, and Co^{2+} with depth in chlorite-illite matrix

■: Cs^+ ●: Ba^{2+} ▲: Co^{2+}

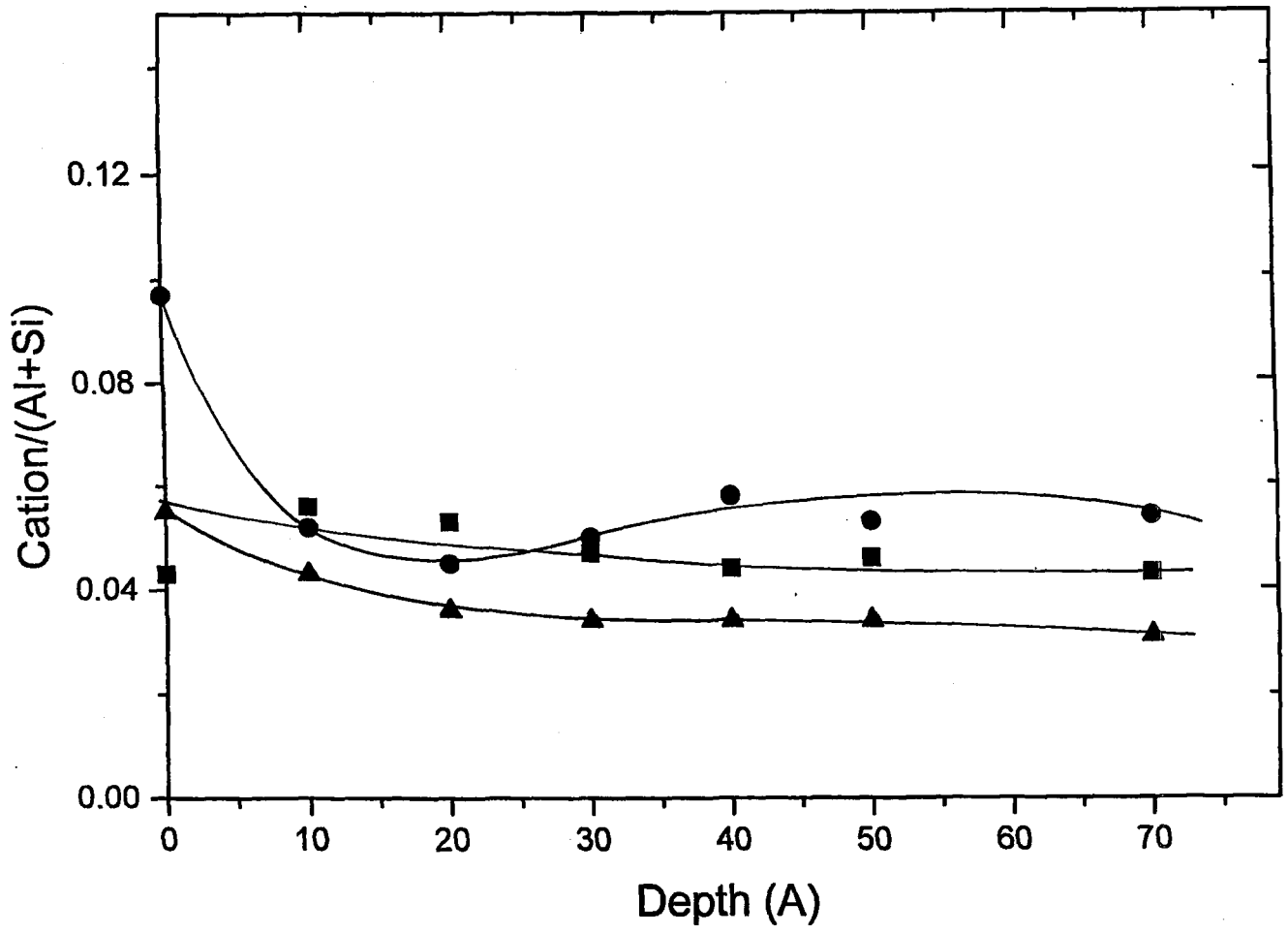

Fig. 4.33: The variation of sorbed amounts of Cs^+, Ba^{2+}, and Co^{2+} with depth in bentonite matrix ■: Cs^+ ●: Ba^{2+} ▲: Co^{2+}

4.4- Sorption Studies Using XPS

Along with ToF-SIMS studies, the sorption of Cs^+, and Ba^{2+} on kaolinite, chlorite-illite, and bentonite clays were studied using XPS technique. XPS is a powerful surface sensitive technique that can be used in the surface characterization of the clays. The XPS studies provided information about the sorbed ions on different clays and the depletion of ions in the clay structure. Compared with ToF-SIMS, the major drawback of XPS is its poorer detection limits. Furthermore, when comparing ToF-SIMS results with XPS results one must keep in mind the fact that the escape depths of each technique is different.

The XPS data were obtained in the form of kinetic energies of the ejected electrons of different elements versus their intensities. The binding energies (B.E=hν- K.E, eV) were then calculated from the kinetic energies and drawn as a function of the corresponding intensities. Figs. 4.34, 4.35, 4.36 give typical XPS spectra of natural, Cs-, and Ba-sorbed kaolinite, chlorite-illite, and bentonite, respectively. As a first approximation, the intensity of an XPS signal can be considered to be proportional with the quantity of an element. However, performing a meaningful quantitative analysis requires correcting the peak intensities with the corresponding cross section values (given usually in the form of sensitivity factors calculated relative to C 1s line). The peak energies and sensitivity factors of different elements considered in this study are given in Table 4.12. As in ToF-SIMS analysis, in order to establish a basis for comparing the clay contents prior to and

following sorption, the data of different elements were normalized relative to Al+Si content. The resulting values for depleted and sorbed elements upon sorption of Cs^+ and Ba^{2+} on the three clays are given in Table 4.13. Compared with ToF-SIMS only a limited number of elemnts could be detected using XPS. The XPS findings are generally in line with those of ToF-SIMS, but the major difference is the absence of Mg and partially of Fe signals in the XPS spectra (for full data listings see Appendix E).

Table 4.12: The elements detected by XPS in the clays structures, their binding energies (eV), and their sensitivity factors

Element	**Binding Energy (eV)**	**Sensitivity Factor**
C 1s	291.0 - 293.0	1.000
Al $2p_{1/2}$	80.8 - 83.05	0.570
Si $2p_{1/2}$	109.0 - 110.9	0.865
Na $1s_{1/2}$	1079	7.990
K $2p_{3/2}$	298.3 - 300.8	2.670
Ca $2p_{1/2}$	353.0 - 354.0	5.130
Fe $2p_{3/2}$	718.0	10.540
Cs $3d_{5/2}$	732.1 - 732.3	22.930
Ba $3d_{5/2}$	787.6 - 789.2	24.750

For sorption of Cs^+ and Ba^{2+} on kaolinite, K^+ and Ca^{2+} were detected as the depleted ions with K^+ showing larger depletion upon Cs^+ sorption. Ca^{2+} existed in larger amounts than K^+ and its presence was not detected upon sorption of Cs^+ and Ba^{2+}, indicating a large depletion. Depletion of K^+ and Ca^{2+} was also detected in chlorite-illite samples upon sorption. Ca^{2+} existed in larger amount compared with K^+, which showed discrepancies in Cs^+ case, and was more depleted upon sorption of Ba^{2+}. For the bentonite case, depletion of only Na^+ was detected in both of sorption cases. No Na^+ signal was obtained in the sorbed samples of the clay, indicating a large loss of this ion from the clay matrix upon sorption. In all cases, amounts of sorbed Ba^{2+} are larger than those of sorbed Cs^+. These results are to a large extent inline with ToF-SIMS findings except for the absence of Mg^{2+}. The reason for this might be the extremely low sensitivity factor of Mg^{2+} (0.360 for Mg 2p) compared to 7.990, 2.670, and 5.130 for Na 1s, K 2p, and Ca 2p respectively.

The fact that the pH-independent ion exchange is the primary sorption mechanism, the thing discussed in the previous section based on ToF-SIMS data, is -to a large extent- verified also by XPS results. Except for the case of Cs^+ sorption on bentonite, the equivalent depleted amounts (EDA) are comparable with the equivalent sorbed amounts in all other sorption cases as shown in Table 4.13.

Table 4.13: The initial and final amounts, R_i and R_f, (normalized to Al+Si contents), the Equivalent Depleted Amounts (EDA) of different depleted elements, and the Equivalent Sorbed Amounts (ESA) obtained from XPS data of Cs^+ and Ba^{2+} sorption on kaolinite, chlorite-illite, and bentonite

			Cs-Sorption		Ba-Sorption	
Clay	**Element**	**R_i**	**R_f**	**EDA**	**R_f**	**EDA**
Kaolinite	K	0.009	0.0	0.009	0.006	0.003
	Ca	0.015	0.0	0.030	0.0	0.030
	Σ EDA			0.039		0.033
	ESA			0.028		0.031
Chlorite-Illite	K	0.016	0.026	0.0	0.008	0.008
	Ca	0.101	0.090	0.022	0.0	0.202
	Σ EDA			0.022		0.210
	ESA			0.036		0.223
Bentonite	Na	0.093	0.0	0.093	0.0	0.093
	Σ EDA			0.093		0.093
	ESA			0.050		0.116

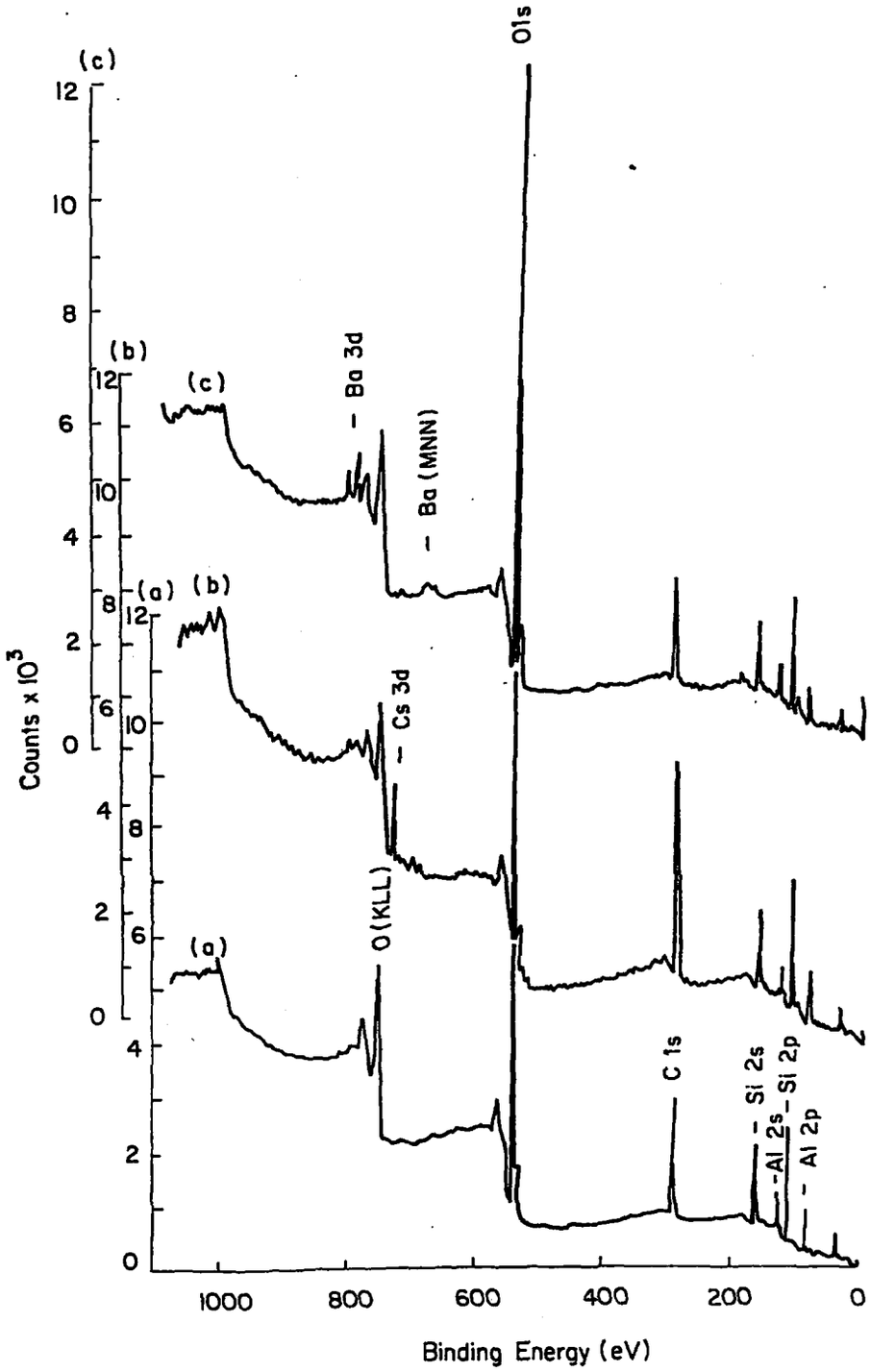

Fig. 4.34: XPS spectra of : (a) natural kaolinite, (b) Cs-sorbed kaolinite, and (c) Ba-sorbed kaolinite

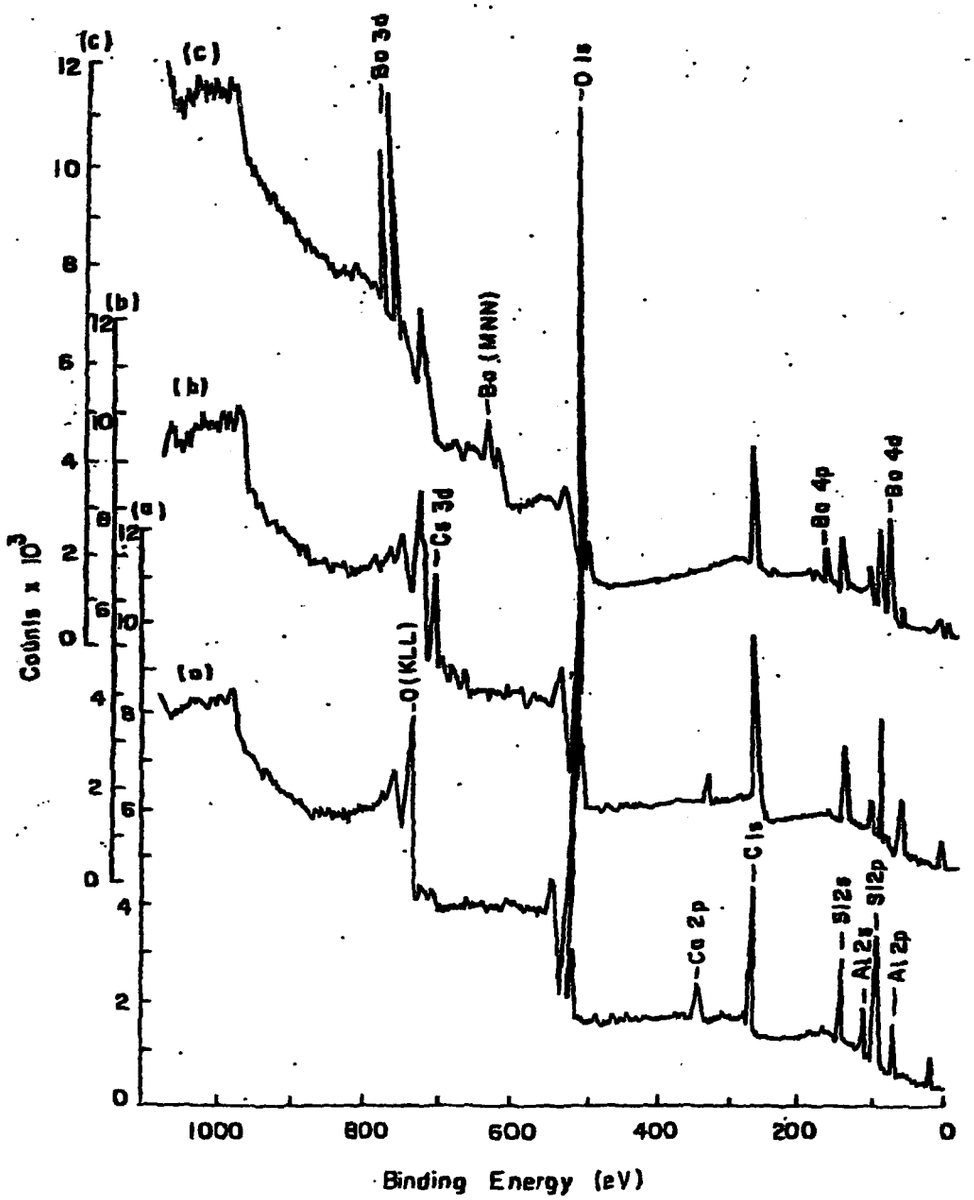

Fig. 4.35: XPS spectra of : (a) natural chlorite-illite, (b) Cs-sorbed chlorite-illite, and (c) Ba-sorbed chlorite-illite

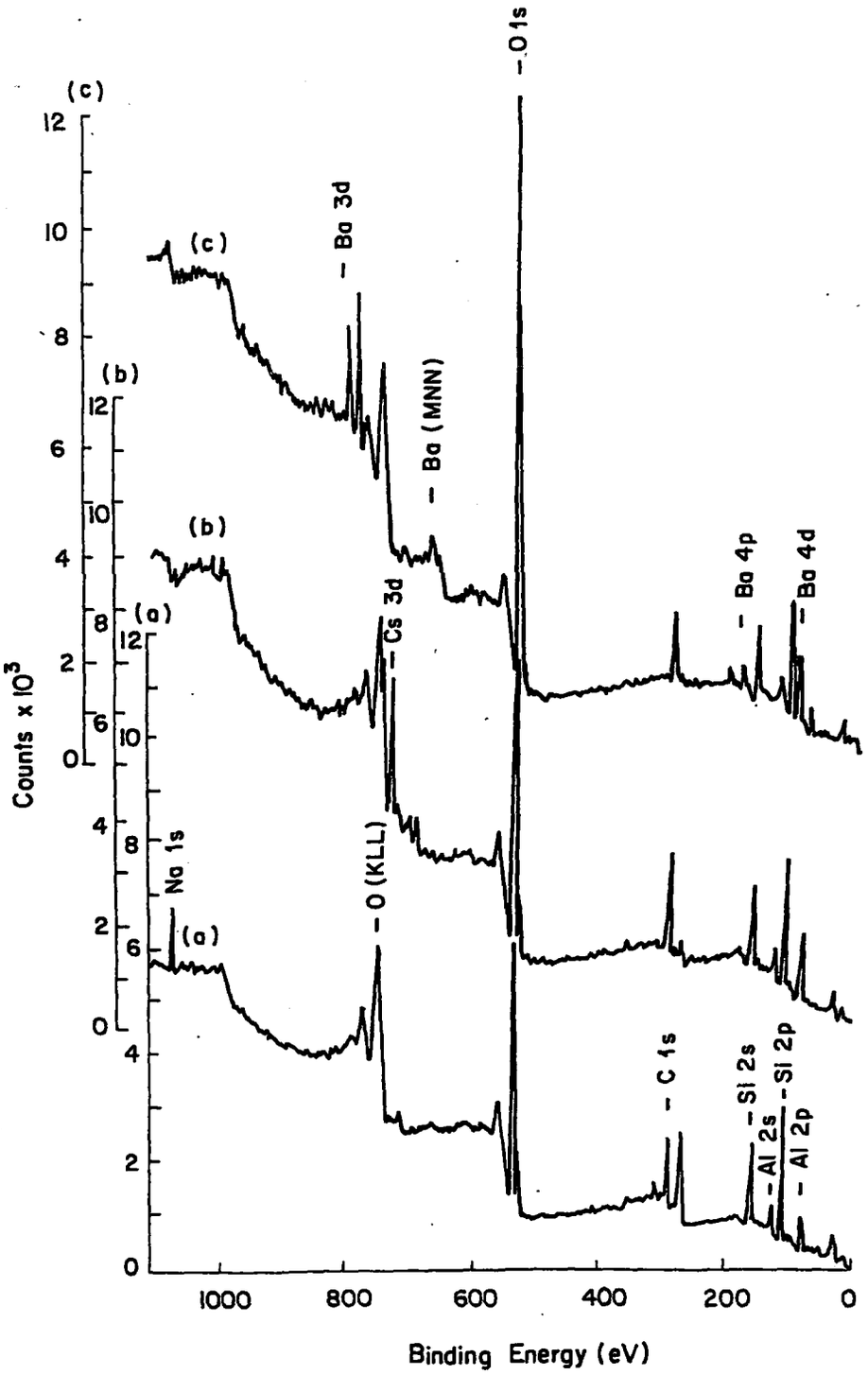

Fig. 4.36: XPS spectra of : (a) natural bentonite, (b) Cs-sorbed bentonite, and (c) Ba-sorbed bentonite

4.5- X-Ray Diffraction (XRD) Studies

In addition to its use in the characterization of the clay samples, XRD was also used to examine any structural changes that accompanied sorption of Cs^+, Ba^{2+}, and Co^{2+} on the natural clays under consideration. The peak intensities in natural and Cs-, Ba-, and Co-sorbed clay spectra were normalized to the corresponding intensities of quartz (101) peak which showed no changes upon sorption. This step facilitated comparing the spectra of natural clays with those corresponding to exchanged ones. The results are given in Appendix F (Tables F1, F2, F3) for natural and exchanged kaolinite, chlorite-illite, and bentonite, respectively.

The XRD spectra corresponding to kaolinite, chlorite-illite, and bentonite prior to and after Cs^+, Ba^{2+}, and Co^{2+} sorption are shown in Figs. 4.37, 4.38, 4.39, respectively. According to the spectra and the tabulated results, whereas no major structural changes were observed in the case of Cs^+ and Co^{2+} sorption, new features appeared in the Ba^{2+} sorbed chlorite-illite and bentonite samples. These features were identified as $BaCO_3$ with the major peak appearing at d_{hkl}=3.696. The formation of $BaCO_3$ was accompanied with a severe reduction in peak intensity of calcite (104), which existed in minor quantities in the clay samples. This suggests that $BaCO_3$ was probably formed as a result of calcite dissolution followed by precipitation of $BaCO_3$ and/or Ba^{2+} exchange with Ca^{2+} in the calcite matrix. In the literature it is reported that sorption of Ba^{2+} on calcite occurs in the form of

coprecipitation to produce $(Ca,Ba)CO_3$ [70], but such a possibility would not lead to the formation of a distinct $BaCO_3$ structure as seen in our case.

No evidence of Cs- or Co-carbonate formation was obtained from the XRD spectra of the three clays. In the literature, it is reported that calcite is a poor sorbent of Cs and that its sorption properties could be enhanced only in the presence of SO_4^{2-} ions that forms a bridge between the calcite surface and Cs^+ ions [71]. On the other hand, the sorption of Co^{2+} on calcite is believed to occur via various mechanisms, the most significant of which is the 'burial' of Co^{2+} ions between the dissolved and reprecipitated calcite layers [72].

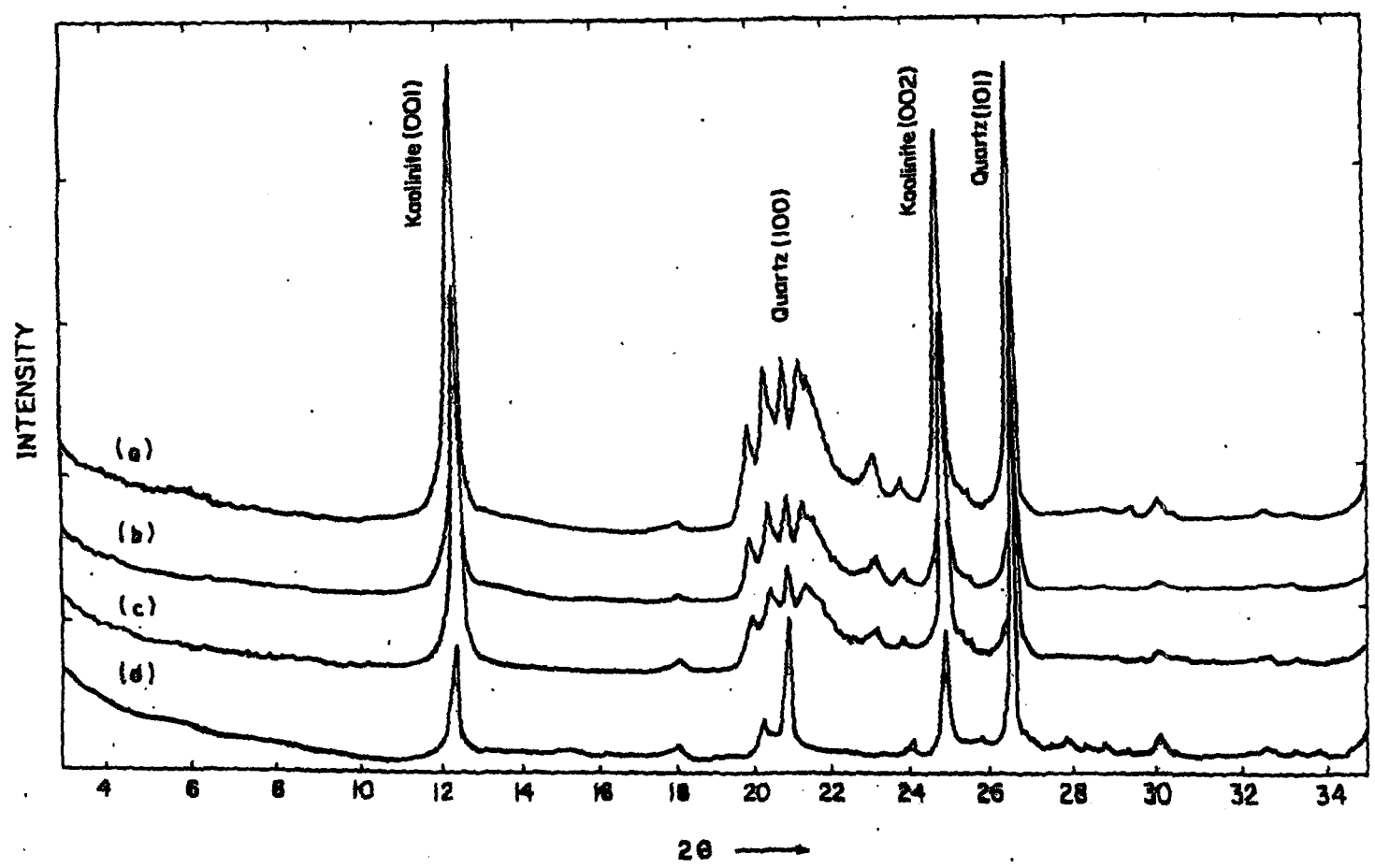

Fig. 4.37: XRD spectra of; (a) natural kaolinite, (b) Ba-sorbed kaolinite, (c) Cs-sorbed kaolinite, and (d) Co-sorbed kaolinite

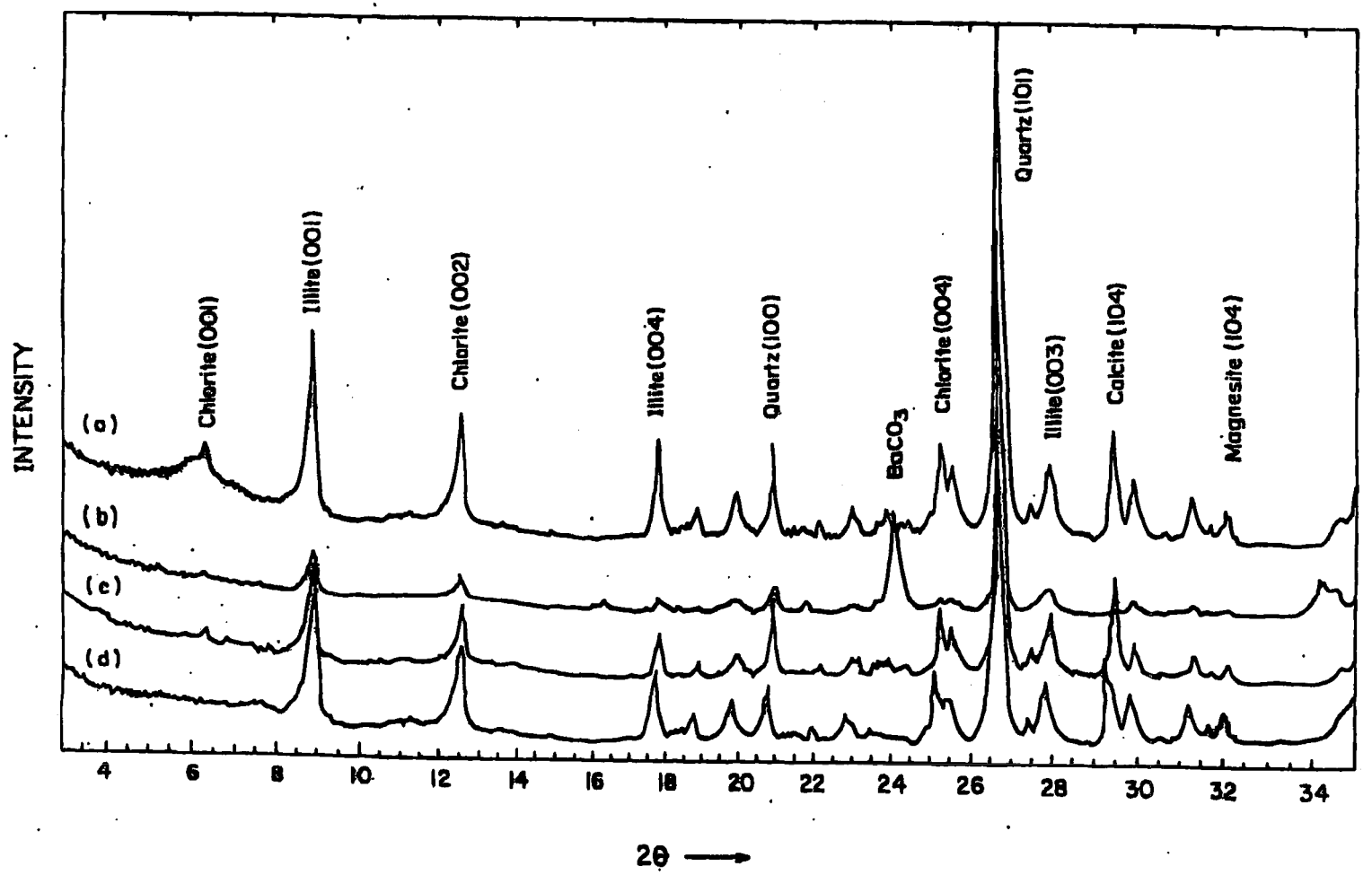

Fig. 4.38: XRD spectra of; (a) natural chlorite-illite, (b) Ba-sorbed chlorite-illite, (c) Cs-sorbed chlorite-illite, and (d) Co-sorbed chlorite-illite

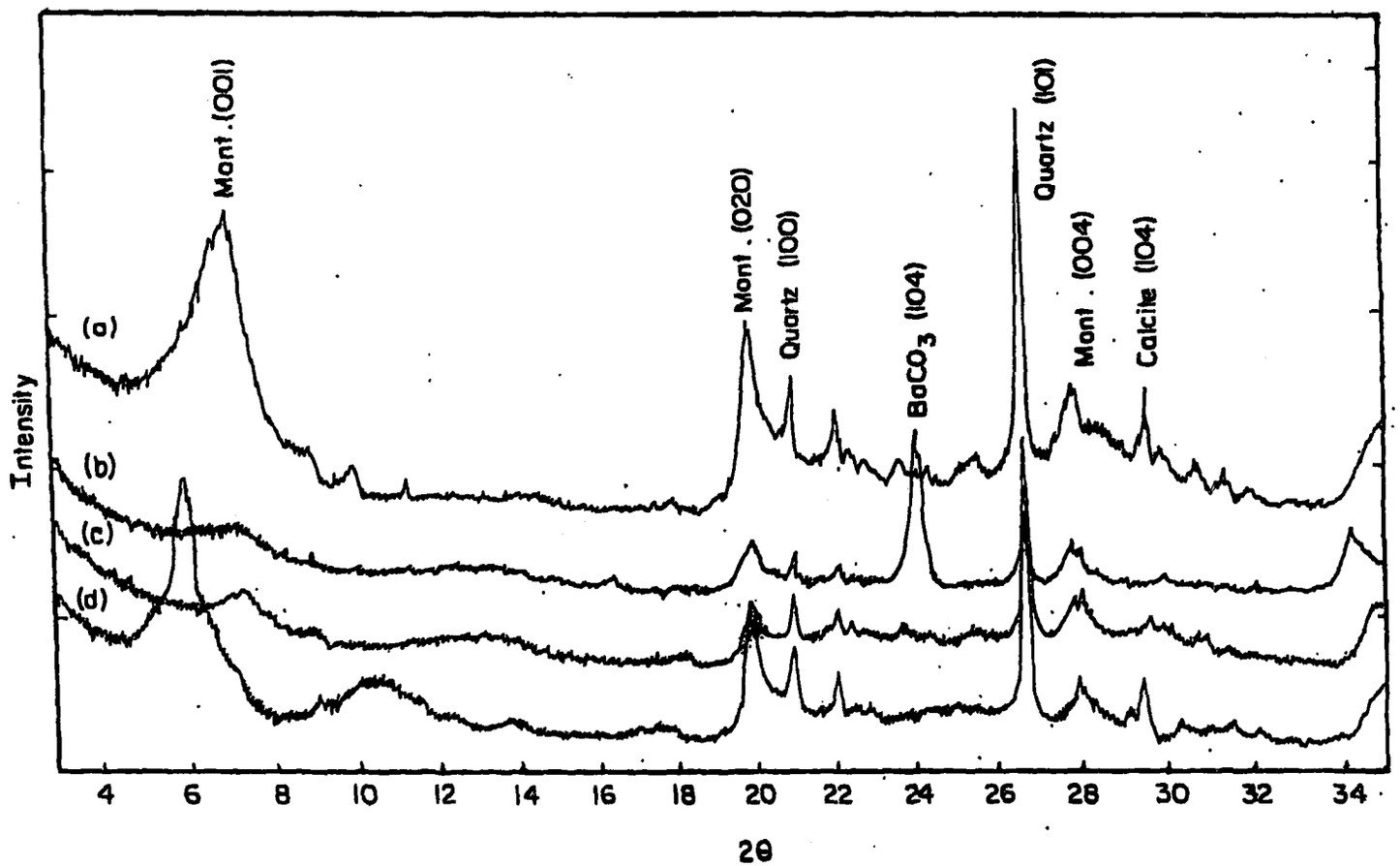

Fig. 4.39: XRD spectra of; (a) natural bentonite, (b) Ba-sorbed bentonite, (c) Cs-sorbed bentonite, and (d) Co-sorbed bentonite

4.6- Empirical Equations

4.6.1- Equations Based on Data Obtained Using Radiochemical Studies

Among the isotherm models applied in this study, Freundlich isotherm model provided the best description of the experimental data. Hence, empirical equations that relates R_d to the equilibrium concentration in the liquid phase were developed utilizing the Freundlich isotherm parameters, n and k. As was shown in section (2.2.2.), starting with Freundlich isotherm equation, R_d can be related to the equilibrium concentration in the liquid phase to yield equation (2.11), which is given as:

$$R_d = k\,[C]_l^{n-1}$$

This equation may be viewed as a modified expression of Freundlich isotherm. As the term 'isotherm' implies, the values of Freundlich parameters, k and n, can be obtained for experiments conducted at different loading conditions while temperature is kept constant. If the variation of k and/or n is expressed as a function of temperature, then the equation above would be an expression that is helpful in predicting R_d values for various loading and temperature conditions.

The values of n and k were given for different sorption cases in Table 4.2. As the table shows, while the values of n are almost temperature independent, those of k varies considerably with temperature in most of the sorption cases. As a result the n values at different temperatures may be expressed in terms of average values that

cover the entire temperature range. The k values, on the other hand, were plotted as a function of temperature and expressed using a linear function (k=A+BT), except for the cases of Cs^+ and Ba^{2+} sorption on chlorite-illite, where an average was used since k values did not show significant changes with varying temperature. Variation of the k values with absolute temperature is shown in Fig. 4.40. Based on this, R_d can be expressed using the general equation:

$$R_d = (A + B\,T)\,[C]_l^{\,N-1} \qquad (4.1)$$

where (A+BT) corresponds to k, A and B are constants, T is the temperature (K), and N is the average of n values obtained from Freundlich isotherm fits. The values of A, B, and N for sorption of Cs^+, Ba^{2+}, and Co^{2+} on kaolinite, chlorite-illite, and bentonite are given in Table 4.14. As an illustrative example, the variation of R_d with equilibrium aqueous concentration and temperature was plotted on a three-dimensional space for the case of Cs^+ sorption on bentonite as shown in Fig. 4.41. In this figure, the significance of the resulting surface is its incorporation of the R_d values corresponding to any entire combination of concentration and temperature. Consequently, the surface can aid in the prediction of the loading curves and sorption isotherms at various temperatrures in addition to Arrhenius plots used in the calculations of the thermodynamic parameters.

Table 4.14: The values of A, B, and N for the sorption of Cs^+, Ba^{2+}, and Co^{2+} on kaolinite, chlorite-illite, and bentonite

Clay	Sorbed Ion	A	B	N
Kaolinite	Cs^+	96.1	-0.28	0.87
	Ba^{2+}	21.5	-0.045	0.73
	Co^{2+}	-36.2	0.25	0.87
Chlorite-Illite	Cs^+	22.4	0.0	0.71
	Ba^{2+}	36.9	0.0	0.78
	Co^{2+}	-1018.1	3.64	0.87
Bentonite	Cs^+	1965.9	-5.40	0.92
	Ba^{2+}	1070.5	-2.72	0.95
	Co^{2+}	-1872.4	6.80	0.91

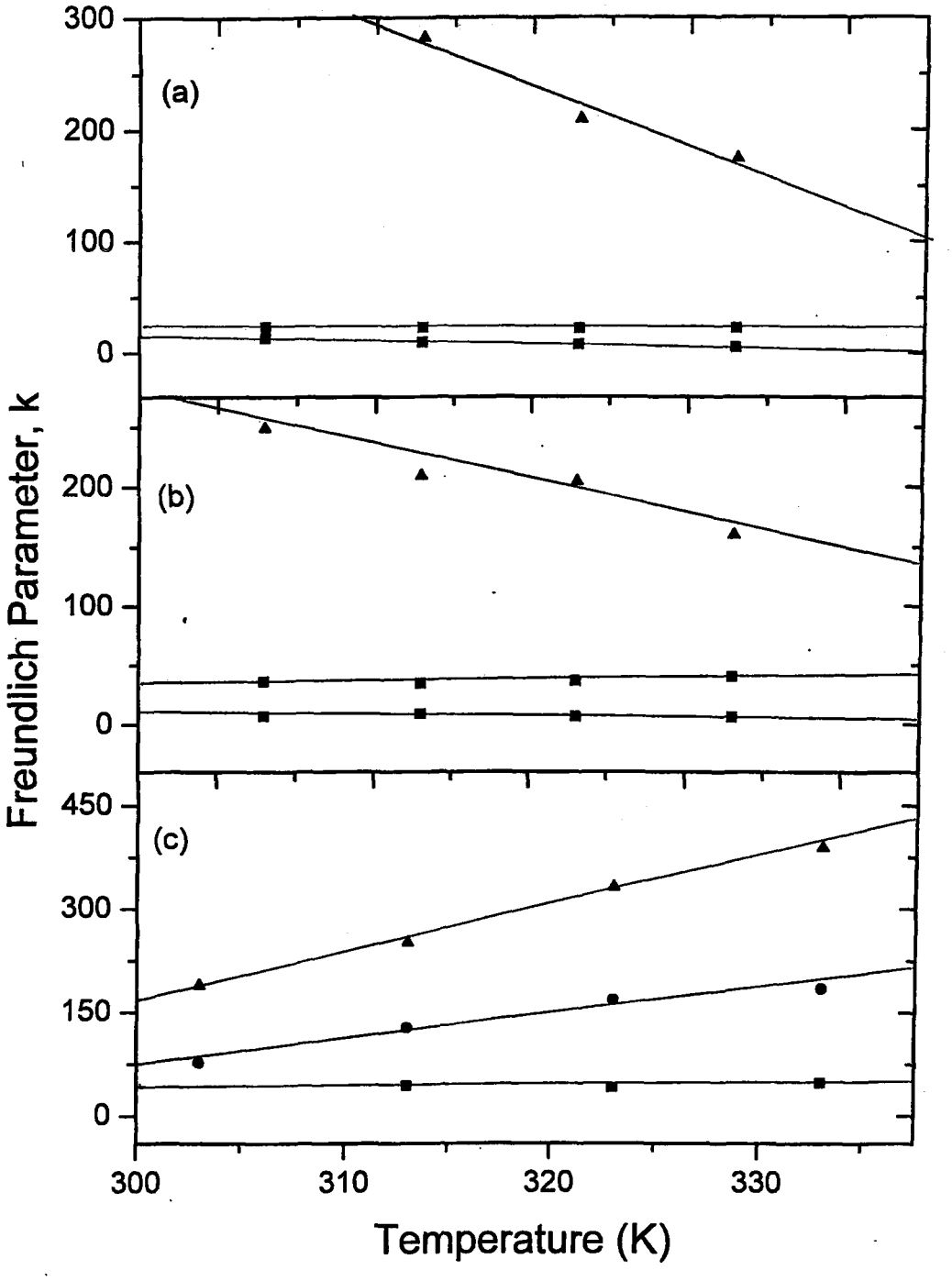

Fig. 4.40: The variation of the Freundlich Parameter, k, with Temperature for the Sorption of (a) Cs^{+}, (b) Ba^{2+}, and (c) Co^{2+} on Kaolinite, Chlorite-Illite, and Bentonite ■ Kaolinite ● Chlorite-Illite ▲ Bentonite

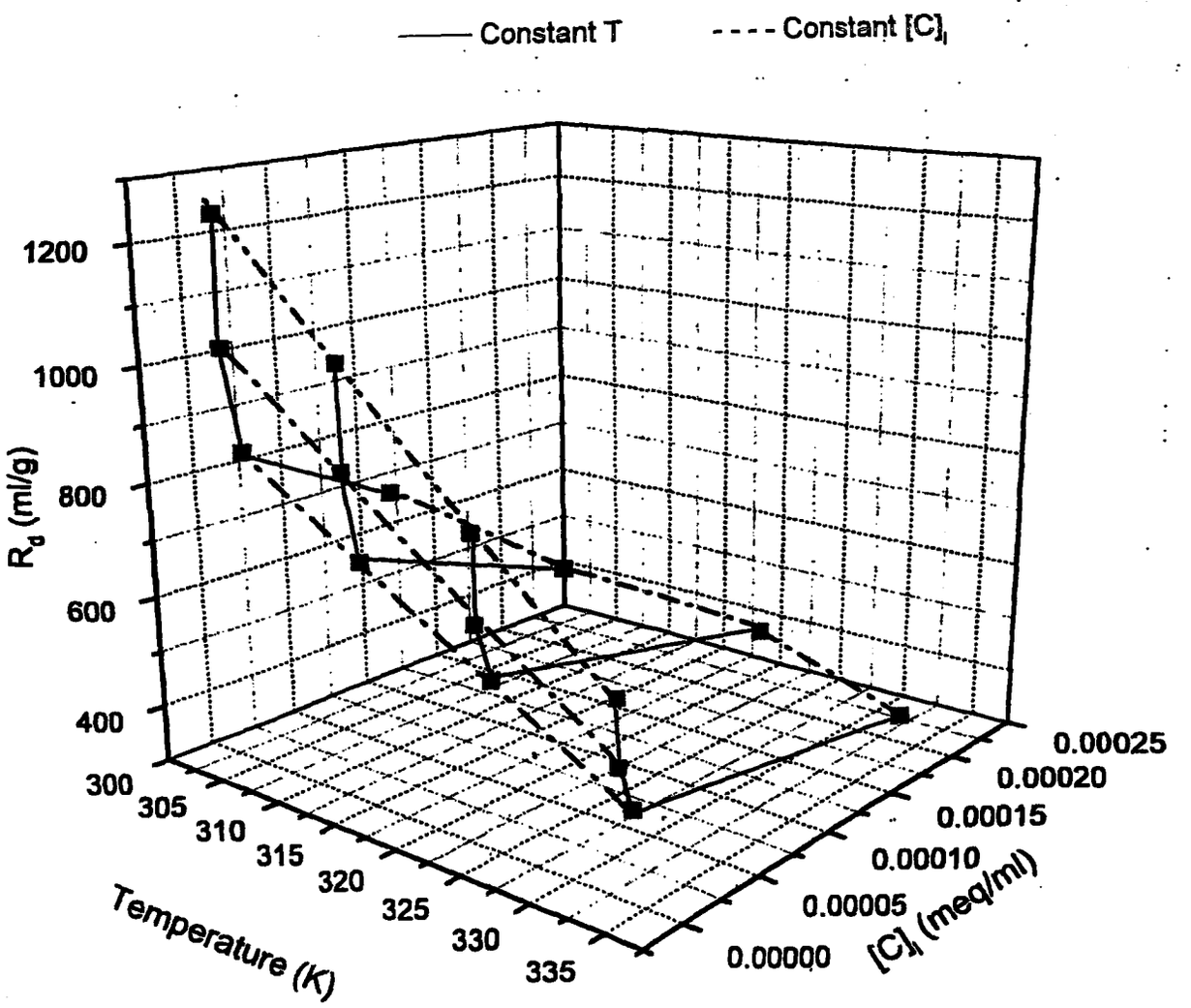

Fig. 4.41: Variation of the R_d Values with Equilibrium Aqueous Concentration, $[C]_l$ (meq/ml), and Temperature (K) as Predicted by the Empirical Equation Corresponding to Cs^+ Sorption on Bentonite

4.6.2- Equations Based on Data Obtained Using ToF-SIMS Studies

The sorbed amounts of Cs^+, Ba^{2+}, and Co^{2+} on the three clays as a function of depth were fitted to an equation which refers to a one-dimensional sorption from an infinitely thin source, given as:

$$C = C_o \exp(-x^2 / D) \qquad (4.2)$$

where C is the sorbed amount at any depth, x is the depth in clay matrix (Å) and C_o, D are constants. The value of C_o was obtained from the intercept of the figure constructed by plotting ln C against x^2, and refers to the sorbed amount at x=0. The constant D is obtained from the slope of the same figure and is related to the diffusion coefficient.

According to this model, the total sorbed amount is assumed to initially exist on an infinitely thin plate centered at x=0. As time passes, the initial amount of sorbed ion on the uppermost surface decreases as a result of diffusion of those ions into internal pores of the solid. At equilibrium a sorption profile of sorbed ions is developed that is characterized by the values of the constants C_o and D.

This type of model is widely applied for sorption on compacted clays. It is used to describe sorption resulting from two diffusion mechanisms; one through the interconnected pores between the clay particles, and another across the pores of the clay particles (surface transport) [73,74]. By applying this model to our sorption cases, it is assumed that the total sorbed amount of a particular ion accumulates

initially as a thin film on the solution-clay interface, which is a fast process. This is followed by a slower process where the accumulated ions diffuse into the internal sorption sites of the clay particles. Here the only diffusion mechanism responsible for sorption is the surface transport and the given equations corresponds to sorption after equilibrium is achieved.

Fig. 4.42 shows the plots ln C versus x^2 plots for the sorption cases of Cs^+, Ba^{2+}, and Co^{2+} ions on kaolinite, chlorite-illite, and bentonite. The points in the figure refer to the experimental values, whereas the lines refer to the fitting functions. The values of the constants C_o and D for different sorption cases are given in Table 4.15. Utilizing the individual equations, the amount sorbed at different depths at equilibrium are can be predicted.

Table 4.15: The values of the constants C_o and D for the Cs^+, Ba^{2+}, and Co^{2+} sorption on kaolinite, chlorite-illite, and bentonite obtained from the diffusion model based on ToF-SIMS data

	Kaolinite		**Chlorite-Illite**		**Bentonite**	
Sorbed Ion	**C_o**	**D**	**C_o**	**D**	**C_o**	**D**
Cs^+	0.024	4545.4	0.045	14285.7	0.052	25000.0
Ba^{2+}	0.056	25000.0	0.061	20000.0	0.059	33333.3
Co^{2+}	0.067	6666.7	0.064	25000.0	0.042	12500.0

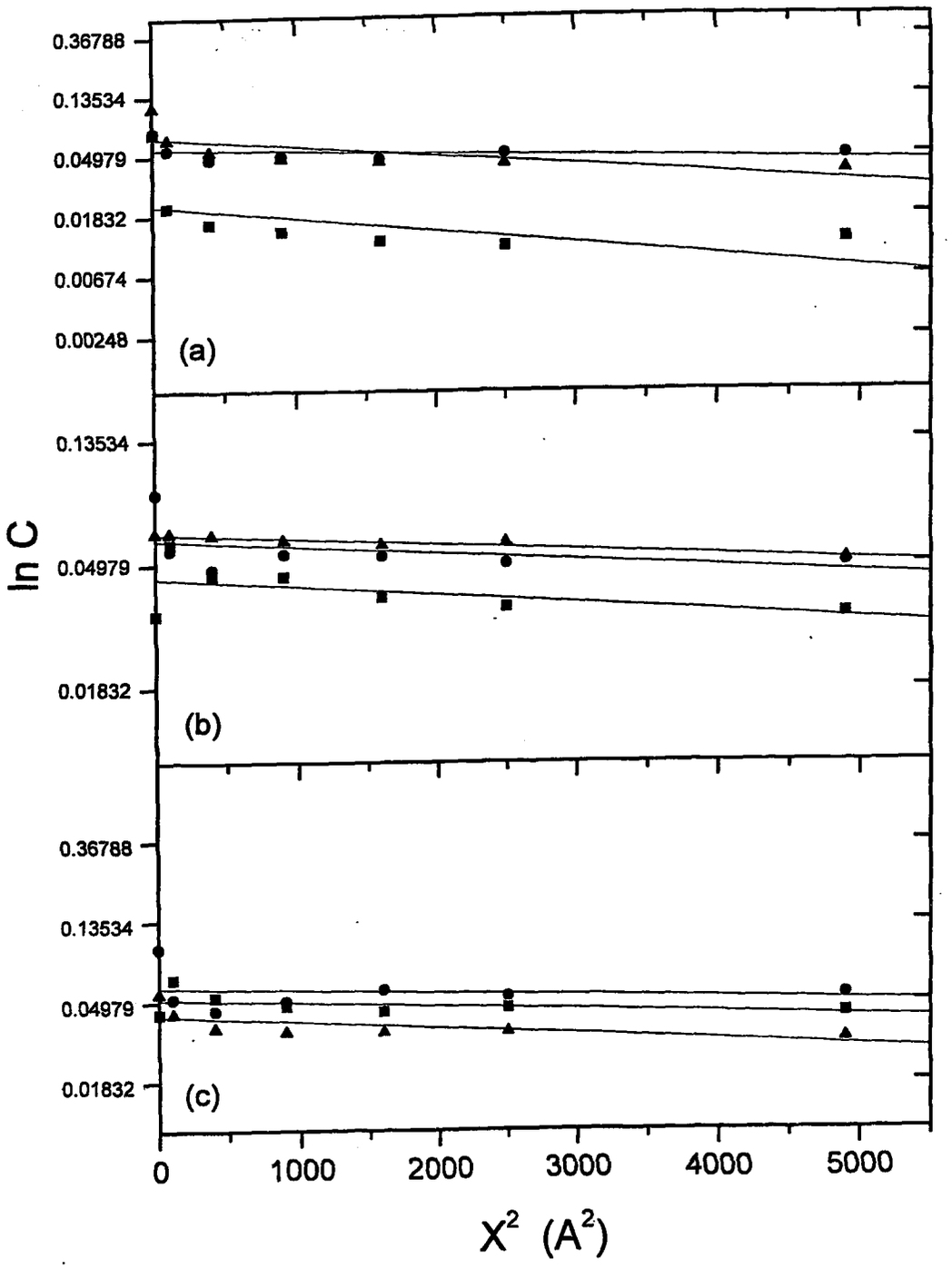

Fig. 4.42: Variation of ln C with x^2 for the sorption cases of Cs^+, Ba^{2+}, and Co^{2+} on;

(a) kaolinite, (b) chlorite-illite, and (c) bentonite

■: Cs^+ ●: Ba^{2+} ▲:Co^{2+}

5. CONCLUSIONS

Based on the results of this study, the following major conclusions may be obtained:

- Equilibrium in sorption is achieved within hours of contact between the solutions of sorbed ions and the clay samples indicating that fast sorption steps are involved and that sorption is mainly a surface phenomena.

- In all cases, the sorption process is nonlinear. The degree of nonlinearity is smallest for bentonite and largest for chlorite-illite. The nonlinearity implies an increase in the sorption barrier as loading is increased.

- The sorption data is well described using Freundlich and Dubinin-Radushkevich isotherm models. According to the k and C_m parameters of the two isotherms , the order of sorption affinity (based on k values) and sorption capacity (based on C_m values) of Cs^+, Ba^{2+}, and Co^{2+} is; bentonite > chlorite-illite > kaolinite. Hence bentonite seems to be the most appropriate clay in retarding the migration of those cations.

- Whereas Cs^+ and Ba^{2+} sorption on the three clay types is exothermic, that of Co^{2+} is endothermic. This means that while Cs^+ and Ba^{2+} sorption favors lower temperatures, Co^{2+} sorption favors higher temperatures. The values of the mean free energy of Sorption, E, and the Gibbs Free Energy, ΔG^o, are generally in the energy range 8-16 (kJ/mol) that corresponds to ion exchange type of sorption.

- ToF-SIMS seems to be an adequate tool in the detailed study of the sorption process. By virtue of its large sensitivity and very low detection limits, ToF-SIMS can aid in identifying the exchanged cations and quantifying the extent of depletion and sorption on the clay surface. The main complexity in ToF-SIMS analysis of clay samples may arise from the surface heterogeneity, the effect of which can be minimized by performing measurements at different locations on the surface and averaging the results. According ToF-SIMS results - that were also to a large extent supported by XPS results- the primary mechanism of sorption is the ion exchange between some alkali and alkaline-earth elements originally present in the clay sample and the sorbed ions. Moreover, ToF-SIMS depth profiling experiments have shown that uppermost surface sorption is more pronounced in the case of kaolinite than the other two clays indicating a relatively less diffusion inside the kaolinite matrix, in line with the structural properties of the clays.

- The XRD results indicate that Ba^{2+} sorption on chlorite-illite and bentonite involves a precipitate formation in the form of $BaCO_3$. No precipitate formation

was, however, observed for Cs^+ and Co^{2+} sorption on the three clays.

- The empirical equations based on the radiochemical data can be used to model the R_d variation with different loading and temperature conditions. Empirical equations that covers wider ranges of loadings and temperatures and provides better predictions can be obtained by extending the experiments to lower concentrations and performing more experiments at closer loading and temperature values.

- The sorption model corresponding to a one-dimensional diffusion provides good predictions for the distribution of the sorbed ions across the surface of different clays. The sorbed amounts used in the fits of the model were the ones corresponding to equilibrium case, where time is not a variable. The model can be used in its time-dependent form if analysis is performed for samples obtained from sorption experiments prior to achieving equilibrium.

REFERENCES

[1] Lieser, K. H. Radionuclides in the Geosphere: Sources, Mobility, Reactions in Natural Waters and Interactions with Solids. Radiochim. Acta, 70/71, 355-375 (1995).

[2] Chapman, N.A., McKinely, I.G. The Geological Disposal of Nuclear Waste. John Wiley and Sons (1987).

[3] Durrance, E. M. Radioactivity in Geology: Principles and Applications. John Wiley and Sons, (1989).

[4] Larsson, A., Thomas, K.T. The IAEA Program for the Underground Disposal of Radioactive Wastes IAEA-CN-43/171 (1982).

[5] Underground Disposal of Radioactive Wastes, Safety Series, No. 54, International Atomic Energy Agency, Vienna (1981).

[6] Jedinakova-Krizova, V. Migration of Radionuclides in the Environment. J. Radioanal. Nucl. Chem., 229/1-2, 13-18, (1998).

[7] Jedinakova-Krizova, V. Radionuclides Migration in the Geosphere and Their Sorption on Natural Sorbents. J. Radioanal. Nucl. Chem., 208/2, 559-575, (1996).

[8] Drever, J. I. The Geochemistry of Natural Waters. Prentice-Hall, (1982).

[9] Brown, G.: The X-Ray Identification and Crystal Structures of Clay Minerals. Mineralogical Society, London (1972).

[10] Gillman, G.P. A Proposed Method for the Measurement of Exchange Properties of Highly Weathered Soils. Aust. J. Soil Res., 17, 129-139 (1979).

[11] Searle, P.L. The Measurement of Soil Cation Exchange Properties Using the Single Extraction, Silver Thiourea Method. Aust. J. Soil Res., 24, 193-200 (1986).

[12] Matsue, N., Wada, K. A New Equilibrium Method for Cation Exchange Capacity Measurement. Soil Sci. Soc. Am. J., 49 (1985).

[13] Grim, R.A. Clay Mineralogy. Mc Graw-Hill Inc., New York (1953)

[14] Goodman, B. A. Adsorption of Metal ions and Complexes on Aluminosilicate Minerals.

[15] Stumm, W., and Morgan, J. J. Aquatic Chemistry. John Wiley & Sons (1981).

[16] Harrison, R.M., de More, S.J., Repsomanikis, S., Johnston, W.R. Introductory Chemistry for the Environmental Sciences. Cambridge University Press (1991).

[17] Sorption, Modelling and Measurement for Nuclear Waste Disposal Studies. Summary of Nuclear Energy Agency Workshop held in Paris, (1983).

[18] Tornstenfelt, B., Andresson, K., Allard, B. Sorption of Sr and Cs on Rocks and Minerals, Part 1: Sorption in Groundwater Report Prav 4.29, National Council for Radioactive Wastes, Stockholm (1981).

[19] Gronthe, I. Thermodynamics in Migration Chemistry, Radiochim. Acta, 52/53, 425-432, (1991).

[20] Sundstrom, D.W., Klei, H.E. Waste Water Treatment. Prentice-Hall Inc.(1983).

[21] Eylem, C., Erten, H. N., and Gokturk, H.: Sorption-Desorption Behavior of Barium on Clays. J. Environ. Radioactivity, 11, 183 (1990).

[22] Hatipoglu, S., Eylem, C., Gokturk, H., and Erten, H. N.: Sorption of Strontium and Barium on Clays and Soil Fractions. Sci. Geol. Mem., 86, 79 (1990).

[23] Erten, H. N., and Gokmenoglu, Z.: Sorption Behavior of Co^{2+}, Zn^{2+}, and Ba^{2+} ions on Alumina, Kaolinite, and Magnesite. J. Radioanal. Nucl. Chem., 182/2, 375 (1994).

[24] Brouwer E., Baeyers B., & Cramers A. Cesium and Rubidium Ion Equilibria in Illite Clay. J. Phys. Chem., 87, 1213-1219, (1986)

[25] Poinssot, C., Bayens, B., and Bradburg, M. H. Experimental and Modelling Studies of Caesium Sorption on Illite. Geochimica et Cosmochimica Acta. 63/19-20, 3217-3227 (1999).

[26] Grutter, A., von Gunten, H.R., Rossler, E., and Keil, R. Sorption of Nickel and Cobalt on Size-Fraction of Unconsolidated Deposits and Clay Minerals. Radiochim. Acta, 65, 181-187 (1994)

[27] Grutter, A., von Gunten, H. R. and Rossler, E. Sorption of Barium on Unconsolidated Glaciofluvial Deposits and Clay Minerals. 58/59, 259-265 (1992)

[28] Oscarson D.W., Watson R.L., & Miller H.G. The Intteraction of Trace Levels of Cesium with Monmorillonite and Illite Clays. App. Clay Sci., 2, 29-39, (1987)

[29] Benes P., Cernik M., & Lam Ramos P. Factors Affecting Interaction of Radiocesium with Fresh Water Solids. J. Radioanal. Nucl. Chem., 159/2, 201-218, (1992)

[30] Leiser K.H., and Steinkopff Th. Chemistry of Radioactive Cesium in the Hydroshere and in the Geosphere. Radiochim. Acta, 46, 39, (1989).

[31] Pacheco, G., Nava-Galva, G., Bosch, B., and Bulbulian S. ^{60}Co Sorption-Desorption in Mexican Montmorillonite. J. Radioanal. Nucl. Chem., 200/3, 259-264 (1995).

[32] Atun, G., Bilgin, B., and Mardinli, A. Sorption of Cesium on Montmorillonite and Effects of Salt Concentration. J. Radioanal. Nucl. Chem., 211/2, 435-442 (1996).

[33] Cui, D., and Eriksen, T.E. On the Sorption of Co and Cs on Stripo Granite Fracture-Filling Material. Radiochimica Acta, 79, 29-35 (1997).

[34] Adelye, S. A., and Clay, P. G. Sorption of Caesium, Strontium, and Europium Ions on Clay Minerals. J. Material Sci. 29, 954-958 (1994).

[35] Ghoneimy H. F. Adsorption of Co^{2+} and Zn^{2+} on Cryptomelane-Type Hydrous Mangenese Oxide. J. Radioanal. Nucl. Chem. 223/1-2, 61-65 (1997).

[36] Hakem, N., Fourest, B., Guillanmount, R., Marmier, N. Sorption of Iodine and Cesium on Some Mineral Oxide Colloids. Radiochim. Acta, 74, 225-230 (1996).

[37] Cho, Y., Jeong, C., and Hahn, P. Sorption Characteristics of ^{137}Cs onto Clay Minerals. Effect of Mineral Structure and Ionic Strength. J. Radioanal. Nucl. Chem. 204/1, 33-43 (1996).

[38] Wilson, M. J. Clay Mineralogy. Chapmann and Hall (1994).

[39] Davison, N., and Mc Whinnie W.R. X-ray Photoelectron Spectroscopic Study of Cobalt (II) on Hectorite and Montmorillonite Clays. Clay and Clay Minerals, 39/1, 22-27 (1991).

[40] Koppelman, M., and Dillard, J.G. An X-ray Photoelectron Spectroscopic (XPS) Study of Cobalt Adsorbed on the Clay Mineral Chlorite. J. Colloid. Interface Sci., 66/2, 345-351 (1978).

[41] Adams, J. M., Evans, S., Reid, P. I., Thomas, J. M., and Walters, M. J. Quantitative Analysis of Aluminosilicates and Other Soils by X-ray Photoelectron Spectroscopy. Analytical Chemistry, 49/13, 2001-2008 (1977).

[42] Bancroft, G. M., Brown, J. R., and Fyfe, W. S. Quantitative X-ray Photoelectron Spectroscopy (ESCA): Studies of Ba^{2+} Sorption on Calcite. Chem. Geol., 19, 131-144 (1977).

[43] Briggs, D., and Seah, M. Practical Surface Analysis: Volume 1: Auger and X-ray Photoelectron Spectroscopy. John Wiley and Sons (1990).

[44] Brule, D. G., Brown, J. R., Bancroft, G. M., and Fufe, W. S. Cation Adsorption by Hydrous Mangenese Dioxide: a Semi-Quantitative X-ray Photoelectron (ESCA) Study. Chem. Geol., 28, 331-339 (1980).

[45] Hochella, M. F. Auger Electron and X-ray Photoelectron Spectroscopies in Spectroscopic Methods in Mineralogy and Geology; F.C. Hawthorn Ed. Reviews in Mineralogy 18, Mineralogical Society of America Washington, 573-633. (1988)

[46] Perry, D. L., Application of Surface techniques to Chemical Bonding Studies of Minerals. Asm. Chem. Soc., 389-402 (1986)

[47] Aksoyoglu, S. Sorption of U(VI) on Granite. J. Radioanal Nucl. Chem. 134/2, 393-403 (1989).

[48] Tadjiki S. Radiochronology of Sediments from Various Regions of the Mediterranean. M.S. Thesis. Bilkent University (1992).

[49] Aksoyoglu, S. Sorption/Desorption Studies of Cesium and Neptunium on Some Clays and Soil. Ph. D. Thesis. Middle East Technical University (1987).

[50] Mishra, S. P., Tiwary, D. Ion Exchangers in Radioactive Waste Management. J. Radioanal. Nucl. Chem., 196/2, 353-361 (1995).

[51] Grutter, A., von Gunten, H. R., Kohler, M., and Rossler, E.: Sorption, Desorption and Exchange of Cesium on Gluciofluvial Deposits. Radiochim. Acta, 50, 177 (1990).

[52] Kim, Y., Kirkpatrick, R. J., and Cygan, R. T. 133Cs NMR Study of Cesium on the Surfaces of Kaolinite and Illite. Geochim. et Cosmochim. Acta, 60/21, 4059-4074 (1996)

[53] Erbel, D. D. Alkali Cation Selectivity and Fixation by Clay Minerals. Clay and Clay Minerals, 28/3, 161-172 (1980)

[54] Cotton, F. A. Advanced Inorganic Chemistry. Wiley (1988)

[55] Kozai, N., Ohunki, T., Matsumoto, J., Banba, T., and Ito, Y. A study of Specific Sorption of Neptunium (V) on Smectite in Low pH Solutions. Radiochim. Acta 75, 149-158 (1996).

[56] Helferrich, F. Ion Exchange. McGraw Hill (1962).

[57] Levine, I. N. Physical Chemistry. Mc Graw Hill (1988).

[58] Panday, K. K., Prasad, J., and Singh, V. N. Removal of Cr (VI) from Aqueous Solutions by Adsorption on Fly Ash-Wollastonite. J. Chem. Tech. Biotech. 34A, 367-374 (1984)

[59] Khan S. A., Reman, R., and Khan, M. A. Sorptiopn of Cs(I), Sr(II), and Co(II) on Al_2O_3. J. Radioanal. Nucl. Chem. 190, 81-96 (1995).

[60] Shahwan, T., Suzer, S., and Erten, H. N. Sorption Studies of Cs^+ and Ba^{2+} Cations on Magnesite. Appl. Radiat. Isot., 49/8, 915-920 (1998).

[61] Kwang, K., Kun-Jai, L., and Jae-Heum, B. Characterization of Cobalt Adsorption on Prepared TiO_2 and Fe-Ti-O Adsorbents in High Temperature Water. Separ. Sci. Tech., 30/6, 963-979 (1995).

[62] Khan, S. A., Reman, R. U., and Khan, M. A. Sorption of Cobalt on Bentonite. J. Radioanal. Nucl. Chem., 207/1, 19-37 (1996).

[63] Qadeer, R., Hanif, J., Saleem, M., and Afzal, M. Surface Characterization and Thermodynamics of Adsorption of Sr^{2+}, Ce^{3+}, Sm^{3+}, Cd^{3+}, Th^{4+}, UO_2^{3+} on Activated Charcoal from Aqueous Solution. Colloid. Polym. Sci., 271, 83-90 (1993).

[64] Briggs, D., and Seah, M. P. Practical Surface Analysis, Volume 2: Ion and Neutral Spectroscopy. John Wiley and Sons (1996).

[65] Schauer, S. N., and Williams P. Doubly Charged Ions of Fourth Raw Elements. Proceedings of the Eighth International Conference on Secondary Ion Mass Spectrometry (SIMS VIII). John Wiley and Sons (1992).

[66] Bennett, J., and Simons, D. Factors Influencing Quantitative SIMS Using a Microfocused Ga Ion Beam and TOF-MS. Proceedings of the Eighth International Conference on Secondary Ion Mass Spectrometry (SIMS VIII). John Wiley and Sons (1992).

[67] Sparrow, G. R. Quantitative SIMS Approximations for General Applications in Surface Science. 25th Conf. Mass Spec. & Allied Topics, May 29-June3, Washington D.C (1977)..

[68] Groenewold, G.S., Ingram, J.C., McLing, T., and Gianotto, A.K. Cs+ Speciation on Soil Particles by ToF-SIMS Imaging. Anal. Chem., 70, 534-539 (1998)

[69] Westrich, H.R., Brady P.V., Cygan, R.T, Gruenhagen, S.E., Anderson, H.L., and Nagy, K.L. Characterization of Retardation Mechanisms in Soil. NUREG/CR-6603 SAND98-0419 RW Report, Washington-USA (1998).

[70] Pingitore, N. E. Modes of Co-precipitation of Ba^{2+} and Sr^{2+} with Calcite. Am. Chem. Soc. Whashington D. C., 547-586 (1986).

[71] Fujikawa, Y. and Fukui, M. Radionuclide Sorption to Rocks and Minerals: Effects of pH and Inorganic Anions, Part 1. Sorption of Cesium, Cobalt, Strontium, and mangenese. Radiochim. Acta, 76, 153-162 (1997).

[72] Michael, N. X., Hochella JR. F., Brown JR. G. E., and Parks, G. A. Co(II) Sorption at the Calcite-Water Interface: I. X-ray Photoelectron Spectroscopyic Study. Geochim. et Cosmochim. Acta, 60/15, 2801-2815 (1996).

[73] Torstenfelt, B. Migration of Fission Products Strontium, Technetium, Iodine, and Cesium in Clay. Radiochimica Acta, 39, 97-104 (1986).

[74] Kozaki, T., Sato, H., Sato, S., and Ohashi, H. Diffusion Mechanism of Cesium Ions in Compacted Montmorillonite. Engineering Geology, 54, 223-230 (1999)

APPENDICES

APPENDIX A

Table A1: Variation of R_d Values with Shaking Time for Cs^+, Ba^{2+}, and Co^{2+} Sorption on Kaolinite

	R_d (mL/g)		
Shaking Time	**Cs-kaolinite**	**Ba-kaolinite**	**Co-kaolinite**
1 h	24	56	136
6 h	20	66	149
12 h	21	52	134
1 d	18	56	143
2 d	17	57	137
3 d	19	59	120
5 d	19	50	122
7 d	16	54	127

Table A2: Variation of R_d Values with Shaking Time for Cs^+, Ba^{2+}, and Co^{2+} Sorption on Chlorite-Illite

	R_d (mL/g)		
Shaking Time	**Cs- chlorite-illite**	**Ba- chlorite-illite**	**Co- chlorite-illite**
1 h	207	150	227
6 h	195	148	219
12 h	202	162	234
1 d	151	187	241
2 d	157	178	238
3 d	154	181	276
5 d	159	160	243
7 d	164	149	256

Table A3: Variation of R_d Values with Shaking Time for Cs^+, Ba^{2+}, and Co^{2+} Sorption on Bentonite

	R_d (mL/g)		
Shaking Time	**Cs- bentonite**	**Ba- bentonite**	**Co- bentonite**
1 h	1052	416	467
6 h	1137	414	482
12 h	1106	429	510
1 d	886	427	638
2 d	871	408	637
3 d	927	416	629
5 d	875	430	641
7 d	917	428	638

APPENDIX B

Table B1: The sorption data of Cs^+, Ba^{2+}, and Co^{2+} on kaolinite at different loadings and temperatures

		303 K			313 K			323 K			333 K		
Sorbed Cation	**$[C]^o$ meq/ml**	**$[C]_l$ meq/ml**	**$[C]_s$ meq/g**	**R_d ml/g**	**$[C]_l$ meq/ml**	**$[C]_s$ meq/g**	**R_d ml/g**	**$[C]_l$ meq/ml**	**$[C]_s$ meq/g**	**R_d ml/g**	**$[C]_l$ meq/ml**	**$[C]_s$ meq/g**	**R_d ml/g**
Cs^+	1.0×10^{-6}	6.1×10^{-7}	3.5×10^{-5}	58	6.2×10^{-7}	3.5×10^{-5}	56	6.3×10^{-7}	3.3×10^{-5}	53	6.5×10^{-7}	3.1×10^{-5}	47
	1.0×10^{-5}	6.5×10^{-6}	3.1×10^{-4}	48	6.7×10^{-6}	3.0×10^{-4}	44	7.0×10^{-6}	2.5×10^{-4}	36	7.3×10^{-6}	2.2×10^{-4}	30
	1.0×10^{-4}	7.1×10^{-5}	2.6×10^{-3}	36	7.3×10^{-5}	2.4×10^{-3}	33	7.6×10^{-5}	2.0×10^{-3}	26	7.8×10^{-5}	1.7×10^{-3}	22
	1.0×10^{-3}	7.6×10^{-4}	2.1×10^{-2}	28	7.9×10^{-4}	1.7×10^{-2}	22	8.1×10^{-4}	1.4×10^{-2}	17	8.3×10^{-4}	1.2×10^{-2}	15
Ba^{2+}	1.0×10^{-6}	2.2×10^{-7}	7.4×10^{-5}	338	2.4×10^{-7}	7.4×10^{-5}	309	2.5×10^{-7}	7.5×10^{-5}	296	2.5×10^{-7}	6.9×10^{-5}	275
	1.0×10^{-5}	2.9×10^{-6}	7.7×10^{-4}	267	2.7×10^{-6}	7.1×10^{-4}	261	2.7×10^{-6}	7.0×10^{-4}	273	2.7×10^{-6}	6.9×10^{-4}	254
	1.0×10^{-4}	3.4×10^{-5}	6.0×10^{-3}	177	3.7×10^{-5}	5.9×10^{-3}	159	3.8×10^{-5}	5.9×10^{-3}	156	4.1×10^{-5}	5.5×10^{-3}	135
	1.0×10^{-3}	7.3×10^{-4}	3.2×10^{-2}	44	6.9×10^{-4}	2.9×10^{-2}	42	7.3×10^{-4}	2.4×10^{-2}	33	7.3×10^{-4}	2.4×10^{-2}	33
Co^{2+}	3.6×10^{-5}	1.7×10^{-5}	2.1×10^{-3}	121	1.2×10^{-5}	2.7×10^{-3}	226	9.6×10^{-6}	3.0×10^{-3}	315	8.9×10^{-6}	3.1×10^{-3}	349
	3.6×10^{-4}	1.7×10^{-4}	1.8×10^{-2}	105	1.3×10^{-4}	2.1×10^{-2}	157	8.7×10^{-5}	2.6×10^{-2}	299	5.9×10^{-5}	2.8×10^{-2}	471
	3.6×10^{-3}	1.8×10^{-3}	1.5×10^{-1}	86	1.7×10^{-3}	1.8×10^{-1}	106	1.6×10^{-3}	1.9×10^{-1}	114	9.8×10^{-4}	2.5×10^{-1}	258
	3.6×10^{-2}	2.0×10^{-2}	1.3×10^{0}	66	1.9×10^{-2}	1.5×10^{0}	78	1.8×10^{-2}	1.6×10^{0}	89	1.2×10^{-2}	2.3×10^{0}	190

Table B2: The sorption data of Cs^+, Ba^{2+}, and Co^{2+} on chlorite-illite at different loadings and temperatures

		303 K			313 K			323 K			333 K		
Sorbed Cation	**$[C]^0$ meq/ml**	**$[C]_l$ meq/ml**	**$[C]_s$ meq/g**	**R_d ml/g**	**$[C]_l$ meq/ml**	**$[C]_s$ meq/g**	**R_d ml/g**	**$[C]_l$ meq/ml**	**$[C]_s$ meq/g**	**R_d ml/g**	**$[C]_l$ meq/ml**	**$[C]_s$ meq/g**	**R_d ml/g**
Cs^+	1.0×10^{-6}	3.6×10^{-8}	9.3×10^{-5}	2581	4.1×10^{-8}	8.9×10^{-5}	2132	4.2×10^{-8}	9.2×10^{-5}	2207	4.7×10^{-8}	9.2×10^{-5}	1966
	1.0×10^{-5}	5.1×10^{-7}	8.9×10^{-4}	1743	5.7×10^{-7}	9.1×10^{-4}	1594	7.3×10^{-7}	1.0×10^{-3}	1384	8.7×10^{-7}	9.0×10^{-4}	1039
	1.0×10^{-4}	7.8×10^{-6}	9.0×10^{-3}	1156	9.2×10^{-6}	9.0×10^{-3}	978	9.5×10^{-6}	8.9×10^{-3}	933	1.0×10^{-5}	8.8×10^{-3}	883
	1.0×10^{-3}	3.3×10^{-4}	5.7×10^{-2}	174	3.8×10^{-4}	5.9×10^{-2}	157	3.8×10^{-4}	5.9×10^{-2}	154	3.9×10^{-4}	5.7×10^{-2}	146
Ba^{2+}	1.0×10^{-6}	7.4×10^{-8}	9.4×10^{-5}	1273	7.6×10^{-8}	9.1×10^{-5}	1205	8.5×10^{-8}	8.9×10^{-5}	1047	9.2×10^{-8}	8.7×10^{-5}	956
	1.0×10^{-5}	1.0×10^{-6}	8.7×10^{-4}	872	1.1×10^{-6}	8.6×10^{-4}	780	1.1×10^{-6}	8.2×10^{-4}	744	1.2×10^{-6}	8.3×10^{-4}	726
	1.0×10^{-4}	1.2×10^{-5}	8.9×10^{-3}	741	1.2×10^{-5}	8.3×10^{-3}	694	1.1×10^{-5}	7.7×10^{-3}	707	1.3×10^{-5}	8.2×10^{-3}	630
	1.0×10^{-3}	3.5×10^{-4}	6.1×10^{-2}	173	3.5×10^{-4}	5.9×10^{-2}	169	3.5×10^{-4}	6.1×10^{-2}	173	3.6×10^{-4}	6.2×10^{-2}	171
Co^{2+}	3.6×10^{-4}	7.9×10^{-5}	2.6×10^{-2}	334	7.1×10^{-5}	2.8×10^{-2}	388	6.0×10^{-5}	2.9×10^{-2}	481	5.5×10^{-5}	3.0×10^{-2}	540
	3.6×10^{-3}	9.1×10^{-4}	2.6×10^{-1}	286	7.6×10^{-4}	2.7×10^{-1}	354	6.5×10^{-4}	2.9×10^{-1}	447	6.2×10^{-4}	3.2×10^{-1}	519
	3.6×10^{-2}	1.4×10^{-2}	2.0×10^{-0}	144	1.1×10^{-2}	2.3×10^{-0}	208	9.5×10^{-3}	2.6×10^{-0}	272	8.4×10^{-3}	2.5×10^{-0}	301

Table B3: The sorption data of Cs^+, Ba^{2+}, and Co^{2+} on bentonite at different loadings and temperatures

		303 K			313 K			323 K			333 K		
Sorbed Cation	**$[C]^o$ meq/ml**	**$[C]_l$ meq/ml**	**$[C]_s$ meq/g**	**R_d ml/g**	**$[C]_l$ meq/ml**	**$[C]_s$ meq/g**	**R_d ml/g**	**$[C]_l$ meq/ml**	**$[C]_s$ meq/g**	**R_d ml/g**	**$[C]_l$ meq/ml**	**$[C]_s$ meq/g**	**R_d ml/g**
Cs^+	1.0×10^{-6}	6.9×10^{-8}	8.9×10^{-5}	1291	7.3×10^{-8}	9.3×10^{-5}	1273	1.0×10^{-7}	8.4×10^{-5}	831	1.1×10^{-7}	8.9×10^{-5}	825
	1.0×10^{-5}	7.6×10^{-7}	9.3×10^{-4}	1223	7.5×10^{-7}	8.9×10^{-4}	1179	1.2×10^{-6}	8.5×10^{-4}	697	1.2×10^{-6}	8.4×10^{-4}	697
	1.0×10^{-4}	8.8×10^{-6}	8.7×10^{-3}	985	9.3×10^{-6}	8.8×10^{-3}	946	1.4×10^{-5}	8.5×10^{-3}	630	1.4×10^{-5}	8.7×10^{-3}	619
	1.0×10^{-3}	9.6×10^{-5}	8.8×10^{-2}	919	1.4×10^{-5}	8.4×10^{-2}	598	1.9×10^{-4}	7.8×10^{-2}	396	2.1×10^{-4}	7.8×10^{-2}	373
Ba^{2+}	1.0×10^{-6}	1.6×10^{-7}	7.9×10^{-5}	494	1.7×10^{-7}	7.7×10^{-5}	454	1.8×10^{-7}	7.5×10^{-5}	417	2.0×10^{-7}	7.4×10^{-5}	369
	1.0×10^{-5}	1.7×10^{-6}	7.9×10^{-4}	466	1.8×10^{-6}	7.9×10^{-4}	541	1.9×10^{-6}	7.6×10^{-4}	403	2.1×10^{-6}	7.5×10^{-4}	357
	1.0×10^{-4}	1.9×10^{-5}	7.5×10^{-3}	395	2.2×10^{-5}	7.5×10^{-3}	342	2.2×10^{-5}	7.3×10^{-3}	332	2.4×10^{-5}	7.0×10^{-3}	288
	1.0×10^{-3}	2.0×10^{-4}	7.5×10^{-2}	374	2.0×10^{-4}	7.6×10^{-2}	382	2.3×10^{-4}	7.3×10^{-2}	318	2.7×10^{-4}	6.9×10^{-2}	254
Co^{2+}	1.0×10^{-6}	8.0×10^{-8}	8.8×10^{-5}	1108	8.0×10^{-8}	9.7×10^{-5}	1224	7.3×10^{-8}	9.6×10^{-5}	1313	6.4×10^{-8}	9.1×10^{-5}	1422
	1.0×10^{-5}	9.3×10^{-7}	8.6×10^{-4}	925	9.0×10^{-7}	9.6×10^{-4}	1064	8.4×10^{-7}	9.3×10^{-4}	1108	7.5×10^{-7}	8.9×10^{-4}	1188
	1.0×10^{-4}	1.3×10^{-5}	8.3×10^{-3}	639	1.1×10^{-5}	8.7×10^{-3}	788	9.0×10^{-6}	8.9×10^{-3}	992	8.3×10^{-6}	9.1×10^{-3}	1097
	1.0×10^{-3}	1.8×10^{-4}	8.4×10^{-2}	464	1.6×10^{-4}	8.4×10^{-2}	545	1.2×10^{-4}	8.4×10^{-2}	699	1.1×10^{-4}	8.8×10^{-2}	796

APPENDIX C

Table C1: The Sorption Data Obtained Using ToF-SIMS for Cs^{+}, Ba^{2+}, and Co^{2+} Sorption on Natural Kaolinite

Natural Kaolinite

Recorded ounts

Element	0A	10A	20A	30A	40A	50A	70A	Total
Li	994	2028	961	895	835	460	241	6414
Na	202	148	68	73	67	45	37	640
Mg	564	670	303	312	300	185	147	2481
Al	4645	13021	7376	7546	7678	4394	3664	48324
Si	2944	4973	2456	2475	2477	1451	1160	17936
K	3492	14488	8613	8756	8777	4745	3669	52540
Ca	891	561	268	261	249	136	86	2452
Fe	350	220	101	98	92	52	32	945
Sensitivity Correction								
Li	0.2840	0.5794	0.2746	0.2557	0.2386	0.1314	0.0689	1.8326
Na	0.1010	0.0740	0.0340	0.0365	0.0335	0.0225	0.0185	0.3200
Mg	3.5250	4.1875	1.8938	1.9500	1.8750	1.1563	0.9188	15.5063
Al	38.7083	108.5083	61.4667	62.8833	63.9833	36.6167	30.5333	402.7000
Si	109.0370	184.1852	90.9630	91.6667	91.7407	53.7407	42.9630	664.2963
K	1.9400	8.0489	4.7850	4.8644	4.8761	2.6361	2.0383	29.1889
Ca	3.5640	2.2440	1.0720	1.0440	0.9960	0.5440	0.3440	9.8080
Fe	16.6667	10.4762	4.8095	4.6667	4.3810	2.4762	1.5238	45.0000
Si/Al	2.8169	1.6974	1.4799	1.4577	1.4338	1.4677	1.4071	1.6496
Al+Si	147.7454	292.6935	152.4296	154.5500	155.7241	90.3574	73.4963	1066.996
Calculation of Ratios								
Li	0.0019	0.0020	0.0018	0.0017	0.0015	0.0015	0.0009	0.0113
Na	0.0007	0.0003	0.0002	0.0002	0.0002	0.0002	0.0003	0.0021
Mg	0.0239	0.0143	0.0124	0.0126	0.0120	0.0128	0.0125	0.1005
Al+Si	1.0000	1.0000	1.0000	1.0000	1.0000	1.0000	1.0000	7.0000
K	0.0131	0.0275	0.0314	0.0315	0.0313	0.0292	0.0277	0.1917
Ca	0.0241	0.0077	0.0070	0.0068	0.0064	0.0060	0.0047	0.0627
Fe	0.1128	0.0358	0.0316	0.0302	0.0281	0.0274	0.0207	0.2866

Calculation of Fractions								
Li	0.1704	0.1755	0.1597	0.1467	0.1358	0.1289	0.0830	1.0000
Na	0.3238	0.1197	0.1056	0.1118	0.1019	0.1179	0.1192	1.0000
Mg	0.2373	0.1423	0.1236	0.1255	0.1198	0.1273	0.1243	1.0000
Al+Si	0.1429	0.1429	0.1429	0.1429	0.1429	0.1429	0.1429	1.0000
K	0.0685	0.1434	0.1637	0.1642	0.1633	0.1522	0.1447	1.0000
Ca	0.3849	0.1223	0.1122	0.1078	0.1021	0.0961	0.0747	1.0000
Fe	0.3936	0.1249	0.1101	0.1054	0.0982	0.0956	0.0723	1.0000

Cs-Sorbed Kaolinitre

Recorded Counts **Element**	**0A**	**10A**	**20A**	**30A**	**40A**	**50A**	**70A**	**Total**
Li	349	423	301	241	203	168	149	1834
Na	20	18	14	13	10	13	12	100
Mg	156	121	97	81	77	81	77	690
Al	1743	3354	3122	2915	2786	2816	2890	19626
Si	1401	1380	1207	1081	1003	1071	977	8120
K	1597	3295	2494	1987	1663	1684	1658	14378
Ca	233	69	59	51	45	48	46	551
Fe	106	60	46	35	27	31	28	333
Cs	3691	1074	790	606	474	481	465	7581
Sensitivity correction								
Li	0.0997	0.1209	0.0860	0.0689	0.0580	0.0480	0.0426	0.5240
Na	0.0100	0.0090	0.0070	0.0065	0.0050	0.0065	0.0060	0.0500
Mg	0.9750	0.7563	0.6063	0.5063	0.4813	0.5063	0.4813	4.3125
Al	14.5250	27.9500	26.0167	24.2917	23.2167	23.4667	24.0833	163.5500
Si	51.8889	51.1111	44.7037	40.0370	37.1481	39.6667	36.1852	300.7407
K	0.8872	1.8306	1.3856	1.1039	0.9239	0.9356	0.9211	7.9878
Ca	0.9320	0.2760	0.2360	0.2040	0.1800	0.1920	0.1840	2.2040
Fe	5.0476	2.8571	2.1905	1.6667	1.2857	1.4762	1.3333	15.8571
Cs	6.1517	1.7900	1.3167	1.0100	0.7900	0.8017	0.7750	12.6350
Si/Al	3.5724	1.8287	1.7183	1.6482	1.6001	1.6903	1.5025	1.8388
CF	0.7885	0.9282	0.8613	0.8844	0.8961	0.8683	0.9365	0.8971
Al+Si	66.4139	79.0611	70.7204	64.3287	60.3648	63.1333	60.2685	464.2907
Calculation of Ratios								
Li	0.0015	0.0015	0.0012	0.0011	0.0010	0.0008	0.0007	0.0077
Na	0.0002	0.0001	0.0001	0.0001	0.0001	0.0001	0.0001	0.0007
Mg	0.0147	0.0096	0.0086	0.0079	0.0080	0.0080	0.0080	0.0647
Al+Si	1.0000	1.0000	1.0000	1.0000	1.0000	1.0000	1.0000	7.0000
K	0.0134	0.0232	0.0196	0.0172	0.0153	0.0148	0.0153	0.1187
Ca	0.0140	0.0035	0.0033	0.0032	0.0030	0.0030	0.0031	0.0331
Fe	0.0760	0.0361	0.0310	0.0259	0.0213	0.0234	0.0221	0.2358
Cs	0.0926	0.0226	0.0186	0.0157	0.0131	0.0127	0.0129	0.1882

Ratios After Correction (=Ratio*CF)

Li	0.0012	0.0014	0.0010	0.0009	0.0009	0.0007	0.0007	0.0068
Na	0.0001	0.0001	0.0001	0.0001	0.0001	0.0001	0.0001	0.0007
Mg	0.0116	0.0089	0.0074	0.0070	0.0071	0.0070	0.0075	0.0564
Al+Si	0.7885	0.9282	0.8613	0.8844	0.8961	0.8683	0.9365	6.1633
K	0.0105	0.0215	0.0169	0.0152	0.0137	0.0129	0.0143	0.1050
Ca	0.0111	0.0032	0.0029	0.0028	0.0027	0.0026	0.0029	0.0282
Fe	0.0599	0.0335	0.0267	0.0229	0.0191	0.0203	0.0207	0.2032
Cs	0.0730	0.0210	0.0160	0.0139	0.0117	0.0110	0.0120	0.1588

Calculation of Fractions

Li	0.1746	0.2093	0.1545	0.1396	0.1270	0.0974	0.0976	1.0000
Na	0.1810	0.1611	0.1300	0.1363	0.1132	0.1363	0.1422	1.0000
Mg	0.2053	0.1575	0.1309	0.1234	0.1267	0.1235	0.1326	1.0000
Al+Si	0.1279	0.1506	0.1397	0.1435	0.1454	0.1409	0.1519	1.0000
K	0.1003	0.2047	0.1607	0.1446	0.1307	0.1226	0.1364	1.0000
Ca	0.3930	0.1151	0.1021	0.0996	0.0949	0.0938	0.1015	1.0000
Fe	0.2950	0.1651	0.1313	0.1128	0.0939	0.0999	0.1020	1.0000
Cs	0.4600	0.1324	0.1010	0.0875	0.0739	0.0694	0.0758	1.0000

Ba-Sorbed Kaolinite

Recorded Counts

Element	0A	10A	20A	30A	40A	50A	70A	Total
Li	569	1156	1078	931	813	774	666	5987
Na	59	86	90	85	75	74	67	536
Mg	211	327	346	328	321	313	302	2148
Al	2799	7606	8595	8576	8364	8433	8233	52606
Si	1936	3493	3733	3601	3412	3363	3226	22764
K	1271	6322	7313	6859	6412	6313	5891	40381
Ca	130	121	122	115	111	105	104	808
Fe	143	164	168	158	152	149	132	1066
Ba	681	1142	1168	1159	1044	1080	1000	7274

Sensitivity Correction

Li	0.1626	0.3303	0.3080	0.2660	0.2323	0.2211	0.1903	1.7106
Na	0.0295	0.0430	0.0450	0.0425	0.0375	0.0370	0.0335	0.2680
Mg	1.3188	2.0438	2.1625	2.0500	2.0063	1.9563	1.8875	13.4250
Al	23.3250	63.3833	71.6250	71.4667	69.7000	70.2750	68.6083	438.3833
Si	71.7037	129.3704	138.2593	133.3704	126.3704	124.5556	119.4815	843.1111
K	0.7061	3.5122	4.0628	3.8106	3.5622	3.5072	3.2728	22.4339
Ca	0.5200	0.4840	0.4880	0.4600	0.4440	0.4200	0.4160	3.2320
Fe	6.8095	7.8095	8.0000	7.5238	7.2381	7.0952	6.2857	50.7619
Ba	7.5667	12.6889	12.9778	12.8778	11.6000	12.0000	11.1111	80.8222

Si/Al	3.0741	2.0411	1.9303	1.8662	1.8131	1.7724	1.7415	1.9232
CF	0.9163	0.8316	0.7666	0.7811	0.7908	0.8281	0.8080	0.8577
Al+Si	95.0287	192.7537	209.8843	204.8370	196.0704	194.8306	188.0898	1281.494
Calculation of Ratios								
Li	0.0017	0.0017	0.0015	0.0013	0.0012	0.0011	0.0010	0.0095
Na	0.0003	0.0002	0.0002	0.0002	0.0002	0.0002	0.0002	0.0015
Mg	0.0139	0.0106	0.0103	0.0100	0.0102	0.0100	0.0100	0.0751
Al+Si	1.0000	1.0000	1.0000	1.0000	1.0000	1.0000	1.0000	7.0000
K	0.0074	0.0182	0.0194	0.0186	0.0182	0.0180	0.0174	0.1172
Ca	0.0055	0.0025	0.0023	0.0022	0.0023	0.0022	0.0022	0.0192
Fe	0.0717	0.0405	0.0381	0.0367	0.0369	0.0364	0.0334	0.2938
Ba	0.0796	0.0658	0.0618	0.0629	0.0592	0.0616	0.0591	0.4500
Ratios After Correction (=Ratio*CF)								
Li	0.0016	0.0014	0.0011	0.0010	0.0009	0.0009	0.0008	0.0078
Na	0.0003	0.0002	0.0002	0.0002	0.0002	0.0002	0.0001	0.0012
Mg	0.0127	0.0088	0.0079	0.0078	0.0081	0.0083	0.0081	0.0618
Al+Si	0.9163	0.8316	0.7666	0.7811	0.7908	0.8281	0.8080	5.7226
K	0.0068	0.0152	0.0148	0.0145	0.0144	0.0149	0.0141	0.0947
Ca	0.0050	0.0021	0.0018	0.0018	0.0018	0.0018	0.0018	0.0160
Fe	0.0657	0.0337	0.0292	0.0287	0.0292	0.0302	0.0270	0.2436
Ba	0.0730	0.0547	0.0474	0.0491	0.0468	0.0510	0.0477	0.3697
Calculation of Fractions								
Li	0.2003	0.1821	0.1438	0.1296	0.1197	0.1201	0.1044	1.0000
Na	0.2278	0.1486	0.1316	0.1298	0.1211	0.1259	0.1152	1.0000
Mg	0.2059	0.1428	0.1279	0.1266	0.1310	0.1346	0.1313	1.0000
Al+Si	0.1601	0.1453	0.1340	0.1365	0.1382	0.1447	0.1412	1.0000
K	0.0719	0.1601	0.1568	0.1535	0.1518	0.1575	0.1485	1.0000
Ca	0.3133	0.1305	0.1114	0.1096	0.1119	0.1116	0.1117	1.0000
Fe	0.2695	0.1383	0.1199	0.1178	0.1198	0.1238	0.1108	1.0000
Ba	0.1973	0.1481	0.1282	0.1328	0.1265	0.1379	0.1291	1.0000

Co-Sorbed Kaolinite

Absolute Values

Element	0A	10A	20A	30A	40A	50A	70A	Total
Li	752	1552	1228	1093	922	824	700	7071
Na	298	104	88	75	72	70	62	769
Mg	213	139	142	131	130	128	127	1010
Al	3977	4515	4573	4737	4708	4682	4682	31874
Si	2979	2129	2034	2018	1949	1886	1927	14922
K	1854	5240	5330	5311	4328	3949	3639	29651
Ca	238	91	71	77	75	75	64	691

Fe	107	77	68	68	62	55	47	484
Co	438	216	185	159	149	132	123	1402
Sensitivity Corrections								
Li	0.2149	0.4434	0.3509	0.3123	0.2634	0.2354	0.2000	2.0203
Na	0.1490	0.0520	0.0440	0.0375	0.0360	0.0350	0.0310	0.3845
Mg	1.3313	0.8688	0.8875	0.8188	0.8125	0.8000	0.7938	6.3125
Al	33.1417	37.6250	38.1083	39.4750	39.2333	39.0167	39.0167	265.6167
Si	110.3333	78.8519	75.3333	74.7407	72.1852	69.8519	71.3704	552.6667
K	1.0300	2.9111	2.9611	2.9506	2.4044	2.1939	2.0217	16.4728
Ca	0.9520	0.3640	0.2840	0.3080	0.3000	0.3000	0.2560	2.7640
Fe	5.0952	3.6667	3.2381	3.2381	2.9524	2.6190	2.2381	23.0476
Co	19.0435	9.3913	8.0435	6.9130	6.4783	5.7391	5.3478	60.9565
Si/Al	3.3291	2.0957	1.9768	1.8934	1.8399	1.7903	1.8292	2.0807
CF	0.8461	0.8099	0.7486	0.7699	0.7793	0.8198	0.7692	0.7928
Al+Si	143.4750	116.4769	113.4417	114.2157	111.4185	108.8685	110.3870	818.2833
Calculation of Ratios								
Li	0.0015	0.0038	0.0031	0.0027	0.0024	0.0022	0.0018	0.0175
Na	0.0010	0.0004	0.0004	0.0003	0.0003	0.0003	0.0003	0.0031
Mg	0.0093	0.0075	0.0078	0.0072	0.0073	0.0073	0.0072	0.0536
Al+Si	1.0000	1.0000	1.0000	1.0000	1.0000	1.0000	1.0000	7.0000
K	0.0072	0.0250	0.0261	0.0258	0.0216	0.0202	0.0183	0.1442
Ca	0.0066	0.0031	0.0025	0.0027	0.0027	0.0028	0.0023	0.0227
Fe	0.0355	0.0315	0.0285	0.0284	0.0265	0.0241	0.0203	0.1947
Co	0.1327	0.0806	0.0709	0.0605	0.0581	0.0527	0.0484	0.5041
Ratios After Correction (=Ratio*CF)								
Li	0.0013	0.0031	0.0023	0.0021	0.0018	0.0018	0.0014	0.0138
Na	0.0009	0.0004	0.0003	0.0003	0.0003	0.0003	0.0002	0.0025
Mg	0.0079	0.0060	0.0059	0.0055	0.0057	0.0060	0.0055	0.0425
Al+Si	0.8461	0.8099	0.7486	0.7699	0.7793	0.8198	0.7692	5.5429
K	0.0061	0.0202	0.0195	0.0199	0.0168	0.0165	0.0141	0.1132
Ca	0.0056	0.0025	0.0019	0.0021	0.0021	0.0023	0.0018	0.0182
Fe	0.0300	0.0255	0.0214	0.0218	0.0206	0.0197	0.0156	0.1547
Co	0.1123	0.0653	0.0531	0.0466	0.0453	0.0432	0.0373	0.4031
Calculation of Fractions								
Li	0.0920	0.2238	0.1680	0.1528	0.1337	0.1286	0.1011	1.0000
Na	0.3494	0.1438	0.1155	0.1005	0.1001	0.1048	0.0859	1.0000
Mg	0.1847	0.1421	0.1378	0.1298	0.1337	0.1417	0.1301	1.0000
Al+Si	0.1527	0.1461	0.1351	0.1389	0.1406	0.1479	0.1388	1.0000
K	0.0537	0.1789	0.1727	0.1757	0.1486	0.1460	0.1245	1.0000
Ca	0.3079	0.1388	0.1028	0.1138	0.1151	0.1239	0.0978	1.0000
Fe	0.1942	0.1648	0.1381	0.1411	0.1335	0.1275	0.1008	1.0000
Co	0.2786	0.1620	0.1317	0.1156	0.1124	0.1072	0.0925	1.0000

Table C2: The Sorption Data Obtained Using ToF-SIMS for Cs^{+}, Ba^{2+}, and Co^{2+} Sorption on Natural Chlorite-Illite

Natural Chlorite-Illite

Recorded Counts

Element	0A	10A	20A	30A	40A	50A	70A	Total
Li	37	39	40	32	37	33	30	248
Na	102	143	152	156	167	161	177	1058
Mg	239	436	445	426	434	416	411	2807
Al	1042	1998	2198	2318	2329	2343	2566	14794
Si	670	1140	1205	1268	1272	1274	1366	8195
K	362	1673	2422	2702	2822	2897	3642	16520
Ca	426	629	654	673	680	665	699	4426
Fe	242	354	366	363	358	349	351	2383
Sensitivity Corrections								
Li	0.0106	0.0111	0.0114	0.0091	0.0106	0.0094	0.0086	0.0709
Na	0.0510	0.0715	0.0760	0.0780	0.0835	0.0805	0.0885	0.5290
Mg	1.4938	2.7250	2.7813	2.6625	2.7125	2.6000	2.5688	17.5438
Al	8.6833	16.6500	18.3167	19.3167	19.4083	19.5250	21.3833	123.2833
Si	24.8148	42.2222	44.6296	46.9630	47.1111	47.1852	50.5926	303.5185
K	0.2011	0.9294	1.3456	1.5011	1.5678	1.6094	2.0233	9.1778
Ca	1.7040	2.5160	2.6160	2.6920	2.7200	2.6600	2.7960	17.7040
Fe	11.5238	16.8571	17.4286	17.2857	17.0476	16.6190	16.7143	113.4762
Si/Al	2.8578	2.5359	2.4366	2.4312	2.4274	2.4167	2.3660	2.4620
Al+Si	33.4981	58.8722	62.9463	66.2796	66.5194	66.7102	71.9759	426.8019
Calculation of Ratios								
Li	0.0003	0.0002	0.0002	0.0001	0.0002	0.0001	0.0001	0.0012
Na	0.0015	0.0012	0.0012	0.0012	0.0013	0.0012	0.0012	0.0088
Mg	0.0446	0.0463	0.0442	0.0402	0.0408	0.0390	0.0357	0.2907
Al+Si	1.0000	1.0000	1.0000	1.0000	1.0000	1.0000	1.0000	7.0000
K	0.0060	0.0158	0.0214	0.0226	0.0236	0.0241	0.0281	0.1416
Ca	0.0509	0.0427	0.0416	0.0406	0.0409	0.0399	0.0388	0.2954
Fe	0.3440	0.2863	0.2769	0.2608	0.2563	0.2491	0.2322	1.9057
Al	0.2592	0.2828	0.2910	0.2914	0.2918	0.2927	0.2971	2.0060
Si	0.7408	0.7172	0.7090	0.7086	0.7082	0.7073	0.7029	4.9940
Calculation of Fractions								
Li	0.2537	0.1522	0.1460	0.1109	0.1278	0.1136	0.0958	1.0000
Na	0.1728	0.1378	0.1370	0.1335	0.1424	0.1369	0.1395	1.0000
Mg	0.1534	0.1592	0.1520	0.1382	0.1403	0.1341	0.1228	1.0000
Al+Si	0.1429	0.1429	0.1429	0.1429	0.1429	0.1429	0.1429	1.0000
K	0.0424	0.1115	0.1509	0.1599	0.1664	0.1704	0.1985	1.0000

Ca	0.1722	0.1447	0.1407	0.1375	0.1384	0.1350	0.1315	1.0000
Fe	0.1805	0.1503	0.1453	0.1369	0.1345	0.1307	0.1219	1.0000
Al	0.1292	0.1410	0.1451	0.1453	0.1454	0.1459	0.1481	1.0000
Si	0.1483	0.1436	0.1420	0.1419	0.1418	0.1416	0.1408	1.0000

Cs-Sorbed Chlorite-Illite

Recorded Counts

Element	**0A**	**10A**	**20A**	**30A**	**40A**	**50A**	**70A**	**Total**
Li	49	31	28	31	23	19	16	197
Na	135	387	377	419	322	264	235	2139
Mg	383	745	709	755	626	534	525	4277
Al	1527	3898	4085	4444	3765	3398	3224	24341
Si	1888	2281	2392	2485	2072	1822	1664	14604
K	459	2921	2767	3088	2306	1925	1690	15156
Ca	331	754	821	935	781	731	687	5040
Fe	332	556	538	564	450	393	349	3182
Cs	3177	4219	3528	3594	2505	2011	1718	20752

Sensitivity Corrections

Li	0.0140	0.0089	0.0080	0.0089	0.0066	0.0054	0.0046	0.0563
Na	0.0675	0.1935	0.1885	0.2095	0.1610	0.1320	0.1175	1.0695
Mg	2.3938	4.6563	4.4313	4.7188	3.9125	3.3375	3.2813	26.7313
Al	12.7250	32.4833	34.0417	37.0333	31.3750	28.3167	26.8667	202.8417
Si	69.9259	84.4815	88.5926	92.0370	76.7407	67.4815	61.6296	540.8889
K	0.2550	1.6228	1.5372	1.7156	1.2811	1.0694	0.9389	8.4200
Ca	1.3240	3.0160	3.2840	3.7400	3.1240	2.9240	2.7480	20.1600
Fe	15.8095	26.4762	25.6190	26.8571	21.4286	18.7143	16.6190	151.5238
Cs	5.2950	7.0317	5.8800	5.9900	4.1750	3.3517	2.8633	34.5867
Si/Al	5.4952	2.6008	2.6025	2.4852	2.4459	2.3831	2.2939	2.6666
CF	0.5200	0.9750	0.9362	0.9783	0.9924	1.0141	1.0314	0.9233
Al+Si	82.6509	116.9648	122.6343	129.0704	108.1157	95.7981	88.4963	743.7306

Calculation of Ratios

Li	0.0002	0.0001	0.0001	0.0001	0.0001	0.0001	0.0001	0.0005
Na	0.0008	0.0017	0.0015	0.0016	0.0015	0.0014	0.0013	0.0098
Mg	0.0290	0.0398	0.0361	0.0366	0.0362	0.0348	0.0371	0.2496
Al+Si	1.0000	1.0000	1.0000	1.0000	1.0000	1.0000	1.0000	7.0000
K	0.0031	0.0139	0.0125	0.0133	0.0118	0.0112	0.0106	0.0764
Ca	0.0160	0.0258	0.0268	0.0290	0.0289	0.0305	0.0311	0.1880
Fe	0.1913	0.2264	0.2089	0.2081	0.1982	0.1954	0.1878	1.4160
Cs	0.0641	0.0601	0.0479	0.0464	0.0386	0.0350	0.0324	0.3245

Ratios After Correction (=Ratio*CF)

Li	0.0001	0.0001	0.0001	0.0001	0.0001	0.0001	0.0001	0.0005

Na	0.0004	0.0016	0.0014	0.0016	0.0015	0.0014	0.0014	0.0093
Mg	0.0151	0.0388	0.0338	0.0358	0.0359	0.0353	0.0382	0.2330
Al+Si	0.5200	0.9750	0.9362	0.9783	0.9924	1.0141	1.0314	6.4475
K	0.0016	0.0135	0.0117	0.0130	0.0118	0.0113	0.0109	0.0739
Ca	0.0083	0.0251	0.0251	0.0283	0.0287	0.0310	0.0320	0.1785
Fe	0.0995	0.2207	0.1956	0.2036	0.1967	0.1981	0.1937	1.3078
Cs	0.0333	0.0586	0.0449	0.0454	0.0383	0.0355	0.0334	0.2894

Calculation of Fractions

Li	0.1910	0.1601	0.1324	0.1456	0.1308	0.1246	0.1155	1.0000
Na	0.0456	0.1733	0.1546	0.1706	0.1587	0.1501	0.1471	1.0000
Mg	0.0647	0.1666	0.1452	0.1535	0.1542	0.1517	0.1642	1.0000
Al+Si	0.0807	0.1512	0.1452	0.1517	0.1539	0.1573	0.1600	1.0000
K	0.0217	0.1831	0.1588	0.1760	0.1591	0.1532	0.1481	1.0000
Ca	0.0467	0.1408	0.1404	0.1588	0.1606	0.1734	0.1794	1.0000
Fe	0.0761	0.1688	0.1496	0.1556	0.1504	0.1515	0.1481	1.0000
Cs	0.1151	0.2025	0.1551	0.1569	0.1324	0.1226	0.1153	1.0000

Ba-Sorbed Chlorite-Illite

Recorded Counts

Element	0A	10A	20A	30A	40A	50A	70A	Total
Li	70	92	69	99	88	62	72	552
Na	127	413	396	576	581	448	579	3120
Mg	695	1452	1277	1408	1471	1022	1432	8757
Al	3672	8564	8000	8805	9203	6453	9238	53935
Si	2261	4495	4332	4371	4767	3252	4781	28259
K	943	6683	6795	8504	8316	6388	7837	45466
Ca	595	1153	1131	1368	1418	1005	1512	8182
Fe	607	1140	963	1045	1063	751	1007	6576
Ba	867	1097	965	1044	1150	726	1106	6955

Sensitivity Corrections

Li	0.0200	0.0263	0.0197	0.0283	0.0251	0.0177	0.0206	0.1577
Na	0.0635	0.2065	0.1980	0.2880	0.2905	0.2240	0.2895	1.5600
Mg	4.3438	9.0750	7.9813	8.8000	9.1938	6.3875	8.9500	54.7313
Al	30.6000	71.3667	66.6667	73.3750	76.6917	53.7750	76.9833	449.4583
Si	83.7407	166.4815	160.4444	161.8889	176.5556	120.4444	177.0741	1046.6296
K	0.5239	3.7128	3.7750	4.7239	4.6200	3.5489	4.3539	25.2583
Ca	2.3800	4.6120	4.5240	5.4720	5.6720	4.0200	6.0480	32.7280
Fe	28.9048	54.2857	45.8571	49.7619	50.6190	35.7619	47.9524	313.1429
Ba	9.6333	12.1889	10.7222	11.6000	12.7778	8.0667	12.2889	77.2778
Si/Al	2.7366	2.3328	2.4067	2.2063	2.3021	2.2398	2.3002	2.3286
CF	1.0443	1.0871	1.0124	1.1019	1.0544	1.0790	1.0286	1.0572

Al+Si	114.3407	237.8481	227.1111	235.2639	253.2472	174.2194	254.0574	1496.0880

Calculation of Ratios

Li	0.0002	0.0001	0.0001	0.0001	0.0001	0.0001	0.0001	0.0008
Na	0.0006	0.0009	0.0009	0.0012	0.0011	0.0013	0.0011	0.0071
Mg	0.0380	0.0382	0.0351	0.0374	0.0363	0.0367	0.0352	0.2569
Al+Si	1.0000	1.0000	1.0000	1.0000	1.0000	1.0000	1.0000	7.0000
K	0.0046	0.0156	0.0166	0.0201	0.0182	0.0204	0.0171	0.1126
Ca	0.0208	0.0194	0.0199	0.0233	0.0224	0.0231	0.0238	0.1527
Fe	0.2528	0.2282	0.2019	0.2115	0.1999	0.2053	0.1887	1.4884
Ba	0.0843	0.0512	0.0472	0.0493	0.0505	0.0463	0.0484	0.3771

Ratios After Correction (=Ratio*CF)

Li	0.0002	0.0001	0.0001	0.0001	0.0001	0.0001	0.0001	0.0008
Na	0.0006	0.0009	0.0009	0.0013	0.0012	0.0014	0.0012	0.0075
Mg	0.0397	0.0415	0.0356	0.0412	0.0383	0.0396	0.0362	0.2720
Al+Si	1.0443	1.0871	1.0124	1.1019	1.0544	1.0790	1.0286	7.4077
K	0.0048	0.0170	0.0168	0.0221	0.0192	0.0220	0.0176	0.1195
Ca	0.0217	0.0211	0.0202	0.0256	0.0236	0.0249	0.0245	0.1616
Fe	0.2640	0.2481	0.2044	0.2331	0.2108	0.2215	0.1941	1.5760
Ba	0.0880	0.0557	0.0478	0.0543	0.0532	0.0500	0.0498	0.3987

Calculation of Fractions

Li	0.2225	0.1464	0.1071	0.1614	0.1275	0.1337	0.1015	1.0000
Na	0.0771	0.1254	0.1173	0.1793	0.1607	0.1844	0.1558	1.0000
Mg	0.1458	0.1525	0.1308	0.1515	0.1407	0.1454	0.1332	1.0000
A+Si	0.1410	0.1467	0.1367	0.1488	0.1423	0.1457	0.1389	1.0000
K	0.0400	0.1419	0.1408	0.1851	0.1609	0.1838	0.1475	1.0000
Ca	0.1345	0.1304	0.1248	0.1586	0.1461	0.1541	0.1515	1.0000
Fe	0.1675	0.1574	0.1297	0.1479	0.1337	0.1405	0.1232	1.0000
Ba	0.2207	0.1397	0.1199	0.1363	0.1334	0.1253	0.1248	1.0000

Co-Sorbed Chlorite-Illite

Recorded Counts

Element	**0A**	**10A**	**20A**	**30A**	**40A**	**50A**	**70A**	**Total**
Li	27	33	32	35	28	33	29	217
Na	103	145	179	173	138	162	125	1025
Mg	558	598	663	640	585	718	620	4382
Al	2691	3611	4209	4210	3942	4785	4271	27719
Si	3896	3965	4338	4210	3898	4529	4106	28942
K	259	1178	1439	1239	955	1226	926	7222
Ca	653	607	700	701	660	796	715	4832
Fe	550	543	619	576	521	609	501	3919
Co	556	502	531	479	427	493	401	3389

Sensitivity Corrections								
Li	0.007714	0.009429	0.009143	0.01	0.008	0.009429	0.008286	0.062
Na	0.0515	0.0725	0.0895	0.0865	0.069	0.081	0.0625	0.5125
Mg	3.4875	3.7375	4.14375	4	3.65625	4.4875	3.875	27.3875
Al	22.425	30.09167	35.075	35.08333	32.85	39.875	35.59167	230.9917
Si	144.2963	146.8519	160.6667	155.9259	144.3704	167.7407	152.0741	1071.926
K	0.143889	0.654444	0.799444	0.688333	0.530556	0.681111	0.514444	4.012222
Ca	2.612	2.428	2.8	2.804	2.64	3.184	2.86	19.328
Fe	26.19048	25.85714	29.47619	27.42857	24.80952	29	23.85714	186.619
Co	24.17391	21.82609	23.08696	20.82609	18.56522	21.43478	17.43478	147.3478
Si/Al	6.434617	4.88015	4.58066	4.444444	4.394836	4.206664	4.272744	4.640539
CF	0.444122	0.519629	0.531923	0.547023	0.552322	0.574482	0.553738	0.530533
Al+Si	166.7213	176.9435	195.7417	191.0093	177.2204	207.6157	187.6657	1302.918
Calculation of Ratios								
Li	4.63E-05	5.33E-05	4.67E-05	5.24E-05	4.51E-05	4.54E-05	4.42E-05	0.000333
Na	0.000309	0.00041	0.000457	0.000453	0.000389	0.00039	0.000333	0.002741
Mg	0.020918	0.021123	0.021169	0.020941	0.020631	0.021614	0.020648	0.147046
Al+Si	1	1	1	1	1	1	1	7
K	0.000863	0.003699	0.004084	0.003604	0.002994	0.003281	0.002741	0.021265
Ca	0.015667	0.013722	0.014305	0.01468	0.014897	0.015336	0.01524	0.103846
Fe	0.157091	0.146132	0.150587	0.143598	0.139993	0.139681	0.127126	1.004208
Co	0.144996	0.123351	0.117946	0.109032	0.104758	0.103243	0.092903	0.796228
Ratios After Correction (=Ratio*CF)								
Li	2.05E-05	2.77E-05	2.48E-05	2.86E-05	2.49E-05	2.61E-05	2.44E-05	0.000177
Na	0.000137	0.000213	0.000243	0.000248	0.000215	0.000224	0.000184	0.001465
Mg	0.00929	0.010976	0.011261	0.011455	0.011395	0.012417	0.011434	0.078228
Al+Si	0.444122	0.519629	0.531923	0.547023	0.552322	0.574482	0.553738	3.72324
K	0.000383	0.001922	0.002172	0.001971	0.001654	0.001885	0.001518	0.011505
Ca	0.006958	0.00713	0.007609	0.00803	0.008228	0.00881	0.008439	0.055204
Fe	0.069768	0.075935	0.080101	0.078552	0.077321	0.080244	0.070394	0.532314
Co	0.064396	0.064097	0.062738	0.059643	0.05786	0.059311	0.051444	0.419489
Calculation of Fractions								
Li	0.115974	0.156264	0.140217	0.161624	0.140709	0.147237	0.137976	1
Na	0.093668	0.145368	0.166058	0.169138	0.146825	0.153029	0.125914	1
Mg	0.118758	0.140307	0.143945	0.146436	0.145664	0.15873	0.14616	1
Al+Si	0.119284	0.139564	0.142866	0.146921	0.148344	0.154296	0.148725	1
K	0.033316	0.167048	0.188827	0.17134	0.143721	0.163811	0.131937	1
Ca	0.12604	0.129162	0.137832	0.145464	0.149042	0.159594	0.152866	1
Fe	0.131065	0.14265	0.150477	0.147566	0.145254	0.150746	0.132242	1
Co	0.15351	0.152797	0.149559	0.14218	0.13793	0.141389	0.122635	1

Table C3: The Sorption Data Obtained Using ToF-SIMS for Cs^{+}, Ba^{2+}, and Co^{2+} Sorption on Natural Bentonite

Natural Bentonite

Recorded Counts

Element	0A	10A	20A	30A	40A	50A	70A	Total
Li	69	72	56	41	40	40	40	358
Na	10154	10941	7498	5533	4299	3428	2828	44681
Mg	884	1546	1512	1464	1383	1302	1302	9393
Al	2227	4563	4911	5093	5193	5096	5302	32385
Si	2770	3750	3482	3392	3458	3369	3241	23462
K	542	1963	1594	1349	1205	1127	1064	8844
Ca	140	209	224	242	246	242	270	1573
Fe	642	954	775	604	499	442	419	4335
Sensitivity Corrections								
Li	0.0197	0.0206	0.0160	0.0117	0.0114	0.0114	0.0114	0.1023
Na	5.0770	5.4705	3.7490	2.7665	2.1495	1.7140	1.4140	22.3405
Mg	5.5250	9.6625	9.4500	9.1500	8.6438	8.1375	8.1375	58.7063
Al	18.5583	38.0250	40.9250	42.4417	43.2750	42.4667	44.1833	269.8750
Si	102.5926	138.8889	128.9630	125.6296	128.0741	124.7778	120.0370	868.9630
K	0.3011	1.0906	0.8856	0.7494	0.6694	0.6261	0.5911	4.9133
Ca	0.5600	0.8360	0.8960	0.9680	0.9840	0.9680	1.0800	6.2920
Fe	30.5714	45.4286	36.9048	28.7619	23.7619	21.0476	19.9524	206.4286
Si/Al	5.5281	3.6526	3.1512	2.9601	2.9595	2.9383	2.7168	23.9065
Al+Si	121.1509	176.9139	169.8880	168.0713	171.3491	167.2444	164.2204	1138.84
Calculation of Ratios								
Li	0.0002	0.0001	0.0001	0.0001	0.0001	0.0001	0.0001	0.0006
Na	0.0419	0.0309	0.0221	0.0165	0.0125	0.0102	0.0086	0.1428
Mg	0.0456	0.0546	0.0556	0.0544	0.0504	0.0487	0.0496	0.3589
Al+Si	1.0000	1.0000	1.0000	1.0000	1.0000	1.0000	1.0000	7.0000
K	0.0025	0.0062	0.0052	0.0045	0.0039	0.0037	0.0036	0.0296
Ca	0.0046	0.0047	0.0053	0.0058	0.0057	0.0058	0.0066	0.0385
Fe	0.2523	0.2568	0.2172	0.1711	0.1387	0.1258	0.1215	1.2835
Calculation of Fractions								
Li	0.2513	0.1796	0.1454	0.1076	0.1030	0.1055	0.1075	1.0000
Na	0.2935	0.2166	0.1546	0.1153	0.0879	0.0718	0.0603	1.0000
Mg	0.1271	0.1522	0.1550	0.1517	0.1405	0.1356	0.1381	1.0000
Al+Si	0.1429	0.1429	0.1429	0.1429	0.1429	0.1429	0.1429	1.0000
K	0.0840	0.2085	0.1763	0.1508	0.1321	0.1266	0.1217	1.0000
Ca	0.1201	0.1228	0.1370	0.1496	0.1492	0.1504	0.1709	1.0000
Fe	0.1966	0.2001	0.1692	0.1333	0.1080	0.0981	0.0947	1.0000

Cs-Sorbed Bentonite

Recorded Counts

Li	34	26	20	18	15	15	16	144

Na	2144	751	580	498	459	471	461	5364
Mg	1206	1136	1064	1051	998	1015	1020	7490
Al	2612	3670	3864	4101	4027	4199	4306	26779
Si	4098	3182	2974	2974	2915	2847	2798	21788
K	236	1004	860	792	781	784	797	5254
Ca	194	287	304	321	327	345	363	2141
Fe	792	700	532	457	403	392	365	3641
Cs	5645	6178	4870	4420	4070	3942	3796	32921
Sensitivity Corrections								
Li	0.0097	0.0074	0.0057	0.0051	0.0043	0.0043	0.0046	0.0411
Na	1.0720	0.3755	0.2900	0.2490	0.2295	0.2355	0.2305	2.6820
Mg	7.5375	7.1000	6.6500	6.5688	6.2375	6.3438	6.3750	46.8125
Al	21.7667	30.5833	32.2000	34.1750	33.5583	34.9917	35.8833	223.1583
Si	151.7778	117.8519	110.1481	110.1481	107.9630	105.4444	103.6296	806.9630
K	0.1311	0.5578	0.4778	0.4400	0.4339	0.4356	0.4428	2.9189
Ca	0.7760	1.1480	1.2160	1.2840	1.3080	1.3800	1.4520	8.5640
Fe	37.7143	33.3333	25.3333	21.7619	19.1905	18.6667	17.3810	173.3810
Cs	9.4083	10.2967	8.1167	7.3667	6.7833	6.5700	6.3267	54.8683
Si/Al	6.9729	3.8535	3.4207	3.2231	3.2172	3.0134	2.8880	26.5888
CF	0.7928	0.9479	0.9212	0.9184	0.9199	0.9751	0.9407	0.8991
Al+Si	173.5444	148.4352	142.3481	144.3231	141.5213	140.4361	139.5130	1030.12
Calculation of Ratios								
Li	0.0001	0.0001	0.0000	0.0000	0.0000	0.0000	0.0000	0.0003
Na	0.0062	0.0025	0.0020	0.0017	0.0016	0.0017	0.0017	0.0174
Mg	0.0434	0.0478	0.0467	0.0455	0.0441	0.0452	0.0457	0.3184
Al+Si	1.0000	1.0000	1.0000	1.0000	1.0000	1.0000	1.0000	7.0000
K	0.0008	0.0038	0.0034	0.0030	0.0031	0.0031	0.0032	0.0203
Ca	0.0045	0.0077	0.0085	0.0089	0.0092	0.0098	0.0104	0.0591
Fe	0.2173	0.2246	0.1780	0.1508	0.1356	0.1329	0.1246	1.1637
Cs	0.0542	0.0694	0.0570	0.0510	0.0479	0.0468	0.0453	0.3717
Calculation of Corrected Ratios (Ratio*CF)								
Li	0.0000	0.0000	0.0000	0.0000	0.0000	0.0000	0.0000	0.0002
Na	0.0049	0.0024	0.0019	0.0016	0.0015	0.0016	0.0016	0.0154
Mg	0.0344	0.0453	0.0430	0.0418	0.0405	0.0440	0.0430	0.2922
Al+Si	0.7928	0.9479	0.9212	0.9184	0.9199	0.9751	0.9407	6.4160
K	0.0006	0.0036	0.0031	0.0028	0.0028	0.0030	0.0030	0.0189
Ca	0.0035	0.0073	0.0079	0.0082	0.0085	0.0096	0.0098	0.0548
Fe	0.1723	0.2129	0.1639	0.1385	0.1247	0.1296	0.1172	1.0591
Cs	0.0430	0.0658	0.0525	0.0469	0.0441	0.0456	0.0427	0.3405
Calculation of Fractions								
Li	0.1775	0.1898	0.1479	0.1309	0.1115	0.1190	0.1233	1.0000
Na	0.3172	0.1553	0.1216	0.1026	0.0966	0.1059	0.1007	1.0000
Mg	0.1178	0.1552	0.1473	0.1431	0.1388	0.1507	0.1471	1.0000
Al+Si	0.1236	0.1477	0.1436	0.1431	0.1434	0.1520	0.1466	1.0000
K	0.0317	0.1886	0.1637	0.1483	0.1494	0.1602	0.1581	1.0000

Ca	0.0647	0.1338	0.1436	0.1491	0.1552	0.1749	0.1787	1.0000
Fe	0.1627	0.2010	0.1548	0.1308	0.1178	0.1224	0.1107	1.0000
Cs	0.1262	0.1931	0.1543	0.1377	0.1295	0.1340	0.1253	1.0000

Ba-Sorbed Bentonite

Recorded Counts

Element	0A	10A	20A	30A	40A	50A	70A	Total
Li	65	52	45	37	43	42	37	321
Na	471	1031	936	810	742	748	787	5525
Mg	1032	978	1034	981	934	922	894	6775
Al	2574	3086	3730	3836	3862	3928	3999	25015
Si	3174	3321	3207	3052	2784	2902	2767	21207
K	382	973	855	761	733	755	786	5245
Ca	140	246	300	314	349	633	429	2411
Fe	713	702	625	807	478	480	450	4255
Ba	1202	911	736	779	765	747	734	6611
Sensitivity Corrections								
Li	0.0186	0.0149	0.0129	0.0106	0.0123	0.0120	0.0106	0.0917
Na	0.2355	0.5155	0.4680	0.4050	0.3710	0.3740	0.3935	2.7625
Mg	6.4500	6.1125	6.4625	6.1313	5.8375	5.7625	5.5875	42.3438
Al	21.4500	25.7167	31.0833	31.9667	32.1833	32.7333	33.3250	208.4583
Si	117.5556	123.0000	118.7778	113.0370	103.1111	107.4815	102.4815	785.4444
K	0.2122	0.5406	0.4750	0.4228	0.4072	0.4194	0.4367	2.9139
Ca	0.5600	0.9840	1.2000	1.2560	1.3960	2.5320	1.7160	9.6440
Fe	33.9524	33.4286	29.7619	38.4286	22.7619	22.8571	21.4286	202.6190
Ba	13.3579	10.1264	8.1824	8.6565	8.4965	8.3007	8.1484	73.4512
Si/Al	5.4804	4.7829	3.8213	3.5361	3.2039	3.2835	3.0752	3.7679
CF	1.0087	0.7637	0.8246	0.8371	0.9237	0.8948	0.8834	6.3448
Al+Si	139.0056	148.7167	149.8611	145.0037	135.2944	140.2148	135.8065	993.9028
Calculation of Ratios								
Li	0.0001	0.0001	0.0001	0.0001	0.0001	0.0001	0.0001	0.0006
Na	0.0017	0.0035	0.0031	0.0028	0.0027	0.0027	0.0029	0.0194
Mg	0.0464	0.0411	0.0431	0.0423	0.0431	0.0411	0.0411	0.2983
Al+Si	1.0000	1.0000	1.0000	1.0000	1.0000	1.0000	1.0000	7.0000
K	0.0015	0.0036	0.0032	0.0029	0.0030	0.0030	0.0032	0.0205
Ca	0.0040	0.0066	0.0080	0.0087	0.0103	0.0181	0.0126	0.0683
Fe	0.2443	0.2248	0.1986	0.2650	0.1682	0.1630	0.1578	1.4217
Ba	0.0961	0.0681	0.0546	0.0597	0.0628	0.0592	0.0600	0.4509
Calculation of Ratios After Correction (Ratio*CF)								
Li	0.0001	0.0001	0.0001	0.0001	0.0001	0.0001	0.0001	0.0006
Na	0.0017	0.0026	0.0026	0.0023	0.0025	0.0024	0.0026	0.0167
Mg	0.0468	0.0314	0.0356	0.0354	0.0399	0.0368	0.0363	0.2621
Al+Si	1.0087	0.7637	0.8246	0.8371	0.9237	0.8948	0.8834	6.1361
K	0.0015	0.0028	0.0026	0.0024	0.0028	0.0027	0.0028	0.0177
Ca	0.0041	0.0051	0.0066	0.0073	0.0095	0.0162	0.0112	0.0598
Fe	0.2464	0.1717	0.1638	0.2218	0.1554	0.1459	0.1394	1.2443

Ba	0.0970	0.0521	0.0453	0.0504	0.0579	0.0528	0.0532	0.4087
Calculation of Fractions								
Li	0.2356	0.1334	0.1237	0.1067	0.1466	0.1339	0.1202	1.0000
Na	0.1020	0.1580	0.1538	0.1396	0.1512	0.1425	0.1528	1.0000
Mg	0.1786	0.1197	0.1357	0.1350	0.1520	0.1403	0.1387	1.0000
Al+Si	0.1644	0.1245	0.1344	0.1364	0.1505	0.1458	0.1440	1.0000
K	0.0872	0.1571	0.1479	0.1381	0.1574	0.1515	0.1608	1.0000
Ca	0.0679	0.0845	0.1104	0.1212	0.1593	0.2701	0.1866	1.0000
Fe	0.1980	0.1380	0.1316	0.1783	0.1249	0.1172	0.1120	1.0000
Ba	0.2373	0.1275	0.1108	0.1233	0.1417	0.1292	0.1302	1.0000

Cobalt-Sorbed Bentonite

Recorded Counts

Element	0A	10A	20A	30A	40A	50A	70A	Total
Li	31	32	29	27	21	19	19	178
Na	131	596	411	404	374	312	321	2549
Mg	1179	1317	1283	1307	1289	1149	1206	8730
Al	2825	4158	4124	4233	4312	4144	4435	28231
Si	4952	5582	5203	5036	4983	4627	4678	35061
K	198	1083	917	869	827	658	692	5244
Ca	156	226	247	268	277	266	292	1732
Fe	963	989	889	815	757	675	642	5730
Co	368	390	335	310	295	269	258	2225
Sensitivity Corrections								
Li	0.0089	0.0091	0.0083	0.0077	0.0060	0.0054	0.0054	0.0509
Na	0.0655	0.2980	0.2055	0.2020	0.1870	0.1560	0.1605	1.2745
Mg	7.3688	8.2313	8.0188	8.1688	8.0563	7.1813	7.5375	54.5625
Al	23.5417	34.6500	34.3667	35.2750	35.9333	34.5333	36.9583	235.2583
Si	183.4074	206.7407	192.7037	186.5185	184.5556	171.3704	173.2593	1298.56
K	0.1100	0.6017	0.5094	0.4828	0.4594	0.3656	0.3844	2.9133
Ca	0.6240	0.9040	0.9880	1.0720	1.1080	1.0640	1.1680	6.9280
Fe	45.8571	47.0952	42.3333	38.8095	36.0476	32.1429	30.5714	272.8571
Co	16.0000	16.9565	14.5652	13.4783	12.8261	11.6957	11.2174	96.7391
Si/Al	7.7908	5.9665	5.6073	5.2876	5.1361	4.9625	4.6880	39.4386
CF	0.7096	0.6122	0.5620	0.5598	0.5762	0.5921	0.5795	0.6062
Al+Si	206.9491	241.3907	227.0704	221.7935	220.4889	205.9037	210.2176	1533.81
Calculation of Ratios								
Li	0.0000	0.0000	0.0000	0.0000	0.0000	0.0000	0.0000	0.0002
Na	0.0003	0.0012	0.0009	0.0009	0.0008	0.0008	0.0008	0.0057
Mg	0.0356	0.0341	0.0353	0.0368	0.0365	0.0349	0.0359	0.2491
Al+Si	1.0000	1.0000	1.0000	1.0000	1.0000	1.0000	1.0000	7.0000
K	0.0005	0.0025	0.0022	0.0022	0.0021	0.0018	0.0018	0.0131
Ca	0.0030	0.0037	0.0044	0.0048	0.0050	0.0052	0.0056	0.0317
Fe	0.2216	0.1951	0.1864	0.1750	0.1635	0.1561	0.1454	1.2431
Co	0.0773	0.0702	0.0641	0.0608	0.0582	0.0568	0.0534	0.4408

Calculation of Corrected Ratios (Ratio*CF)

Li	0.0000	0.0000	0.0000	0.0000	0.0000	0.0000	0.0000	0.0001
Na	0.0002	0.0008	0.0005	0.0005	0.0005	0.0004	0.0004	0.0034
Mg	0.0253	0.0209	0.0198	0.0206	0.0211	0.0207	0.0208	0.1491
Al+Si	0.7096	0.6122	0.5620	0.5598	0.5762	0.5921	0.5795	4.1914
K	0.0004	0.0015	0.0013	0.0012	0.0012	0.0011	0.0011	0.0077
Ca	0.0021	0.0023	0.0024	0.0027	0.0029	0.0031	0.0032	0.0188
Fe	0.1572	0.1194	0.1048	0.0980	0.0942	0.0924	0.0843	0.7503
Co	0.0549	0.0430	0.0360	0.0340	0.0335	0.0336	0.0309	0.2660

Calculation of Fractions

Li	0.2172	0.1659	0.1467	0.1393	0.1122	0.1117	0.1071	1.0000
Na	0.0665	0.2237	0.1505	0.1509	0.1447	0.1328	0.1310	1.0000
Mg	0.1695	0.1400	0.1331	0.1383	0.1412	0.1385	0.1394	1.0000
Al+Si	0.1693	0.1461	0.1341	0.1336	0.1375	0.1413	0.1383	1.0000
K	0.0490	0.1983	0.1639	0.1584	0.1561	0.1366	0.1377	1.0000
Ca	0.1141	0.1222	0.1304	0.1442	0.1544	0.1631	0.1717	1.0000
Fe	0.2096	0.1592	0.1396	0.1306	0.1256	0.1232	0.1123	1.0000
Co	0.2062	0.1617	0.1355	0.1279	0.1260	0.1264	0.1163	1.0000

APPENDIX D

Table D1: The Depletion Factors of K^+, Mg^{2+}, and Ca^{2+} for Cs^+, Ba^{2+}, and Co^{2+} sorption on kaolinite obtained by ToF-SIMS

Depleted Ion	**Sorbed Ion**	**Depletion Factors at Different Depths in Kaolinite Matriz**						
		0 Å	**10 Å**	**20 Å**	**30 Å**	**40 Å**	**50 Å**	**70 Å**
K^+	Cs^+	0.20	0.22	0.46	0.52	0.56	0.51	0.48
	Ba^{2+}	0.48	0.45	0.53	0.54	0.54	0.49	0.49
	Co^{2+}	0.54	0.26	0.38	0.37	0.46	0.43	0.49
Mg^{2+}	Cs^+	0.51	0.38	0.41	0.45	0.41	0.45	0.40
	Ba^{2+}	0.47	0.38	0.36	0.38	0.33	0.35	0.35
	Co^{2+}	0.67	0.58	0.53	0.56	0.53	0.53	0.56
Ca^{2+}	Cs^+	0.54	0.58	0.59	0.58	0.58	0.57	0.39
	Ba^{2+}	0.79	0.73	0.75	0.74	0.72	0.70	0.62
	Co^{2+}	0.77	0.67	0.73	0.69	0.67	0.62	0.62

Table D2: The Depletion Factors of K^+, Mg^{2+}, and Ca^{2+} for Cs^+, Ba^{2+}, and Co^{2+} sorption on chlorite-illite obtained by ToF-SIMS

Depleted Ion	**Sorbed Ion**	**Depletion Factors at Different Depths in Chlorite-Illite**						
		0 Å	**10 Å**	**20 Å**	**30 Å**	**40 Å**	**50 Å**	**70 Å**
K^+	Cs^+	0.73	0.14	0.45	0.43	0.50	0.53	0.61
	Ba^{2+}	0.20	0.01	0.21	0.02	0.18	0.09	0.37
	Co^{2+}	0.94	0.88	0.90	0.91	0.93	0.92	0.95
Mg^{2+}	Cs^+	0.66	0.16	0.23	0.11	0.12	0.09	0.02
	Ba^{2+}	0.11	0.10	0.19	0.043	0.06	0	0
	Co^{2+}	0.79	0.76	0.75	0.71	0.72	0.68	0.68
Ca^{2+}	Cs^+	0.84	0.41	0.40	0.30	0.30	0.22	0.18
	Ba^{2+}	0.57	0.51	0.51	0.37	0.42	0.38	0.37
	Co^{2+}	0.86	0.83	0.82	0.80	0.80	0.78	0.78

Table D3: The Depletion Factors of Na^+ and Mg^{2+} for Cs^+, Ba^{2+}, and Co^{2+} sorption on bentonite obtained by ToF-SIMS

Depleted Ion	**Sorbed Ion**	**Depletion Factors at Different Depths in Bentonite**						
		0 Å	**10 Å**	**20 Å**	**30 Å**	**40 Å**	**50 Å**	**70 Å**
Na^+	Cs^+	0.88	0.92	0.91	0.90	0.88	0.84	0.82
	Ba^{2+}	0.96	0.91	0.88	0.86	0.80	0.77	0.70
	Co^{2+}	0.99	0.98	0.98	0.97	0.96	0.96	0.95
Mg^{2+}	Cs^+	0.24	0.17	0.23	0.23	0.20	0.09	0.13
	Ba^{2+}	0.02	0.43	0.36	0.35	0.21	0.24	0.27
	Co^{2+}	0.45	0.62	0.64	0.62	0.58	0.58	0.58

APPENDIX E

Table E1: The XPS Results of Cs^+ and Ba^{2+} Sorption on Natural Kaolinite

Natural Kaolinite

Element Identity	*Center (eV)*	*Peak Intensity*	*Sensitivity Factor*	*Corrected Intensity*	*Atomic Percentage*
K 2p3/2	299.90	0.10	2.67	0.04	0.87
Al 2p1/2	81.10	0.72	0.57	1.27	30.34
Si 2p1/2	109.50	2.44	0.87	2.82	67.29
Ca 2p1/2	355.10	0.32	5.13	0.06	1.49

Cs-Sorbed Kaolinite

Element Identity	*Center (eV)*	*Peak Intensity*	*Sensitivity Factor*	*Corrected Intensity*	*Atomic Percentage*
Al 2p1/2	82.24	0.51	0.57	1.12	16.55
Si 2p1/2	110.20	2.15	0.87	2.48	80.71
Cs 3d5/2	732.10	1.94	22.93	0.09	2.75

Ba-Sorbed Kaolinite

Element Identity	*Center (eV)*	*Peak Intensity*	*Sensitivity Factor*	*Corrected Intensity*	*Atomic Percentage*
K 2p3/2	299.80	0.08	2.67	0.03	0.68
Al 2p1/2	81.50	0.73	0.57	1.28	31.2
Si 2p1/2	109.60	2.36	0.87	2.73	66.59
Ba 3d5/2	787.60	1.55	24.75	0.06	1.52

Table E2: The XPS Results of Cs^{+} and Ba^{2+} Sorption on Natural Chlorite-Illite

Natural Chlorite-Illite

Element Identity	*Center (eV)*	*Peak Intensity*	*Sensitivity Factor*	*Corrected Intensity*	*Atomic Percentage*
K 2p3/2	299.30	0.12	2.67	0.05	1.42
Al 2p1/2	80.80	0.51	0.57	0.89	27.78
Si 2p1/2	109.00	1.67	0.87	1.93	60.36
Fe 2p3/2	718.00	0.53	10.54	0.05	1.56
Ca 2p1/2	353.90	1.46	5.13	0.28	8.87

Cs-Sorbed Chlorite-Illite

Element Identity	*Center (eV)*	*Peak Intensity*	*Sensitivity Factor*	*Corrected Intensity*	*Atomic Percentage*
K 2p3/2	300.80	0.17	2.67	0.06	2.28
Al 2p1/2	82.38	0.46	0.57	0.46	70.24
Si 2p1/2	110.00	1.68	0.87	1.94	16.57
Cs 3d5/2	732.30	1.98	22.93	0.09	3.12
Ca 2p1/2	354.03	1.11	5.13	0.22	7.79

Ba-Sorbed Chlorite-Illite

Element Identity	*Center (eV)*	*Peak Intensity*	*Sensitivity Factor*	*Corrected Intensity*	*Atomic Percentage*
K 2p3/2	298.30	0.19	2.67	0.07	2.81
Al 2p1/2	82.70	0.33	0.57	0.59	23.35
Si 2p1/2	110.90	1.39	0.87	1.61	64.08
Ba 3d5/2	789.00	6.07	24.75	0.25	9.76

Table E3: The XPS Results of Cs^+ and Ba^{2+} Sorption on Natural Bentonite

Natural Bentonite

Element Identity	*Center (eV)*	*Peak Intensity*	*Sensitivity Factor*	*Corrected Intensity*	*Atomic Percentage*
Al 2p1/2	80.90	0.37	0.57	0.65	21.08
Si 2p1/2	109.00	1.86	0.87	2.15	70.43
Na 1s	1078.98	2.07	7.99	0.26	8.48

Cs-Sorbed Bentonite

Element Identity	*Center (eV)*	*Peak Intensity*	*Sensitivity Factor*	*Corrected Intensity*	*Atomic Percentage*
Al 2p1/2	83.05	0.54	0.57	0.54	71.14
Si 2p1/2	110.40	1.37	0.87	1.58	24.09
Cs 3d5/2	732.10	2.43	22.93	0.11	4.77

Ba-Siorbed Bentonite

Element Identity	*Center (eV)*	*Peak Intensity*	*Sensitivity Factor*	*Corrected Intensity*	*Atomic Percentage*
Al 2p1/2	82.70	0.24	0.57	0.42	20.11
Si 2p1/2	110.90	1.35	0.87	1.56	74.04
Ba 3d5/2	789.20	3.05	24.75	0.12	6.15

APPENDIX F

Table F1: The intensities (normalized to Quartz (101) peak) of major peaks corresponding to the main mineralogical fractions in natural and Cs-, Ba-, and Co-sorbed Kaolinite determined using XRD measurements.

Mineral Fraction	Nat. Kaolinite		Cs-kaolinite		Ba-kaolinite		Co-kaolinite	
	d_{hkl}	Intensity	d_{hkl}	Intensity	d_{hkl}	Intensity	d_{hkl}	Intensity
Quartz (101)	3.34	100	3.34	100	3.34	100	3.35	100
Kaolinite (001)	7.14	120	7.12	125	7.13	110	7.16	42
Kaolinite (002)	3.57	76	3.57	73	3.57	78	3.57	29
Kaolinite (110)	4.34	7	4.34	6	4.34	6	4.36	1
Quartz (100)	4.25	5	4.24	5	4.25	4	4.26	5
Kaolinite(020)	4.45	4	4.45	4	4.45	3	4.46	2

Table F2: The intensities (normalized to Quartz (101) peak) of major peaks corresponding to the main mineralogical fractions in natural and Cs-, Ba-, and Co-sorbed Chlorite-Illite (CI) determined using XRD measurements.

Mineral Fraction	Nat. CI		Cs-CI		Ba-CI		Co-CI	
	d_{hkl}	Intensity	d_{hkl}	Intensity	d_{hkl}	Intensity	d_{hkl}	Intensity
Quartz (101)	3.34	100	3.33	100	3.33	100	3.34	100
Illite (001)	9.95	36	9.95	21	10.1	21	10.02	37
Chlorite (002)	7.05	20	7.04	13	7.07	13	7.09	23
Calcite (104)	3.03	16	3.03	17	3.03	2	3.04	11
Illite (003)	3.20	13	3.20	8	3.20	8	3.21	15
Quartz (100)	4.24	11	4.24	13	4.25	12	4.25	11
Chlorite (004)	3.52	14	3.53	10	3.52	7	3.53	18
Chlorite (001)	14.08	14	14.08	2	14.08	2	14.31	12
$BaCO_3$ (104)	-	-	-	-	3.70	96	-	-

Table F3: The intensities (normalized to Quartz (101) peak) of major peaks corresponding to the main mineralogical fractions in natural and Cs-, Ba-, and Co-sorbed bentonite determined using XRD measurements.

Mineral	**Nat. Bentonite**		**Cs-bentonite**		**Ba-bentonite**		**Co-bentonite**	
Fraction	d_{hkl}	**Intensity**	d_{hkl}	**Intensity**	d_{hkl}	**Intensity**	d_{hkl}	**Intensity**
Quartz (101)	3.34	100	3.33	100	3.33	100	3.33	100
Montm. (001)	12.63	540	12.31	45	12.49	35	12.68	111
Montm. (110)	4.47	66	4.46	25	4.47	20	4.49	52
Montm. (004)	3.19	18	3.18	17	3.18	12	3.19	14
Quartz (100)	4.25	13	4.24	14	4.24	14	4.25	13
Feldspar	4.03	10	4.03	9	4.03	10	4.03	10
Calcite (104)	3.01	7	3.01	3	2.97	1	3.01	4
$BaCO_3$ (104)	-	-	-	-	3.69	196	-	-